THE UNIVERSITY
of EDINBURGH

Carbon dynamics of African miombo woodlands:

from the leaf to the landscape

Emily Skovmand Woollen

Doctor of Philosophy

The University of Edinburgh

School of GeoSciences

February 2013

Declaration

I declare that this thesis has been composed by myself and has not been submitted for any other degree. The work described is my own, except where otherwise indicated.

Emily S. Woollen

Abstract

Africa's carbon (C) cycle is one of the least well understood components of the global C cycle. Miombo woodlands are the most common woodland type in southern Africa, but despite their vast extent and importance in the biogeochemical cycles of Africa, their C dynamics are not well understood. This thesis addresses a set of science questions related to miombo woodland C dynamics that cover a range of scales, from the leaf to the landscape. The questions are related to seasonal controls on C uptake at the leaf level, to spatial distributions and scales of variation of C stocks in the landscape, and to the drivers and spatial patterns of deforestation and degradation at the regional scale.

In miombo woodlands, the seasonality of productivity remains poorly understood, and it is unclear whether stomatal limitations or variations in leaf traits cause seasonal changes in productivity. I use data of leaf gas exchange and leaf traits collected in dry and wet seasons to assess the response of photosynthesis to seasonality. I found a large degree of inter-specific responses, where photosynthetic capacity was maintained between seasons in some tree species but not in others. This was linked to inter-specific stomatal regulation on leaf gas exchange, access to soil water and varied leaf traits, indicating differing timing of leaf development during the dry season. Differing timing of leaf flushing can create niche separation, facilitating the co-existence of miombo woodland tree species.

I use data collected along a 5 km transect through miombo woodland to characterise the spatial distributions and scales of variation of C stocks in woody biomass and soils, and assess the links between them. I found that on the scale of a few meters, soil C stocks varied in relation to soil texture. At the kilometre scale,

surface soil and woody C stocks were coupled, and varied in relation to topography. By understanding the scales of variation I was able to make recommendations for optimal sampling of C stocks in a miombo woodland landscape for improved C stock assessments.

I developed and tested a simple spatial model of deforestation and degradation, using a rule-based approach, to produce risk maps of areas more likely to be affected by deforestation and degradation for a study site in central Mozambique. I found that my model was able to accurately predict the locality of high risk areas, and that roads were the major axis for forest biomass loss. Risk maps created from this method are useful for exploring the drivers of deforestation and degradation in a region dominated by miombo woodland, and for targeting policy and management efforts.

Overall, this thesis has contributed significantly to our understanding of natural and human driven miombo woodland C dynamics over a range of scales, from the leaf to the landscape. In the final chapter, I discuss the implications of each chapter for our understanding of miombo woodland C dynamics, and suggest areas for further research.

Acknowledgements

First and foremost I would like to thank my supervisor Mathew Williams for guiding me through the PhD, and for always having patience, a wealth of ideas and encouraging words when most needed. I would also like to thank John Grace, my second supervisor, whom has always been a source of inspiration and has supported me to pursue my ambitions right from the start of my undergraduate degree. Casey Ryan has always made time to discuss theories and hypotheses, and has been a large part of the thesis work from the beginning. I have learnt a lot from his experiences and have benefited from his work on miombo woodlands immensely. Thank you for all your inputs.

To the staff of Envirotrade Ltd. and the people of Nhambita I owe a huge dept of gratitude. The field staff Albasine 'Joey' Mucavele, Alfonso Jornal, Ramaio Saimone, Neto Moulinho and Zito Lindo were indispensable during field work, and lugged at least a ton of soil for me, and never complained even when asked to get up before dawn for no apparent reason. The van Zyl family, whom fed me well and showed me wonderful sights which I will never forget. Lucy Goodman and Philip Powell, for your friendship and amazing company. Gary Goss, who helped me out in numerous sticky situations and was always ready to enjoy a beer and share his stories. Lastly, to all the people who made my stay at Nhambita fun and who shared their time with me, I thank you.

Several people have helped me in various ways over the last few years. Jennifer Wright, Theresa Meacham and Silvia Caldararu shared this experience with me from day one, and I could not have asked for more energetic, enthusiastic and inspiring friends to struggle through with. Eddy Barratt, for the many adventures that

have been and have yet to come. Sheldon Goss, for doing a lot of my lab work. All the people in the Attic (you know who you are!): you are probably the most crazy bunch of people I will ever have the pleasure of working alongside. You made these years fun, and your friendships and outrageous conversations kept me sane.

Finally, I would like to thank my family for their unwavering support and encouragement, without which I would never have made it through. The endless trips to museums, botanical gardens, tree houses, safari's, and world wide travels have always been the source of my wonder of the natural world. I dedicate this thesis to my parents, Astrid and Charles.

"No doubt my voyage would seem a grander thing if I omitted mention of the help I received, but - well, there was a German gentleman once who evolved a camel out of his inner consciousness. It was a wonderful thing; still, you know, it was not a good camel, only a thing which people personally unacquainted with camels could believe in. Now I am ambitious to make a picture, if I make one at all, that people who do know the original can believe in - even if they criticise its points - and so I give you details a more showy artist would omit."

Mary Kingsley (1897), Travels in West Africa

Contents

1. Introduction

Thesis context: the uncertainty of Africa in the global carbon cycle

The global carbon cycle

The global carbon cycle is a biogeochemical cycle in which carbon (C) is exchanged amongst the earth's biosphere, pedosphere, geosphere, hydrosphere, and atmosphere. The exchange of C between the atmosphere, the oceans and the land surface are the largest annually, and determine the global C balance. The global C balance has fluctuated for hundreds of millennia (Augustin et al. 2004; Luethi et al. 2008; Petit et al. 1999), evidenced by changing atmospheric concentrations, and in the past has been tightly coupled to glacial cycles and climate (Petit et al. 1999; Shakun et al. 2012), driven by orbital forcing (Imbrie et al. 1992).

Over the past few centuries, human impacts on the global C balance have resulted in an increased flux of C to the atmosphere, estimated at 9.9 ± 0.9 Pg C $year^{-1}$ in 2008, mainly from fossil fuel emissions and land use change activities (Le Quere et al. 2009). Anthropogenic emissions have increased atmospheric carbon dioxide (CO_2) concentrations to a global average of 390 ppm in 2011 (Conway & Tans, NOAA/ESRL), a 40 % increase since pre-industrial values (280 ppm) (Etheridge et al. 1996). The unprecedented concentrations and rates of increased atmospheric CO_2 are perturbing the climate system, resulting in global warming and rapid climate change (IPCC 2007). The global mean surface temperature has risen faster over the past decade than previously, and the highest recorded 12 month running mean

temperature was reached in 2010, ~0.6 ^{o}C above the 1951-1980 mean (Hansen et al. 2010).

The oceans and the land surface store large amounts of C and act as natural C sinks, absorbing C from the atmosphere and offsetting approximately half of the human induced flux of C to the atmosphere (Le Quere et al. 2009). These natural sinks are not constant, however, resulting in large interannual variability in the amount of anthropogenic C emissions remaining in the atmosphere (Canadell et al. 2007; Le Quere et al. 2009). The interannual variability in the global C balance is largely caused by interannual variability in the land surface sink. The terrestrial C balance is determined by the balance between gross primary productivity and heterotrophic respiration, and forest re-growth and human land use change. Most of the interannual variability in the land C balance is due to the complex responses of terrestrial vegetation to climate variability (Houghton 2000). Land use change emissions, on the other hand, have remained fairly constant (Le Quere et al. 2009). Overall, the terrestrial biosphere acts as a net C sink, but the sink size and location remain uncertain.

Current estimates of the land sink strength are approximately 2.6 ± 0.7 Pg C yr^{-1} (Canadell et al. 2007; Le Quere et al. 2009), but with large uncertainty surrounding this value. The land sink has not been determined from direct measurements of the land surface C balance, as measurements are sparse and suffer from bias towards temperate regions. However, recent estimates from land based inventories and C studies suggests a global forest sink of 2.4 ± 0.4 Pg C $year^{-1}$ from 1990-2007 (Pan et al. 2011). This is almost equivalent to the estimated global terrestrial sink for the same period, deduced from balancing the C pools, suggesting

global forests can account for almost the entire terrestrial C sink. The land sink is partly offset by emissions from land use change, ranging from global estimates of 1.1 to 2.2 Pg C $year^{-1}$ (Houghton 2010), dominated by emissions from tropical deforestation (DeFries et al. 2002). Uncertainties surrounding the land use change emission estimates are associated with large spatial heterogeneity in forest biomass, and a lack of knowledge of biomass distributions, densities, and rates of deforestation, especially in the tropics (Houghton 2005; Houghton 2010).

Positive feedbacks between a changing climate and the C cycle have been predicted by several coupled climate-carbon cycle models (Cox et al. 2000; Friedlingstein et al. 2006), possibly decreasing the land and ocean sink efficiencies and amplifying climate changes further (Canadell et al. 2007; Le Quere et al. 2009). Although, more recent studies suggest an increased uptake by land and ocean sinks on a global scale (Ballantyne et al. 2012). Uncertainty surrounding the continued emissions rates and the variability and efficiency of the natural sinks make it difficult to forecast future atmospheric CO_2 levels and consequent climate change (IPCC 2007). In particular, a greater understanding of the land surface C cycle, and its response to a changing climate is needed if we are to reduce the uncertainty surrounding the global C budget and future climate projections. Given that global forests account for nearly the entire terrestrial C sink, and contribute the most to land use change emissions, further understanding of forest C cycles, changes, and responses to climate variability is essential for understanding the terrestrial C cycle. Furthermore, a greater knowledge of the amount and distribution of C stores in forest biomass and soils, particularly in the tropics, can constrain land use change emission estimates further.

Africa's role in the global carbon cycle

The African continent plays a large role in the global C cycle, accounting for an estimated 20 % of global land area, 17 % of global net land use change emissions (Canadell et al. 2009), 14-27 % of global net primary productivity (Weber et al. 2009) and 40 % of global biomass burning (Ciais et al. 2011; Williams et al. 2007). Furthermore, large temporal variability of the African C balance exists, caused by interannual variability in net ecosystem productivity (Ciais et al. 2009; Weber et al. 2009), contributing up to 50 % of the year-to-year variation in the global C balance (Williams et al. 2007). Despite Africa's importance in the global C cycle, the continent contributes one of the largest uncertainties to the global C budget, due to limited long-term measurements and sparse sampling networks (Ciais et al. 2011).

Uncertainties in the current knowledge of Africa's C budget are reflected in the large range of C balance estimates (Table 1) (Ciais et al. 2011). Estimates from *in situ* measurements (Bombelli et al. 2009) and models (Ciais et al. 2009) find that Africa is a net sink of C, in the order of 0.15-1 Pg C yr^{-1} (excluding fossil fuel emissions). Others claim Africa has a neutral long term C budget (Williams et al. 2007). However, both claims are subject to large uncertainties in their estimates. Africa has a unique emissions profile, where the majority of emissions are caused by land use change and fires, rather than fossil fuel emissions (Bombelli et al. 2009). Africa is only responsible for approximately 4 % of global fossil fuel emissions, but Africa's share of global emissions is likely to increase (Canadell et al. 2009), with the potential to turn the African C balance from a net sink to a source.

Table 1: Comparison between estimates of C uptake through net ecosystem productivity (NEP, includes forest and savanna), and C emissions from land use change (LUC, includes deforestation and degradation), savanna fires (SF), fossil fuel emissions (FF), and agricultural emissions (A). Net total C flux estimates are shown for each study specifying a value. Negative values represent a source of C to the atmosphere.

Source	**Uptake**	**Emissions**				**Net total**
	(Pg C yr^{-1})	**(Pg C yr^{-1})**				**(Pg C yr^{-1})**
	NEP	LUC	SF	FF	A	
Weber et al. (2009)	4.46 [a]					
Canadell et al. (2009)		-0.24		-0.26 [d]		
Williams et al. (2007)	2.07 [b]	-0.4	-1.47	-0.2		0
Ciais et al. (2009)	0.28 [c]	-0.13				0.15
Bombelli et al. (2009)	2.23	-0.33	-0.79	-0.18	-0.11	0.82

[a] value as presented in Bombelli et al. (2009) for sub-Saharan Africa
[b] Williams et al. assume a neutral C balance, therefore uptake must equal emissions
[c] deduced from balancing LUC emissions and net total flux. If we include all other emissions, the NEP estimate is likely to increase in order to obtain the net total flux 0.15 Pg C yr^{-1}
[d] value for all of Africa including north Africa, sub-Saharan values shown in Bombelli value for FF

Savannas and woodlands cover up to 40-50 % of the African land surface (Mayaux et al. 2004) and play a dominant role in Africa's C balance due to their large extent, frequent fires, and strong interannual variability in plant productivity (Bombelli et al. 2009). Savannas are productive ecosystems, but fluxes are highly seasonal and have large interannual variability caused by seasonality of plant productivity and fires (Grace et al. 2006; Scholes and Andreae 2000). Large interannual variability in photosynthesis occurs in savannas and woodlands of southern and eastern Africa, driven by variability in rainfall, contributing significantly to the interannual variability of Africa's C balance (Ciais et al. 2009; Weber et al. 2009). The role of savannas and woodlands in Africa's C balance is, however, still highly uncertain and there is a need for further research on the C dynamics of savannas and woodlands for a better understanding of their role in the dynamics of the African C cycle.

Africa's population is increasing rapidly (United Nations 2011), increasing pressure on ecosystem services. Rapidly increasing urban populations are placing higher demands on agricultural and forest products, increasing rates of deforestation and land use change (DeFries et al. 2010). There is an urgent need for *in situ* measurements and an integrated C observing system across Africa, for a more precise assessment of Africa's C cycle and sensitivity to anthropogenic pressures and future climate change (Ciais et al. 2011). In particular, savannas and woodlands of Africa require attention, as they contribute the most to the uncertainty of Africa's C balance.

Miombo woodlands of Africa

The most common woodland type in the southern hemisphere is miombo woodland, which covers more than 2.7 million km^2 of southern, central and eastern Africa (Campbell 1996), spanning from Tanzania in the north, Angola in the west, and Mozambique in the south and east (Fig. 1). Miombo woodlands (Fig. 2) are the dominant element of the Zambezian phytochorological region, and are characterised by the dominance of trees of the genera *Brachystegia*, *Julbernardia* and/or *Isoberlinia*, all from the legume family (Fabaceae, subfamily Caesalpinioideae) (White 1983). Miombo has variously been defined as savanna, woodland and forest due to the large range of vegetation structures found, ranging from open sparse wooded grassland to closed canopy woodlands or forest. Savanna ecosystems are broadly characterised by the presence of scattered trees and a continuous grass layer co-existing in the landscape (Scholes and Archer 1997), and miombo falls within the broader classification of savanna due to having a continuous C_4 grass layer. The large variability in canopy cover and vegetation structure occurs due to a hierarchy of

factors at a range of scales; climate and rainfall at a regional level, soil properties at the landscape, and various disturbance factors locally (Frost 1996).

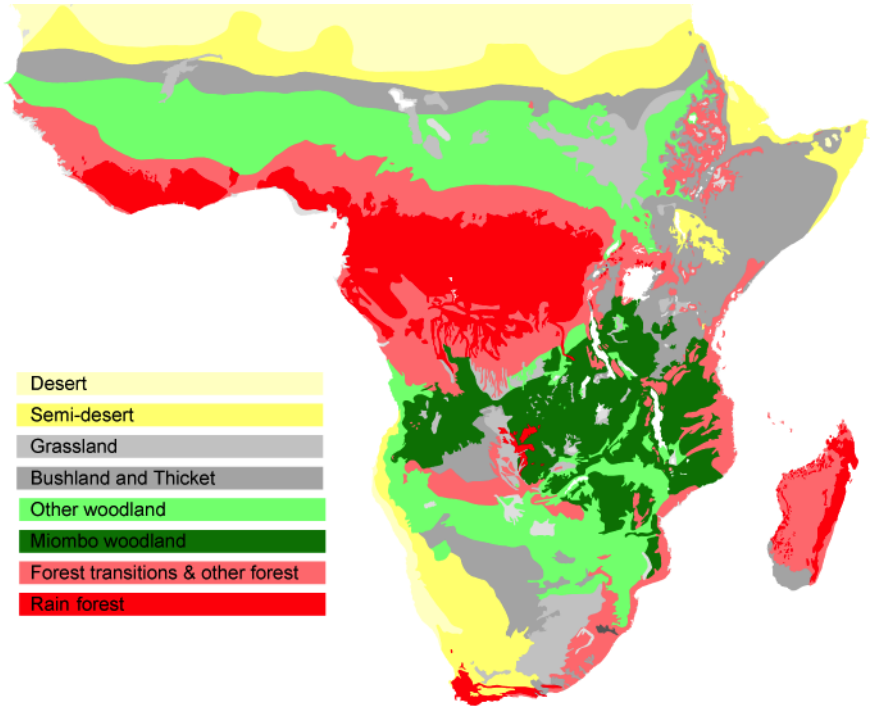

Fig. 1: Vegetation map of Africa, showing Miombo woodlands in dark green. The map was created by White (1983), and edited by Casey Ryan (data available from http://gcmd.gsfc.nasa.gov)

Fig. 2: Mature miombo woodland with characteristic canopy tree species of *Brachystegia spiciformis* and *Julbernardia globiflora*, with a continuous C_4 grass layer. Photo was taken at the study site in central Mozambique (see Fig. 6) during the wet season by Casey Ryan.

The miombo region has an estimated 8500 species of higher plants, where over half of these are endemic (Rodgers et al. 1996). Mean annual rainfall varies from 540 to 1700 mm with large seasonality in precipitation, where more than 95% of annual rainfall occurs in a 5-7 month wet season (Frost 1996). They are seasonally dry deciduous woodlands, and characteristically produce new leaves 1-2 months before the start of the rains (Chidumayo 1994; Fuller 1999; Ryan 2009). Miombo generally occurs on highly weathered, acidic soils with low nutrient and C content (Bird et al. 2000; Frost 1996). Soils are classed as sandy loam, loamy sands, or sandy clay loam, which are often more than 3 m deep and freely draining (Frost 1996). However, soil properties are diverse and vary within a landscape, mainly due to changes in slope, termite presence and land use. The dominance of tree species with ectomycorrhizal root associations, for increased nutrient uptake, may enable miombo tree species to exploit infertile soils more efficiently than other groups, explaining their dominance on nutrient poor soils (Hogberg 1986a; Hogberg 1986b). Rooting profiles of miombo trees are largely unknown, but they are thought to have extensive lateral roots and deep tap roots extending several meters down (Fig. 3) (Timberlake and Calvert 1993). Approximately 40 % of woody biomass is allocated to below-ground structures and 60 % to above, but miombo C stocks are dominated by soil C (Ryan et al. 2011).

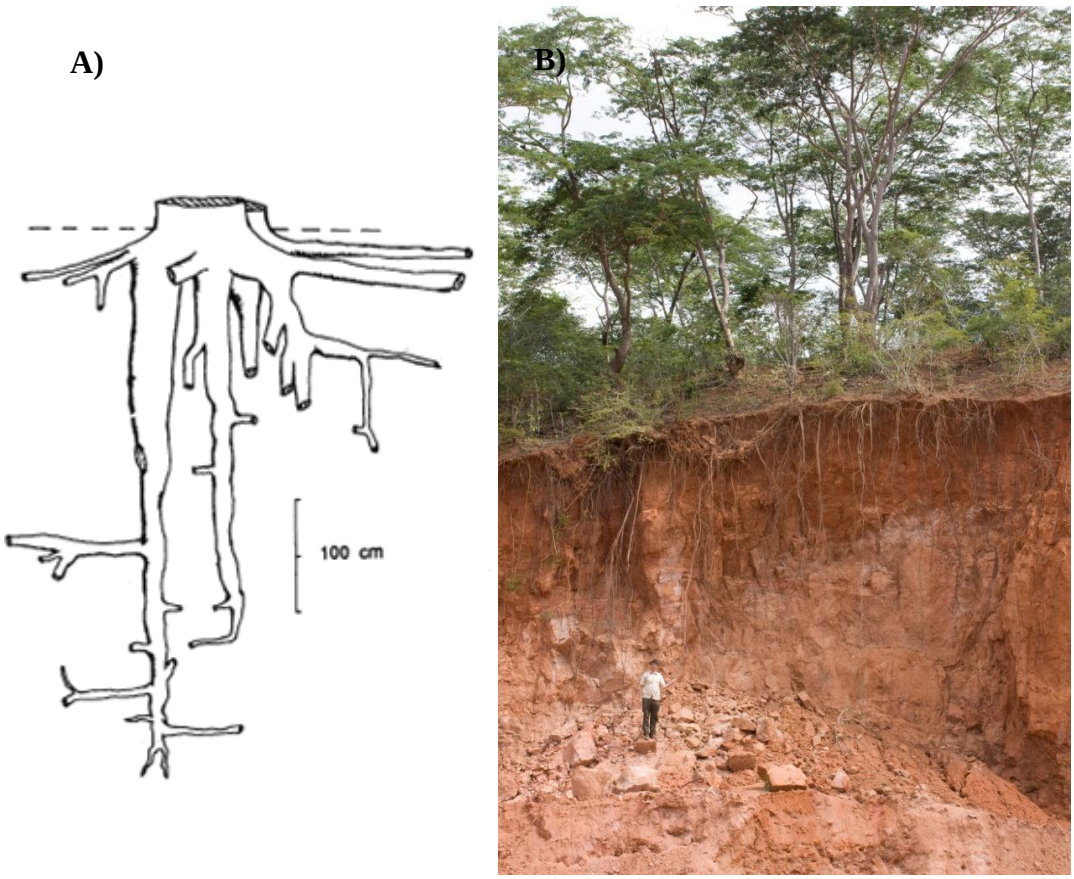

Fig. 3: Rooting profile of miombo woodland trees. A) typical rooting structure of mature *Brachystegia spiciformis* [from Timberlake and Calvert (1993), p. 39], B) excavated hill slope where roots are seen to extend several meters (~ 6 m) down. Picture by Mathew Williams, featuring Casey Ryan.

Frequent fires are a characteristic feature of miombo woodland, majority of which are human induced, and have been part of the miombo woodland dynamics for centuries (Chidumayo 1997). Fire return intervals are between 1 to 3 years, and occur mainly in the 6 month dry season when dry grass fuel loads are high (Frost 1996). Fire is a key ecological determinant in the savanna biome (Furley et al. 2008; Trapnell 1959), where frequent fires can transform woodlands into open tall grass savanna, and protection from fire promotes canopy closure (Fig. 4). The intensity and timing of burning can have further selective impacts on miombo woodlands, affecting the structure and composition of trees (Ryan and Williams 2011), and

decreasing soil C stocks (Bird et al. 2000). Fire is therefore a complex disturbance force, with considerable implications for the dynamics of miombo woodland. Grazing by herbivores is limited in miombo (Frost 1996), but elephants can have a significant impact on the woodland structure (Guy 1981). Furthermore, interactions between fires and elephants can have an important role in ecosystem structure, composition and extent (Ribeiro et al. 2008; Yang and Prince 2000).

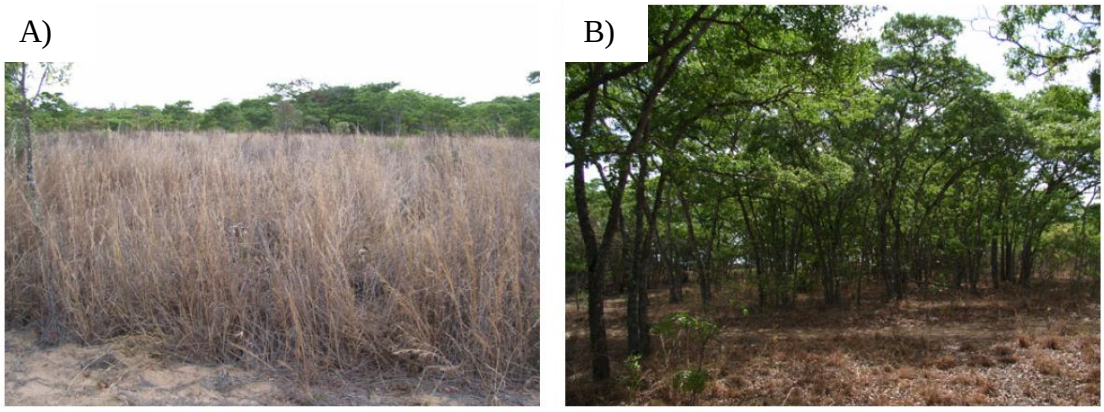

Fig. 4: The effect of fire in miombo at Marondera, Zimbabwe. A) A plot that was burned annually for 50 years. B) A plot that has been protected from fire during the same period. See Furley et al. (2008) for further details. Pictures by Casey Ryan.

Miombo woodlands are central to the livelihoods of millions of rural and urban dwellers by providing fuel wood, building materials, medicines, food and ecosystem services (Campbell et al. 2007). Increasing populations and demand has meant land use change and shifting agriculture is increasing (Fig. 5) (Houghton and Hackler 2006). Re-growth and recovery of miombo woodland from land clearing can take several decades (Williams et al. 2008b), and below ground C stocks may not recover to pre-clearing values even after 30 years of fallow (Walker and Desanker 2004; Williams et al. 2008b). In more recent years, there has been an observed change from shifting cultivation to more permanent types of agriculture (Jansen et al. 2008), causing altered, but largely unknown, impacts to miombo woodlands. With a

population growth of ~2 % annually (United Nations 2011), humans play an ever increasing role in the dynamic ecosystem of miombo woodland.

Fig. 5: Example of shifting agriculture where the stumps of felled trees are visible throughout the field, and some trees still remain. The *machamba* is surrounded by the original woodland. Photo was taken near Mbulawa in central Mozambique (see Fig. 6).

Overview of the study site

The thesis study site was located in the Nhambita community area, Gorongosa district, Sofala province, central Mozambique (18°59'24''S, 34°10'23''E) (Fig. 6). The Nhambita community is situated immediately west of Gorongosa National Park, and the area is predominantly classified as miombo woodland (Mushove 2003). Miombo is predominantly found on brown granite gneiss on higher ground in the study site, but large variability in vegetation and soil type occurs throughout the landscape, where *Acacia* and *Combretum* savanna is more common

on grey hydromorphic, grey soils, and non-hydromorphic alluvia soils on the low grounds (Tinley 1977). Mean annual rainfall is 850 ± 269 mm (± standard deviation) and is highly seasonal, with 82 % falling in the 5 month wet season between November and March, and mean monthly temperatures range from 20 ^{o}C in the mid-dry season to 30 ^{o}C in the mid-wet season (Ryan 2009).

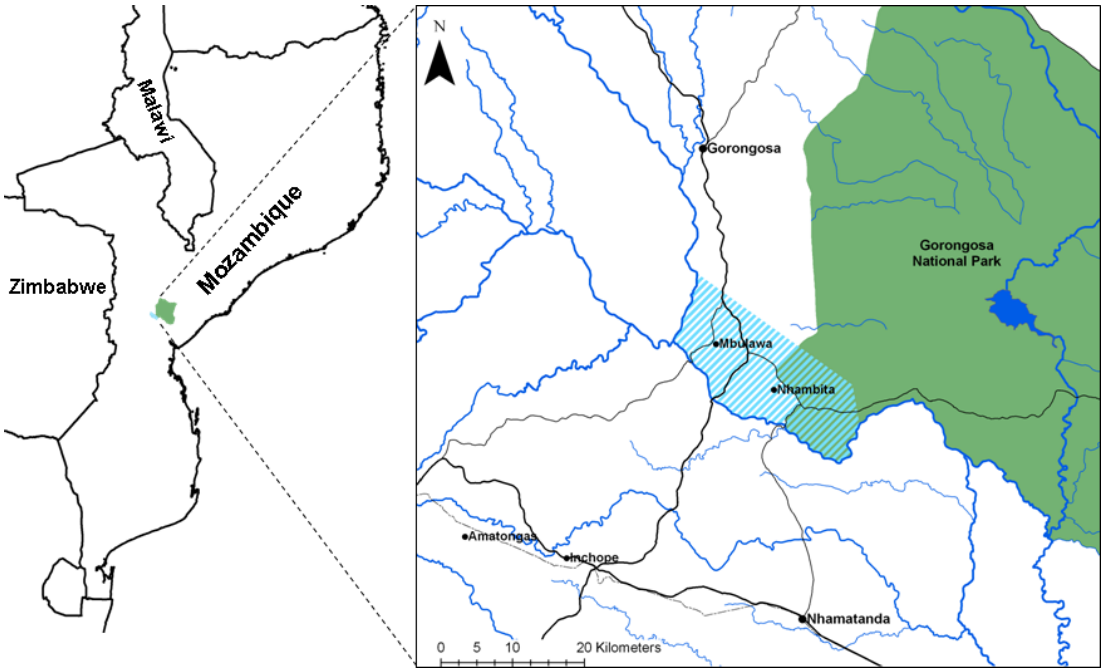

Fig. 6: Map of Nhambita community area (blue stripped area), Sofala Province, central Mozambique. Rivers and lakes are shown in blue and roads in black. Gorongosa National Park is the green area to the east.

The Nhambita community has a population of a few thousand people, consisting of widely scattered homesteads. Subsistence agriculture and shifting cultivation is common, and *machambas* occur throughout the study site but are kept outside the National Park borders. The population largely depends on natural products and ecosystem services for their livelihoods, and hunting, wood fuel collection, and extraction of building materials from the surrounding woodland is common practice. The area was heavily impacted by the war for independence (1964-1975), followed by the civil war (1977-1992), displacing the people of

Nhambita and causing the abandonment of industrial agriculture (mainly cotton) in the area. The National Park was also affected, with a large loss of animal populations. Since the end of the civil war, the area has been resettled by its previous inhabitants and now has a growing population. The Park has largely been restored and their animal populations are still increasing, but industrial agriculture was never re-established.

The Sofala Community Carbon Project, a pilot project to store carbon as biomass to create carbon credits for sale on the voluntary carbon market, was established in 2003 in the Nhambita area (Grace et al. 2010). The project creates carbon credits through tree planting (e.g. agroforestry by inter-cropping and boundary planting of trees along fields) and avoided deforestation. The project was the initiative of a commercial company, Evirotrade Ltd (http://www.envirotrade .co.uk), in conjunction with the University of Edinburgh and other consultants, whom provided technical expertise (Grace et al. 2010). Between 2003 and 2009 the project was able to establish and sell carbon credits corresponding to 156,000 t CO_2. The project has also had large ancillary benefits, including increased employment, income, literacy, schooling, and greater access to health care. The project is still in operation today, and has created alternative livelihoods and improved standards of living for many people in the Nhambita area.

Thesis rationale: a better understanding of African miombo woodland carbon dynamics on several scales

The current state of knowledge on Africa's C cycle is limited. Despite the vast extent and importance in the biogeochemical cycles of Africa, miombo woodlands remain relatively understudied. Miombo woodlands are dynamic ecosystems and are driven by multiple disturbances and environmental variability at a range of scales, with complex interactions, defining the C dynamics of miombo woodlands. However, very few studies have quantified the C stocks and changes of miombo woodland, or assessed the impacts of climate variability and anthropogenic pressures on C dynamics. The aim of this thesis is to contribute towards a better understanding of miombo woodland C dynamics by addressing key unknown aspects of the C cycle at a range of scales, from the leaf to the landscape. These include 1) seasonal controls on C uptake at the leaf level, 2) spatial distributions and scales of variation of C stocks in the landscape, and 3) drivers and spatial patterns of deforestation and degradation at the regional scale.

Previous work (Ciais et al. 2009; Weber et al. 2009; Williams et al. 2008a), suggests that the variability in Africa's primary productivity is linked to interannual variability in rainfall and acute soil water stress, with the highest variability occurring in southern and eastern Africa. In miombo woodlands, the seasonality of productivity remains poorly understood. Photosynthetic capacity of miombo woodland trees is known to increase initially with leaf development during the late dry season (Tuohy and Choinski 1990), increasing to their highest potentials during the wet season (Choinski and Johnson 1993), and scaling linearly with increasing leaf nitrogen content (Tuohy et al. 1991). However, the mechanisms contributing to

the increased photosynthetic capacities in the wet season are still largely unknown, and it is unclear whether stomatal limitations or variations in leaf traits cause seasonal changes in productivity. A better understanding of how leaf level photosynthesis and gas exchange responds to seasonality of climate and water availability in miombo woodlands would contribute towards a better understanding of the mechanisms driving the seasonality of Africa's primary productivity.

Miombo woodlands are characterised by large heterogeneity in tree and grass cover, determined by multiple mechanisms. The heterogeneity of miombo translates into highly varied above and below ground C stocks (Rossi et al. 2009; Ryan et al. 2011; Williams et al. 2008b), which complicates estimates of their C stocks and their monitoring requirements, leading to significant uncertainty in the assessment of C stocks and changes at the landscape scale. Woody biomass and soil C stock distributions have been linked to slope and soil physical properties (Chidumayo 1997; Frost 1996). However, these links are unclear (Ryan et al. 2011), due to other disturbances such as fire (Bird et al. 2000; Ryan and Williams 2011) and human influences (Chidumayo 2002; Williams et al. 2008b) impacting on vegetation structure, and de-coupling above- and below-ground C stocks (Ryan et al. 2011). In order to reduce uncertainty surrounding C stock assessments in a miombo woodland landscape, there is a need to understand what determines the distributions of C stocks in soils and vegetation and at what scales they vary.

A flux of C to the atmosphere from land use/cover change offsets part of the sink strength of the global land surface (Le Quere et al. 2009), attributed largely to tropical deforestation (Baccini et al. 2012; DeFries et al. 2002). Deforestation is a spatially complex issue caused by many factors, created by human activities and

social processes (Geist and Lambin 2002). By understanding the drivers of deforestation, and incorporating such information into spatial models, managers are better able to predict the likely locations and quantities of forest biomass loss, to support resource management efforts (Lambin 1997). However, these spatial models tend to be complex and lack transparency, comprehension and credibility, and are not always practical if sufficient data and expertise are lacking. A simpler approach to spatial modelling of forest cover change might therefore be preferable (Liu et al. 1993; Mertens and Lambin 1997). By incorporating drivers of miombo woodland deforestation into a simple spatial model it would enable us to test our understanding of the drivers of deforestation, and predict locations of forest loss, providing valuable information for management and policy efforts.

Thesis objectives:

The objectives of this thesis are to improve our understanding of miombo woodland C cycles at a range of scales by answering key unknown questions relating to processes of C uptake, C stock distributions and variability, and C stock changes. Specifically:

1) What are the controls on photosynthetic productivity of miombo woodland tree species on a diurnal to seasonal time scale?
2) How do C stocks in soil and vegetation vary across a miombo woodland landscape, and to what degree and at what scales are these stocks linked?
3) Based on our understanding of drivers of deforestation and degradation, can we create a simple spatial model to accurately predict risk of forest biomass loss in a region of central Mozambique?

Overview of thesis chapters:

This thesis is structured as a series of three papers, which are either published or intended for publication. Each paper stands alone as an independent research article. There are also three appendices, which include other data collected as part of the thesis but not included in the papers, further analyses of data, and other published work where the data was used in this thesis. Each of the thesis papers content and purpose are outlined below. In the final chapter of the thesis, I outline the main conclusions, discuss the implications of each paper for our understanding of miombo woodland C dynamics, and suggest areas for further research.

Paper 1 - Seasonal limitations to leaf level productivity in African miombo woodland tree species

The objective of this chapter was to determine the controls on photosynthetic productivity of miombo woodland tree species on a diurnal to seasonal time scale, by assessing the response of leaf level gas exchange to seasonal drought and leaf trait variations between seasons. We expected photosynthetic productivity to increase in the wet season, and hypothesised that decreased rates during the dry season would be caused by stomatal limitations to leaf gas exchange, and/or seasonal changes to leaf traits related to photosynthetic capacity. Contrary to our expectations, we found that two out of the three tree species maintained photosynthetic capacities between seasons, whereas one had lower rates during the dry season. The inter-specific differences were a result of differing stomatal control on leaf gas exchange, varied access to soil water, and variable leaf traits, suggesting differing stages of leaf development during the dry season. We suggest that varied timing of leaf flushing

creates niche separation with regards to resource competition during the early growing season, facilitating the co-existence of miombo woodland tree species.

Paper 2 - Carbon stocks in and African woodland landscape: spatial distributions and scales of variation

The objectives of this chapter were to assess what the spatial distributions of C stocks in soils and vegetation were, determine if C stocks were linked, and assess at what scales they varied in a miombo woodland landscape. In order to assess spatial distributions and scales of variation of C stocks, a 5 km transect was used to sample C stocks and other related variables across a miombo woodland landscape. We found that soil C stocks varied significantly at scales of a few meters, and woody biomass C stocks varied significantly at kilometre scales. Soil textural distributions and woody biomass C stocks were linked to topography, where coarse textured soils and greater biomass volumes were found on hill tops and elevated ground. Top-soil C stocks were linked to vegetation, but deeper soil C stocks were coupled to soil clay content. We discuss the mechanisms controlling C stock distributions, and suggest optimal sampling strategies for C stock assessments in miombo based on our findings.

Paper 3 - Spatial modelling of areas at risk of deforestation and degradation using a simple rule-based approach: a case study in central Mozambique

The objective of this study was to develop and test a simple rule-based model of deforestation and degradation. The model was based on the hypothesis that if land is accessible, cultivable, has extractable value and is unprotected (the ACEU

hypothesis) it will be at high risk of deforestation and degradation. We incorporated our understanding of the drivers of deforestation and degradation in our study site in central Mozambique into the ACEU model. By using geographic information system techniques, we applied the model in a spatial context, and produce a risk map of areas more likely to be affected by deforestation and degradation processes. We tested our model assumptions and compared our results to measured biomass changes using a time series of remotely sensed biomass maps over a three year period. We found that the model was able to accurately predict the areas at high risk of deforestation and degradation in most cases. We found that roads were the major axis of forest loss and that biomass resources were being degraded at an unsustainable rate in the region during the study period. The risk map created from this method is useful for targeting further monitoring, policy and management efforts to areas at high risk of forest loss in the near future.

Appendix 1:

Appendix 1 presents additional analyses of some of the data presented in paper 1 of this thesis, and additional ecophysiological measurement data collected during the wet season on miombo woodland tree species.

Appendix 2:

Appendix 2 is an additional study I did on leaf trait relations of miombo woodland trees.

Appendix 3:

Appendix 3 is a published article by Ryan et al. (2012) in which I am a co-author, as data collected as part of this thesis work (paper 2) was used in the publication. I also use the time series of biomass maps produced by this article in paper 3 of this thesis.

References

Augustin L et al. (2004) Eight glacial cycles from an Antarctic ice core. Nature 429:623-628

Baccini A et al. (2012) Estimated carbon dioxide emissions from tropical deforestation improved by carbon-density maps. Nature Advance online publication

Ballantyne AP, Alden CB, Miller JB, Tans PP, White JWC (2012) Increase in observed net carbon dioxide uptake by land and oceans during the past 50 years. Nature 488:70-73

Bird MI, Veenendaal EM, Moyo C, Lloyd J, Frost P (2000) Effect of fire and soil texture on soil carbon in a sub-humid savanna (Matopos, Zimbabwe). Geoderma 94:71-90

Bombelli A et al. (2009) The sub-saharan Africa carbon balance, an overview. Biogeosciences Discuss. 6:2085-2123

Campbell BM (1996) The Miombo in Transition: Woodlands and Welfare in Africa. Center for International Forestry Research, Bogor, Indonesia

Campbell BM, Angelsen A, Cunningham A, Katerere Y, Sitoe A, Wunder S (2007) Miombo woodlands - opportunities and barriers to sustainable forest management. Centre for International Forestry Research, Bogor, Indonesia

Canadell JG et al. (2007) Contributions to accelerating atmospheric CO(2) growth from economic activity, carbon intensity, and efficiency of natural sinks. Proceedings of the National Academy of Sciences of the United States of America 104:18866-18870

Canadell JG, Raupach MR, Houghton RA (2009) Anthropogenic CO2 emissions in Africa. Biogeosciences 6:463-468

Chidumayo EN (1994) Phenology and Nutrition of Miombo Woodland Trees in Zambia. Trees-Structure and Function 9:67-72

Chidumayo EN (1997) Miombo Ecology and Management: an Introduction. Intermediate Technology Publications, London

Chidumayo EN (2002) Changes in miombo woodland structure under different land tenure and use systems in central Zambia. Journal of Biogeography 29:1619-1626

Choinski JS, Johnson JM (1993) Changes in Photosynthesis and Water Status of Developing Leaves of Brachystegia-Spiciformis Benth. Tree Physiology 13:17-27

Ciais P et al. (2011) The carbon balance of Africa: synthesis of recent research studies. Philosophical Transactions of the Royal Society a-Mathematical Physical and Engineering Sciences 369:2038-2057

Ciais P, Piao SL, Cadule P, Friedlingstein P, Chedin A (2009) Variability and recent trends in the African terrestrial carbon balance. Biogeosciences 6:1935-1948

Cox PM, Betts RA, Jones CD, Spall SA, Totterdell IJ (2000) Acceleration of global warming due to carbon-cycle feedbacks in a coupled climate model. Nature 408:184-187

DeFries RS, Houghton RA, Hansen MC, Field CB, Skole D, Townshend J (2002) Carbon emissions from tropical deforestation and regrowth based on satellite observations for the 1980s and

1990s. Proceedings of the National Academy of Sciences of the United States of America 99:14256-14261

DeFries RS, Rudel T, Uriarte M, Hansen M (2010) Deforestation driven by urban population growth and agricultural trade in the twenty-first century. Nature Geoscience 3:178-181

Etheridge DM, Steele LP, Langenfelds RL, Francey RJ, Barnola JM, Morgan VI (1996) Natural and anthropogenic changes in atmospheric CO2 over the last 1000 years from air in Antarctic ice and firn. Journal of Geophysical Research-Atmospheres 101:4115-4128

Friedlingstein P et al. (2006) Climate-carbon cycle feedback analysis: Results from the C(4)MIP model intercomparison. Journal of Climate 19:3337-3353

Frost P (1996) The ecology of miombo woodlands. In: Campbell B (ed) The Miombo in Transition: Woodlands and Welfare in Africa. Center for International Forestry Research, Bogor, Indonesia, pp 11-57

Fuller DO (1999) Canopy phenology of some mopane and miombo woodlands in eastern Zambia. Global Ecology and Biogeography 8:199-209

Furley PA, Rees RM, Ryan CM, Saiz G (2008) Savanna burning and the assessment of long-term fire experiments with particular reference to Zimbabwe. Progress in Physical Geography 32:611-634

Geist HJ, Lambin EF (2002) Proximate causes and underlying driving forces of tropical deforestation. Bioscience 52:143-150

Grace J, Ryan CM, Williams M, Powell P, Goodman L, Tipper R (2010) A pilot project to store carbon as biomass in African woodlands. Carbon Management 1:227-235

Grace J, San Jose J, Meir P, Miranda HS, Montes RA (2006) Productivity and carbon fluxes of tropical savannas. Journal of Biogeography 33:387-400

Guy PR (1981) Changes in the Biomass and Productivity of Woodlands in the Sengwa Wildlife Research Area, Zimbabwe. Journal of Applied Ecology 18:507-519

Hansen J, Ruedy R, Sato M, Lo K (2010) Global surface temperature change. Reviews of Geophysics 48

Hogberg P (1986a) Nitrogen fixation and nutrient relations in savanna woodland trees (Tanzania). Journal of Applied Ecology 23:675-688

Hogberg P (1986b) Soil nutrient availability, root symbioses and tree species composition in tropical Africa: a review. Journal of Tropical Ecology 2:359-372

Houghton RA (2000) Interannual variability in the global carbon cycle. Journal of Geophysical Research-Atmospheres 105:20121-20130

Houghton RA (2005) Aboveground forest biomass and the global carbon balance. Global Change Biology 11:945-958

Houghton RA (2010) How well do we know the flux of CO(2) from land-use change? Tellus Series B-Chemical and Physical Meteorology 62:337-351

Houghton RA, Hackler JL (2006) Emissions of carbon from land use change in sub-Saharan Africa. Journal of Geophysical Research-Biogeosciences 111

Imbrie J et al. (1992) On the structure and origin of major glaciation cycles 1. Linear responses to Milankovich forcing. Paleoceanography 7:701-738

IPCC (2007) Fourth Assessment Report: Climate Change 2007 (AR4). Geneva, Switzerland

Jansen LJM, Bagnoli M, Focacci M (2008) Analysis of land-cover/use change dynamics in Manica Province in Mozambique in a period of transition (1990-2004). Forest Ecology and Management 254:308-326

Lambin EF (1997) Modelling and monitoring land-cover change processes in tropical regions. Progress in Physical Geography 21:375-393

Le Quere C et al. (2009) Trends in the sources and sinks of carbon dioxide. Nature Geoscience 2:831-836

Liu DS, Iverson LR, Brown S (1993) Rates and patterns of deforestation in the Philippines: application of geogrpahic information system analysis. Forest Ecology and Management 57:1-16

Luethi D et al. (2008) High-resolution carbon dioxide concentration record 650,000-800,000 years before present. Nature 453:379-382

Mayaux P, Bartholome E, Fritz S, Belward A (2004) A new land-cover map of Africa for the year 2000. Journal of Biogeography 31:861-877

Mertens B, Lambin EF (1997) Spatial modelling of deforestation in southern Cameroon - Spatial disaggregation of diverse deforestation processes. Applied Geography 17:143-162

Mushove P (2003) Preliminary inventory of Nhambita community forest, Gorongosa district, Mozambique. ERMAL Natural Resources Consultancy, Harare

Pan Y et al. (2011) A Large and Persistent Carbon Sink in the World's Forests. Science 333:988-993

Petit JR et al. (1999) Climate and atmospheric history of the past 420,000 years from the Vostok ice core, Antarctica. Nature 399:429-436

Ribeiro NS, Shugart HH, Washington-Allen R (2008) The effects of fire and elephants on species composition and structure of the Niassa Reserve, northern Mozambique. Forest Ecology and Management 255:1626-1636

Rodgers A, Salehe J, Howard G (1996) The biodiversity of miombo woodlands. In: Campbell B (ed) The Miombo in Transition: Woodlands and Welfare in Africa. Center for International Forestry Research, Bogor, Indonesia

Rossi J et al. (2009) Spatial structures of soil organic carbon in tropical forests-A case study of Southeastern Tanzania. Catena 77:19-27

Ryan CM (2009) Carbon Cycling, Fire and Phenology in a Tropical Savanna Woodland in Nhambita, Mozambique. PhD thesis, School of GeoSciences, The University of Edinburgh, Edinburgh

Ryan CM et al. (2012) Quantifying small-scale deforestation and forest degradation in African woodlands using radar imagery. Global Change Biology 18:243-257

Ryan CM, Williams M (2011) How does fire intensity and frequency affect miombo woodland tree populations and biomass? Ecological Applications 21:48-60

Ryan CM, Williams M, Grace J (2011) Above- and belowground carbon stocks in a miombo woodland landscape of Mozambique. Biotropica 43:423-432

Scholes M, Andreae MO (2000) Biogenic and pyrogenic emissions from Africa and their impact on the global atmosphere. Ambio 29:23-29

Scholes RJ, Archer SR (1997) Tree-grass interactions in savannas. Annual Review of Ecology and Systematics 28:517-544

Shakun JD et al. (2012) Global warming preceded by increasing carbon dioxide concentrations during the last deglaciation. Nature 484:49-+

Timberlake JR, Calvert GM (1993) Preliminary Root Atlast for Zimbabwe and Zambia. Zimbabwe Bulletin of Forestry Research

Tinley KL (1977) Framework of the Gorongosa Ecosystem. PhD thesis, Faculty of Science, University of Pretoria, Pretoria

Trapnell CG (1959) Ecological results of woodland and burning experiments in nothern Rhodisia. Journal of Ecology 47:129-168

Tuohy JM, Choinski JS (1990) Comparative Photosynthesis in Developing Leaves of Brachystegia-Spiciformis Benth. Journal of Experimental Botany 41:919-923

Tuohy JM, Prior JAB, Stewart GR (1991) Photosynthesis in Relation to Leaf Nitrogen and Phosphorus-Content in Zimbabwean Trees. Oecologia 88:378-382

United Nations (2011) World Population Prospects: The 2010 Revision. Department of Economic and Social Affairs, Population Division, New York

Walker SM, Desanker PV (2004) The impact of land use on soil carbon in Miombo Woodlands of Malawi. Forest Ecology and Management 203:345-360

Weber U et al. (2009) The interannual variability of Africa's ecosystem productivity: a multi-model analysis. Biogeosciences 6:285-295

White F (1983) The Vegetation of Africa: a descriptive memoir to accompany the Unesco/AETFAT/UNSO vegetation map of Africa. UNESCO, Paris

Williams CA, Hanan NP, Baker I, Collatz GJ, Berry J, Denning AS (2008a) Interannual variability of photosynthesis across Africa and its attribution. Journal of Geophysical Research-Biogeosciences 113

Williams CA et al. (2007) Africa and the global carbon cycle. Carbon Balance and Management 2:3

Williams M, Ryan CM, Rees RM, Sambane E, Fernando J, Grace J (2008b) Carbon sequestration and biodiversity of re-growing miombo woodlands in Mozambique. Forest Ecology and Management 254:145-155

Yang J, Prince SD (2000) Remote sensing of savanna vegetation changes in Eastern Zambia 1972-1989. International Journal of Remote Sensing 21:301-322

2a. Seasonal limitations to leaf level productivity in African miombo woodland tree species

E. Woollen[1] and M. Williams[1]

[1] School of GeoSciences, The University of Edinburgh, Edinburgh, EH9 3JN, UK

(*intended for submission to Tree Physiology*)

Abstract

Africa's carbon cycle is one of the least well understood components of the global carbon cycle. The savannas and woodlands of southern Africa play a major but uncertain role in Africa's carbon cycle, due, in part, to their large extent and inter-annual variability in primary productivity. Miombo woodlands, which cover over 2.7 M km^2 of Southern Africa, are seasonally dry deciduous woodlands, developing new leaves at the end of the dry season before the start of the rains. Very little is known of their leaf-level productivity and seasonal fluctuations in photosynthesis, so that it is unclear whether increased wet season productivity is caused by changes to stomatal limitations on leaf gas exchange or leaf trait variations. The objectives of this study were to quantify the controls on photosynthetic productivity of miombo woodland tree species on a diurnal to seasonal time scale, by assessing the seasonal changes in leaf traits (including rates of carboxylation and electron transport, leaf chemical and physical structure, and leaf specific conductance), leaf water relations and stomatal conductance. Contrary to expectations, we found that two dominant tree species, *Julbernardia globiflora* and *Diplorhynchus condylocarpon*, maintained stomatal conductances and assimilation rates between seasons. *Brachystegia spiciformis*, however, had lower stomatal conductance and assimilation rates in the dry season. The inter-specific differences were a result of differing stomatal regulation on leaf gas exchange, photosynthetic capacities and leaf traits between species, and varied access to soil water during the dry season. Despite strong stomatal down-regulation at high evaporative demands in the dry season, *B. spiciformis* maintained internal to ambient CO_2 ratios between seasons, and showed no apparent stomatal limitations to photosynthetic productivity.

B. spiciformis did, however, have lower leaf N content and photosynthetic capacity in the dry season, whereas *J. globiflora* and *D. condylocarpon* showed little to no change in leaf traits between seasons. The differences in leaf traits were attributed to differing stages of leaf development during the time of measurement in the dry season. It was unclear what caused the varied phenological timing, but varied timing of leaf flushing can create niche separation with regards to resource competition during the early growing season, facilitating the co-existence of tree species in miombo woodlands.

Key words: leaf gas exchange, CO_2 response curves, leaf water potential, leaf traits, *Brachystegia spiciformis, Julbernardia globiflora, Diplorhynchus condylocarpon*, miombo woodland, Mozambique

Abbreviations: A, net CO_2 assimilation rate; A_{max}, maximum assimilation rate; BS, *Brachystegia spiciformis*; C, carbon; C_i, internal CO_2 concentration; DC, *Diplorhynchus condylocarpon*; E, transpiration rate; E_{max}, maximum transpiration rate; g_s, stomatal conductance; $g_{s\,max}$, maximum stomatal conductance; JG, *Julbernardia globiflora*; J_{max}, maximum electron transport rate; *LMA*, leaf-mass-per-area; *LSC*, leaf specific conductance; N, nitrogen; *PAR*, photosynthetically active radiation; T_l, leaf temperature; $T_{l\,Amax}$, leaf temperature at the time of maximum assimilation rates; V_{cmax}, maximum carboxylation rate; *VPD*, vapour pressure deficit; Ψ_l, leaf water potential; Ψ_{min}, minimum leaf water potential; Ψ_{pd} , pre-dawn leaf water potential.

Introduction

Africa's carbon (C) cycle is one of the least well understood components of the global C cycle (Bombelli et al. 2009; Ciais et al. 2011; Williams et al. 2007). The savannas and woodlands of southern Africa play a major role in the overall C balance of Africa, but are also the most uncertain, due to their large extent, frequent fires, and large inter-annual variability in primary production (Bombelli et al. 2009), driven by variable rainfall and acute soil water stress (Ciais et al. 2009; Weber et al. 2009; Williams et al. 2008a). The most common woodland type in southern Africa is miombo woodland, covering 2.7 million km^2 of southern and central Africa (Campbell 1996; White 1983). Despite the vast extent of miombo woodland, and therefore its importance in biogeochemical cycles of Africa, no studies have measured the fundamental photosynthetic parameters (*sensu* Farquhar et al. (1980)) of these woodlands. Likewise, the magnitude of and controls on seasonal fluctuations in photosynthesis remain poorly known. Expected climate changes for Africa are for increased temperatures and more severe droughts (IPCC 2007), increasing the need for a more detailed understanding of how primary productivity responds to changes in climate and water availability.

Miombo woodlands are characterised by the presence of leguminous trees (family *Fabaceae*, sub-family *Caesalpinioideae*) of the genera *Brachystegia*, *Julbernardia* and/or *Isoberlinia* occurring on nutrient poor soils (Chidumayo 1997; Frost 1996). They are seasonally dry deciduous woodland, largely leafless during the dry season, but developing new leaves 1-2 months before the start of the rains when water availability is low (Chidumayo and Frost 1996; Chidumayo 2001; Fuller 1999). This paradox is common amongst other seasonally dry tropical forests

(Borchert 1994; Elliott et al. 2006; Williams et al. 1997). Photosynthetic rates of miombo tree species have been observed to initially increase with increasing leaf development during leaf flush (Tuohy and Choinski 1990), and once fully developed C assimilation rates scale linearly with increasing leaf nitrogen (N) content (Tuohy et al. 1991). With the onset of the rainy season, substantial increases in photosynthetic rates have been observed (Choinski and Johnson 1993), but the mechanisms contributing to the increased productivity are still unknown.

Photosynthesis and C assimilation in plants is a complex biogeochemical process, determined by several environmental factors and metabolic processes. Plants regulate leaf gas exchange through stomatal control, optimising C gain and minimising water loss, and stomatal control is influenced by several environmental factors including light, temperature, evaporative demands, and plant water status (Flexas and Medrano 2002; Lambers et al. 2008; Lawlor and Cornic 2002; Oren et al. 1999). Photosynthetic capacity (maximum rate of carboxylation and maximum rate of electron transport) co-varies with other leaf traits such as leaf chemical composition, in particular leaf nitrogen content (Field and Mooney 1986), and leaf physical structure (Reich et al. 1997; Wright et al. 2004). Changes to leaf traits can therefore affect photosynthetic capacity. The dynamic properties of plants resulting from interacting leaf traits and the environment determine the ultimate controls on photosynthesis.

The key question of this study was to determine what controls photosynthetic productivity of miombo woodland tree species on a diurnal to seasonal time scale. We assessed the diurnal variations in leaf-level photosynthetic activity, leaf gas exchange, and leaf water relations for key tree species in wet and dry seasons, and

tested how these were linked to seasonal shifts in leaf traits and environmental variables. While we expect photosynthetic capacity to be lower in the dry season, it is yet unclear whether this difference is caused by stomatal limitations to productivity or by leaf trait variations. Our overall hypothesis is:

H1. During the dry season, maximum assimilation rates (highest rate reached during the day) will be less than during the wet season.

Our related hypotheses are:

H2a. This reduction will be driven by reduced stomatal conductance during the dry season due to increased evaporative demand and lower soil water availability. To disprove this hypothesis, we would expect little response of stomata to increasing vapour pressure deficits and decreasing soil water availability, and minor stomatal limitations on assimilation.

H2b. This reduction will be driven by differences in leaf traits, related to photosynthetic capacity. To disprove this hypothesis, we would expect leaf traits to remain constant between seasons.

H3. All species will exhibit similar seasonal patterns of leaf gas exchange and photosynthetic capacities. To disprove this hypothesis, inter-specific differences in stomatal control, leaf trait variations, and maximum assimilation rates will occur between species.

We collected data on leaf traits (maximum carboxylation capacity, maximum rate of electron transport, leaf nitrogen content, leaf mass per area, leaf specific conductance and minimum leaf water potential) and took ambient gas exchange and leaf water potential measurements across dry and wet seasons (2009 - 2010) on two

key miombo canopy tree species, *Brachystegia spiciformis* and *Julbernardia globiflora*, and one commonly co-occurring understory tree species, *Diplorhynchus condylocarpon*, in miombo woodlands of central Mozambique (Williams et al. 2008b). The sparse existing leaf trait and gas exchange data in dry woodlands, and in particular African dry woodlands, makes our measurements an important addition to global datasets (e.g. TRY Plant Trait Database, http://www.try-db.org/TryWeb/Home.php).

Methods

Study site

The study site was based in the Nhambita community area of Gorongosa District, adjacent to the south-west boundary of Gorongosa National Park in the Sofala Province, central Mozambique (18.979^{o}S, 34.176^{o}E). The Nhambita community area covers approximately 348 km^2 and is predominantly classified as miombo woodland vegetation (Williams et al. 2008b), with a continuous layer of co-occurring C_4 grasses. Miombo woodlands occur on well drained coarse textured sandy soils on elevated ground (Woollen et al. 2012), and invest 1/3 of total biomass to below ground roots (Ryan et al. 2011). Most of the fine roots are thought to occur in the top 1-2 m of soil, with deep tap roots extending several meters down (Timberlake and Calvert 1993). The soils found in the Nhambita area are mostly sandy fersiallitic soils derived from metamorphic migmatitic gneisses and granite (Tinley 1977). The Nhambita area receives 850±269 mm mean annual precipitation (± standard deviation) with strong seasonality, where 82 % of precipitation falls in the wet season between November and March (Ryan 2009). Daily mean

temperatures range from 30º C in December to 20ºC in July. Fire is a frequent occurrence, causing most of the vegetation to be burned every 1-3 years during the dry season between June to October (Ryan and Williams 2011).

Leaf gas exchange measurements

Leaf gas exchange and meteorological parameters were measured in two seasons, one at the end of the dry season (October-November 2009), and the second at the end of the following wet season (April-May 2010). Measurements were taken on three C_3 woody plant species, *Brachystegia spiciformis* (BS), *Julbernardia globiflora* (JG) and *Diplorhynchus condylocarpon* (DC), which were chosen due to their characterisation of miombo woodland (BS and JG) canopy species, and under-story dominance (DC) at the study site (Williams et al. 2008b). Each plant used in measurements was identified to species in the field by several local botanists. All leaf gas exchange measurements were conducted using an infra-red-gas-analyser (IRGA) portable photosynthesis system (model LI-6400, LI-COR Inc.), which was zeroed every day before measurements using CO_2 and H_2O free air.

Leaf gas exchange measurements were taken at two sites within the study area; site one was within the national park boundary, and site two 2 km away outside the park boundary. Both sites where characterised as miombo woodland, due to the presence of key miombo tree species, with soils classed as loamy sand (approx. 76% sand, 20 % silt, 4% clay) (Ryan, pers. comm.) at an elevation of 100-120 meters above-sea-level. Both sites had a similar floristic structure with similar tree species composition and an open canopy, but site two had no *B. spiciformis* present. The leaf area index, as measured using hemispherical photos and analysis software (Gap Light Analyzer, Version 2.0, Frazer and Canham (1999)), was between 0.3-0.6 at the

end of the dry season, when new leaves emerge, increasing to 1.5-2.0 at the end of the wet season.

Diurnal leaf gas exchange and leaf water potential measurements

To characterise diurnal patterns of leaf gas exchange, ambient measurements were taken on several individual trees at two hour intervals from pre-dawn to sun-down (06:00 - 18:00, Central Africa Time) in each season, taking measurements on several leaves (n = 4 – 8) at each time step on each tree to allow averaging (Table 1). A total of 14 diurnal measurements (6 in the dry season and 8 in the wet season) were taken over two seasons and all species. Due to technical constraints and damage by fire, it was not always possible to conduct diurnal measurements on the same trees between seasons. Selection of trees for diurnal measurements was limited to those that were accessible from the ground, as no crane or tower was available to access the canopy. This meant that all the trees used in diurnal measurements (apart from *D. condylocarpon*, which has a smaller stature) were saplings, but due to the open nature of the woodland, all studied leaves were sunlit for some part of the day. Diurnal measurements were taken using the standard ambient light clear top leaf chamber (LI-COR, LI-6400), keeping temperature and humidity as close to ambient conditions as possible, but with CO_2 concentrations at a constant 400 μmol CO_2 mol^{-1}. Some errors in measurements occurred in the pre-dawn hours (06:00), caused by dew forming on the leaves, increasing water vapour in the chamber and causing erroneous stomatal conductance and transpiration measures. Clear outliers at this time step were therefore excluded. Leaf water potentials (Ψ_l) were measured on two excised leaves (n = 2) at each time step on each tree, as above, using a pressure bomb system (model SKPM 1400 Plant moisture system, Skye Instruments Ltd.). Soil

water potentials were estimated to be equal to pre-dawn (6:00) leaf water potentials (Ψ_{pd}).

Table 1: Details of individual trees measured for diurnal leaf gas exchange and leaf water potentials during the dry and wet season on miombo tree species (BS: *Brachystegia spiciformis*, JG: *Julbernardia globiflora*, and DC: *Diplorhynchus condylocarpon*). On each tree, several leaves (n = 4 – 8) were used in leaf gas exchange measurements.

Date of measurement		Tree ID	Site	Stem diameter	Tree height
Dry	*Wet*			(cm)	(m)
3/11/2009	27/04/2010	BS1*	1	5.0	4
9/11/2009	04/05/2010	BS2	1	5.0	5
3/11/2009	27/04/2010	JG1*	1	2.0	3
5/11/2009	29/04/2010	JG2	2	2.5	2
9/11/2009		JG3	1	2.5	2
	04/05/2010	JG4	1	2.0	3
5/11/2009	29/04/2010	DC1*	2	5.0	3
	27/04/2010	DC2	1	8.0	6
	04/05/2010	DC3	1	15.0	8

* indicates those trees used in Figure 2

To characterise changes to environmental variables between seasons, maximum incident *PAR* (PAR_{max}), *VPD* of air (VPD_{max}) and temperature of air (T_{max}) were assessed for each diurnal measurement in each season (Table 1). Maximum assimilation rates (A_{max}), transpiration rates (E_{max}), and stomatal conductance ($g_{s\ max}$) in each season were assessed as the maximum rates reached during the course of the day (i.e. at the same time step) of several leaves (n = 4 - 8) on several individual trees of each species in each season (Table 1). Leaf temperatures at the time of A_{max} ($T_{l\ Amax}$) were also determined. Leaf temperatures were measured with a thermocouple inside the leaf chamber during diurnal measurements. The mean daily ratios of internal to ambient CO_2 concentrations (C_i/C_a) for each diurnal measurement were also determined, to assess if stomatal limitations to internal C_i values occurred.

Mean values and standard errors of the mean were calculated for each maximum rate of leaf gas exchange, $T_{l\,Amax}$ and C_i/C_a using data split by season and by species. To test for significant differences between mean values between seasons, a two sample *t*-test was used with a 95% confidence interval ($P < 0.05$). All analyses were conducted using Matlab routines (MathWorks 2012).

CO_2 response curves

CO_2 response curves (A/C_i curves) were made on a combined total of 26 leaves (BS = 7, JG = 12, DC = 7 leaves) on 14 individual trees (BS = 4, JG = 5, DC = 5 trees) in the dry season, and 57 leaves (BS = 20, JG = 19, DC = 18 leaves) on 15 individual trees (5 individual trees for each species) in the wet season. Where possible, measurements were taken on the same individual trees in both the wet and dry seasons. A/C_i curve measurements were taken using the IRGA and an artificial light source leaf chamber (6400-02B LED Light Source, LI-COR Inc.), following the method outlined in Long and Bernacchi (2003), where assimilation rates were measured over a range of leaf chamber CO_2 concentrations, varying from ambient concentrations down to 100 μmol CO_2 mol^{-1} and up to a maximum of 2000 μmol CO_2 mol^{-1}. Block temperature and humidity were kept constant at ambient conditions throughout the measurement, and irradiance at a constant saturating level of 2000 μmol m^{-1} s^{-1}.

During A/C_i measurements it was necessary to eliminate other limiting factors, such as water and stomatal conductance, in order to isolate and measure the response of A to changes in C_i only. Therefore, during the dry season A/C_i curves were measured on excised branches, taken from the sunlit canopy of mature and sapling trees, placed in a bucket of water and then re-cut under water to avoid air

entering the xylem. During the wet season A/C_i measurements were taken on intact branches, as excising branches from trees meant stomatal conductance decreased substantially, limiting internal C_i to low levels (see supplementary data for issues with comparing intact and excised branch measurements). If stomatal conductance went below 0.1 mol H_2O m^{-1} s^{-1} during a measurement the measurement was discarded due to the observed stomatal restrictions on internal C_i, creating erroneous A/C_i curves. This was a serious problem during the dry season, resulting in more than half of all measurements to be discarded.

Leaf traits

The CO_2 response curves were used to estimate maximum rate of carboxylation (V_{cmax}), and maximum electron transport rate (J_{max}) of photosynthesis by applying the Farquhar et al. (1980) biochemical model of photosynthesis to the measured response (Long and Bernacchi 2003; Sharkey et al. 2007; Wullschleger 1993). Several studies have pointed out the effects of diffusion leaks of IRGA leaf chamber measurements on estimates of photosynthetic parameters (Flexas et al. 2007; Rodeghiero et al. 2007). Therefore, diffusion leaks through the leaf chamber gasket were accounted for by using diffusion equations outlined in the LI-6400 manual (LI-COR, Using the LI-6400, Version 6, Ch. 4, pp:44-48), and diffusion leaks were temperature corrected using equations outlined in Bruhn et al. (2002). Measured assimilation rates in each CO_2 response curve were corrected by applying the calculated leak rates at each CO_2 concentration step, and corrected values were used in subsequent analyses of photosynthetic parameter estimates.

We use a maximum likelihood analysis to fit curves to the A/C_i data, as employed in the leaf biochemical sub-model of the Soil-Plant-Atmosphere model

(Williams et al. 1996), to find the best estimation of V_{cmax} and J_{max}. No measure of mesophyll conductance was taken; we therefore assumed an infinite internal conductance term. Temperature corrections for estimated photosynthetic parameters at 25 ^{o}C were conducted using the Arrhenius equation, using measured leaf temperatures.

To characterise leaf structural traits, leaf-mass-per-area (*LMA*) was measured using dry weights of leaves divided by the fresh leaf area in both seasons (g m^{-2}). To determine fresh leaf area, several leaves with petioles removed were taken from each individual tree used in leaf gas exchange measurements and placed between two Perspex panes to flatten them. A digital image was taken of the flattened leaves, and each image was analysed for estimation of leaf area (m^2) using ImageJ software (Abramoff et al. 2004; Rasband 1997-2011). The leaves were then dried at 70 ^{o}C to constant weight, and the collective dry weight (g) determined for all the leaves used in each image using a high precision balance. This method was repeated four to six times for each individual tree to obtain a mean *LMA* (g m^{-2}) in each season and for each tree (n = 14 trees in the dry, n = 15 trees in the wet season) used in measurements.

To characterise leaf chemical traits, leaf N content was determined for each leaf used in A/C_i curves in both seasons (n = 27 in the dry, n = 57 leaves in the wet season). Each leaf was dried at 60 ^{o}C to constant weight, and ground to a fine powder using a ball-mill. A 4 mg sub-sample was analysed in a Carbo-Erba/400 automated CN analyser to give % N measurements for each leaf (i.e. leaf N content on a mass basis). Leaf N content on an area basis (g m^{-2}) was estimated as follows,

$$N_a = L_m N_m \qquad \text{(Eq. 1)}$$

where the leaf N content on an area basis (N_a) was a function of the mean *LMA* (L_m), and the measured N content (N_m, %) on a mass basis.

Leaf specific conductance (*LSC*), a measure of the hydraulic capacity of the tree to supply the leaves with water, can be described by Darcy's Law [as described in Hubbard et al. (1999)]:

$$L_{sc} = \frac{E}{\Psi_s - \Psi_l} \quad \text{(Eq. 2)}$$

where E is flux of liquid water per unit leaf area in the xylem tissue, and Ψ_s and Ψ_l are soil and leaf water potentials, respectively. We used diurnal maximum rates of transpiration (E_{max}) for several leaves on several individual trees of each species and the difference in pre-dawn (i.e. soil water potential) and minimum leaf water potentials to calculate *LSC* in each species and season.

Minimum daily leaf water potential (Ψ_{min}) reflects the maximum water deficits that leaves must tolerate to maintain physiological activity, and depends on the balance between soil water availability, rate of leaf water loss, and the capacity of the plant to supply water to the leaves (Bhaskar and Ackerly 2006). Minimum daily leaf water potentials were determined for every diurnal measurement from pressure bomb measurements for several leaves, on several individual trees, for each species and season.

Summary statistics were calculated for each leaf trait parameter using data split by season and by species. To test for significant differences between mean leaf trait values between seasons, a two sample *t*-test was used with a 99% confidence interval ($P < 0.01$). All analyses were conducted using Matlab routines (MathWorks 2012).

Results

Seasonal patterns in environmental variables

The seasonal variations in evaporative demand and water availability are reflected in the differences in vapour pressure deficits of the air and soil water potentials between seasons. Maximum daily air temperatures were on average 7 ^{o}C higher in the dry season as compared to the wet (Fig. 1 A), and maximum daily vapour pressure deficit (*VPD*) of air was on average three times higher in the dry season as compared to the wet season (Fig. 1 B). Maximum incident photosynthetic active radiation (*PAR*) was 66 % higher in the dry season (Fig. 1 C). *VPD* of air (Fig. 2 M-O), incident *PAR* (Fig. 2 P-R) and air temperature (data not shown) varied throughout the day due to variable sun angle, cloud cover and over story canopy shading. Soil water potentials, as estimated from pre-dawn leaf water potentials, were significantly (two sample *t*-test, $P < 0.05$) lower by 0.9-1.1 MPa during the dry season, although *D. condylocarpon* showed no significant change between seasons (Fig. 3 A).

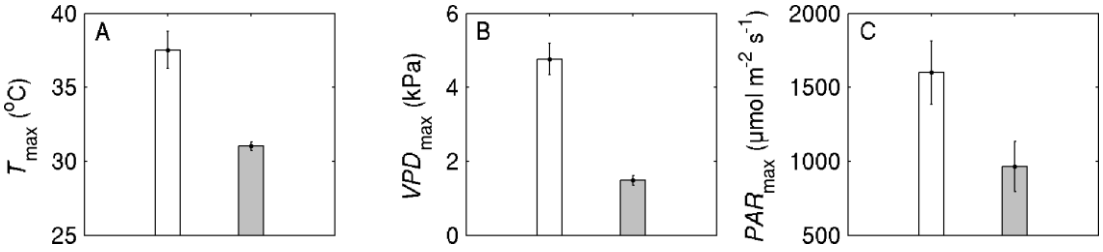

Fig 1: Mean (± standard error) maximum A) air temperature, B) vapour pressure deficit of air, C) incident photosynthetic active radiation measured in dry (white bars) and wet (grey bars) seasons. All means are significantly different between seasons (two-sample *t*-test, $P < 0.05$).

Diurnal patterns of leaf gas exchange

Dry Season

On a diurnal time scale, leaf gas exchange had similar patterns in all three species during the dry season. Assimilation rates (Fig. 2 A-C), stomatal conductance (Fig. 2 D-F) and transpiration rates (Fig. 2 G-I) peaked in the morning hours, when *VPD* was at its lowest (Fig. 2 M-O). Following the morning peak, assimilation rates, stomatal conductance and transpiration rates decreased gradually over the course of the day, as *VPD* increased. Assimilation rates in *B. spiciformis* and *J. globiflora* did not increase in the afternoon, despite a peak in *PAR* (Fig. 2 P-Q), as stomatal conductance was very low in the afternoon. Transpiration rates and stomatal conductance were twice as high in *D. condylocarpon* as those found in *B. spiciformis* and *J. globiflora* during the dry season.

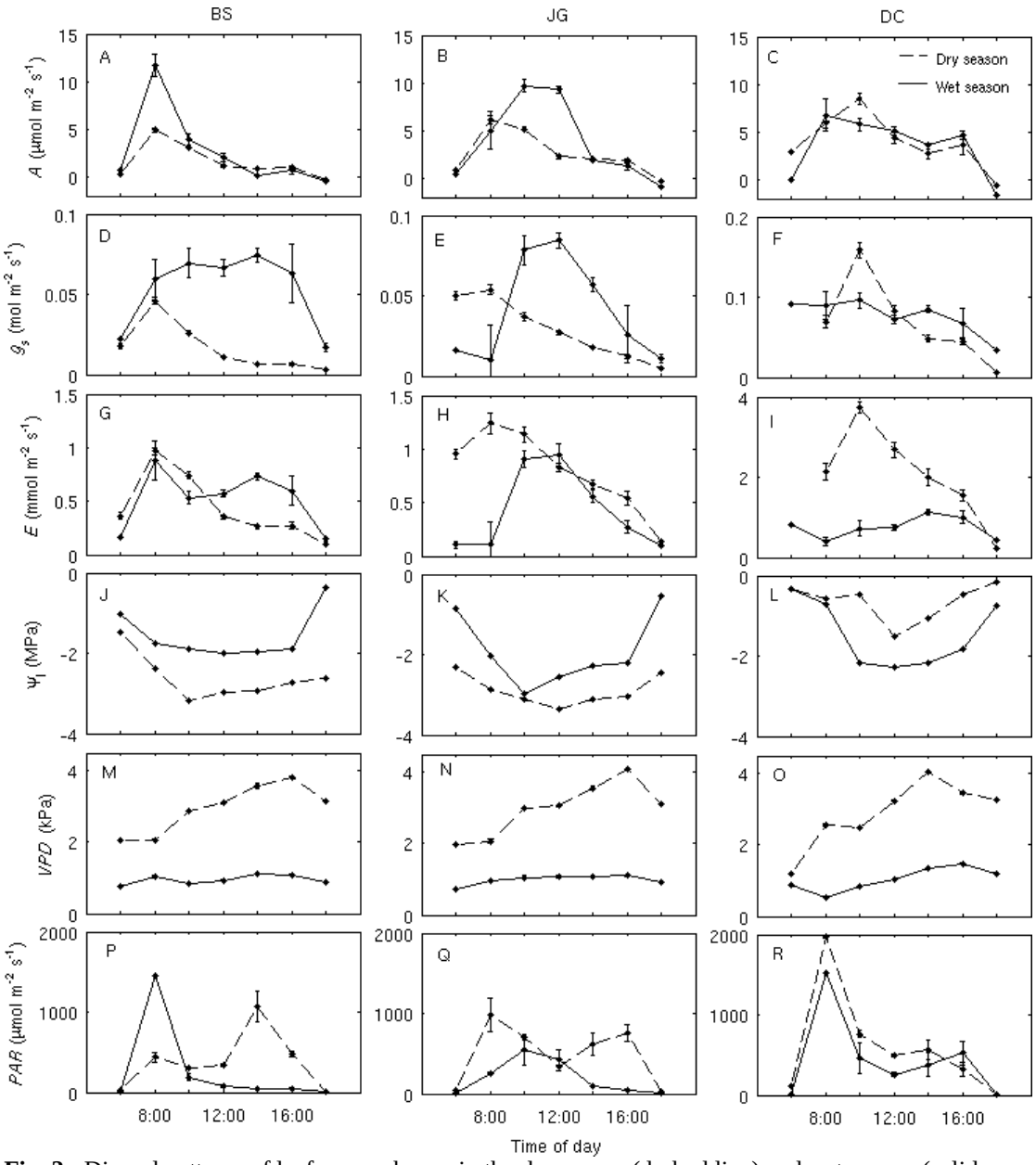

Fig. 2: Diurnal patterns of leaf gas exchange in the dry season (dashed line) and wet season (solid line) for one individual tree of *Brachystegia spiciformis* (left panel), *Julbernardia globiflora* (middle panel), and *Diplorhynchus condylocarpon* (right panel) (see Table 1). A-C) net CO_2 assimilation rate, D-F) stomatal conductance, G-I) transpiration rates, J-L) leaf water potential, M-O) vapour pressure deficit of air, and P-R) incident photosynthetically active radiation are shown for each species over time. Each point is the mean of 4-8 leaf measurements at each time step. Errors are standard errors of the mean. No error estimates are shown for Ψ_l as only two measurements were taken at each time step. No measures of g_s or E are shown for DC at 6:00, as dew on the leaves caused erroneous measurements at this time step.

Wet season

Diurnal leaf gas exchange varied among species during the wet season. *B. spiciformis* and *J. globiflora* stomatal conductance (Fig. 2 D-E) and transpiration

rates (Fig. 2 G-H) show a hump-shaped pattern. *B. spiciformis* assimilation rates peaked in the morning, 40 % greater than dry season rates (Fig. 2 A). Rates decreased rapidly in the afternoon, despite continued high stomatal conductance, due to decreased *PAR* levels (Fig. 2 P). *J. globiflora* assimilation rates showed similar patterns to stomatal conductance during the wet season (Fig. 2 B), and assimilation rates increased to 57 % greater than dry season rates. Assimilation rates (Fig. 2 C) and stomatal conductance (Fig. 2 F) were not markedly different between seasons in *D. condylocarpon*, but transpiration rates were 70 % lower in the wet season (Fig. 2 I), linked to lower *VPD* (Fig. 2 O). *PAR* showed similar patterns and levels between seasons for *D. condylocarpon* (Fig. 2 R).

Diurnal and seasonal patterns in leaf water potentials

Diurnal leaf water potentials (Ψ_l) for all species and seasons show a U-shaped pattern (Fig. 2 J-L), decreasing from pre-dawn values to a minimum during the mid-day and recovering again in the late afternoon. During the dry season *B. spiciformis* reached Ψ_{min} which was significantly (*t*-test, $P < 0.05$) lower than in the wet season, by 1.1 MPa (Fig. 3 B). *D. condylocarpon*, however, had the opposite behaviour where dry season Ψ_{min} was significantly (*t*-test, $P < 0.05$) higher, by 0.7 MPa, as compared to the wet season (Fig. 3 B). Large fluctuations in Ψ_l occurred throughout the day in both seasons and in all species. The difference between Ψ_{pd} and Ψ_{min} ranged from 1.2-1.4 MPa in the dry season to 1.1-2.1 MPa in the wet, and the change in Ψ_l was not significantly different (two-sample *t*-test, $P > 0.05$) between seasons, when species data was combined.

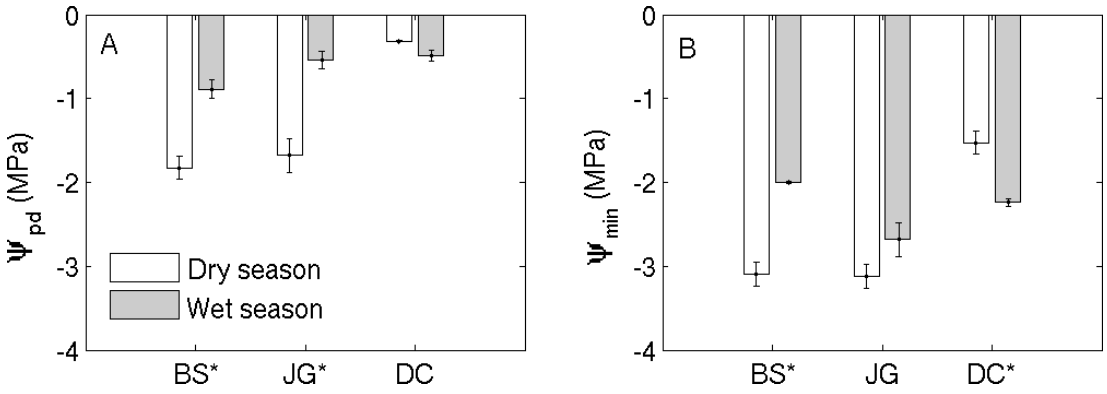

Fig. 3: Mean (± standard error) of A) pre-dawn leaf water potential, and B) minimum leaf water potential for trees of species *Brachystegia spiciformis* (BS), *Julbernardia globiflora* (JG) and *Diplorhynchus condylocarpon* (DC) in the dry and the wet season. Each mean is based on several leaf measurements (n = 2-3) on several individual trees of each species in each season (see Table 1). * indicates when means were significantly (two sample t-test, $P < 0.05$) different between seasons.

Stomatal regulation of leaf gas exchange

Stomatal conductance in *B. spiciformis* and *J. globiflora* was closely related to the *VPD* of air (Fig. 4 A & C), with stomatal conductance decreasing as *VPD* increased. Despite the down-regulation of stomatal conductance with increased *VPD*, Ψ_l also decreased and was constrained to a lower limit by *VPD* (Fig. 4 B & D). For *D. condylocarpon*, however, stomatal conductance shows a less sensitive response to increasing *VPD* (Fig. 4 E) and was able to maintain Ψ_l even at high *VPD* during the dry season (Fig. 4 F).

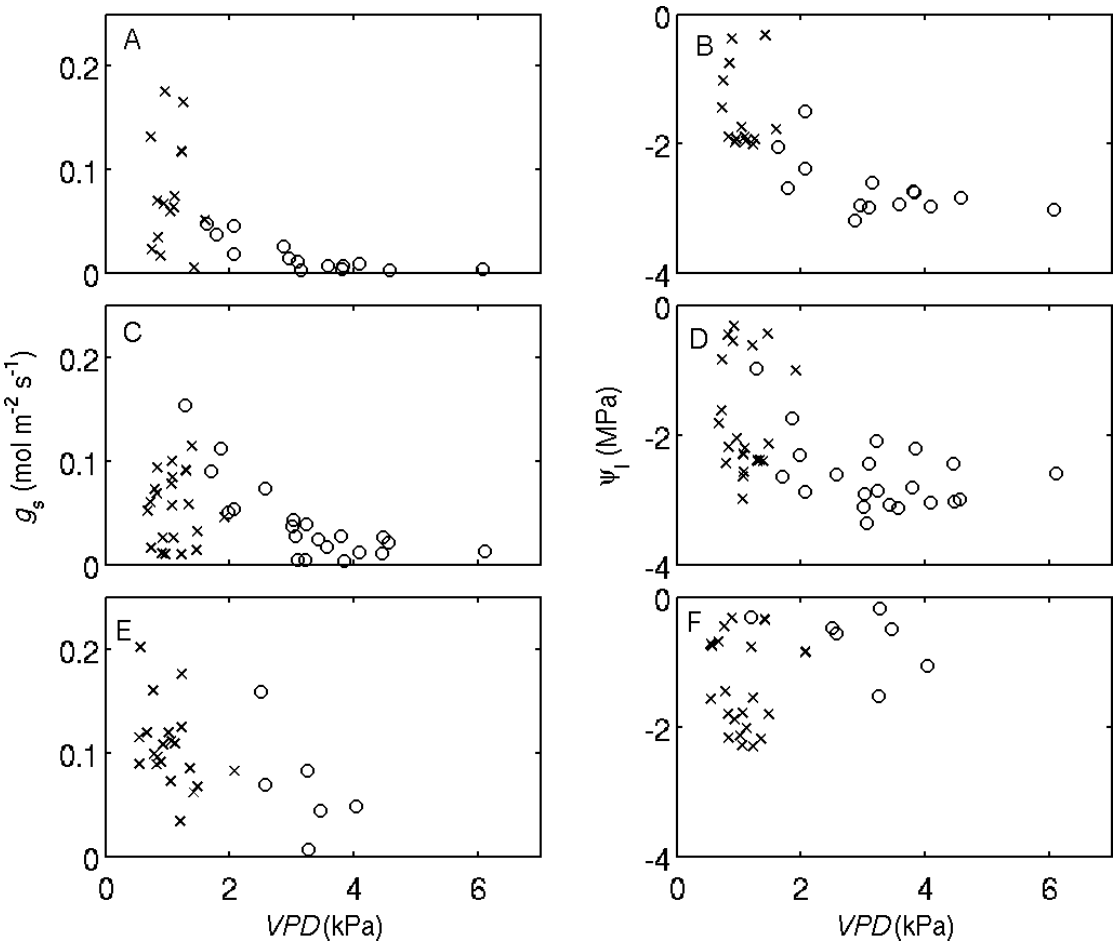

Fig. 4: Stomatal conductance (g_s) (left panel) and leaf water potential (Ψ_l) (right panel) response to vapour pressure deficit of the air (*VPD*) in the dry (o) and the wet (x) season for all individuals of species *Brachystegia spiciformis* (A-B), *Julbernardia globiflora* (C-D), and *Diplorhynchus condylocarpon* (E-F) (see Table 1). Each point in the left panel is the mean of 4-8 leaf measurements, and the right on 2-3 leaf measurements, on one individual tree, at one time step over the course of a day.

The relationship between assimilation rates and stomatal conductance was similar in both seasons for all species (Fig. 5, left panel). Thus, rates of C uptake were consistent for each species at a given stomatal conductance, whether during dry or wet season. Contrastingly, transpiration reached higher rates during the dry season at any given stomatal conductance in all species (Fig. 5, right panel), due to higher *VPD*. The maximum stomatal conductance in *B. spiciformis* was smaller during the dry season, leading to restriction on the maximum values of assimilation and transpiration rates (Fig. 5 A-B). Stomatal conductance and assimilation rates had

similar maxima in both seasons in *J. globiflora* and *D. condylocarpon* (Fig. 5 C & E).

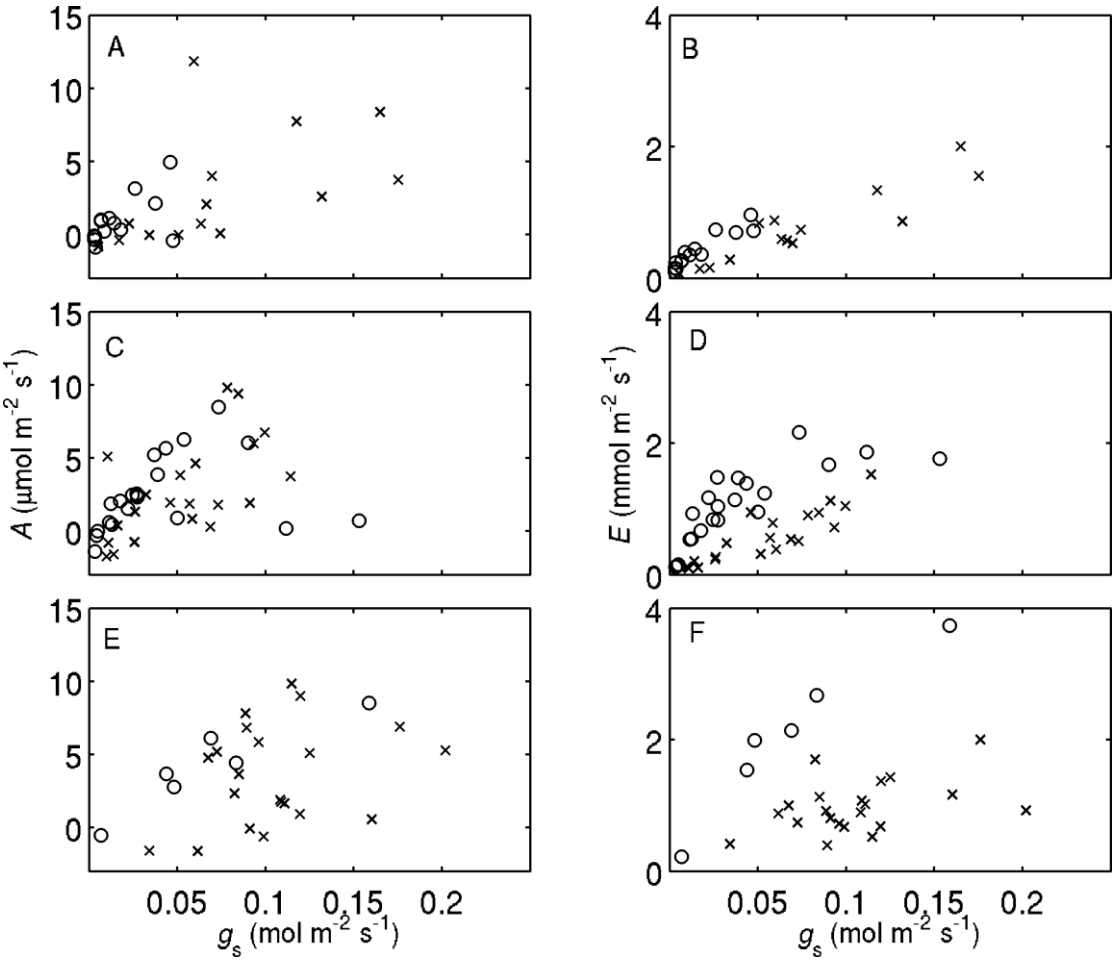

Fig. 5: Response of diurnal assimilation rates (left panel) and transpiration rates (right panel) to stomatal conductance (g_s) during the dry (o) and the wet (x) season for all individuals of species A-B) *Brachystegia spiciformis*, C-D) *Julbernardia globiflora*, and E-F) *Diplorhynchus condylocarpon* (see Table 1). Each point is the mean of 4-8 leaf measurements, on one individual tree, at one time step over the course of a day.

Seasonal changes to maximum leaf gas exchange rates, leaf temperature at A_{max} and internal CO_2

The diurnal maximum assimilation rates for *B. spiciformis* were significantly different between seasons (two sample *t*-test, $P < 0.05$), with a 185 % average increase from the dry to the wet season (Fig. 6 A). *J. globiflora* and *D.*

condylocarpon showed no significant (*t*-test, $P > 0.05$) differences in maximum diurnal assimilation rates between seasons (Fig. 6 A). Higher assimilation rates during the wet season in *B. spiciformis* were accompanied by significantly ($P < 0.05$) higher transpiration rates (Fig. 6 B) and maximum stomatal conductance (Fig. 6 C) during the wet season, which increased by 168 % from the dry to the wet season. *J. globiflora* and *D. condylocarpon*, however, had significantly ($P < 0.05$) higher maximum transpiration rates in the dry season (Fig. 6 B), which were on average 32 and 60 % greater, respectively, than in the wet season. *J. globiflora* and *D. condylocarpon* had similar maximum stomatal conductance values in both seasons (Fig. 6 C). Leaf temperatures at the time of A_{max} were significantly ($P < 0.05$) lower in the dry season for *B. spiciformis* by ~2 ^{o}C, but were significantly higher in *J. globiflora* and *D. condyclocarpon* by 2-3 ^{o}C in the dry season (Fig. 6 D). The mean daily internal to ambient CO_2 ratios were above 0.7 for all species and seasons (Fig. 6 E). These ratios did not change significantly between seasons in *B. spiciformis* or *D. condylocarpon*, but were significantly ($P < 0.05$) lower in *J. globiflora* by 15 % in the dry season (for diurnal patterns of C_i/C_a see supplementary material Fig. S2).

Comparing among species, during the dry season maximum assimilation rates in *B. spiciformis* were 48-58 % lower than rates in the other two species, but then increased to 12-33 % higher during the wet season (Fig. 6 A). During the dry season maximum transpiration rates were 117 and 343 % higher in *D. condylocarpon*, as compared to *J. globiflora* and *B. spiciformis*, respectively (Fig. 6 B).

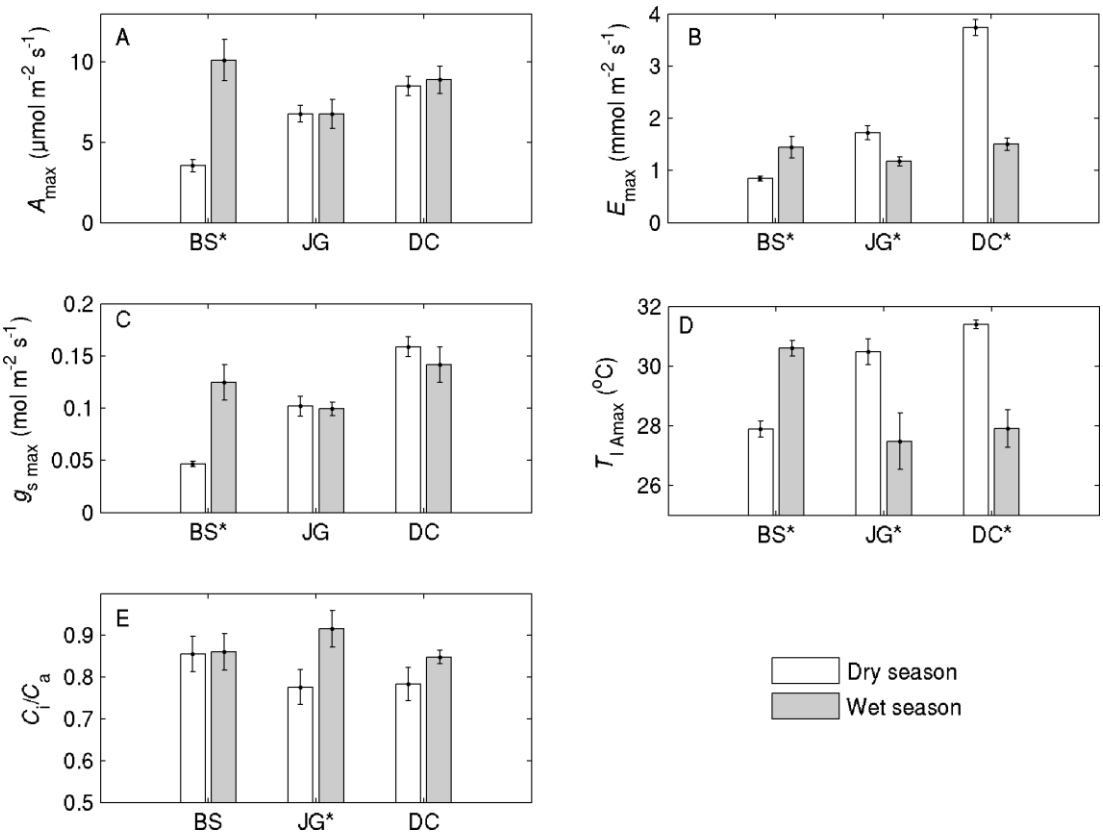

Fig. 6: Mean values (± standard error) of diurnal maximum A) assimilation rates, B) transpiration rates, C) stomatal conductance, D) leaf temperature at the time of A_{max}, and E) mean daily internal to ambient CO_2 concentration ratios for trees of species *Brachystegia spiciformis* (BS), *Julbernardia globiflora* (JG) and *Diplorhynchus condylocarpon* (DC) in the dry and the wet seasons. Each mean is from several leaf measurements (n = 4-8) at one time step (i.e. time of day when maximum values were reached), over the course of the day, on several trees for each species in each season (Table 1). * indicates when mean values were significantly different (two sample t-test, $P < 0.05$) between seasons.

Seasonal leaf trait variations

B. spiciformis had significantly (two sample t-tests, P <0.01) different leaf traits between seasons with 30-55 % lower J_{max} rates (Fig. 7 A), V_{cmax} rates (Fig. 7 B), leaf N content (Fig. 7 C), and *LSC* (Fig. 7 E) in the dry season. *J. globiflora* had significantly ($P < 0.01$) lower J_{max} rates by 27 % (Fig. 7 A) and significantly ($P <$ 0.01) higher *LSC* by 118 % (Fig. 7 E) in the dry season, consistent with higher transpiration rates (Fig. 6 B), but all other leaf traits did not change between seasons. The only leaf trait to change significantly ($P < 0.01$) between seasons for *D.*

condylocarpon was *LSC*, where dry season *LSC* was 260 % above the wet season mean value, consistent with very high transpiration rates in the dry season (Fig. 6 B). There was no significant change ($P > 0.01$) in *LMA* between seasons for *J. globiflora* or *D. condylocarpon* (Fig. 7 D), but *LMA* was significantly different between seasons in *B. spiciformis* at the 95% confidence level (*t*-test, $P < 0.05$).

Comparing between species, *B. spiciformis* had 35-38 % lower J_{max} rates and 46-52 % lower V_{cmax} rates as compared to the other two species during the dry season. *D. condylocarpon* had 34-35 % lower J_{max} rates, 31-35 % lower V_{cmax} rates, and 31-40 % lower leaf N content as compared to the other two species during the wet season. *LSC* was 159 and 363 % higher in *D. condylocarpon* as compared to *J. globiflora* and *B. spiciformis*, respectively, during the dry season (Fig. 7 E).

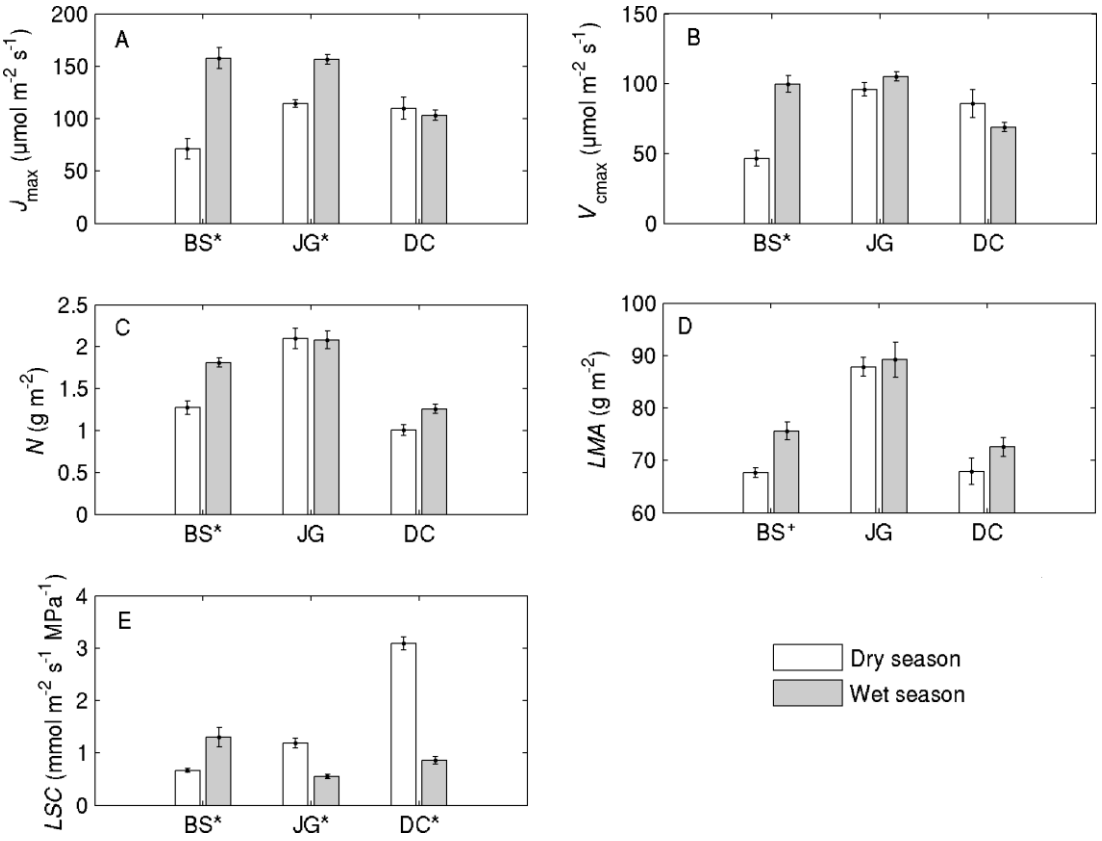

Fig 7: Estimates of mean leaf traits (± standard error) for species of *B. spiciformis* (BS), *J. globiflora* (JG), and *D. condylocarpon* (DC) in the dry and the wet season. Mean leaf trait estimates are A) maximum electron transport rate, B) maximum carboxylation rate, C) leaf nitrogen content, D) leaf mass per area, and E) leaf specific conductance. J_{max} and V_{cmax} are corrected to 25 ^{o}C. * indicates when means are significantly different (two sample *t*-test, $P < 0.01$) between seasons at the 99 % confidence interval, and $^{+}$ at the 95 % confidence interval ($P < 0.05$). See supplementary material Table S1 for values and additional leaf traits.

Discussion

The objectives of this study were to test some key hypotheses related to seasonal limitations and changes to photosynthetic productivity of miombo woodland tree species on a diurnal to seasonal time scale, by assessing the response of leaf gas exchange and leaf water relations to seasonal drought, and determining leaf trait variations between seasons. Conversely to our expectations, we found that only one species, *B. spiciformis*, had lower maximum assimilation rates in the dry season. *J. globiflora* and *D. condylocarpon* had similar assimilation rates between seasons.

This result was due to inter-specific differences in stomatal regulation of leaf gas exchange and leaf traits during the dry season.

Stomatal limitations to leaf gas exchange

We hypothesised that reduced assimilation rates in the dry season would be driven by reduced stomatal conductance due to increased evaporative demand and lower soil water availability in the dry season. To disprove this hypothesis, we would expect little response of stomata to increasing evaporative demands and decreasing soil water availability, and no clear stomatal limitations on assimilation.

Stomatal down-regulation of leaf gas exchange were apparent in all three tree species during the afternoon in the dry season (Fig. 2 A-I), in response to increasing evaporative demands (Fig. 2 M-O). During the wet season, assimilation rates were more closely related to *PAR* (Fig. 2 P-R). However, inter-specific stomatal sensitivity to vapour pressure deficits (Fig. 4) resulted in lower maximum stomatal conductance in *B. spiciformis* (Fig. 5 A-B), restricting transpiration rates in the dry season (Fig. 6 B). Maximum assimilation rates were also lower in the dry season in *B. spiciformis* (Fig. 6 A), but this was not related to stomatal limitations on leaf gas exchange, as internal to ambient CO_2 concentration ratios remained constant between seasons (Fig. 6 E). In contrast, stomatal conductance and assimilation rates were not different between seasons in *J. globiflora* and *D. condylocarpon* (Fig. 5 C & E, Fig. 6 A & C), and transpiration rates were higher during the dry season (Fig. 5 D & F, Fig. 6 B). A large degree of inter-specific variation in sensitivity of stomatal conductance to vapour pressure deficit exists (Oren et al. 1999), and co-occurring species can exhibit a range of stomatal control linked to local hydrological conditions and drought tolerance (Bonal and Guehl 2001).

Variations between measured pre-dawn leaf water potentials (Fig. 3 A), minimum daily leaf water potentials (Fig. 3 B), and rates of transpiration (Fig. 6 B) between species suggests varied access to deep soil water occurred during the dry season. It has previously been assumed that miombo trees can access deep soil water during the dry season through their extensive root systems (Timberlake and Calvert 1993) in order to support leaf flushing (Choinski and Johnson 1993; Frost 1996), and the ability of all the trees to transpire during the dry season (Fig. 2 G-I) and maintain leaf water potentials above a mid-day minimum (Fig. 2 J-L) supports this hypothesis. *D. condylocarpon* had high stomatal conductance (Fig. 6 C) and very high transpiration rates (Fig. 6 B) during the dry season, and maintained leaf water potentials even at high evaporative demands (Fig. 4 F), linked to maintained access to soil water between seasons (Fig. 3 A). *J. globiflora* had higher maximal stomatal conductance (Fig. 6 C) and transpiration rates (Fig. 6 B) as compared to *B. spiciformis* in the dry season, despite having similar low pre-dawn leaf water potentials (Fig. 3 A), suggesting similar soil water access. Therefore, differing access to soil water does not fully explain the inter-specific differences we observed in stomatal control, and other limitations could be occurring in *B. spiciformis*.

Photosynthesis is strongly affected by temperature, arising from the intrinsic temperature dependence of enzyme reactions and the photosynthetic apparatus, and differences in the ability to maintain functional integrity at high temperatures and potential for acclimation is variable between plant species (Berry and Bjorkman 1980). Leaf temperatures at the time of maximum assimilation reached values above 30 ^{o}C in *J. globiflora* and *D. condylocarpon* in the dry season, whereas leaf temperatures at the time of A_{max} was several degrees lower in *B. spiciformis* (Fig. 6

D). The maintained assimilation rates between seasons, despite the higher leaf temperatures during the dry seasons, indicate a greater ability of *J. globiflora* and *D. condylocarpon* to manage high temperatures without the loss of C uptake during the dry season. The lower leaf temperature in *B. spiciformis* at the time of A_{max} suggests a lower tolerance to high temperatures, decreasing photosynthetic potentials.

Despite the low stomatal conductance in *B. spiciformis*, and thus restricted CO_2 diffusion, the internal CO_2 concentration was not decreased to lower values in the dry season (Fig. 6 E). This suggests that changes to internal photosynthetic processes may be determining C_i values, where lower demands for C_i in the dry season in *B. spiciformis* maintained C_i /C_a ratios between seasons (Lambers et al. 2008). Diurnal patterns of C_i were linked to diurnal variations in the supply and demand of CO_2 (see supplementary material Fig. S2). The maintained C_i /C_a between seasons suggest that photosynthesis was not limited by stomatal limitations to CO_2 (i.e. supply) and other limitations to photosynthesis were occurring in *B. spiciformis* in the dry season decreasing the demand for C_i.

Seasonal leaf trait variations

We hypothesised that reduced assimilation rates in the dry season would be driven by differences in leaf traits, related to photosynthetic capacity. To disprove this hypothesis, we would expect leaf traits to remain constant between seasons. Inter-specific difference in seasonal leaf trait variations occurred, and differences in photosynthetic capacity between species can be related to differences in leaf traits. The lower photosynthetic metabolic processes and leaf N content of *B. spiciformis* (Fig. 7 A-C) are consistent with the lower maximal assimilation rates of *B. spiciformis* during the dry season (Fig. 6 A); photosynthetic capacity is strongly

linked to leaf N content (Field and Mooney 1986), and assimilation rates scale linearly with increasing leaf N content in miombo trees (Tuohy et al. 1991). The maintained assimilation rates between seasons in *J. globiflora* and *D. condylocarpon* is consistent with little to no seasonal variations in leaf traits. *J. globiflora* exhibited lower electron transport rates during the dry season (Fig. 7 A), but with no apparent limitations to maximum assimilation rates of ambient measurements (Fig. 6 A), where other limitations are likely to be more important.

Newly flushed leaves of *B. spiciformis* typically exhibit lower leaf nitrogen content, stomatal conductance, assimilation and transpiration rates (Choinski and Johnson 1993), and in conjunction with lower LMA (Fig. 7 D), suggests that the leaves of *B. spiciformis* were not fully developed at the time of measurement during the dry season (see supplementary material Fig. S3 & 4), accounting for seasonal changes to leaf traits. *J. globiflora* and *D. condylocarpon* showed little to no changes in leaf traits between seasons, suggesting the leaves were fully developed at the time of measurement in the dry season. We therefore suggest that inter-specific differences in assimilation rates were due to differing stages of leaf development between the three species at the time of measurement in the dry season.

Differing leaf specific conductivity between species and seasons (Fig. 7 E) suggests hydraulic conductivity could be an important mechanism determining the inter-specific responses of stomatal sensitivity to *VPD* (Fig. 4), leaf water relations (Fig. 3), and photosynthetic capacities (Fig. 6 A) to seasonal drought (Hubbard et al. 1999; Sperry et al. 2002). A recent study in miombo woodlands has shown that differing cavitation resistance between miombo tree species occurs, where higher resistance to cavitation (embolism) was associated with lower leaf specific

conductance (Vinya et al. 2009). The high pre-dawn leaf water potentials for *D. condylocarpon* in the dry season (Fig. 3 A) suggests a continued supply of water, and with high *LSC* (Fig. 7 E), *D. condylocarpon* was able to maintain minimum leaf water potentials to higher values in the dry season (Fig. 3 B), avoiding cavitation even at high evaporative demands. Lower *LSC* in *B. spiciformis* and *J. globiflora* (Fig. 7 E) decreases the risk of embolism (Sperry et al. 2002), consistent with lower pre-dawn leaf water potentials (Fig. 3 A), and increased cavitation resistance allows a greater tolerance for lower leaf water potentials (Fig. 3 B). Therefore, the inter-specific differences in *LSC* and concomitant cavitation resistance is co-ordinated to match a particular water use niche (Sperry et al. 2002), presumably caused by roots drawing water from a particular temporal or spatial niche in the soil environment.

Inter-specific differences and ecological implications

We hypothesised that all species would exhibit similar seasonal patterns of leaf gas exchange and photosynthetic capacities. To disprove this hypothesis, inter-specific differences in stomatal control, leaf trait variations, and maximum assimilation rates would occur between species. We observed inter-specific differences in stomatal control (Fig. 4 & 5), photosynthetic capacities (Fig. 6 A) and leaf traits (Fig. 7) between species, falsifying this hypothesis. From our results we have shown that miombo trees can tolerate very low leaf water potentials, and continue to transpire even when water availability is seemingly very low, allowing positive carbon uptake even in the dry season. However, inter-specific differences occurred where *J. globiflora* and *D. condylocarpon* had a higher assimilation capacity in the dry season, but at the cost of higher transpired water losses. *B. spiciformis* postponed leaf development and full photosynthetic capacity till later in

the dry season, and compensated for lower assimilation rates in the dry season with higher rates in the wet season and overall lower water losses.

The differences in leaf developmental stage between species indicate slightly differing phenological timing, where *B. spiciformis* postponed leaf flushing to a later stage of the dry season than *J. globiflora* and *D. condylocarpon* did (see supplementary material Fig. S4). Varied timing of leaf flushing occurs in other seasonally dry tropical forests, and has been suggested to occur due to varied access to soil water and tree size (Elliott et al. 2006; Shackleton 1999). Smaller trees are less able to access deep soil water due to less extensive root systems (Eamus 1999). In this study we have shown that miombo trees can access deep soil water, but that access is varied. It is yet unclear why varied soil water access occurs between miombo trees within close proximity and of similar stature, but variations in topography and soil texture could cause varied soil water access (Shackleton 1999). However, all the trees measured occurred on similar soils and with no obvious topographic differences between sites. A further possibility is varied stem water storage capacity between species (Alves de Lima et al. 2012; Borchert 1994), but the similar wood densities of the three species (0.60-0.63 Mg m^{-3}) (Williams et al. 2008b) suggests that they do not differ in their stem water storage capacities.

It is unclear why differing timing of leaf development and photosynthetic capacity occurs between the co-existing miombo tree species, but it may create niche separation with regards to light, water and nutrient competition during the early growing season, facilitating co-existence (Simioni et al. 2004). The development of fully functional leaves during dry season flush would give the under-story tree *D. condylocarpon* a competitive advantage over co-occurring over-story species of *B.*

spiciformis and *J. globiflora,* increasing the growing season and taking full advantage of the higher light conditions (Fig. 1 C) during the dry season. The development of leaves in *J. globiflora* before *B. spiciformis* would give *J. globiflora* a competitive advantage to soil water and nutrient uptake, if they shared the same rooting profiles. For *B. spiciformis* the postponement of full photosynthetic capacity till later in the dry season decreases transpired water losses and avoids severe desiccation during the dry season.

Conclusions

The objectives of this study were to quantify the controls on photosynthetic uptake of miombo woodland tree species on a diurnal to seasonal time scale, by assessing the diurnal variations in leaf-level photosynthetic activity, leaf gas exchange, and water relations, as well as seasonal shifts in leaf traits for key miombo tree species in wet and dry seasons. We found inter-specific responses of leaf level gas exchange and photosynthetic productivity to seasonal drought amongst tree species of miombo woodland. *J. globiflora* and *D. condylocarpon* maintained similar maximum stomatal conductance and assimilation rates in dry and wet seasons. However, *B. spiciformis* had a greater stomatal sensitivity to increasing evaporative demands, and its maximum stomatal conductance, transpiration and assimilation rates were lower during the dry season. The inter-specific differences in stomatal response and assimilation rates were attributed to differing leaf traits and photosynthetic capacities between species during the dry season. *B. spiciformis* had lower leaf N content and photosynthetic capacity in the dry season, whereas *J. globiflora* and *D. condylocarpon* showed little to no change in leaf traits from the dry to wet season. There was also some indication of differing access to soil water,

where *D. condylocarpon* did not experience higher soil water deficits in the dry season, allowing higher stomatal conductance, transpiration rates, and leaf specific conductance, while maintaining leaf water potentials in the dry season.

It was suggested that differing photosynthetic capacities between species were due to differing stages of leaf development during the dry season at the time of measurement. It was unclear what caused the differing timing of leaf development between species, but the staggered timing of new leaf flushing may facilitate niche separation with regards to light, water and nutrient competition during the growing season, allowing these tree species to co-exist in miombo woodlands.

Several questions arise from this study, including whether rooting depth and access to soil water and nutrients differ between species and tree size classes, and if so, does root niche separation determine the inter-specific response of photosynthesis to seasonal drought and timing of leaf flush? Further studies on rooting depths and profiles of miombo woodland trees, in conjunction with an assessment of soil water and nutrient availability of trees would be needed to fully understand the inter-specific differences of miombo tree responses to seasonal drought. Furthermore, a greater sampling effort across different sites and trees of different sizes and species would be needed in order to fully understand the responses of leaf gas exchange and photosynthetic productivity of miombo woodlands to diurnal and seasonal fluctuations in water availability.

Acknowledgements

We thank staff at Envirotrade Ltd. for facilitating fieldwork and the field staff Albasine ‘Joey’ Mucavele, Alfonso Jornal, Ramaio Saimone, Neto Moulinho and Zito Lindo. We thank Tomas Domingues and Joana Zaragoza-Castells for extensive technical advice and discussion. We thank Jennifer Wright for useful comments on the manuscript. Emily Woollen was funded by a Natural Environment Research Council CASE studentship.

References

Abramoff MD, Magalhaes PJ, Ram SJ (2004) Image processing with ImageJ. Biophotonics International 11:36-42

Alves de Lima AL, de Sa Barretto Sampaio EV, de Castro CC, Nogueira Rodal MJ, Dantas Antonino AC, de Melo AL (2012) Do the phenology and functional stem attributes of woody species allow for the identification of functional groups in the semiarid region of Brazil? Trees-Structure and Function 26:1605-1616

Berry J, Bjorkman O (1980) Photosynthetic response and adaptation to temperature in higher plants. Annual Review of Plant Physiology and Plant Molecular Biology 31:491-543

Bhaskar R, Ackerly DD (2006) Ecological relevance of minimum seasonal water potentials. Physiologia Plantarum 127:353-359

Bombelli A et al. (2009) The sub-saharan Africa carbon balance, an overview. Biogeosciences Discuss. 6:2085-2123

Bonal D, Guehl JM (2001) Contrasting patterns of leaf water potential and gas exchange responses to drought in seedlings of tropical rainforest species. Functional Ecology 15:490-496

Borchert R (1994) Soil and stem water storage determine phenology and distribution of tropical dry forest trees. Ecology 75:1437-1449

Bruhn D, Mikkelsen TN, Atkin OK (2002) Does the direct effect of atmospheric CO2 concentration on leaf respiration vary with temperature? Responses in two species of Plantago that differ in relative growth rate. Physiologia Plantarum 114:57-64

Campbell BM (1996) The Miombo in Transition: Woodlands and Welfare in Africa. Center for International Forestry Research, Bogor, Indonesia

Chidumayo E, Frost P (1996) Population biology of miombo trees. In: Campbell B (ed) The Miombo in Transition: Woodlands and Welfare in Africa. Center for International Forestry Research, Bogor, Indonesia, pp 59-72

Chidumayo EN (1997) Miombo Ecology and Management: an Introduction. Intermediate Technology Publications, London

Chidumayo EN (2001) Climate and phenology of savanna vegetation in southern Africa. Journal of Vegetation Science 12:347-354

Choinski JS, Johnson JM (1993) Changes in Photosynthesis and Water Status of Developing Leaves of Brachystegia-Spiciformis Benth. Tree Physiology 13:17-27

Ciais P et al. (2011) The carbon balance of Africa: synthesis of recent research studies. Philosophical Transactions of the Royal Society a-Mathematical Physical and Engineering Sciences 369:2038-2057

Ciais P, Piao SL, Cadule P, Friedlingstein P, Chedin A (2009) Variability and recent trends in the African terrestrial carbon balance. Biogeosciences 6:1935-1948

Eamus D (1999) Ecophysiological traits of deciduous and evergreen woody species in the seasonally dry tropics. Trends in Ecology & Evolution 14:11-16

Elliott S, Baker PJ, Borchert R (2006) Leaf flushing during the dry season: the paradox of Asian monsoon forests. Global Ecology and Biogeography 15:248-257

Farquhar GD, Caemmerer SV, Berry JA (1980) A Biochemical Model of Photosynthetic CO2 Assimilation in Leaves of C3 Species. Planta 149:78-90

Field CB, Mooney HA (1986) The photosynthesis-nitrogen relationship in wild plants In: Givnish TJ (ed) On the Economy of Plant Form and Function. Cambridge University Press, Cambridge, pp 25-55

Flexas J et al. (2007) Analysis of leakage in IRGA's leaf chambers of open gas exchange systems: quantification and its effects in photosynthesis parameterization. Journal of Experimental Botany 58:1533-1543

Flexas J, Medrano H (2002) Drought-inhibition of photosynthesis in C-3 plants: Stomatal and non-stomatal limitations revisited. Annals of Botany 89:183-189

Frazer GW, Canham CD (1999) Gap Light Analyzer (Version 2.0). Simon Fraser University & Institute of Ecosystem Studies, British Columbia & New York

Frost P (1996) The ecology of miombo woodlands. In: Campbell B (ed) The Miombo in Transition: Woodlands and Welfare in Africa. Center for International Forestry Research, Bogor, Indonesia, pp 11-57

Fuller DO (1999) Canopy phenology of some mopane and miombo woodlands in eastern Zambia. Global Ecology and Biogeography 8:199-209

Hubbard RM, Bond BJ, Ryan MG (1999) Evidence that hydraulic conductance limits photosynthesis in old Pinus ponderosa trees. Tree Physiology 19:165-172

IPCC (2007) Fourth Assessment Report: Climate Change 2007 (AR4). Geneva, Switzerland

Lambers H, Chapin FS, Pons TL (2008) Plant Physiological Ecology, 2nd edn. Springer Science, New York, USA

Lawlor DW, Cornic G (2002) Photosynthetic carbon assimilation and associated metabolism in relation to water deficits in higher plants. Plant Cell and Environment 25:275-294

Long SP, Bernacchi CJ (2003) Gas exchange measurements, what can they tell us about the underlying limitations to photosynthesis? Procedures and sources of error. Journal of Experimental Botany 54:2393-2401

MathWorks (2012) Matlab (Version 7.14.0.739). The MathWorks Inc., Natick, MA.

Oren R et al. (1999) Survey and synthesis of intra- and interspecific variation in stomatal sensitivity to vapour pressure deficit. Plant Cell and Environment 22:1515-1526

Rasband WS (1997-2011) ImageJ. National Institutes of Health, Bethesda, Maryland, USA

Reich PB, Walters MB, Ellsworth DS (1997) From tropics to tundra: Global convergence in plant functioning. Proceedings of the National Academy of Sciences of the United States of America 94:13730-13734

Rodeghiero M, Niinemets U, Cescatti A (2007) Major diffusion leaks of clamp-on leaf cuvettes still unaccounted: how erroneous are the estimates of Farquhar et al. model parameters? Plant Cell and Environment 30:1006-1022

Ryan CM (2009) Carbon Cycling, Fire and Phenology in a Tropical Savanna Woodland in Nhambita, Mozambique. PhD thesis, School of GeoSciences, The University of Edinburgh, Edinburgh

Ryan CM, Williams M (2011) How does fire intensity and frequency affect miombo woodland tree populations and biomass? Ecological Applications 21:48-60

Ryan CM, Williams M, Grace J (2011) Above- and belowground carbon stocks in a miombo woodland landscape of Mozambique. Biotropica 43:423-432

Santiago LS, Mulkey SS (2003) A test of gas exchange measurements on excised canopy branches of ten tropical tree species. Photosynthetica 41:343-347

Shackleton CM (1999) Rainfall and topo-edaphic influences on woody community phenology in South African savannas. Global Ecology and Biogeography 8:125-136

Sharkey TD, Bernacchi CJ, Farquhar GD, Singsaas EL (2007) Fitting photosynthetic carbon dioxide response curves for C-3 leaves. Plant Cell and Environment 30:1035-1040

Simioni G, Gignoux J, Le Roux X, Appe R, Benest D (2004) Spatial and temporal variations in leaf area index, specific leaf area and leaf nitrogen of two co-occurring savanna tree species. Tree Physiology 24:205-216

Sperry JS, Hacke UG, Oren R, Comstock JP (2002) Water deficits and hydraulic limits to leaf water supply. Plant Cell and Environment 25:251-263

Timberlake JR, Calvert GM (1993) Preliminary Root Atlast for Zimbabwe and Zambia. Zimbabwe Bulletin of Forestry Research

Tinley KL (1977) Framework of the Gorongosa Ecosystem. PhD thesis, Faculty of Science, University of Pretoria, Pretoria

Tuohy JM, Choinski JS (1990) Comparative Photosynthesis in Developing Leaves of Brachystegia-Spiciformis Benth. Journal of Experimental Botany 41:919-923

Tuohy JM, Prior JAB, Stewart GR (1991) Photosynthesis in Relation to Leaf Nitrogen and Phosphorus-Content in Zimbabwean Trees. Oecologia 88:378-382

Vinya R, Malhi Y, Brown N (2009) Xylem vulnerability to cavitation for ten miombo canopy tree species with varying habitat preference. Comparative Biochemistry and Physiology a-Molecular & Integrative Physiology 153A:S213-S213

Weber U et al. (2009) The interannual variability of Africa's ecosystem productivity: a multi-model analysis. Biogeosciences 6:285-295

White F (1983) The Vegetation of Africa: a descriptive memoir to accompany the Unesco/AETFAT/UNSO vegetation map of Africa. UNESCO, Paris

Williams CA, Hanan NP, Baker I, Collatz GJ, Berry J, Denning AS (2008a) Interannual variability of photosynthesis across Africa and its attribution. Journal of Geophysical Research-Biogeosciences 113

Williams CA et al. (2007) Africa and the global carbon cycle. Carbon Balance Manag 2:3

Williams M et al. (1996) Modelling the soil-plant-atmosphere continuum in a Quercus-Acer stand at Harvard forest: The regulation of stomatal conductance by light, nitrogen and soil/plant hydraulic properties. Plant Cell and Environment 19:911-927

Williams M, Ryan CM, Rees RM, Sambane E, Fernando J, Grace J (2008b) Carbon sequestration and biodiversity of re-growing miombo woodlands in Mozambique. Forest Ecology and Management 254:145-155

Williams RJ, Myers BA, Muller WJ, Duff GA, Eamus D (1997) Leaf phenology of woody species in a North Australian tropical savanna. Ecology 78:2542-2558

Woollen E, Ryan CM, Williams M (2012) Carbon Stocks in an African Woodland Landscape: Spatial Distributions and Scales of Variation. Ecosystems 15:804-818

Wright IJ et al. (2004) The worldwide leaf economics spectrum. Nature 428:821-827

Wullschleger SD (1993) Biochemical Limitations to Carbon Assimilation in C3 Plants - A Retrospective Analysis of the A/Ci Curves from 109 Species. Journal of Experimental Botany 44:907-920

2b. Seasonal limitations to leaf level productivity in African miombo woodland tree species - supplementary material

E. Woollen[1] and M. Williams[1]

[1] School of GeoSciences, The University of Edinburgh, Edinburgh, EH9 3JN, UK

CO_2 response curve measurements on intact vs. excised branches

Caution when comparing results from the A/C_i measurements in the two seasons is required, as measurements on excised branches have been found to decrease photosynthetic rates, J_{max} and V_{cmax} estimates relative to intact branches (Santiago and Mulkey 2003). To test this theory A/C_i curves were taken on leaves of intact branches of two individual trees and species during the wet season. The same branches were then excised and further A/C_i curves were taken on adjacent leaves on the same branch. We find that a reduction in mean parameter estimates of J_{max}, V_{cmax} and A_{sat} occurs in excised branches in two individual trees of the species *B. spiciformis* and *D. condylocarpon* (Fig. S1). In *B. spiciformis*, J_{max} decreased by 28% from its intact estimate, V_{cmax} by 46% and A_{sat} by 37%. In *D. condylocarpon*, J_{max} and V_{cmax} both decreased by 34% from its intact estimate, but A_{sat} was not significantly decreased. However, the sample size (n = 4 leaves in intact and n = 2 leaves in excised branches for both trees) was small, and results are therefore only indicative of a potential decline in parameter estimations when branches are excised, and are not necessarily significantly different.

However, the % difference on A/C_i measurement on the same tree in the same season shows a large range of estimates, between 8-65% difference in V_{cmax}, J_{max} and A_{sat}. Therefore, the change shown to occur between intact and excised branches is not greater than the % differences we find between individual leaves on the same tree in the same season (i.e. where the same method was used within each season). Therefore, it is unclear whether the different methodologies used between seasons will influence CO_2 response curve measurements, but the large variability between individual leaves on the same tree suggests that is it not necessarily a methodological

effect which causes varied estimates, but most likely caused by other varying influencing factors between leaves.

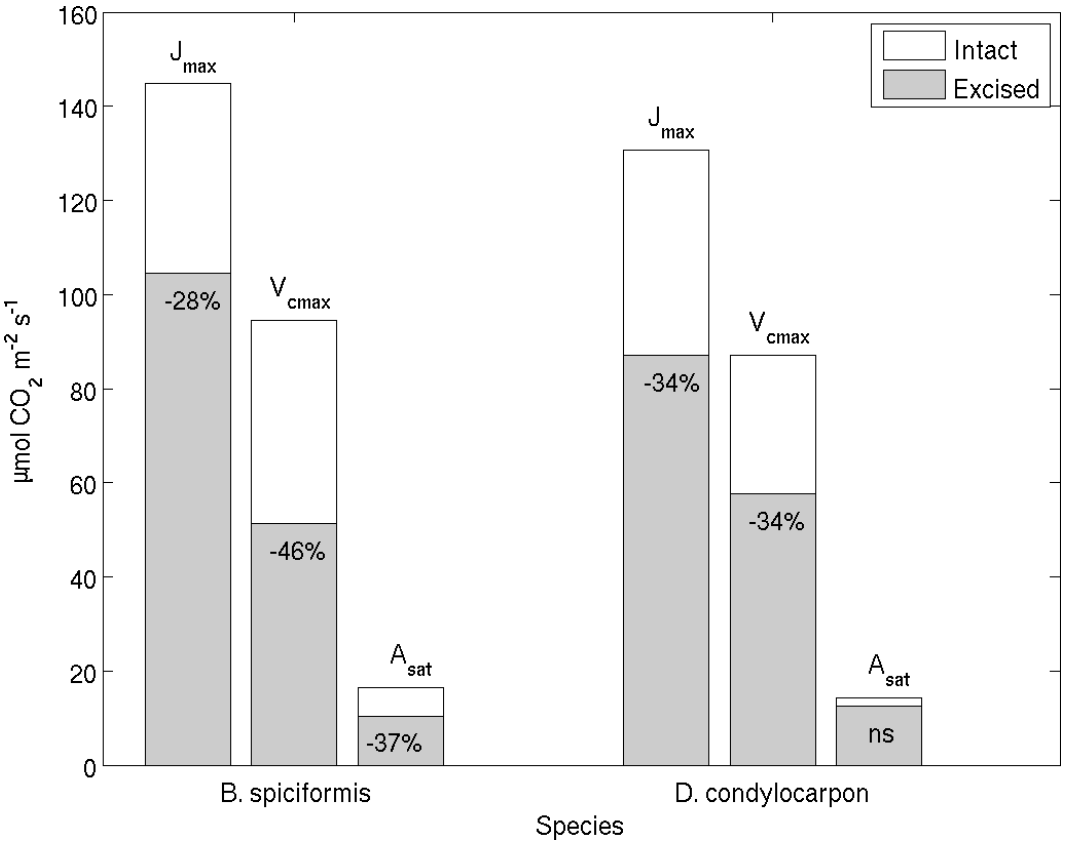

Fig. S1: Comparison of mean parameter estimates of J_{max}, V_{cmax} and A_{sat} on intact and excised branches of one individual tree of the species *Brachystegia spiciformis* and *Diplorhynchus condylocarpon*. Sample size for intact (n = 4 leaves) and excised (n = 2 leaves) branches for each tree was small. ns indicates a small change, which is unlikely to be significant.

C_i/C_a diurnal variations

The diurnal patterns of C_i/C_a for each species and season show that C_i/C_a was closely related to assimilation rate (i.e. the demand for internal CO_2) and stomatal conductance (i.e. the supply of CO_2) in both seasons. In the dry season, C_i/C_a decreases throughout the day as A and g_s decrease until after sunset (18:00), where a large increase in C_i/C_a occurs due to leaf respiration. In the wet season greater

variations in C_i/C_a occur due to more variable A and/or g_s throughout the day. Diurnal patterns of C_i/C_a do not differ markedly between seasons for *J. globiflora* or *D. condylocarpon*, but *B. spiciformis* shows some deviations due to higher A and g_s in the wet season.

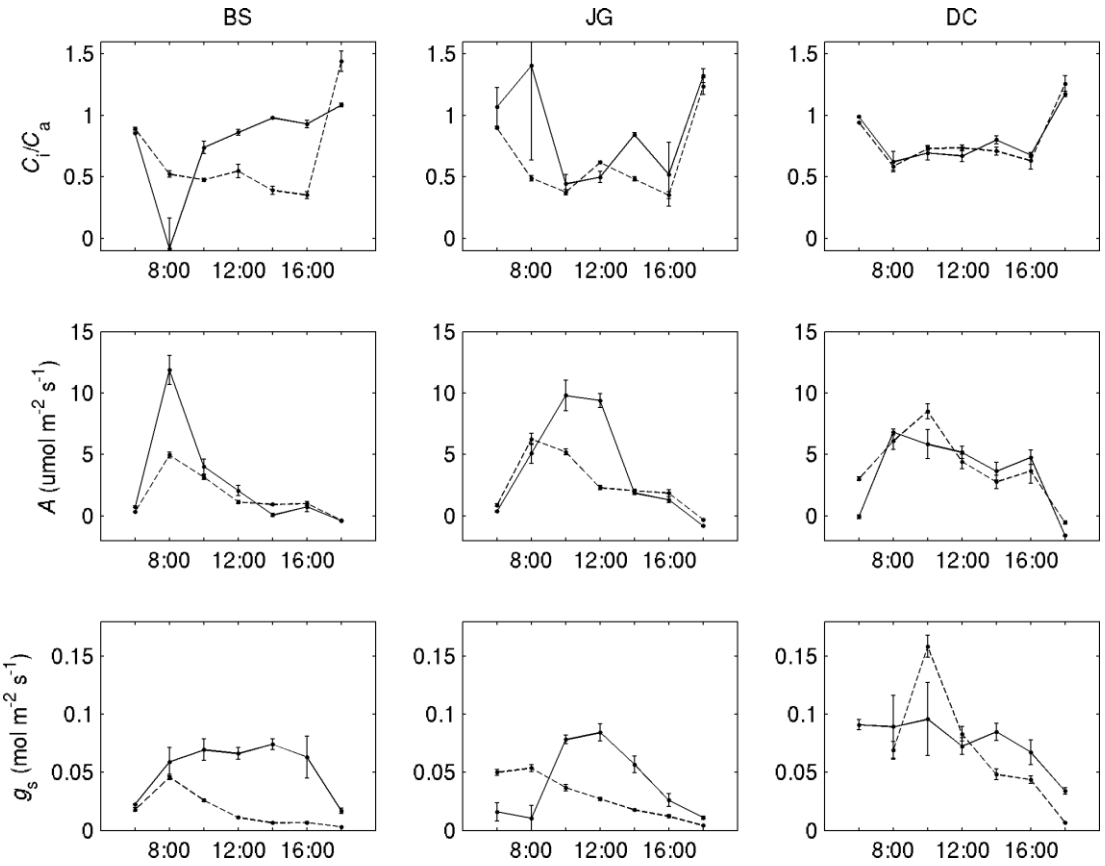

Fig. S2: Diurnal patterns of internal to ambient CO_2 concentrations (top panel), net assimilation rates (middle panel) and stomatal conductance (bottom panel) in dry (dashed line) and wet (solid line) seasons for one diurnal measurement on three tree species (see Fig. 2).

Additional leaf trait measurements

From the CO_2 response curves further leaf traits were determined, including light saturated assimilation rates (A_{sat}) and dark respiration rates (R_d). Values used in figure 7 are also shown in Table S1.

Table S1: Estimates of mean leaf traits for all three tree species combined and for individual species at 25 ^{o}C in two seasons. Number of replicates (i.e. number of leaves) used for each mean were n = 26 in the dry season (BS: n = 7, JG: n=12, DC: n =7) and n = 57 in the wet season (BS: n =20, JG: n =19, DC: n =18). Error estimates are standard errors of the mean.

Season	Leaf trait	All species	*B. spiciformis*	*J. globiflora*	*D. condylocarpon*
Dry	A_{sat} (μmol CO_2 m^{-2} s^{-1})	10.23 ± 0.55*	6.40 ± 0.38 [a]*	12.55 ± 0.35 [a]*	10.07 ± 0.43 [a]
	V_{cmax} (μmol m^{-2} s^{-1})	79.88 ± 5.49	46.54 ± 5.63[ab]*	95.96 ± 4.74[a]	85.67 ± 10.01[b]
	J_{max} (μmol m^{-2} s^{-1})	101.54 ± 5.45*	71.00 ± 9.75[ab]*	114.42 ± 3.39[a]*	110 ± 10.66[b]
	J_{max}:V_{cmax} (ratio)	1.31*	1.51[a]	1.21[a]*	1.30*
	R_d (μmol CO_2 m^{-2} s^{-1})	0.27 ± 0.04	0.34 ± 0.08	0.18 ± 0.05	0.36 ± 0.09
	N_m (mg g^{-1})	20.0 ± 0.01	18.9 ± 0.14[a]*	23.8 ± 0.11[a]	14.8 ± 0.06[a]
	N_a (g m^{-2})	1.58 ± 0.11	1.27 ± 0.08[a]*	2.10 ± 0.12[ab]	1.00 ± 0.06[b]
	LMA (g m^{-2})	77.0 ± 2.26	67.63 ±0.94[a]	87.85 ± 1.77[ab]	67.92 ± 2.51[b]
Wet	A_{sat} (μmol CO_2 m^{-2} s^{-1})	16.10 ± 0.54*	17.35 ± 0.82[a]*	17.93 ± 0.76[b]*	12.78 ± 0.79[ab]
	V_{cmax} (μmol m^{-2} s^{-1})	91.87 ± 3.30	99.82 ± 5.94[a]*	105.26 ± 3.39[b]	68.92 ± 3.29[ab]
	J_{max} (μmol m^{-2} s^{-1})	140.17 ± 5.26*	157.70 ± 9.95[a]*	156.63 ± 4.71[b]*	103.33 ± 4.93[ab]
	J_{max}:V_{cmax}	1.53*	1.57	1.50*	1.50*
	R_d (μmol CO_2 m^{-2} s^{-1})	0.20 ± 0.02	0.23 ± 0.02	0.19 ± 0.03	0.20 ± 0.06
	N_m (mg g^{-1})	21.7 ± 0.06	24.0 ± 0.07[a]*	23.4 ± 0.09[b]	17.3 ± 0.07[ab]
	N_a (g m^{-2})	1.73 ± 0.06	1.80 ± 0.05[a]*	2.08 ± 0.11[a]	1.26 ± 0.05[a]
	LMA (g m^{-2})	79.19 ± 1.67	75.62 ± 1.69[a]	89.21 ± 3.38[ab]	72.57 ± 1.78[b]

[a-b] The same letter indicates means are significantly different (ANOVA, $P < 0.05$) across species in the same season

* indicates means are significantly different (two sampled t-test, $P < 0.01$) between seasons

Inter-specific temporal variation in new leaf development

Temporal variation in leaf flushing occurs between individual trees (Fig. S3), and between species (Fig. S4) during the late dry season at our study site. Observations of leaf flushing behaviour when in the field indicated that leaves of *B. spiciformis* generally turned green at a later stage as compared to *J. globiflora* and *D. condylocarpon* during the dry season (Fig. S4). Many of the *B. spiciformis* trees had not flushed out new leaves in early October, whereas several trees of *J. globiflora* and *D. condylocarpon* had. The observations would suggest an inter-specific timing of leaf flushing between the three species studied, but only by a few weeks. In an attempt to control for varied stages of leaf development, all our measurements were

conducted on green leaves, as very new leaves are typically reddish/ pink in colour. However, despite this, our leaf trait results suggest that leaves of different species were at differing stages of leaf development during the dry season.

Fig S3: Varied stages of new leaf development during early October (7/10/2009) between individual trees of various species, where some trees had fully expanded green leaves, others newly flushed red/pink leaves, and some were still bare.

Fig. S4: Varied colour and stages of leaf development in A) *Brachystegia spiciformis* (red leafed tree in centre), B) *Julbernardia globiflora* (tall green leafed tree in centre), and C) *Diplorhynchus condylocarpon* (small green leafed tree in centre) during the dry season (October 2009) at our study site in central Mozambique. The red colour of *B. spiciformis* is due to anthocyanin pigments in leaves, typical for very young leaves (Tuohy and Choinski 1990).

3a. Carbon stocks in an African woodland landscape: spatial distributions and scales of variation

E. Woollen[1], C. M. Ryan[1] and M. Williams[1]

[1] School of GeoSciences, The University of Edinburgh, Edinburgh EH9 3JN, UK

(published in Ecosystems as Woollen E, Ryan CM, Williams M (2012) Carbon Stocks in an African Woodland Landscape: Spatial Distributions and Scales of Variation. Ecosystems 15:804-818 *)*

Abstract

Current knowledge of Africa's carbon (C) pools is limited despite its importance in the global C budget. To increase understanding of C stocks in African woodlands, we asked how do C stocks in soil and vegetation vary across a miombo woodland landscape and to what degree and at what scales are these stocks linked? We sampled along a 5 km transect using a cyclic sampling scheme to allow geostatistical analyses. Soil C stocks in the top 5 cm (12.1 ± 0.6 Mg C ha^{-1} (± SE)) and 30 cm depths (40.1 ± 2.5 Mg C ha^{-1}) varied significantly at scales of a few meters (autocorrelation distance 14 m in 0-5 cm and 26 m in 0-30 cm interval), and above-ground (AG) woody C stocks (20.7 ± 1.8 Mg C ha^{-1}) varied significantly at kilometre scales (1430 m). Soil textural distributions were linked to topography (r^2 = 0.54) as were large-tree AG C stocks (r^2 = 0.70). AG C stocks were constrained to an upper boundary by soil texture with greater AG C being associated with coarser textured soils. Vegetation and soil C stocks were coupled in the landscape in the top 5 cm of soil (r^2 = 0.24) but not with deeper soil C stocks, which were coupled to soil clay content (r^2 = 0.38). This study is one of the most complete transect studies in an African miombo woodland, and suggests that C stock distributions are strongly linked to topography and soil texture. To optimise sampling strategies for C stock assessments in miombo, soil C should be sampled at > 26 m apart, and AG C should be sampled at > 1430 m apart in plots > 0.5 ha.

Key-words: Africa, miombo woodland, spatial, savanna, tree-grass co-existence, geostatistics, Mozambique

Introduction

Despite being the second largest continent on earth, and the largest land area in the tropics, knowledge on Africa's carbon (C) pools is limited (Ciais et al. 2011). The most widespread vegetation types in Africa are savannas and open woodlands, which cover over half of the continent. Bombelli *et al*. (2009) highlight the importance of savannas in sub-Saharan Africa's carbon balance, due to their extent, fire regimes and high interannual variability in net ecosystem productivity, and notes that they are a major uncertainty in the overall C budget of Africa. The terrestrial C cycle plays a critical role in global climate change and thus in the consequent development of related international treaties, which has heightened the need for accurate assessments of terrestrial C stores on landscape scales (IPCC 2007). Despite their importance to human welfare, large extents, and potential for C storage, African savannas and woodlands are relatively understudied and poorly understood compared to other biomes (Jeltsch et al. 2000; Scholes and Archer 1997).

The most common woodland in sub-Saharan Africa is miombo covering 2.7 million km^2 (Campbell 1996). It is a seasonally dry deciduous woodland dominated by *Brachystegia*, *Julbernardia* and/or *Isoberlinia* tree species with a continuous understory of C_4 grasses (White 1983). Savannas are broadly defined as having a continuous grass cover with discontinuous tree cover, and the term has been widely used and variously defined (Scholes and Archer 1997). Here we define miombo as a woodland but consider them part of the broader definition of savannas, due to the coexistence of trees and grasses. Miombo is a highly heterogeneous woodland with interchangeable domination of tree and grass cover. The mechanisms allowing tree-grass coexistence in savannas are largely debated (Bond 2008; Jeltsch et al. 2000;

Sankaran et al. 2004; Scholes and Archer 1997) and are generally polarized into competition-based or disturbance-based mechanisms. However, multiple mechanisms are likely to be important in determining vegetation cover and patterning. The heterogeneity of miombo translates into highly varied above and below ground C stocks (Rossi et al. 2009; Ryan et al. 2011; Williams et al. 2008), which complicates estimates of their C stocks and their monitoring requirements.

Previous studies have described miombo structure and ecology (Chidumayo 1997; Frost 1996) but little information is available regarding small-scale patterns (but see Campbell et al. 1995). It has previously been observed that miombo woodland trees tend to prefer well drained soils (Chidumayo 1997; Frost 1996), suggesting a link between soil physical properties and floristic composition. However, these links are unclear (Ryan et al. 2011; Williams et al. 2008), perhaps because vegetation structure is partly determined by frequent fire disturbance (Ryan and Williams 2011) and by increasing human usage (Campbell et al. 2007). Soil C stocks have also been linked to soil physical properties (Bird et al. 2000; Ryan et al. 2011) but sampling has shown complex variations in miombo landscapes (Rossi et al. 2009). A link between woody biomass and soil C stocks might be expected due to organic matter inputs to the soil from the trees, and empirical evidence for this is presented in Bird et al. (2000) and Wang et al. (2009). However, other studies find no correlations between woody biomass and soil C stocks, attributed to disturbance factors, such as fire de-coupling above-ground and below-ground C stocks (Ryan et al. 2011).

Thus the critical questions to be addressed are: 1) How do C stocks in soils and vegetation vary across miombo landscapes? 2) To what degree and at what

scales are these stocks linked? and 3) What are the appropriate scales for sampling C stocks? Woody biomass C stocks could vary at scales of a few meters, determined by local perturbation factors such as disturbance and/or soil properties, or at scales of kilometers if determined by larger landscape physical factors such as topography and/or rainfall gradients. Soil C on the other hand might also be expected to vary significantly at scales of a few meters, largely driven by local soil physical factors and tree cover. In light of current knowledge we hypothesise the following:

H1. The distribution of soil textural properties is linked to topography, due to soil formation and runoff processes.

H2. Woody biomass C stocks vary with soil textural properties, with higher biomass on well drained soils.

H3. Soil C and vegetation C stocks are coupled in the landscape, and clear correlation and co-variation across the landscape will be evident.

This paper aims to address these hypotheses by determining spatially explicit vegetation and soil C stocks, and analysing their relationships with other variables. We sampled soils and vegetation along a 5 km transect through a miombo woodland landscape of central Mozambique. The spatial structure of C stores was determined using a cyclic sampling scheme to allow geostatistical analyses of the data (Burrows et al. 2002). Multiple variables were sampled simultaneously along the transect to allow correlation analyses to be performed. This paper is novel in that it presents the most complete transect study undertaken in miombo woodlands, describing the spatial structure and pattern of vegetation and soil C stores, describing the links between them and suggests mechanisms controlling their distributions.

Methods and materials

Study Site

The study site was based in the Nhambita community area of Gorongosa District, adjacent to the south-west boundary and within the buffer zone of Gorongosa National Park in the Sofala Province, central Mozambique (18.979^{o}S, 34.176^{o}E) (Fig. 1). The Nhambita community area covers approximately 348 km^{2} and is predominantly classified as miombo woodland vegetation (Williams et al. 2008). The area receives 850±269 mm (± SD) mean annual precipitation and is strongly seasonal, with 82 % falling in the wet season between November and March (Ryan 2009). Daily mean temperatures range from 30º C in December to 20ºC in July. Fire is a frequent occurrence, causing most of the vegetation to be burned every 1-3 years during the dry season between June to October (Ryan and Williams 2011).

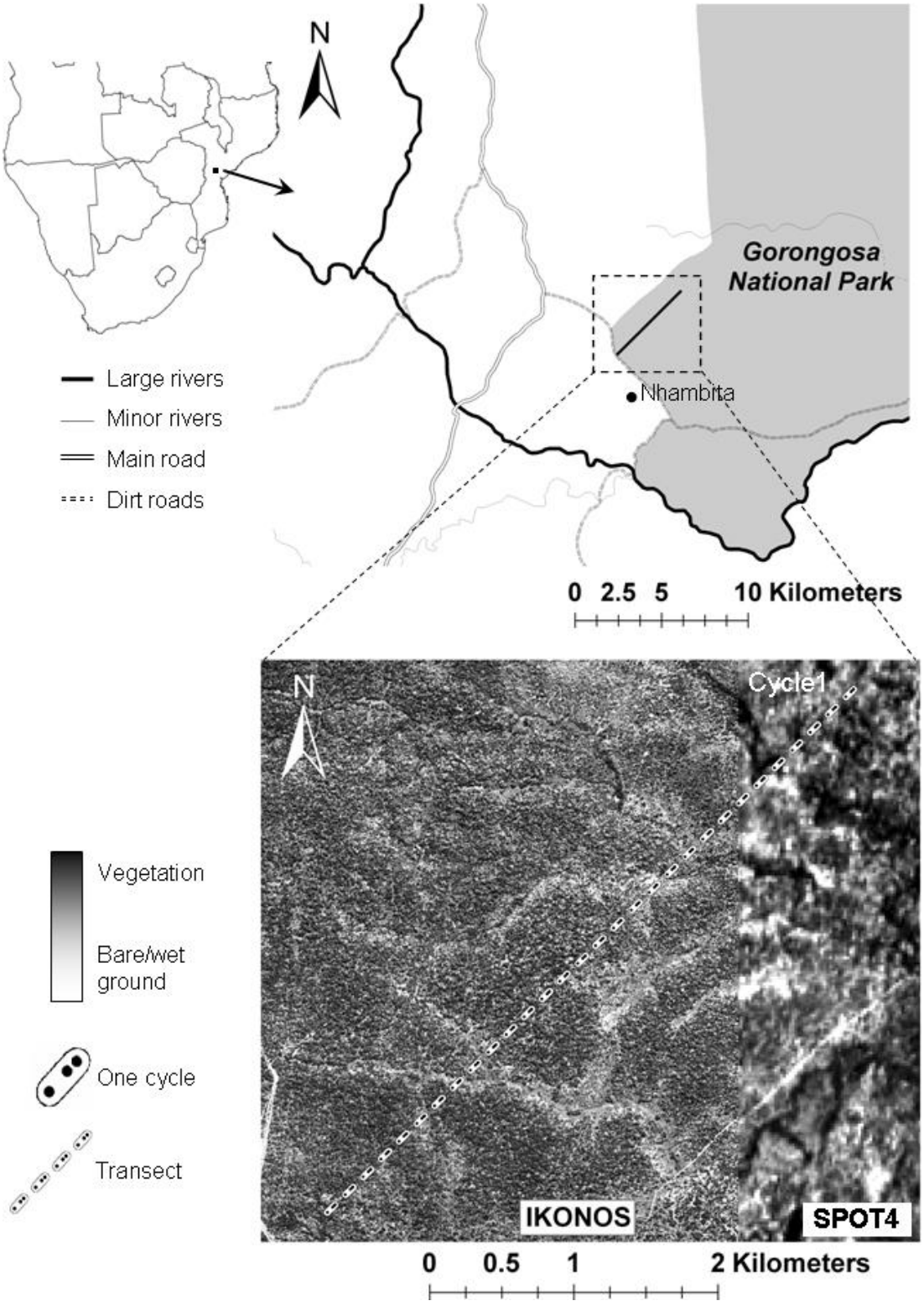

Fig. 1: Top panel: Nhambita community area and the south-west Gorongosa national park zone, Sofala province, central Mozambique. Bottom panel: the transect showing individual cycles overlain on greyscale IKONOS imagery (band 2) and SPOT 4 imagery (band 2).

The soils found in the Nhambita area are mostly sandy fersiallitic soils derived from metamorphic migmatitic gneisses and granite (Tinley 1977). A soil map of the area, illustrated in Tinley (1977), shows a mosaic of soils across the Nhambita area varying from free draining soils in the north-west high grounds, to more hydromorphic soils in the bottomlands of the south-east. Most of the soils to the north-west consist of brown granite-gneiss derived from acid rocks supporting *Brachystegia* savanna or woodlands. Networks of hydromorphic soils supporting dambo grassland occur on the lower grounds of the gently undulating landscape. Dambos (a.k.a *vlei*) are shallow, seasonally waterlogged depressions and typically tree-less grass-covered wetlands (von der Heyden 2004). Dambos have low hydraulic conductivity and permeability due to the accumulation of clays. Termite mounds form islands of loamy fertile soils often supporting a dense cover of vegetation.

Cyclic Sampling

To address the need for spatially explicit measurements of C stores, fieldwork was carried out in April 2009 along a straight line transect (5.15 km) using a nested cyclic sampling design (Fig. 2). One cycle was characterised as a 75 m stretch within which five 1 m^2 quadrats and three 314 m^2 (0.03 ha) circular plots (10 m radius) were placed, around which was one 0.57 ha round-ended rectangular (RER) plot (Fig. 2). A new cycle repeated 100 m from the end of the last cycle, until the end of the 5 km transect, creating a total of 30 cycles. This sampling design allows analyses of data at several different spatial scales; the spatial scale at which data are collected and aggregated (e.g. size of plots), or the geographical extent, or distance, over which comparisons are made.

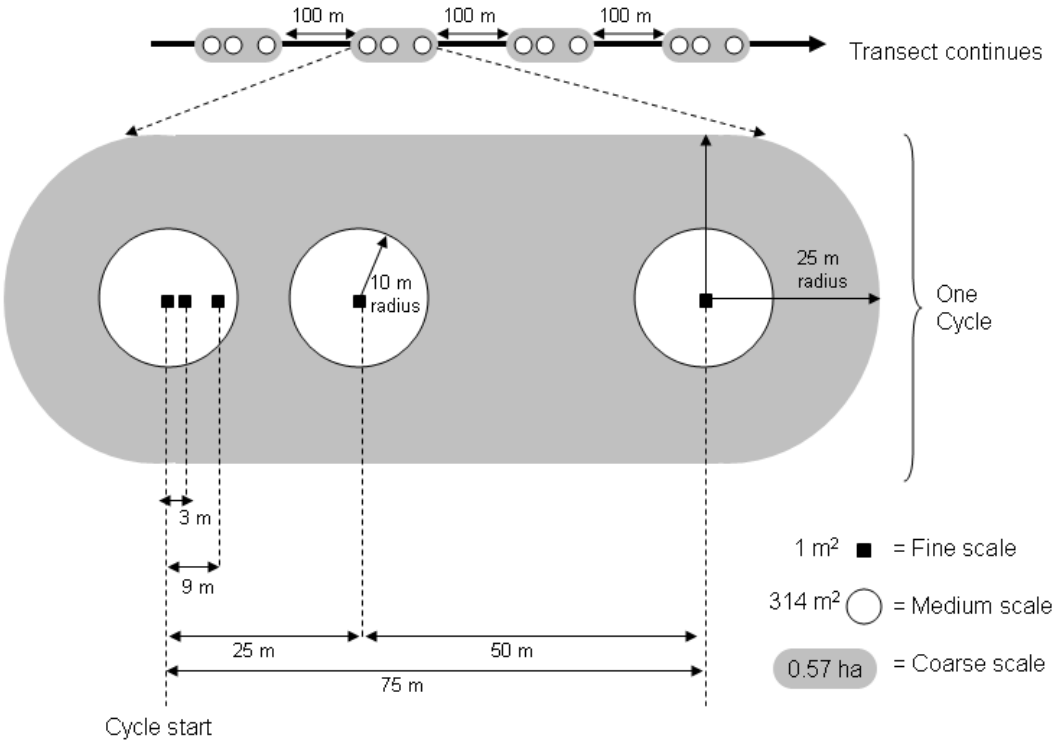

Fig. 2: Diagram of transect cyclic sampling showing sample locations at three spatial grain scales within one cycle: fine (1 m^2 black squares), medium (314 m^2 white circles), and coarse (grey round-ended rectangle 0.57 ha plots). Each cycle is 75 m long within which there are 5 fine scale and 3 medium scale sample plots. The coarse scale plots encompass an entire cycle. The cycle repeats 100 m from the last so that there are 30 cycles in total along a 5 km transect.

For clarification, we distinguish between the two meanings of spatial scale by referring to spatial scales of sampling (i.e. plot sizes) as spatial grain, and geographical spatial scales as spatial extent, as described in Whittaker et al. (2001). The nested cycling sampling design used achieves three spatial grain scales of measurements along the transect, fine (i.e. quadrats, n = 150), medium (circular plots, n = 90) and coarse (RER plots, n = 30), and by using different and unequal spacing between the three different plot sizes we achieve three sets of spatial extent scales as well, small (resolution 3 m), intermediate (resolution 25 m) and large (resolution 100 m).

The transect was located within the Gorongosa National Park in an area known to contain miombo woodland with little recent human disturbance. The study area has high variability in vegetation, occurring as patches surrounded by networks of less dense tree cover and/or bare ground as seen on satellite imagery (Fig. 1). Some evidence of tree extraction was observed along the transect, but cut stems only accounted for 1 % of total tree stem count. Evidence of previous fire occurrence was observed throughout the transect by tree trunk charring. Each cycle start location was pre-determined and located in the field using a GPS (Garmin Ltd., Kansas, USA, GPS 60). To ensure a straight line, a 75 m rope, with each of the five 1 m^2 sample locations marked on it, was extended from the cycle start at a bearing of 240° SW for each cycle. Elevation was measured continuously using a GPS with a barometric altimeter (apart from two days when power sources were exhausted).

Soil samples of the top 0-5 cm ($soil_5$) and 0-30 cm ($soil_{30}$) were taken within each 1 m^2 quadrat (n = 150) and total soil C, bulk density, and soil texture analyses were performed on each sample (see supplementary material for full details of methods used). Total soil carbon on an area basis (Mg C ha^{-1}) was calculated for the two depth profiles using bulk density, percent C and soil fraction measurements. Litter was collected and total dry litter mass (g m^{-2}) was calculated within each 1 m^2 quadrat. Within each 0.03 ha circular plot (n = 90) all standing woody stems > 5 cm diameter-at-breast-height (DBH) were recorded and their local names noted by local persons knowledgeable in botany. Species botanical names were derived using a vernacular key developed for the area by Meg Coates-Palgrave (pers. com.). Within each 0.57 ha RER plot (n = 30) the DBH and species of large trees (defined as having a DBH > 30 cm) were recorded. Small trees (5 < DBH < 30 cm) were not

recorded in the area outside of the 0.03 ha circle plots. Above-ground (AG) woody stem C stocks were calculated using a locally derived allometric equation (Ryan et al. 2011) on all live trees, giving kg of C for each tree stem. LAI measurements were taken in the centre of each 0.03 ha plot (n = 90) using a digital camera (Nikon Coolpix 4500) with a fisheye lens, mounted on a levelled tripod at 1.6 m height from the ground. All LAI images were processed using Gap-Light-Analyser software (Frazer and Canham 1999) to calculate LAI for each image location. Grass biomass was measured by using a disc-pasture-meter (Dorgeloh 2002), which was calibrated in the Nhambita area prior to use (linear calibration curve n = 68, r^2 = 0.48). Mean above-ground dry grass biomass was calculated for each RER plot, however, logistical constraints meant that grass biomass measurements were only taken in cycles 19 to 30 (n = 12), limiting its inclusion in geostatistical analyses.

Statistical Analyses

Spearman's rank correlations and significance values were calculated to describe the strength of monotonic relationships between variables in the landscape, without assuming normal distributions (Quinn and Keough 2002). Where significant correlations were indicated, we visually inspected scatterplots to identify the form of the relationship between dependent and independent variables. In all cases, we undertook linear regression analyses, as our ecological reasoning did not support the fitting of curvilinear relations, and a linear relationship was the simplest assumption. Clearly, extrapolation of these relationships should not be undertaken. Normality of distributions was tested using the Jarque-Bera test, where $P > 0.05$ indicated that the distribution of data was not significantly different from the normal distribution (Jarque and Bera 1987). A log transform on data was performed when necessary to

comply with assumptions of normality and equal variances of the error terms. All calculations were done using Matlab software routines (MathWorks 2007).

We used a 90th percentile linear quantile regression, as implemented in the 'quantreg' library (Koenker 2011) in the statistical package R, to estimate the upper boundary to which 90 % of the dependent variable data lies beneath the fitted line. Confidence intervals of the quantile regression estimated parameters enabled us to test whether the regression slope parameter was significantly different from zero (Koenker 2011).

Geostatistics were used to examine spatially structured variability in the data (i.e. geographical spatial scales). All geostatistical analyses were performed using Matlab. Semivariograms (Webster and Oliver 2001) were calculated for all variables at all three spatial extent scales of data. The data sets were tested for linear trends, and linear trends were removed when present. The empirical semivariograms were calculated by the method of moments (Matheron 1965), and a maximum separation distance was limited to half the total length of the transect to ensure sufficient sample sizes for each lag distance. A spherical model was fitted to each empirical semivariogram, using a weighted non-linear-least-squares method (Cressie 1985), to produce comparable parameter estimates of nugget, sill and range. Webster and Oliver (2001) define the parameters as follows: the nugget reflects the variability at zero distance (finer spatial extent scales than data resolution), or the variability due to measurement error; the sill represents the maximum variability reached; the range is the separation distance at which data points are no longer autocorrelated. A further parameter was calculated, the nugget-to-sill ratio, which indicates the degree of spatial dependence in the data. A strong spatial dependence in the data set is defined

by a ratio less than 0.25, and a ratio between 0.25 and 0.75 a moderate spatial dependence (Rossi et al. 2009). Lack of spatial dependence will occur if measurement errors are large at zero separation distances (i.e. large nuggets), or if large variability occurs at smaller spatial extents than data resolution. The spherical model calculation and fit were achieved using available Matlab code, "Variogramfit", created by Schwanghart (2010).

Results

Transect characteristics

The transect started (cycle 1-4) in open canopy grassy savanna dominated by tree species *Acacia robusta, A. nigrescens, Combretum adenogonium,* and *Tabernaemontana elegans* at an elevation of 85-90 m (Fig. 3 g), the lowest along the transect (see supplementary material Fig. S1). A Vertisol was present at cycle 2 and was a unique soil type along the transect, with unusually high soil C and clay content (Fig. 3 d-f). Cycle 5 crosses a river (approx. 6 m across) with gallery forest causing a peak in AG C stocks due to many large trees at this site (Fig. 3 c). Tree species diversity (H' = 2.69) was the highest at cycle 5 and tree species *C. adenogonium, Rhoicissus revoilii, Dalbergia melanoxylon, Diplorhynchus condylocarpon, Sclerocarya birrea, Cleistanthus schlechteri*, and *Brackenridgea zanguebarica* were common. Cycles 6-13 had several smaller rivers and dambos present in low lying or concave sites and tree species of genera *D. condylocarpon, C. adenogonium, S. birrea, and Julbernardia globiflora* were more common. At cycle 14-21 elevation increased to a peak of 126 m (Fig. 3 g). No rivers or dambos were present in these cycles, and typical miombo tree species of *J. globiflora* and *Brachystegia spiciformis*

were present with an understory of *D. condylocarpon* were dominant. Cycles 22-30 covered a plateau with minor undulations where dambos appear in the depressions. Typical miombo tree species dominated in these cycles. Termite mounds occurred throughout the transect at a density of 1.4 per hectare. Overall tree species diversity had a mean Shannon-index of 1.98, which ranged from 1.40 to 2.65 between cycles.

Spatial trends

Soil trends

Soil C stocks and texture varied significantly (one-way ANOVA, d.f. = 29, all *p*-values < 0.05) between cycles across the landscape (Fig. 3 d-f). Mean $soil_5$ C stocks were 12.1 ± 0.6 Mg C ha^{-1} (± S.E), ranging by 17 Mg C ha^{-1} between cycles, and mean $soil_{30}$ C stocks were 40.1 ± 2.5 Mg C ha^{-1}, ranging by 63 Mg C ha^{-1} between cycles (Table 1). Both $soil_5$ and $soil_{30}$ C content were log-normally distributed. Soil clay content along the transect had a mean of 5.7 ± 0.3 % (± S.E) ranging from 3.5 – 9.5 % (Table 1). The peak in mean soil C content (22.6 ± 1.1 Mg C ha^{-1} in $soil_5$, and 86.2 ± 6.3 Mg C ha^{-1} in $soil_{30}$), and % clay content (9.5 ± 0.5 %) in cycle 2 is associated with the Vertisol at that location.

Vegetation trends

Total AG stem wood C stocks had an overall mean of 20.7 ± 1.8 Mg C ha^{-1} (± S.E), which ranged by as much as 34 Mg C ha^{-1} between cycles (Table 1). On average 70 % of total AG C stocks were found in large trees (DBH > 30 cm) (Table 1). Total AG C and large-tree AG C were normally distributed in the landscape but small-tree AG C (5 cm < DBH < 30 cm) showed a non-normal distribution pattern (Table 1). Mean small-tree AG C was 6.2 ± 0.6 Mg C ha^{-1}, and ranged by 16.7 Mg C

ha^{-1}. Cycle 5 shows a peak (Fig. 3 c) in AG C stocks (36.1 ± 10.8 Mg C ha^{-1}) compared to the surrounding cycles, associated with the gallery forest along a larger river.

Total litter biomass followed the same pattern as total AG C stocks (Fig. 3 b), but had a log normal distribution (Table 1). Total litter biomass had a mean of 1.2 ± 0.2 Mg ha^{-1} and ranged by as much as 4 Mg ha^{-1} between cycles. LAI had an overall mean of 0.8 ± 0.1, which ranged from 0.2 to 1.3 between cycles, and had a normal distribution in the landscape (Table 1). However, LAI coefficients of variation (CV) were large (n = 3 per cycle, mean CV = 59 %, CV range 2-171 % between cycles), indicating high variability in LAI within cycles (Fig. 3 a). Grass biomass, measured for the last 12 cycles only, had a mean of 1.5 ± 0.2 Mg ha^{-1} (± S.E) with a range of 1.8 Mg ha^{-1} between cycles, and was normally distributed in the landscape (Table 1).

Due to cycle 2 and 5 having unique attributes (i.e. crossing a Vertisol and a large river) that were unrepresentative of the broader landscape of miombo woodland, they were excluded from any further analyses as outliers in the dataset. When cycle 2 and 5 were excluded as outliers in the data set, $soil_5$ and $soil_{30}$ data were normally distributed at the coarse spatial grain scale.

Table 1: Descriptive statistics of measured variables for coarse grain scale data sets (RER plots). Number of samples (N) for grass biomass and elevation are less due to lack of data for some cycles. Means, standard errors of the mean (SE), minimum (Min), median (Med), maximum (Max) and skewness (skew) values for each variable are shown. Distributions of variables are indicated. Abbreviations are above-ground (AG), leaf area index (LAI), and carbon (C).

Variable	Units	N	Mean	SE	Min	Med	Max	Skew	Distributions
Total AG C	Mg C ha^{-1}	30	20.7	1.8	8.4	21.2	42.2	0.8	Normal
Large-tree AG C	Mg C ha^{-1}	30	14.5	1.7	3.9	13.9	38.4	0.9	Normal
Small-tree AG C	Mg C ha^{-1}	30	6.2	0.6	0.8	6.6	17.5	1.5	*non-normal*
LAI	m^2 m^{-2}	30	0.8	0.1	0.2	0.8	1.3	0.2	Normal
Total Litter	Mg ha^{-1}	30	1.2	0.2	0.1	1.0	4.5	1.5	Log normal
$Soil_5$ C	Mg C ha^{-1}	30	12.1	0.6	5.8	12.3	22.6	0.8	Log normal
$Soil_{30}$ C	Mg C ha^{-1}	30	40.1	2.5	22.9	37.2	86.2	1.5	Log normal
Soil clay content	%	30	5.7	0.3	3.5	5.5	9.5	0.8	Log normal
Grass biomass	Mg ha^{-1}	12	1.5	0.2	0.7	1.3	2.6	0.8	Normal
Elevation	m	28	105.2	2.3	84.0	109.4	126.0	-0.3	Normal

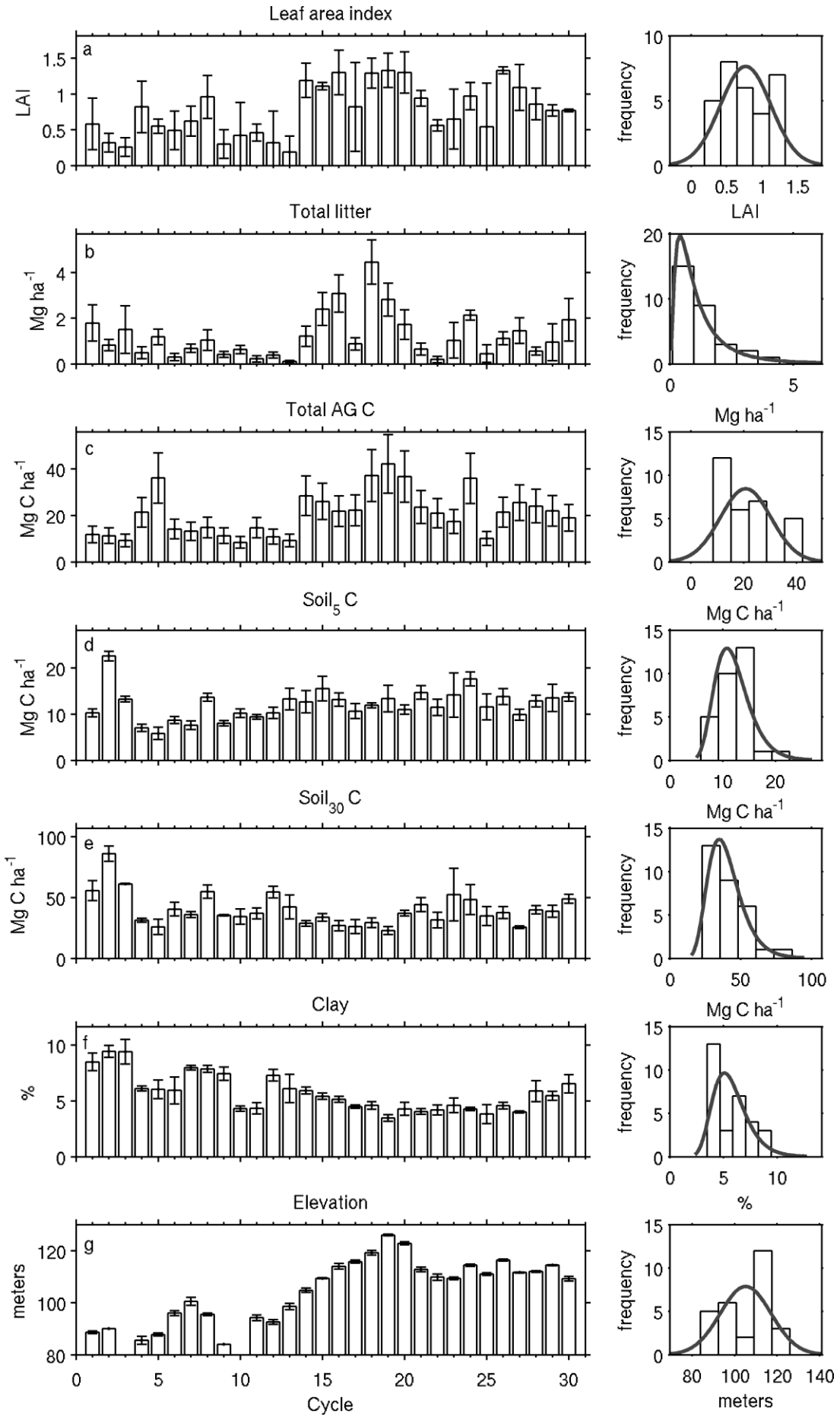
Leaf area index
a
LAI
frequency
LAI
Total litter
b
Mg ha-1
frequency
Mg ha-1
Total AG C
c
Mg C ha-1
frequency
Mg C ha-1
Soil5 C
d
Mg C ha-1
frequency
Mg C ha-1
Soil30 C
e
Mg C ha-1
frequency
Mg C ha-1
Clay
f
%
frequency
%
Elevation
g
meters
frequency
meters
Cycle

Fig. 3: (overleaf) Means (± S.E) of a) leaf-area-index (LAI) (n = 3), b) total litter (n = 5), c) total above-ground woody carbon (C) stock (n = 1), d) soil (0-5 cm) carbon content (n = 5), e) soil (0-30 cm) carbon content (n = 5), f) soil clay content (n = 3) and g) elevation (n = 5) at each cycle along the transect on left panel. Histograms of each variable and their distributions are shown on right panel. Error bars for total above-ground woody carbon are errors associated with the allometric used to calculate biomass (± 30 %). Elevation data has two missing data points at cycles 3 and 10.

Spatial dependence

Semivariograms were produced for all variables at each of the three spatial extent scales of measurement (small, intermediate and large), to enable comparison between variables at similar spatial grain scales and to determine at what geographical scales variation occurs in each variable.

Small spatial extent (resolution 3 m)

There was strong spatial dependence in total litter, $soil_5$ and $soil_{30}$ C content over a small spatial extent, shown by the very small nugget-to-sill ratios (Table 2). The spherical model described the spatial behaviour well at these scales for $soil_5$ C (r^2 = 0.77), $soil_{30}$ C (r^2 = 0.80) and total litter (r^2 = 0.71). The soil C content nearer the surface was more variable in space than the deeper soil C content, shown by the shorter range of autocorrelation in $soil_5$ (14 m) than $soil_{30}$ C (26 m). Total litter had a similar range of autocorrelation (17 m). The semivariograms show very small nuggets, indicating very low measurement errors, and an appropriate resolution (3 m) to account for almost all spatial extent variations of these variables.

Intermediate spatial extent (resolution 25 m)

At intermediate spatial extents there is a marked increase in the distances at which samples are autocorrelated. $Soil_{30}$ C (1056 m) and total litter (771 m) ranges of autocorrelation increased by up to two orders of magnitude, but with very weak

spatial dependence ($soil_{30}$ C = 0.86, and total litter = 0.60 nugget/sill ratios), and $soil_5$ C showed no spatial dependence (pure nugget effect) (Table 2). Soil clay content (662 m) and LAI (1264 m) showed large ranges and moderate to weak spatial dependences (clay = 0.47 and LAI = 0.71 nugget/sill ratios), despite a good-fit to the spherical model (clay $r^2 = 0.78$ and LAI $r^2 = 0.75$) (Table 2). The lack of any strong spatial dependence evidenced by the large nugget-to-sill ratios in total litter, LAI and $soil_{30}$ C content indicate that the spatial variation of these variables was not well characterised at intermediate spatial extents (25 m resolution).

Total AG C stocks had a relatively short range of autocorrelation (70 m) and a moderate spatial dependence (nugget/sill ratio of 0.48) (Table 2). Smaller sample plot sizes (0.03 ha) are more likely to miss the larger rarer trees, evidenced by the fact that 45 % of the 0.03 ha plots did not include any large trees despite their presence in all of the 0.57 ha RER plots, causing a very large sill and nugget in total AG C stocks, as the chance inclusion of a few large-trees within a 0.03 ha plot will cause large variation between plots.

Table 2: Semivariogram parameter estimates of range, sill, nugget, nugget-to-sill ratio and goodness-of-fit (r^2) for measured variables derived from fitted spherical models on three spatial extent scales of data. Abbreviations are above-ground (AG), leaf area index (LAI), and carbon (C).

Spatial extent	Variable	Transformed	Units	Range (m)	Sill $(units)^2$	Nugget $(units)^2$	Nugget/sill ratio	r^2
Large	$Soil_5$ C	Log	Mg C ha^{-1}	-	-	-	1	-
(100 m)	$Soil_{30}$ C	Log	Mg C ha^{-1}	1114	0.07	0.04	0.57	0.48
	Total litter	Log	Mg ha^{-1}	949	0.98	0.40	0.41	0.58
	Soil clay	Log	%	2279	0.06	0.02	0.43	0.77
	LAI	-	LAI	1127	0.14	0.05	0.37	0.79
	Total AG C	-	Mg C ha^{-1}	1426	93.59	31.49	0.34	0.55
Intermediate	$Soil_5$ C	Log	Mg C ha^{-1}	-	-	-	1	-
(25 m)	$Soil_{30}$ C	Log	Mg C ha^{-1}	1056	0.20	0.17	0.86	0.57
	Total litter	Log	Mg ha^{-1}	771	2.52	1.51	0.60	0.86
	Soil clay	Log	%	662	0.07	0.03	0.47	0.78
	LAI	-	LAI	1264	0.27	0.19	0.71	0.75
	Total AG C	-	Mg C ha^{-1}	70	450.04	216.17	0.48	0.37
Small	$Soil_5$ C	Log	Mg C ha^{-1}	14	0.13	0.01	0.04	0.77
(3 m)	$Soil_{30}$ C	Log	Mg C ha^{-1}	26	0.16	0.02	0.10	0.80
	Total litter	Log	Mg ha^{-1}	17	1.96	0.01	0.01	0.71

Large spatial extent (resolution 100 m)

At larger spatial extents the range of autocorrelation for all variables was large (approx. 1-2 km) (Table 2). However, unlike at intermediate spatial extents there was a moderate spatial dependence in all variables shown by the lower nugget-to-sill ratios, caused by the aggregation of small scale variability within each RER plot, decreasing overall variability between plots. $Soil_5$ C did not show any spatial dependence, and was a pure nugget effect. Total AG C range of autocorrelation (1426 m) increased by one order of magnitude from that at intermediate spatial extents. The larger sampling area used was better able to sample total AG C, as large trees were more likely to be included, reducing variability between samples and lowering the sill.

Spatial co-variation

Spearman's rank correlation analyses showed a number of significant co-variations between measured variables along the transect at the coarse spatial granularity. Elevation had significant ($P < 0.05$) correlations to every other variable along the transect, except for small-tree AG C stocks, $soil_{30}$ C and grass biomass (Table 3). Most significant was a very strong positive relationship between elevation and large-tree AG C stocks, where a linear relationship (Fig. 4 a) revealed that elevation could explain as much as 70 % of variability in large-tree AG C stocks ($P < 0.01$). Small-tree AG C had no relationships to any other measured variable. Elevation also had a strong negative correlation with soil clay content, and a negative linear relationship could explain 54 % ($P < 0.01$) of the variation in soil clay content (Fig. 4 b).

Table 3: Spearmans rank correlations between measured variable at the coarse grain scale excluding cycles 2 and 5 (n = 28). n = 12 for grass biomass as data is only available from cycles 19-30. Correlation coefficients are shown in bottom left hand of the table. *P*-values for significance of correlations (at the 95 % confidence interval) are shown in top-right hand of the table. Abbreviations are above-ground (AG), leaf area index (LAI), and carbon (C).

Variable	Elevation	$Soil_5$ C	$Soil_{30}$ C	Total litter	LAI	Soil clay	Total AG C	Small-tree AG C	Large-tree AG C	Grass biomass
Elevation		0.01	0.06	0.01	0.00	0.00	0.00	0.87	0.00	0.10
$Soil_5$ C	0.48		0.12	0.01	0.03	0.35	0.07	0.40	0.01	0.67
$Soil_{30}$ C	-0.37	0.30		0.49	0.02	0.01	0.02	0.58	0.04	0.25
Total litter	0.53	0.46	-0.14		0.00	0.69	0.00	0.41	0.00	0.97
LAI	0.71	0.40	-0.43	0.71		0.03	0.00	0.06	0.00	0.24
Soil clay	-0.71	-0.19	0.52	-0.08	-0.41		0.01	0.17	0.00	0.02
Total AG C	0.73	0.35	-0.46	0.60	0.87	-0.48		0.05	0.00	0.18
Small-tree AG C	-0.03	-0.17	-0.11	0.16	0.36	0.27	0.37		0.93	0.79
Large-tree AG C	0.82	0.50	-0.39	0.58	0.77	-0.66	0.88	-0.02		0.27
Grass biomass	-0.49	-0.14	0.36	0.01	-0.37	0.65	-0.41	0.09	-0.35	

$Soil_5$ and $soil_{30}$ C showed no significant relationship to each other and where $soil_5$ C was positively correlated to a variable, $soil_{30}$ C was negatively correlated, and vice versa (Table 3). The strongest correlation for $soil_5$ C was with large-tree AG C stocks, and a linear relationship explained 24 % ($P < 0.05$) of $soil_5$ C variability (Fig. 4 c). Total litter was positively correlated to $soil_5$ C content, but litter had no significant relationship to deeper $soil_{30}$ C (Table 3). $Soil_{30}$ C had a strong positive correlation to soil clay content, and a linear relationship was able to explain 38 % of variability ($P < 0.01$) in $soil_{30}$ C (Fig. 4 d). $Soil_5$ C shows no significant relationship to soil clay content (Table 3).

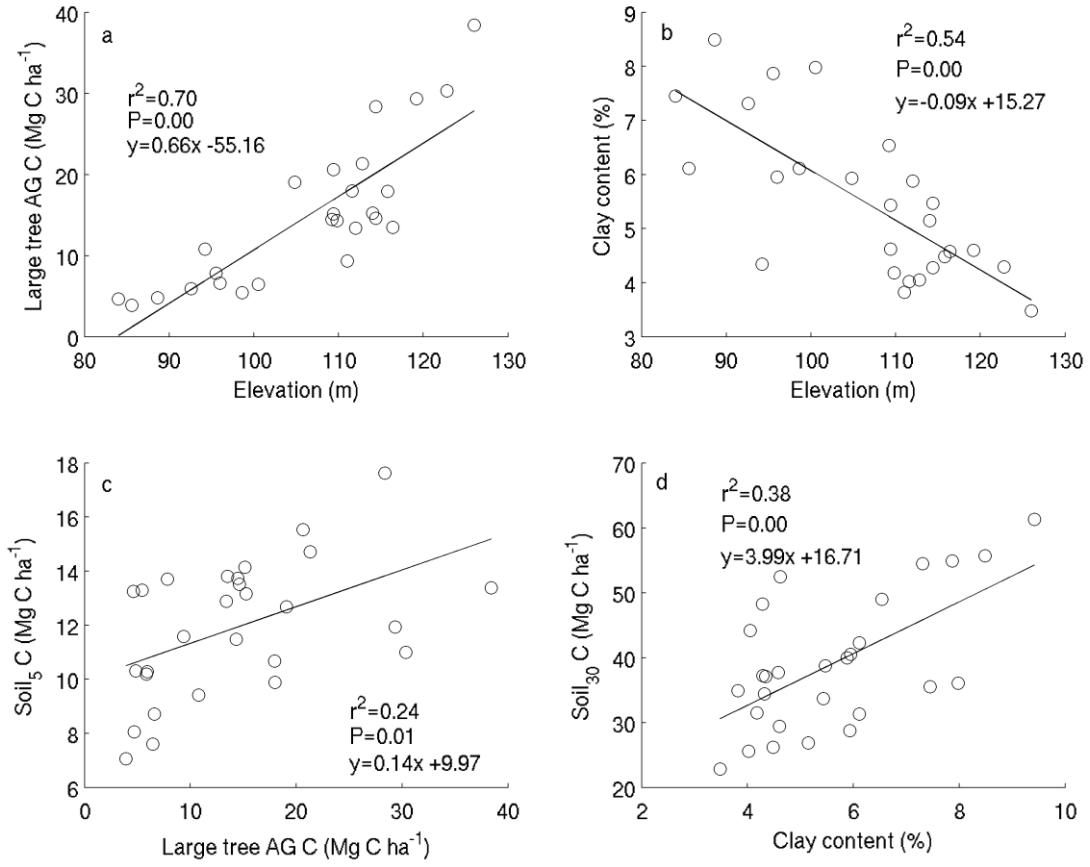

Fig. 4: Ordinary-least-squares linear regression analyses of a) large-tree above-ground (AG) woody carbon (C) against elevation, b) soil clay content against elevation, c) soil (0-5 cm) carbon content against large tree AG woody carbon, and d) soil (0-30 cm) carbon content against soil clay content. A *P*-value < 0.05 indicates a significant linear correlation at the 95 % confidence level.

A scatterplot of large-tree AG C and soil clay content (Fig.5 a) showed a unique relationship, where soil clay content seems to constrain large-tree AG C to an upper limit. Grass biomass showed no significant correlations with any other variable (but $n = 12$), except for soil clay content (Table 3). A positive linear relationship between grass biomass and soil clay content was able to explain 51 % ($P < 0.01$) of grass biomass variability (Fig. 5 b).

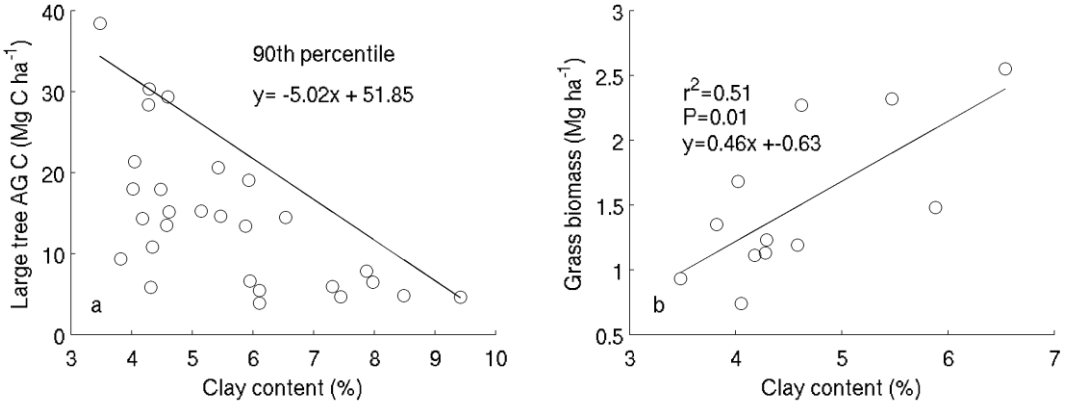

Fig. 5: Quantile linear regression of a) large-tree above-ground (AG) woody carbon (C) stocks against soil clay content fitted at the 90th percentile, and b) an ordinary-least-squares linear regression of grass biomass against soil clay content. A *P*-value < 0.05 indicates a significant linear correlation at the 95 % confidence interval.

Discussion

In this study we asked how do C stocks in soils and vegetation vary across miombo woodland landscapes, and to what degree and at what scales were C stocks linked? A conceptual model, based on our results, illustrates and summarises the relationships found between C stocks in soil and vegetation and their distribution patterns in a miombo woodland landscape (Fig. 6). A similar study conducted in a mountainous forest landscape in Japan (Li et al. 2010) also found positive correlations of soil C stocks with aboveground vegetation, and negative correlations

between soil C stocks and elevation and slope. Similar patterns were found in a shortgrass steppe landscape in Colorado (Hook and Burke 2000) and in a subtropical savanna in Texas (Liu et al. 2010), which were linked to soil textural patterns. However, these studies found greater amounts of vegetation at lower elevation on fine textured soils, in contrast to this study. In a high-elevation Norway spruce forest in Germany, no links between soil C and vegetation were found (Spielvogel et al. 2009), and in a subtropical forest in Puerto Rico (Johnson et al. 2011) positive correlations with soil C stocks and elevation were found. The contrasts between these studies suggest that ecological mechanisms controlling spatial distributions of soil and vegetation C stocks are site specific. Our results largely support our hypotheses, but we cannot assess causality or explain what the underlying mechanisms are which give rise to the distribution patterns in miombo woodland. The underlying mechanisms which could be controlling the observed distribution patterns will be discussed in context of our key findings.

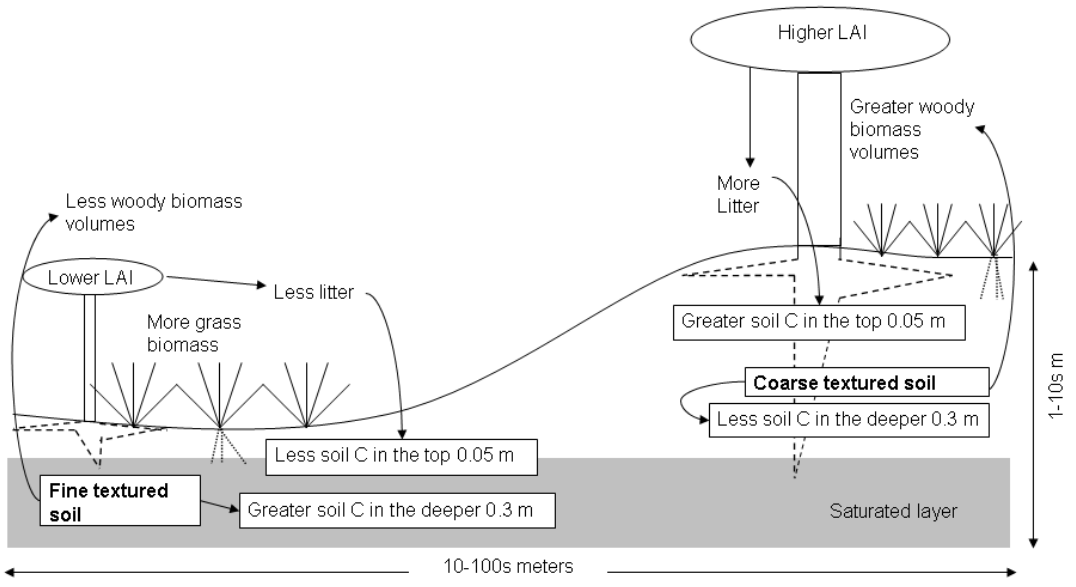

Fig. 6: A conceptual model of carbon stock distributions and the links between them in a miombo woodland landscape.

Variation in soil texture

Areas along the transect that were low lying, concave, and/or shallow sloped were areas where dambo grassland tended to occur, which have high soil clay content (von der Heyden 2004). Qualitative observations of typical sites for dambos were made by Tinley (1977; 1982), who describes the catena sequences of free draining hill soils and the hydromorphic gley soils of the bottomland dambos in the Gorongosa Park area. In a recent review on dambos (von der Heyden 2004) two theories for the reason why dambos have higher soil clay content as compared to the generally deeply weathered freely draining interfluves are discussed. The first ascribes the higher soil clay content of dambos to transportational sorting where sodic soils deflocculate clay particles, which are then transported down slope to the low lying areas where they accumulate due to impeded drainage (Whitlow 1985). The second ascribes higher clay content in dambos to an *in situ* weathering process, where advanced bedrock weathering has occurred in dambos as compared to the interfluves due to differing bedrock geology (McFarlane 1989). Which of these processes governs the spatial patterning of soil clay content observed in this study is unclear, as information on the chemical properties of the soils and underlying geology were not assessed. However, there is a clear link between topography and soil textural distributions, creating clay rich dambos in low relief depressions and well drained coarser textured soils on the ridges and mounds.

Linking woody biomass to soil texture

The role of belowground processes in determining the distribution and composition of savanna vegetation has not been extensively studied, particularly soil textural differences are not a well established determinant of savanna structure

(Furley 2010). On a landscape scale, soil moisture related to a topographic index has been seen to influence savanna vegetation distribution (Reed et al. 2009). Others argue that soil moisture balance controlled by pan horizons is the most important factor in determining vegetation patterns (Tinley 1982). The results found here strongly suggest that distribution of woody biomass in miombo woodland is linked to elevation (Fig. 4 a) and is constrained to an upper limit by soil clay content (Fig. 5 a). However, there was large variability below the soil texture-controlled upper bound, indicating that other factors could be interacting to reduce woody biomass below the threshold. The link between soil texture and woody tree cover is complex. Some studies in African savanna find that fine textured soils support more tree cover (Bucini and Hanan 2007; Groen et al. 2008), while studies in miombo woodland find seemingly opposite relationships (Chidumayo 1997; Frost 1996). Campbell *et al.* (1995) found that some of the miombo woody vegetation spatial heterogeneity correlated to permeability and nutrient content of the soils, with more open woodlands found in less permeable nutrient poor sites.

It is still unclear why miombo trees prefer well drained coarse soils, but several explanations are possible. The first such explanation is that fine textured soil sites along the transect were predominantly classified as dambos, which become seasonally waterlogged due to higher soil water retention capacities and impermeable horizons creating perched water tables (von der Heyden 2004). Inundated soils would inhibit tree growth during the wet season, limiting woody biomass distributions to better drained sites (Tinley 1982). A second explanation is that of the root niche separation hypothesis (Walter 1971). Very little information is available on miombo tree species rooting structures, but it has been observed that they have

very deep tap roots which can extend several meters down (Timberlake and Calvert 1993), giving miombo trees a competitive advantage over co-existing grasses for deep soil water (Fig. 6). Empirical evidence for the root niche separation hypothesis has been found in Brazilian cerrado savanna (Rossatto et al. 2012), where vegetation structure was linked to the depth of water uptake in woody plants along a topographic gradient. However, water may not be the primary root niche axis and other resources such as nitrogen and phosphorus can cause competitive interactions (February and Higgins 2010; Hogberg 1986). Other factors such as simple light competition may also explain the tree-grass distribution patterns (Scholes and Archer 1997), although this would only account for grass distributions and not for trees.

The de-coupling between woody biomass and grass biomass distributions could be further exacerbated by the impacts of fire and fire feedbacks in response to fuel load. Woodlands are amongst the most frequently burnt ecosystems and at local scales the frequency and intensity of fire can alter vegetation structure (Ryan and Williams 2011). Sites that have greater fuel loads in the form of grass biomass and litter are more likely to have high intensity fires, increasing tree top-kill rates (Ryan and Williams 2011), further encouraging grass growth creating a strong negative feedback loop between grasses and trees (see Frost (1996): p.54). It seems that any one mechanism, be it competition-based or disturbance-based, cannot explain the vegetation patterns observed in miombo woodland and it is more likely that a combination of factors interact to determine vegetation cover.

Coupled soil and vegetation carbon stocks

Several studies in savanna and woodland ecosystems found that spatial variability in vegetation was a key component in determining top-soil C variability

(Bird et al. 2000; Jobbagy and Jackson 2000; Rossi et al. 2009; Wang et al. 2009). The spatial distributions of $soil_5$ C was strongly influenced by vegetation cover, (Table 3) and similar ranges of autocorrelation were found between $soil_5$ C and total litter at the small spatial extent (Table 2). Top-soil C was not correlated to grass biomass, suggesting that woody biomass inputs contribute more to the top-soil C pool than grass biomass does. Similar results were found by Wang *et al.* (2009) in a miombo woodland site in western Zambia where ~90 % of top-soil C was derived from C_3 vegetation. The spatial distribution of deeper $soil_{30}$ C stores showed no correlations to vegetation, but was strongly influenced by soil clay content (Fig. 4 d), and top-soil C (0-5 cm) and deep-soil C (0-30 cm) content were de-coupled at the landscape scale (Table 3). Texture of soil is also an important factor in determining soil carbon content; higher clay and silt content are associated with higher soil C storage capacities in tropical soils (Feller and Beare 1997). Jobbagy and Jackson (2000) similarly found, using a global dataset, that surface soil C was influenced by climate and vegetation, whereas deeper soil C was more strongly influenced by soil physical properties.

The history of fire occurrence is likely to de-couple soil C in the surface layers and soil C in the deeper layers. When a fire occurs the immediate effects include loss of soil C in the top few centimetres to the atmosphere (Bird et al. 2000). Furthermore, fire accelerates the incorporation of fine particulate organic matter to the soil C pool where fine minerals (i.e. clay) can chemically stabilise and physically protect particulate carbon from decomposition (Bird et al. 2000). Therefore, occurrence of fire will de-couple the surface soil C stocks from the deeper soil C stocks by inducing surface soil C loss at the same time as increasing fine particulate

C deposition, which is more effectively stored in fine textured soils. Fire and fire feedbacks could be an important factor in explaining the observed distribution patterns of soil C stocks, where areas with fine textured soils and greater grass biomass had lower top soil C but more soil C in the deeper layers as compared to higher elevation low grass biomass sites (Fig. 6).

Implications for measuring C stocks

Sampling woody biomass C stocks

The geographical spatial variability of AG C was largely dependent on the spatial granularity of measurement. When total AG C stocks were divided into small (DBH< 30 cm) and large (DBH> 30 cm) trees we found that 70 % of total AG C was stored in large-trees and only 30 % was stored in small-trees (Table 1). The smaller plots (0.03 ha) were ineffective at sampling total AG C stocks, as the large-trees with the majority of AG C were not sampled optimally. The results of this study highlight the importance of considering the spatial structure of stem distributions when sampling total AG C stocks in miombo woodland, and plot size is an important factor to consider. The geographical scales of autocorrelation found show that plots that are > 0.5 ha in size should be separated at distances >1426 m to avoid autocorrelation between sample plots. However, the range of autocorrelation found at the large spatial extent scale describe the spatial variability of the patches of woodland seen on satellite imagery (Fig. 1), and are most likely reflecting the periodicity of elevation sampled along the transect (~1500 m) caused by the close correlation found between large-tree AG C and elevation. If smaller sample plots are utilised, the geographical

scales of autocorrelation are reduced significantly, and greater sampling effort is needed to get satisfactory low error estimates.

Sampling soil C stocks

Previous studies have not found any normal or log normal distributions of soil C in miombo woodland and show large variability (Williams et al. 2008), most likely due small sample sizes and the use of random sampling techniques, which yield large variability when soil C varies significantly at short geographical spatial scales. The short geographical scales of autocorrelation reported here, similar to those of Rossi *et al*. (2009), can be used to design optimal sampling strategies in future studies of soil C stocks in miombo woodland. Studies that are designed to compare soil C stocks of several locations that have experienced change should consider that at separation distances greater than 14 m or 26 m, depending on depth sampled, the two samples are no longer correlated spatially and might result in erroneous change detection between sites. If on the other hand a study wishes to sample an area to obtain average soil C stocks, then separation distances between samples should exceed 14 m or 26 m to avoid sampling what can be considered as the same C pool, and to optimise sampling efforts. However, regardless of which strategy is utilised the high spatial variability of soil C make adequate sampling of soil C stocks difficult and will require a large sampling effort to get satisfactory low error estimates (Rossi et al. 2009).

Conclusions

In this study we asked how do C stocks in soils and vegetation vary across a miombo woodland landscape, and to what degree and at what scales are these stocks

linked? We hypothesised that vegetation C stock distributions were linked to soil textural properties, preferring well drained soils, and soil textural distributions would be determined by topography. We also hypothesised that vegetation and soil C stocks would be coupled in the landscape. We tested these hypotheses against a dataset collected along a 5 km transect where vegetation and soil C stocks, litter biomass, leaf-area-index, soil texture, and elevation were sampled. Correlation analyses largely corroborate our hypotheses and shows that spatial distributions of vegetation and soil C stocks in a miombo woodland are linked to topography and soil textural distributions. In particular, large-tree AG C stocks were tightly linked to topography as were soil textural distributions. Further to this, soil textural properties seemed to restrict woody C stocks to an upper limit so that coarser soils were able to support greater woody AG C stocks. Coupling between vegetation and surface soil C stocks was found, but deeper soil C stocks were de-coupled from them both and were more closely coupled to soil clay content. Geostatistical analyses conducted at three spatial scales revealed that soil C stocks varied significantly at metre scales whereas vegetation C stocks varied significantly at kilometer scales, reflecting the patchy heterogeneity of miombo woodland vegetation.

This study is one of the most complete transect studies ever conducted in a natural miombo woodland and provides some of the first quantitative insights into the relationships between C stocks, soil properties, vegetation and topography in miombo woodlands over multiple scales. This information can inform future studies on optimal sampling for C stock assessments. However, this study was not able to assess causation of the observed relationships found between measured variables, and several mechanisms are possible in determining the observed distribution

patterns including tree-grass competition, fire feedbacks and soil formation processes. In particular, more work is needed to understand why miombo woodland trees prefer well drained soils on elevated ground, as a large proportion of their variability was linked to this key finding.

Acknowledgements

The Nhambita community and staff at Envirotrade Ltd. facilitated fieldwork. Meg Coates-Palgrave aided in tree species identification. Gorongosa National Park granted access to the park. The GeoEye Foundation provided the IKONOS image. OASIS provided the SPOT4 image. Emily Woollen is funded by the Natural Environment Research Council by a CASE studentship. We thank the anonymous reviewers for their helpful comments.

References

Bird MI, Veenendaal EM, Moyo C, Lloyd J, Frost P (2000) Effect of fire and soil texture on soil carbon in a sub-humid savanna (Matopos, Zimbabwe). Geoderma 94:71-90

Bombelli A et al. (2009) The sub-saharan Africa carbon balance, an overview. Biogeosciences Discuss. 6:2085-2123

Bond WJ (2008) What Limits Trees in C-4 Grasslands and Savannas? Annual Review of Ecology Evolution and Systematics 39:641-659

Bucini G, Hanan NP (2007) A continental-scale analysis of tree cover in African savannas. Global Ecology and Biogeography 16:593-605

Burrows SN et al. (2002) Application of geostatistics to characterize leaf area index (LAI) from flux tower to landscape scales using a cyclic sampling design. Ecosystems 5:667-679

Campbell BM (1996) The Miombo in Transition: Woodlands and Welfare in Africa. Center for International Forestry Research, Bogor, Indonesia

Campbell BM, Angelsen A, Cunningham A, Katerere Y, Sitoe A, Wunder S (2007) Miombo woodlands - opportunities and barriers to sustainable forest management. Centre for International Forestry Research, Bogor, Indonesia

Campbell BM, Cunliffe RN, Gambizia J (1995) Vegetation structure and small-scale pattern in Miombo woodland, Marondera, Zimbabwe. Bothalia 25:121-126

Chidumayo EN (1997) Miombo Ecology and Management: an Introduction. Intermediate Technology Publications, London

Ciais P et al. (2011) The carbon balance of Africa: synthesis of recent research studies. Philosophical Transactions of the Royal Society a-Mathematical Physical and Engineering Sciences 369:2038-2057

Cressie N (1985) Fitting variogram models by weighted least-squares. Journal of the International Association for Mathematical Geology 17:563-586

Dorgeloh WG (2002) Calibrating a disc pasture meter to estimate above-ground standing biomass in Mixed Bushveld, South Africa. African Journal of Ecology 40:100-102

February EC, Higgins SI (2010) The distribution of tree and grass roots in savannas in relation to soil nitrogen and water. South African Journal of Botany 76:517-523

Feller C, Beare MH (1997) Physical control of soil organic matter dynamics in the tropics. Geoderma 79:69-116

Frazer GW, Canham CD (1999) Gap Light Analyzer (Version 2.0). Simon Fraser University & Institute of Ecosystem Studies, British Columbia & New York

Frost P (1996) The ecology of miombo woodlands. In: Campbell B (ed) The Miombo in Transition: Woodlands and Welfare in Africa. Center for International Forestry Research, Bogor, Indonesia, pp 11-57

Furley P (2010) Tropical savannas: Biomass, plant ecology, and the role of fire and soil on vegetation. Progress in Physical Geography 34:563-585

Groen TA, van Langevelde F, de Vijver C, Govender N, Prins HHT (2008) Soil clay content and fire frequency affect clustering in trees in South African savannas. Journal of Tropical Ecology 24:269-279

Hogberg P (1986) Soil nutrient availability, root symbioses and tree species composition in tropical Africa: a review. Journal of Tropical Ecology 2:359-372

Hook PB, Burke IC (2000) Biogeochemistry in a shortgrass landscape: Control by topography, soil texture, and microclimate. Ecology 81:2686-2703

IPCC (2007) Fourth Assessment Report: Climate Change 2007 (AR4). Geneva, Switzerland

Jarque CM, Bera AK (1987) A test for normality of observations and regression residuals International Statistical Review 55:163-172

Jeltsch F, Weber GE, Grimm V (2000) Ecological buffering mechanisms in savannas: A unifying theory of long-term tree-grass coexistence. Plant Ecology 150:161-171

Jobbagy EG, Jackson RB (2000) The vertical distribution of soil organic carbon and its relation to climate and vegetation. Ecological Applications 10:423-436

Johnson KD, Scatena FN, Silver WL (2011) Atypical soil carbon distribution across a tropical steepland forest catena. Catena 87:391-397

Koenker R (2011) Quantile regression. CRAN (http://cran.r-project.org/web/packages/quantreg/index.html)

Li P, Wang Q, Endo T, Zhao X, Kakubari Y (2010) Soil organic carbon stock is closely related to aboveground vegetation properties in cold-temperate mountainous forests. Geoderma 154:407-415

Liu F, Wu XB, Bai E, Boutton TW, Archer SR (2010) Spatial scaling of ecosystem C and N in a subtropical savanna landscape. Global Change Biology 16:2213-2223

Matheron G (1965) Les variables régionalisées et leur estimation. Universite de Paris, Masson, Paris, p 305

MathWorks (2007) Matlab (Version 7.4). The MathWorks Inc., Natick, MA.

McFarlane MJ (1989) Dambos–their characteristics and geomorphological evolution in parts of Malawi and Zimbabwe, with particular reference to their role in the hydrogeological regime of surviving areas of African surface. In: Proceedings of the groundwater exploration and development in crystalline basement aquifers workshop, Commonwealth Science Council Technical Paper 273 vol. 1. Commonwealth Science Council, Harare, pp 254-302

Quinn GP, Keough MJ (2002) Experimental Design and Data Analysis for Biologists. Cambridge University Press, Cambridge

Reed DN, Anderson TM, Dempewolf J, Metzger K, Serneels S (2009) The spatial distribution of vegetation types in the Serengeti ecosystem: the influence of rainfall and topographic relief on vegetation patch characteristics. Journal of Biogeography 36:770-782

Rossatto DR, Silva LDR, Villalobos-Vega R, Sternberg LDL, Franco AC (2012) Depth of water uptake in woody plants relates to groundwater level and vegetation structure along a topographic gradient in a neotropical savanna. Environmental and Experimental Botany 77:259-266

Rossi J et al. (2009) Spatial structures of soil organic carbon in tropical forests-A case study of Southeastern Tanzania. Catena 77:19-27

Ryan CM (2009) Carbon Cycling, Fire and Phenology in a Tropical Savanna Woodland in Nhambita, Mozambique. PhD thesis, School of GeoSciences, The University of Edinburgh, Edinburgh

Ryan CM, Williams M (2011) How does fire intensity and frequency affect miombo woodland tree populations and biomass? Ecological Applications 21:48-60

Ryan CM, Williams M, Grace J (2011) Above- and belowground carbon stocks in a miombo woodland landscape of Mozambique. Biotropica 43:423-432

Sankaran M, Ratnam J, Hanan NP (2004) Tree-grass coexistence in savannas revisited - insights from an examination of assumptions and mechanisms invoked in existing models. Ecology Letters 7:480-490

Scholes RJ, Archer SR (1997) Tree-grass interactions in savannas. Annual Review of Ecology and Systematics 28:517-544

Schwanghart W (2010) Variogramfit. Mathworks Inc. (http://www.mathworks.co.uk/matlabcentral/fileexchange/25948-variogramfit)

Spielvogel S, Prietzel J, Auerswald K, Koegel-Knabner I (2009) Site-specific spatial patterns of soil organic carbon stocks in different landscape units of a high-elevation forest including a site with forest dieback. Geoderma 152:218-230

Timberlake JR, Calvert GM (1993) Preliminary Root Atlast for Zimbabwe and Zambia. Zimbabwe Bulletin of Forestry Research

Tinley KL (1977) Framework of the Gorongosa Ecosystem. PhD thesis, Faculty of Science, University of Pretoria, Pretoria

Tinley KL (1982) The Influence of Soil Moisture Balance on Ecosystem Patterns in Southern Africa. In: Huntley BJ, Walker BH (eds) Ecology of Tropical Savannas. Springer-Verlag, Berlin, pp 175-192

von der Heyden CJ (2004) The hydrology and hydrogeology of dambos: a review. Progress in Physical Geography 28:544-564

Walter H (1971) Ecology of Tropical and Subtropical Vegetation. Oliver and Boyd, Edinburgh, UK

Wang LX, Okin GS, Caylor KK, Macko SA (2009) Spatial heterogeneity and sources of soil carbon in southern African savannas. Geoderma 149:402-408

Webster R, Oliver MA (2001) Geostatistics for Environmental Scientists. John Wiley & Sons Ltd., Chichester

White F (1983) The Vegetation of Africa: a descriptive memoir to accompany the Unesco/AETFAT/UNSO vegetation map of Africa. UNESCO, Paris

Whitlow JR (1985) Dambos in Zimbabwe: a review. Zeitschrift fur Geomorphologie Supplementbande 52:115-146

Whittaker RJ, Willis KJ, Field R (2001) Scale and species richness: towards a general, hierarchical theory of species diversity. Journal of Biogeography 28:453-470

Williams M, Ryan CM, Rees RM, Sambane E, Fernando J, Grace J (2008) Carbon sequestration and biodiversity of re-growing miombo woodlands in Mozambique. Forest Ecology and Management 254:145-155

3b. Carbon stocks in an African woodland landscape: spatial distributions and scales of variation - supplementary material

E. Woollen[1], C. M. Ryan[1] and M. Williams[1]

[1] School of GeoSciences, The University of Edinburgh, Edinburgh EH9 3JN, UK

Details of methods used

Soil sampling and analysis

Within each 1 m^2 quadrat (n = 150), four surface soil cores of the top 0-5 cm (volume of 63 cm^3 each) were collected and combined to make one composite sample, and one soil core of the 0-30 cm (volume of 377 cm^3) was extracted. All soil samples were dried in an oven at 60-70 °C until constant weight. Dry weights and fresh volumes were used in bulk density calculations. The dry soil samples were then sub-sampled using a riffle splitter box, which splits the soil samples evenly avoiding bias.

Soil texture was analysed for each of the $soil_{30}$ samples taken in the centre of each of the circular 314 m^2 plots (n = 90). The $soil_{30}$ samples were sieved to < 2 mm, and a 0.30 g sub-sample was suspended in a 4 % sodium hexametaphosphate solution for 24 hours and then put in a sonic bath for 10 minutes to dissolve aggregates. The dissolved samples were analysed for percentage by volume of particle sizes (clay < 0.002 mm diameter; silt 0.002 mm < diameter < 0.05 mm; sand 0.05 mm < diameter < 2 mm) using a Beckman Coulter LS Particle Size Analyser. Soil texture was not analysed for all $soil_5$ samples, as mean clay content within the first 18 cycles was not significantly different between the two depths (two-way ANOVA, d.f. = 1 depth, F = 3.41 depth, P > 0.05 depth). Therefore, soil texture from the $soil_{30}$ samples were considered representative of soil texture in the top 0-5 cm interval and any referral to soil texture henceforth refers to the $soil_{30}$ samples.

All sieved (< 2 mm) $soil_5$ and $soil_{30}$ samples (n = 150 each) were ball-milled to a fine powder and analysed in a Carbo-Erba/400 automated CN analyser to give %

C measurements for each sample. Total soil carbon on an area basis was calculated for the two depth profiles, 0-5 cm and 0-30 cm depths:

$$Total\ soil\ C\left(Mg\ area^{-1}\right) = B_D C_{\%} dKG \qquad \text{Eq. 1}$$

where B_D is bulk density (g cm^{-3}), $C_{\%}$ is percent total carbon, d is depth (m), K is a scaling factor (in this case 100 to get per hectare values), and G is the fraction of the soil which was < 2 mm (i.e. not gravel). For G, a mean soil fraction determined from permanent sample plots of 0.8 and 0.78 for the top 5 and 30 cm respectively (Ryan et al. 2011) were used to correct for the presence of gravel to avoid overestimation of soil C stocks. The gravel fraction did not contain any organic C, as the gravel fraction in the study area consists mainly of quartz minerals. Tests for mineral soil C in the < 2 mm fraction, by dilution in weak (10 %) hydrochloric acid, did not indicate that mineral C was present. Therefore, in this paper we consider total soil C and soil organic C to be similar, and terms will be used interchangeably.

Litter biomass

All the litter lying within the 1 m^2 quadrats (n = 150) was collected and fresh weights determined. A small sub-sample of litter from each plot was dried to constant weight using solar ovens and weighed for determination of dry weight. Total dry litter mass (g m^{-2}) was estimated for each plot based on the percentage moisture lost from the sub-samples.

Above-ground woody C stocks

Within each 0.03 ha circular plot (n = 90) all standing woody stems >5 cm diameter-at-breast-height (DBH), measured at 1.3 m from the ground, were recorded. Large trees (i.e. DBH > 30 cm) were additionally recorded within each 0.57 ha RER plot (n = 30). Small trees (5 < DBH < 30 cm) were not recorded in the area outside of the 0.03 ha circle plots. On all trees forking below 1.3 m from the ground DBH was measured on each stem separately. Any stems that were dead or cut were noted and excluded from biomass calculations.

Leaf area index

LAI measurements were taken in the centre of each 0.03 ha plot (n = 90) using a digital camera (Nikon Coolpix 4500) with a fisheye lens, mounted on a levelled tripod at 1.6 m height from the ground. All LAI images were processed using Gap-Light-Analyser software (Frazer and Canham 1999) to calculate LAI for each image. Errors due to sun glare were present in most of the images, as it was not possible to take measurements at an optimal time when the sun was below the horizon or behind a cloud. Errors due to glare from the sun were minimised where possible by visually adjusting the image to mask out sun glare.

Elevation

Elevation was measured continuously using a GPS with a barometric altimeter to measure altitude, apart from two days when power sources were exhausted. The elevation of all sample locations (n = 150) was based on track points nearest to them, as seen on GIS software. In addition, averaged waypoints recorded at each cycle start

whilst in the field increased elevation accuracy by averaging several hundred measurements over time in the same location.

Grass biomass

Grass biomass was measured by using a disc-pasture-meter (Dorgeloh 2002), which was calibrated in the Nhambita area prior to use. Above-ground grass biomass was measured between the cycle start and the last $1m^2$ quadrat within each cycle (75 m length), at intervals of 4 meters. Each measurement was used to calculate dry grass biomass ($g\ m^{-2}$) using a linear calibration curve derived from data collected by Ryan (2009) ($n = 68$, $r^2 = 0.48$). The measurements were used to calculate a mean above-ground dry grass biomass measurement within each cycle. Logistical constraints meant that grass biomass measurements were only taken in cycles 19 to 30 ($n = 12$), limiting its inclusion in geostatistical analyses.

Figures

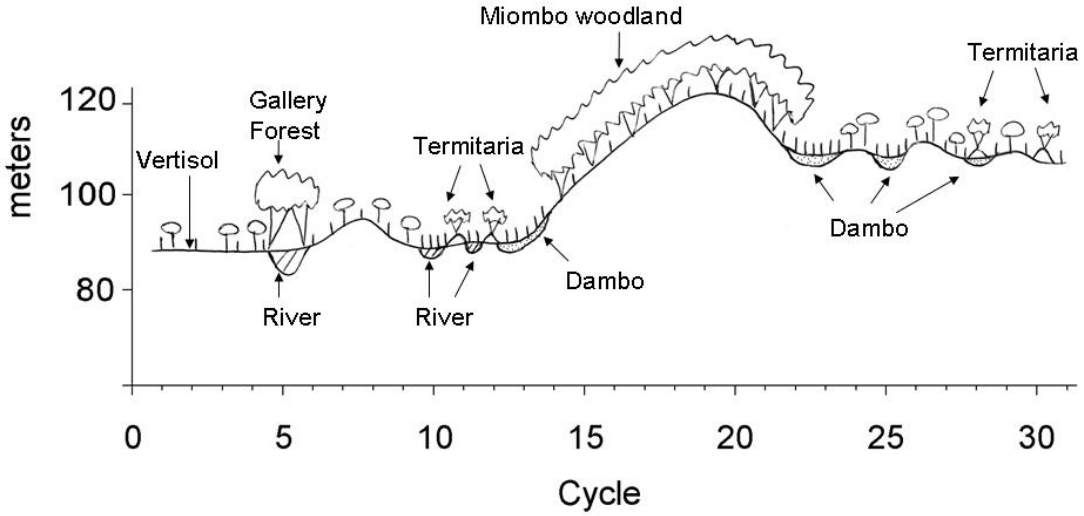

Fig. S1: Graphical representation of the transect characteristics. Approximate elevation is indicated on the y-axis.

4. Spatial modelling of areas at risk of deforestation and degradation using a simple rule-based approach: a case study in central Mozambique

E. Woollen[1], M. Williams[1], C. M. Ryan[1], R. Tipper[2]

[1] School of GeoSciences, The University of Edinburgh, Edinburgh EH9 3JN, UK

[2] Ecometrica, Unit 3B, Kittle Yards, Edinburgh EH9 1PJ, UK

(intended for submission to Carbon Balance and Management)

Abstract

Terrestrial woody biomass is a significant store of global carbon stocks and sequesters carbon dioxide from the atmosphere. However, the sink strength of the land surface is offset by a large but uncertain flux of carbon to the atmosphere from land use change, mainly caused by tropical deforestation driven by agricultural expansion. Land use change in Africa is mainly driven by small-scale agricultural expansion and wood fuel extraction, with millions of hectares deforested every year, resulting in significant carbon losses to the atmosphere. To support resource management efforts, models can predict the locations and quantities of forest loss. However, there is a trade-off for models between complexity and transparency, comprehension and credibility. The objective of this study was to develop and test a simple rule-based model based on the hypothesis that if land is accessible, cultivable, has extractable value and is unprotected (the ACEU hypothesis), it will be at high risk of deforestation and degradation. The ACEU method provides a relatively simple model without large data requirements that can be adapted to specific locations. By using geographic information system techniques we applied the model in a spatial context for a study site in central Mozambique, and produce a risk map of areas more likely to be affected by deforestation and degradation processes. We tested our model assumptions and compared our results to measured biomass changes using a time series of remotely sensed biomass maps over a three year period. We found that the model was able to accurately predict the areas at high risk of deforestation and degradation, but was less able to predict the quantity of biomass lost. We found that roads were the major axis of forest loss and that biomass resources have been degraded at an unsustainable rate in the study region. The risk

maps created from this method are useful for targeting policy and management efforts to areas at high risk of forest loss in the near future.

Key words: risk mapping, miombo woodland, deforestation, degradation, Mozambique, spatial modelling, above-ground biomass.

Introduction

Terrestrial woody biomass plays a significant role in the global carbon (C) cycle by sequestering and storing carbon dioxide from the atmosphere (Le Quere et al. 2009), and provides essential resources for human consumption (Imhoff et al. 2004). However, a flux of C to the atmosphere from land use/cover change (LUCC) offsets part of the sink strength of global forests (Le Quere et al. 2009), attributed largely to tropical deforestation (Baccini et al. 2012; DeFries et al. 2002), though with large uncertainties (Houghton 2010; Houghton et al. 2009). Deforestation is a spatially complex issue caused by many factors, created by human activities and social processes (Geist and Lambin 2002). Deforestation in the tropics has largely been driven by agricultural expansion and increased agricultural trade (DeFries et al. 2010; Geist and Lambin 2002). In Africa agricultural expansion associated with subsistence or smallholder agriculture is increasing (Houghton and Hackler 2006), and wood extraction for fuel, timber and charcoal drive deforestation (Ahrends et al. 2010; Luoga et al. 2005). Deforestation rates for Africa as a whole were estimated as 1.3 million ha $year^{-1}$, resulting in a release of 0.14 Pg C $year^{-1}$ in the 1990's (DeFries et al. 2002) . However, Africa differs from other tropical regions in that increased agricultural expansion and wood extraction is largely for domestic use to supply an

increasing demand from rapidly growing urban populations, rather than for export (DeFries et al. 2010; Fisher 2010).

Over the last few decades large efforts to produce dynamic spatially explicit models to predict and project rates and locations of deforestation have been developed (Agarwal et al. 2005; Lambin 1997; Mas et al. 2004; Mertens and Lambin 1997; Sloan and Pelletier 2012; Soares et al. 2006; Wassenaar et al. 2007). Spatial modelling of deforestation has several advantages: 1) it allows a deeper understanding of the drivers of deforestation, 2) can generate spatial predictions and rates of deforestation, and 3) it can support appropriate management and policy responses (Lambin 1997). However, due to the complex nature of deforestation with its many causal factors (Geist and Lambin 2002), spatial models of deforestation tend to be complex and require large spatial datasets, though with limits to their predictive power and accuracy (Angelsen and Kaimowitz 1999; Sloan and Pelletier 2012). It is not always practical to produce highly complex models of LUCC and deforestation if sufficient data and expertise are lacking, and a simpler approach to spatial modelling of forest-cover change might be preferable for greater transparency, comprehension and credibility. Simpler spatial models using geographic information system analyses, with limited spatial information, have been used effectively to predict the location of areas more susceptible to deforestation pressure in the past (Liu et al. 1993; Mertens and Lambin 1997).

The objective of this study was to develop and test a simple spatial model to estimate risk of deforestation and degradation for a study site in central Mozambique. The model is based on the hypothesis that land areas are at a higher risk of forest loss if the land is easily accessible, suitable for cultivation, has some extractable value

and is unprotected (the ACEU hypothesis) (Grace et al. 2010; Tipper 2008). We test the validity of this hypothesis and the relative importance of each of the four ACEU parameters in explaining the spatial patterns of forest loss occurring at the Mozambican study site.

Using the ACEU framework provides a simple rule-based approach to assessing risk of forest loss, which can theoretically be defined and tailored to any given country or region given that some knowledge of the ACEU parameters is known. Based on our understanding of drivers of deforestation and degradation in our study site in central Mozambique, we assign risk based on the ACEU framework and create a risk map to provide short range projections of the likelihood of biomass loss occurring in defined land areas. We test our risk map against a three year time series of radar derived biomass maps (Ryan et al. 2012), which allows the assessment not only of deforestation but of net biomass change, including degradation and regeneration of woody biomass. We include degradation in our analysis of risk, unlike previous spatial models that deal primarily with deforestation, as forest degradation is a major driver of forest loss in Africa often leading to deforestation (Ahrends et al. 2010).

This study illustrates a novel method of using a simple rule-based approach, with limited spatial data of deforestation and degradation drivers, to create a risk map of land areas more likely to experience forest loss. The methodology tested here is specifically intended for use by forest conservation and management groups that wish to assess risk of forest loss in specific locations in a comprehensive and transparent fashion. We explore the limitations of using this method and test our

assumptions and understanding of the drivers of deforestation and degradation occurring in our study site.

Methods

Study site

The study site covers an area of 1160 km^2 in the Gorongosa and Nhambita districts of Sofala province, central Mozambique (Fig. 1). To the east lies Gorongosa National Park, a protected area, and its associated buffer zone extends up to the east side of the main road connecting Gorongosa town in the north to Inchope and the Beira corridor in the south, a major economic area. The main road (designated EN1) is the only surfaced road in the study area. Several managed avoided-deforestation areas are present outside the national park zone, but some exist inside the park buffer zone. These areas were set up and are maintained by local landowners and Envirotrade, a carbon trading company which supports the conservation and management of existing forests and the planting of new trees to create carbon offsets for the voluntary carbon market, with projects centred around the Nhambita community area (Grace et al. 2010). The Vunduzi river runs from the northeast down to join the Pungue river running west to east. The steepest slopes (>10 ^{o}) mainly occur alongside these large rivers, and the highest elevation (490 m a.s.l.) also occurs to the north and the west of the study site. Moving south and east elevation slowly decreases to a minimum (30-40 m a.s.l.), and the landscape is generally gently undulating with slopes <10^{o} , determined using Shuttle Radar Topography Mission (SRTM) data at a resolution of 90 m (Farr et al. 2007). The vegetation in the area is predominantly classified as miombo woodland with a mean above-ground biomass

(AGB) of 20.7 ± 1.8 Mg C ha^{-1} (Woollen et al. 2012) , but with a gradation from dense woodland on the well drained slopes to the northwest, to more open savanna on the poorly drained valley floor to the southeast (Tinley 1977; Tinley 1982). The area receives 850 ± 269 mm (± SD) mean annual precipitation with strong seasonality in precipitation, with 82 % falling in the wet season between November and March (Ryan 2009).

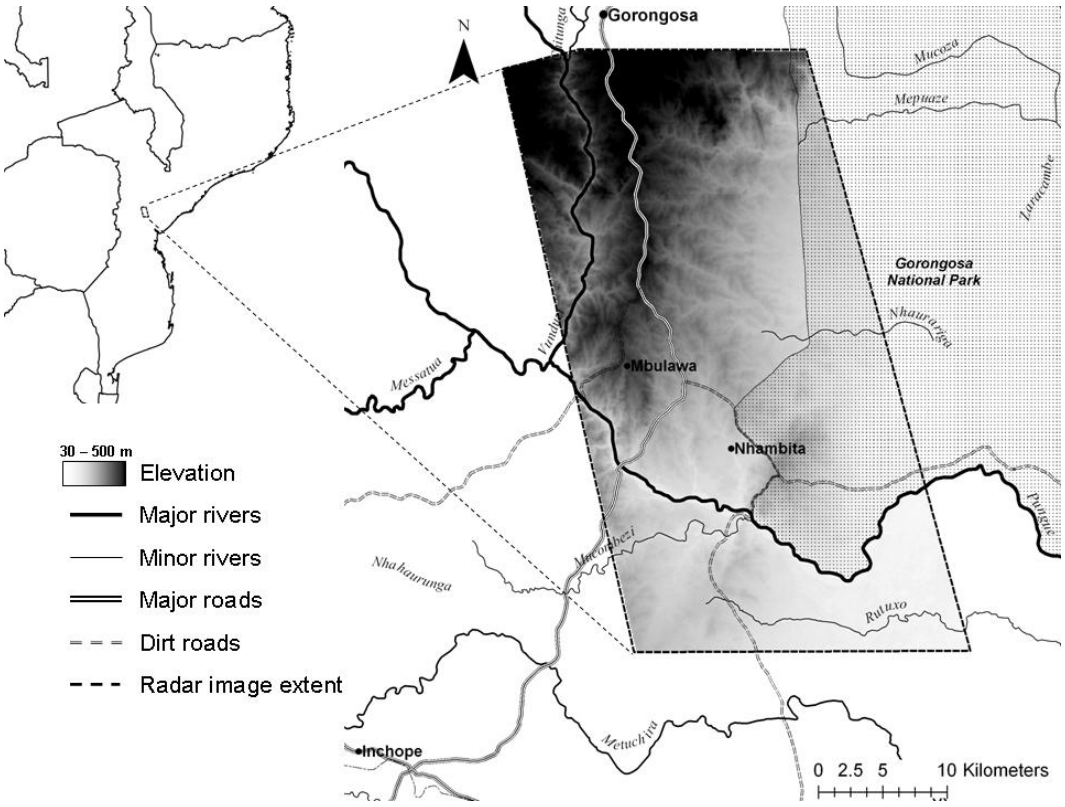

Fig.1: Gorongosa and Nhambita districts in the Sofala province, central Mozambique. The study area is delimited by the radar image extent, covering 1160km^2. Gorongosa is the nearest large town to the north of the image, and the main road (the EN1) links Gorongosa to Inchope and the Beira corridor to the south. Several smaller communities exist, including Mbulawa and Nhambita communities. Vector data courtesy of ARA CENTRO. Elevation data from the Shuttle Radar Topography Mission.

With the end of the Mozambican civil war in 1992, resettlement of the area meant an increase in population. The population of Gorongosa town increased by 50 % from 1997 to 2007, reaching 117,129 inhabitants (INE 2008). During 1999 to 2002 both the main road and the bridge over the Pungue river were re-built, re-

connecting Gorongosa and Nhambita districts to the Beira corridor. There are several smaller communities and settlements in the area, two of which are Nhambita and Mbulawa, with population sizes of a few thousand consisting of scattered homesteads.

The resettlement of people and improved infrastructure has meant the area north of the Pungue is undergoing rapid land-use change, whereas the area south of the Pungue has already largely been deforested (Ryan et al. 2012). The main proximal causes of forest loss are thought to be clearance for small-scale agriculture, and charcoal production. Agriculture is typically shifting cultivation, where areas of ~1 ha are cleared and farmed for a few years until soil fertility decreases, where after they are left fallow. Fire is used for clearing land and for management, and wild fires are a frequent occurrence, where intense and frequent fires can reduce woody biomass significantly (Ryan and Williams 2011). Charcoal production involves the selective logging of tree stems of a preferred size and species, where extraction is concentrated around temporary earthen kilns (Chidumayo 1991; Herd 2007). Charcoal is sold along the EN1 for further transport to Inchope and on to other large urban centres, such as Chimoio and Beira. A smaller amount of charcoal is most likely transported to Gorongosa town, but it is more likely that the people of Gorongosa rely mostly on fire wood for their energy needs.

Study site zonation

In order to map areas at risk, the study area was divided into several discrete zones (Fig. 2). By mapping discrete areas we are able to assign a risk level within each zone, rather than estimate risk as a continuous variable over thousands of grid cells. Using GIS software (ArcGIS 2009) several buffers around Gorongosa town

and the main road were created, based on distance, which were associated with changes in accessibility (A of ACEU) of land (see below for full details of determination of accessibility). Known protected (U of ACEU) areas were overlain onto the distance layers. All areas where slope was > 10^{o}, determined using SRTM data (Farr et al. 2007), were grouped into one zone as very steep slopes were associated with decreased suitability of land for cultivation cultivability (C in ACEU) (see below for further determination of cultivable land). Thereby, a map of discrete zones was created based on unique combinations of overlaid spatial vector data, and each zone was given a unique identifying number (1 to 36) and will be referred to throughout the text. Finally, biomass maps were used to indicate extractable value (E in ACEU) within every zone. This stratified approach simplifies the risk calculation process and negates errors associated with estimating biomass change from radar data on a pixel level, by using mean changes over thousands of pixels rather than single pixel values (Ryan et al. 2012).

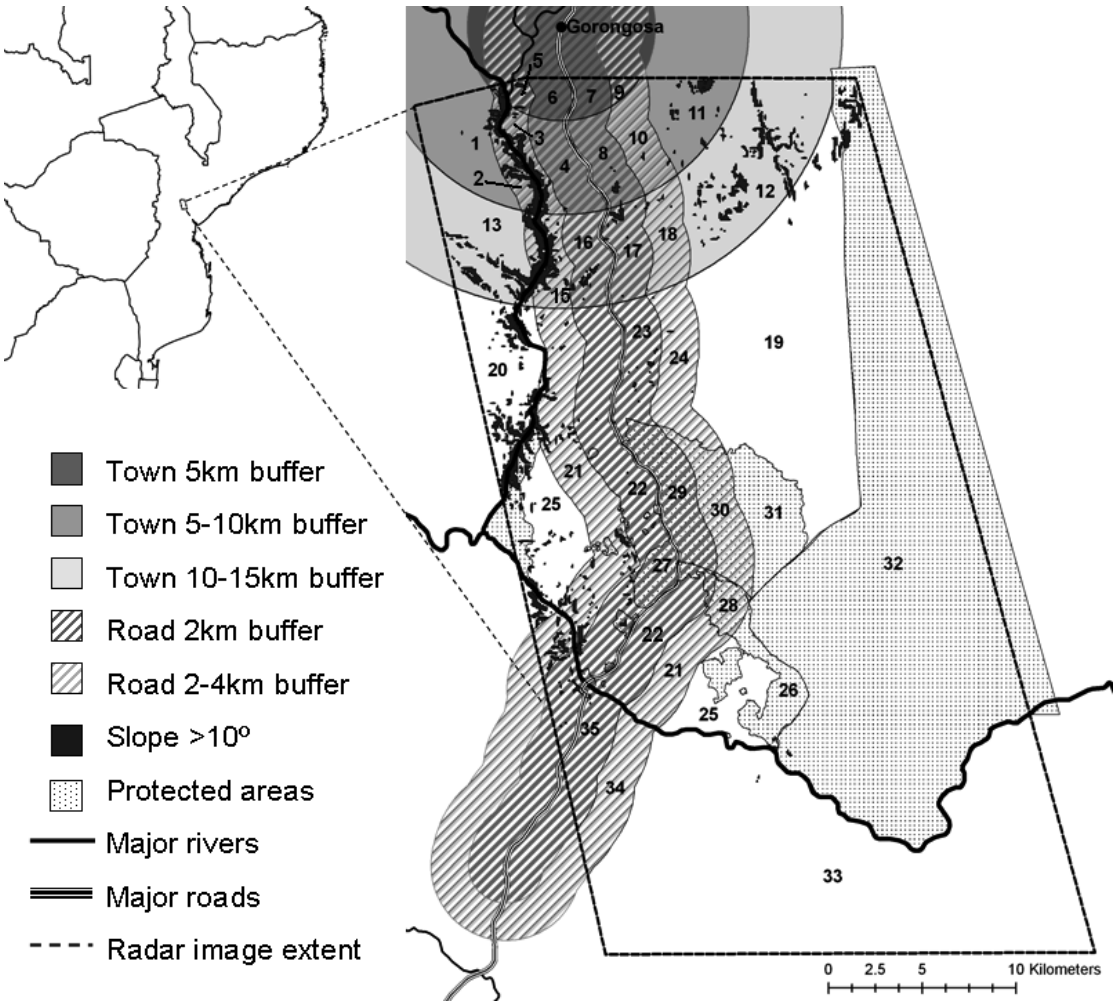

Fig. 2: Map of overlaid spatial vectors of town and road buffers, protected areas, and areas where slope > 10°. Each unique combination of overlaid vectors constitutes an individual zone, labelled 1-36, where zone 36 are all areas where slope was > 10°. Vector data courtesy of ARA CENTRO and Envirotrade Ltd.

Radar biomass maps and biomass change detection

Ten AGB (in units of Mg C ha^{-1}) images were produced from remote sensing data from the phased array L-band synthetic aperture radar sensor aboard the advanced land observing satellite (ALOS PALSAR), spanning the dates 23 June 2007 to 1 October 2010, with a resolution of 25 m for 16 equivalent looks, and calibrated against 96 ground plots. All images were taken in the dry season and two or three images were available for each year. The technical details of the imagery and processing are described in full detail in Ryan et al. (2012). Using GIS software

(ArcGIS 2009) one mean AGB image was produced for 2007 and for 2010, and used in subsequent analyses. The errors associated with the regression analyses used to convert from radar backscatter to aboveground biomass (Ryan et al. 2012) include root-mean-square-error (RMSE) (mean error 9.8 Mg C ha^{-1} for all images) and validation bias (mean absolute bias 1.6 Mg C ha^{-1} for all images). RMSE when propagated over a large number of pixels becomes insignificant, and was therefore disregarded when number of pixels was large (minimum number of pixels per zone was > 2000). The error due to bias was applied as random error through time, despite an indication of temporal correlation. We thereby assume a worst-case-scenario and apply error due to bias to all our change detections to supply a conservative estimate of the probability of mean biomass density in one year being different to that in another year.

To be able to validate the risk map and test our assumptions with measured changes in biomass we used mean AGB density (Mg C ha^{-1}) differences between 2007 and 2010 images within each zone to indicate forest disturbance activities. We do not report changes as a rate per year, as this would assume biomass loss occurs in a linear fashion. Using zonal statistics in GIS software (ArcGIS 2009), mean AGB density values for each zone in each of the two years was calculated. We used Monte Carlo simulations (Manly 2007) to resample the mean AGB density in each year along a distribution of errors, assuming a normal distribution of errors around the mean and a standard deviation equal to the radar bias of 1.6 Mg C ha^{-1}, to get the probability (%) that the mean AGB density in the year 2007 was different to the mean in 2010 (Fig. 3). This resulted in any AGB density change which was ≥ 3.8 Mg

C ha^{-1} having a probability > 95 % of being a 'real' difference in AGB density between 2007 and 2010.

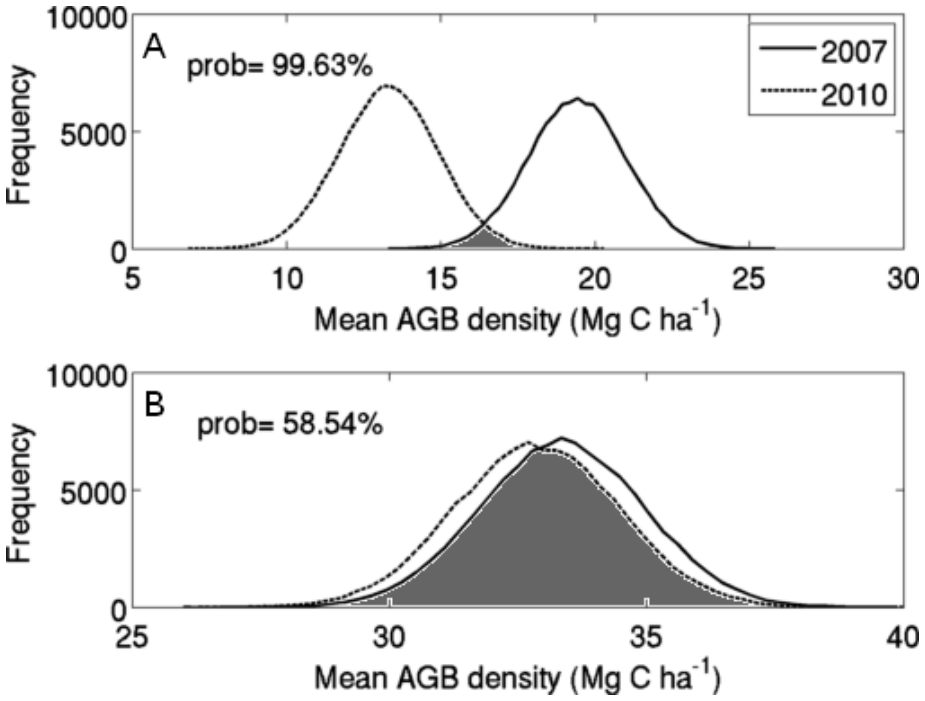

Fig. 3: Example of Monte Carlo re-sampling method of A) zone 22, and B) zone 29 (see Fig. 2). A normal distribution of errors around the mean AGB density in 2007 (solid line) and 2010 (dashed line) with a standard deviation of 1.6 Mg C ha^{-1} was used to test the probability (%) of the change in AGB density detected being real. The greater the overlap (grey area) the lower the probability that the two mean density values for both years were different. The probabilities (%) of the mean densities being different are shown for each case.

Visual comparisons between the risk map and the biomass change map were used to test the accuracy of the ACEU method, and the individual parameter risks, to predict the spatial locations of areas at high risk of biomass loss. To determine how accurate the ACEU method was at predicting biomass loss intensity (Mg C ha^{-1}), a linear correlation between mean AGB density change and the estimated risk level within every zone was assumed. Thereby, we expect biomass loss intensity to increase linearly with increasing risk levels.

Estimating risk of deforestation and degradation

In this study we hypothesise that land areas are at greater risk of deforestation and degradation if they are easily accessible, are suitable for cultivation, have an extractable value, and are unprotected. An overall level of risk is thereby determined as the product of the risks associated with each of the four ACEU parameters:

$$R_i = A_i C_i E_i U_i \qquad \text{(Eq. 1)}$$

where the overall risk level (R) for a defined land area or zone (i) is a function of the risks associated with ease of access (A), suitability for cultivation (C), extractable value (E) and protection status (U) of that zone. Each of the four ACEU parameters are defined and assigned a level of risk as follows:

Access risk (A)

Access was assumed to be related to the proximity to towns and roads. We determine access risk as an exponentially decreasing risk with increasing distance from roads and town centres (Fig. 4). The risk level (a value between 0-1) at a given distance from the road or town centre was thereby determined by assuming an exponentially decreasing risk with increasing distance so that,

$$r_a = e^{-\alpha d} \qquad \text{(Eq. 2)}$$

$$\alpha = \frac{\ln(0.01)}{D} \qquad \text{(Eq. 3)}$$

where access risk (r_a) at a given distance (d, km) from the road or town centre follows a negative exponential function, with a coefficient (α) determined by the distance (D, km) at which risk was assumed to be very low or equal to 0.01. Thereby we only have to estimate one parameter to calculate risk, namely D, and assume an exponential decrease in risk with increasing distance. We calculate access risk as

above with respect to proximity to roads and towns, and use the combined risks of the two to assess total access risk within each zone.

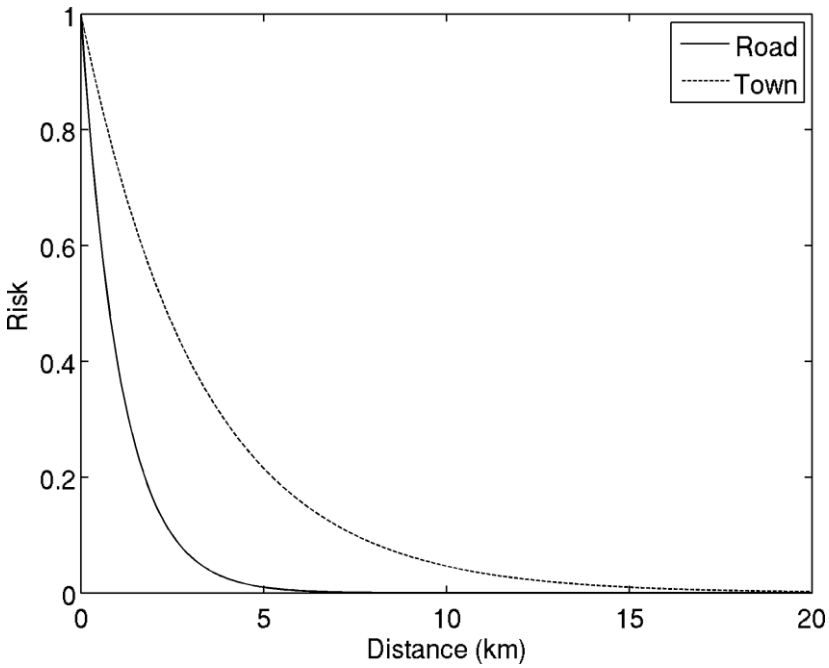

Fig 4: Conceptual model of exponentially decreasing risk with increasing distance from the centre of towns and roads. The conceptual models assume that risk is very low or equal to 0.01 at 5 km distance from roads (solid line), and 15 km distance from Gorongosa town (dashed line).

Access risk with proximity to roads

We assigned an access risk to those roads which were surfaced (i.e the EN1). Unsurfaced roads were ignored as there was no suitable spatial information. Other studies have found that a large proportion of deforestation occurs along roads within a distance of 5 km, with disturbance increasing exponentially with increasing proximity to roads (Jansen et al. 2008; Liu et al. 1993; Mertens and Lambin 1997; Sprague and Oyama 1999). To encompass the area in which most forest disturbance was predicted to occur, two buffer zones were created; an inner buffer zone extending 2 km from the road, and an outer buffer zone extending 4 km from the road (Fig. 2). Access risk, associated with proximity to the road (r_{ar}), was determined

using equations 2 and 3 for each of the two buffers by using the mean distance (d) from the road (i.e. 1 km and 3km, respectively) and a coefficient (α) of -0.92 (if D = 5 km).

Access risk with proximity to towns

To determine the access risk due to proximity to towns, three buffer zones around the centre of Gorongosa town to a maximum distance of 15 km were created (Fig. 2). The smaller towns, such as Nhambita and Mbulawa, were ignored in the analysis of risk associated with proximity to towns, as we did not know enough about the size of the populations or the size of the areas these communities were likely to occupy. The distance (D) at which access risk from Gorongosa town was estimated to be minimal was 15 km (a total area of 707 km^2), as we estimate that the population size of Gorongosa would occupy an area of ~700 km^2 if the population density was similar to that reported by Tabuti et al. (2003) of 170 people km^{-2} for a town of similar population size in Uganda. Furthermore, visual interpretation of deforestation occurring around Gorongosa as seen on Google Earth (Google 2009) confirmed that a maximum distance of 15 km was reasonable. The 15 km buffer around Gorongosa was further divided into three buffer zones, with increments of 5 km from the centre of town, as an estimate of likely distances people were willing to travel on foot on a daily basis for wood fuel extraction and cultivation purposes (Tabuti et al. 2003). Access risk, associated with proximity to towns (r_{at}), was calculated for each buffer using equations 2 and 3, where the mean distance (d) of each buffer from the centre of town (i.e. 2.5, 7.5 and 12.5 km, respectively) and a coefficient (α) of -0.31 (if D = 15 km) was used.

Combined access risk

Total access risk for each defined zone was thereby determined as:

$$A_i = r_{ar} + r_{at} \quad \text{(Eq. 4)}$$

where total access risk (A) within a given zone (i) is the sum of risk due to proximity to roads (r_{ar}) and risk due to proximity to towns (r_{at}) determined for that zone, which was capped at a maximum value of 1. All other areas outside the buffers (i.e. were at least at a distance of 15 km from Gorongosa town and 5 km from roads) were given equal low risk levels of 0.02, as we cannot assume no access occurs outside the buffer zones and therefore assign a uniform low access risk rather than no risk at all.

Cultivation risk (C)

There were no data describing the suitability of land for cultivation based on soil characteristics for the study area. However, a study conducted in the neighbouring province of Manica, to the west of Sofala, found that land cover change was closely related to the land surface slope, where cultivation occurred predominantly on gentle slopes (Jansen et al. 2008). Slope is also related to other relevant factors such as soil erosion, decreased accessibility, and higher input costs for cultivation. Therefore, the slope of the land surface was used as an indicator of the suitability of the land for cultivation.

Using high resolution IKONOS imagery of the study site we delineated visible fields (152 individual fields in total), which were randomly determined throughout the IKONOS imagery but limited to those fields which were distinguishable from the surrounding woody vegetation by their lighter colour and sharp edges, often rectangular in shape. Using SRTM data (Farr et al. 2007), with a resolution of 90 m, we calculated the mean slope within each of the delineated fields

using GIS software (ArcGIS 2009). This analysis yielded a mean slope of 3^{o} with a range of 0-10^{o} for all delineated fields, in close agreement with Jansen et al. (1998). We create a frequency distribution of the number of fields at a given slope, standardising the frequency on the *y*-axis to reflect a risk level of between 0-1 (Fig. 5). A generalized logistic model was fitted to the frequency distribution data:

$$C_i = \frac{1}{1 + e^{b(x_i - m)}} \qquad \text{(Eq. 5)}$$

so that the cultivation risk (*C*) for a given zone (*i*) is a function of the mean slope (*x*) in degrees for that zone. The parameters *b* (value of 4.62) and *m* (value of 0.63) were estimated by optimization methods (Matlab, fminsearch function), minimising the root-mean-square-error (RMSE = 0.40) between measured frequencies and modelled values. Cultivation risk (*C*) is thereby assumed to decrease in a sigmoidal fashion from high risk at low slope angles and low risk at high slope angles (Fig. 5).

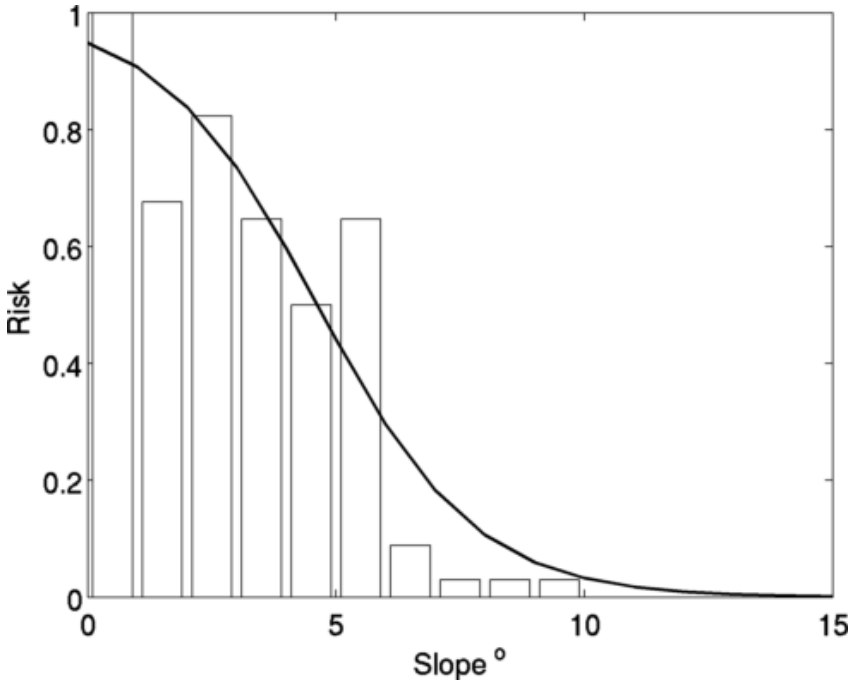

Fig. 5: Standardised frequency (white bars) distribution of the number of cultivated fields with increasing slope of the land surface for the Sofala province, central Mozambique. A generalised logistic model (solid line) fitted to the frequency distribution shows a decreasing risk level with increasing slope angle of the land surface in a sigmoidal fashion.

Extractable value (E)

Charcoal production, timber and construction material extraction involves the selective logging of trees of a preferred size class and species (Ahrends et al. 2010; Chidumayo 1991; Luoga et al. 2002). Wood fuel extraction is primarily collected from dead wood and branches, but some is collected from live trees (Abbot and Homewood 1999; Tabuti et al. 2003). Ideally an indication of extractable value of biomass within every zone would be based on field data of the amount of trees of a desirable size and species for extraction. However, there were no field data available for the whole study area. Therefore, we applied a simple assumption; areas with a greater fraction of land covered by high biomass density will have a higher extractable value. The assumption is that high biomass areas have experienced less extraction and degradation in the past, and therefore still retain high value for extraction. High biomass density was defined as areas with greater than average (i.e. > 20 Mg C ha^{-1}) biomass densities, based on the mean biomass density estimated for a miombo woodland landscape sampled within the study site (Woollen et al. 2012).

To determine the fraction of land covered by high biomass density within every zone we used the radar biomass image for the first year in the time series from 2007. AGB density (Mg C ha^{-1}) measurements for all the pixels within a zone were used to create probability density functions (PDFs) for each individual zone (see for example Fig. 6). The frequencies were standardised so that the area under the curve was equal to 1 (i.e. the total land area of the zone was equal to 1). We apply a threshold at 20 Mg C ha^{-1}, and calculate the area under the curve which is > 20 Mg C ha^{-1}. This fractional area gives an estimate of the extractable value (*E*) from 0-1.

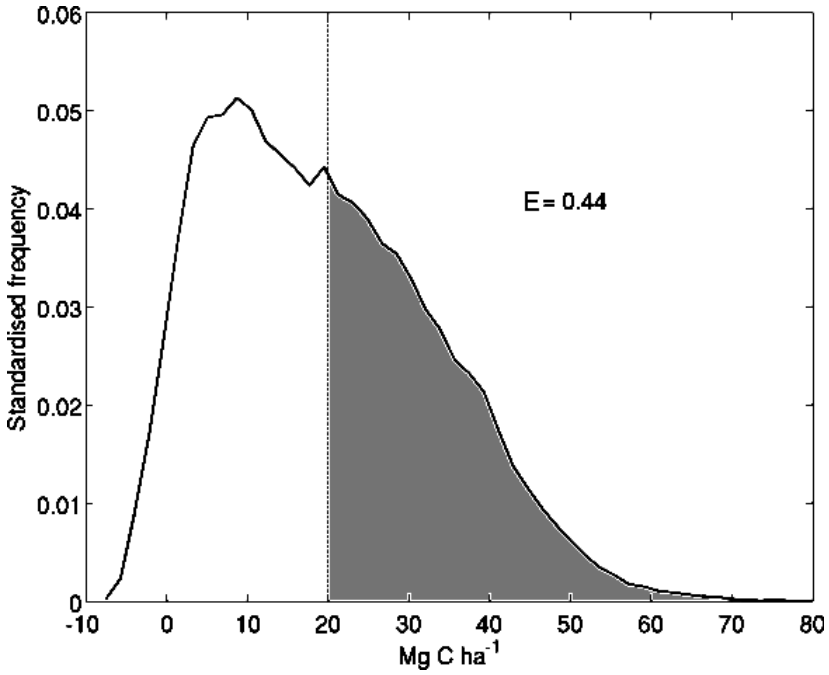

Fig. 6: Probability density function (solid line) of AGB density (Mg C ha^{-1}) of all the pixels in zone number 22 (see Fig. 2). Frequencies are standardised so that the area under the curve is equal to one. Extractable value (*E*) risk was estimated as the area under the curve (grey area) that is above a biomass density threshold of 20 Mg C ha^{-1} (dashed line), i.e. what fraction of the land area has high density biomass, and can be considered as forest/woodland.

Protection status (U)

The Gorongosa national park and several avoided deforestation areas (Fig. 2), set up by the Nhambita Community Carbon Project and established between 2007-2009 (Grace et al. 2010), are managed and protected from deforestation and degradation. The National Park Buffer Zone, extending from the edge of Gorongosa National Park to the east side of the EN1 road, is an area which is managed but not necessarily protected to the same degree as the park. Nhambita community is located inside the buffer zone (Fig. 2), and it is unclear what the perceptions of management are, the extent of policing, and whether perceptions of protection are equally strong throughout the buffer zone. In a similar fashion, areas which are hard to get to due to natural barriers could be considered as 'protected'. However, these areas are difficult to delineate and we have no data on how strong a deterrent any natural barriers such

as rivers might be. Therefore, we made as few assumptions as possible about the management and protection status of land by classing all areas outside of known protected areas as unprotected. The risks associated with the protection status (*U*) are thereby given a risk value of 1 if un-protected, or 0 if protected (Fig.8 U). This assumes that any land outside of clearly defined protected areas is at risk, and that any land which is protected has no risk.

Ranking the risk

In order to visualise the risks associated with each individual zone and how they compare to all other zones within the study area, we ranked the calculated risks from the ACEU model (values between 0-1) to values between 1 to 36 (i.e. the total number of zones). This ranking enhances differences between zones and indicates discrete areas that may be of higher risk than others within a defined study area. Thereby, we assign risk as a qualitative measure on a scale from very high risk (ranking of 31-36), decreasing in steps of 5, to very low risk (ranking of 1-5), creating 7 unique qualitative risk categories.

Results

Observed AGB density change

Large decreases in mean AGB density (probability > 95%) occurred along the main road between 2007 and 2010 in zones 17-18 and 21-23 (see Fig. 2 for zone numbers), with the largest density change (6-7 Mg C ha^{-1}) occurring within 2 km of the main road in zone 22 (Fig. 7). Within the 15 km buffer of Gorongosa town (zones 1-18) large variability in AGB density change occurred, from a possible growth in biomass density in zones 2-3 (probability 50-67 %), to a likely loss of 5-6 Mg C ha^{-1}

in zones 17-18 (probability > 95 %). Moderate to low AGB losses (1-2 and 2-3 Mg C ha^{-1}) occurred elsewhere within the 15 km buffer around Gorongosa.

South of the Pungue river AGB density changes show lower losses south of the river, as compared to their counterparts immediately north of the river (Fig. 7). Zone 35, which was closest to the main road, had the lowest probable AGB losses (1-2 Mg C ha^{-1}) south of the river. The highest likely losses south of the river occurred in zone 34 (3-4 Mg C ha^{-1}), within 2-4 km of the EN1 road. The protected areas (zones 26-32) and the areas with steep slopes (zone 36) show very low probable losses of AGB density and even some growth (-2 to 2 Mg C ha^{-1}, probability 50-81 %). However, there is some indication that protected areas closer to the main road may be experiencing more losses than protected areas further away, though differences are slight and probabilities of an actual change having occurred between years low (50-67 %).

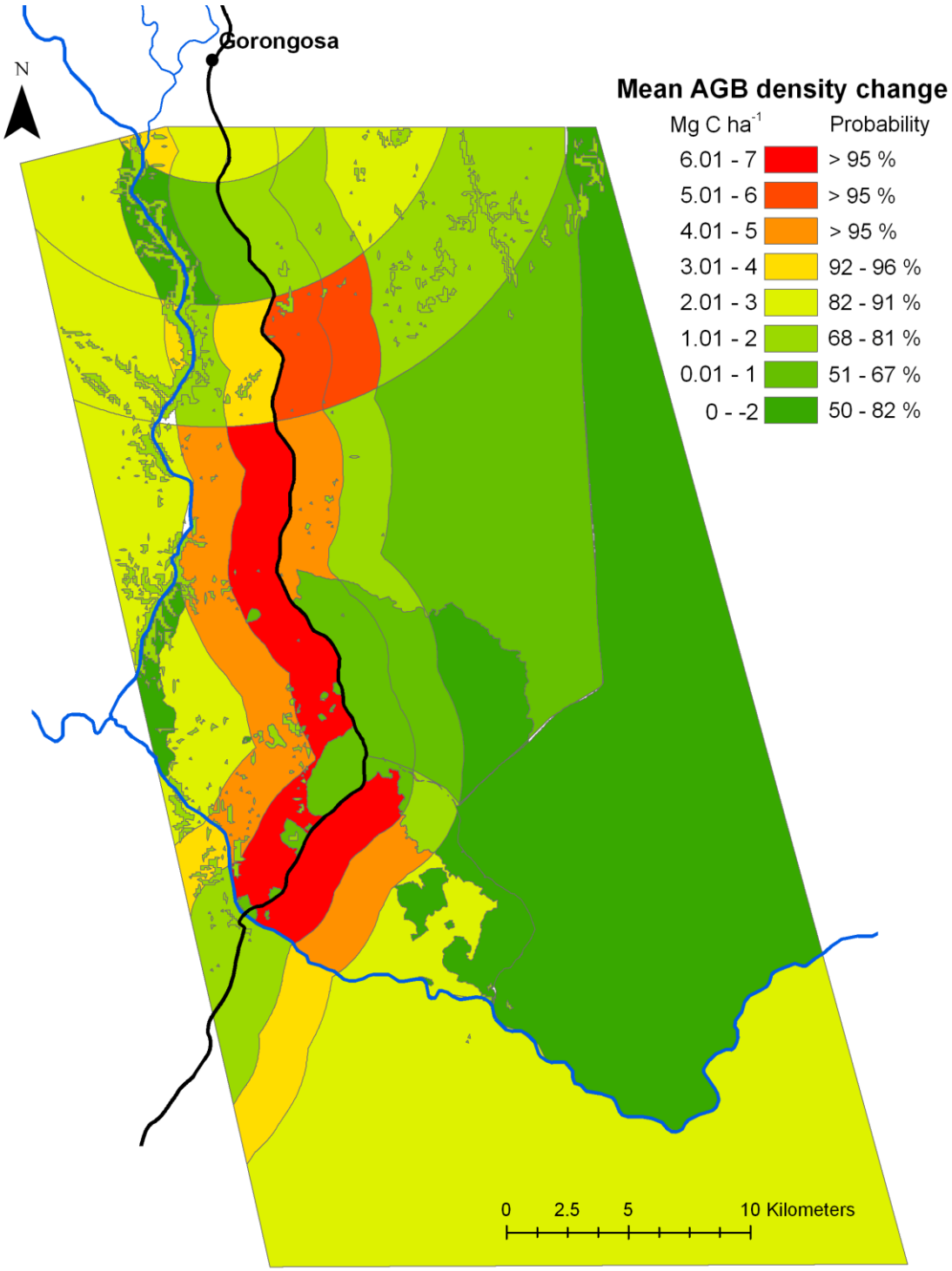

Fig. 7: Measured mean above-ground biomass (AGB) density change (Mg C ha^{-1}) between the year 2007 and 2010, within each of the discrete zones. Positive AGB density changes show a mean loss of biomass, and negative AGB changes show mean growth between years. The probability (%) of the mean AGB density change between years being 'real' (see Fig. 3), is shown for each category of mean AGB density change.

Individual model parameter risk assessment

Each of the four ACEU model parameter estimated risks were mapped individually for a visual assessment of risk associated with each parameter (Fig. 8). As assumed by our model, accessibility increased with proximity to roads and towns (Fig. 8 A). Cultivation risk, based on mean slope of the landscape within each zone, was linked to the topography of the study site where higher risks occurred in the lowland areas to the southeast of the study site and lower risks were associated with the elevated land areas to the northwest and immediately next to the Vunduzi river (Fig. 8 C). Extractable value was lowest around Gorongosa town and south of the Pungue river, indicating greater land use pressure in the past, and highest west of the Vunduzi river and to the east of the EN1 road (Fig. 8 E). Gorongosa National Park had low extractable value most likely due to the natural gradation of lower biomass volumes on lowland areas (Woollen et al. 2012). Known protected areas were assumed to have no risk, whereas all other locations outside of protected areas were un-protected and therefore at risk (Fig. 8 U). Individual model parameter linear regressions showed no significant ($P > 0.05$) correlations between estimated risks and AGB density change (data not shown), and none of the individual ACEU risk maps (Fig. 8) visually matched the spatial patterns of AGB biomass change well (Fig. 7).

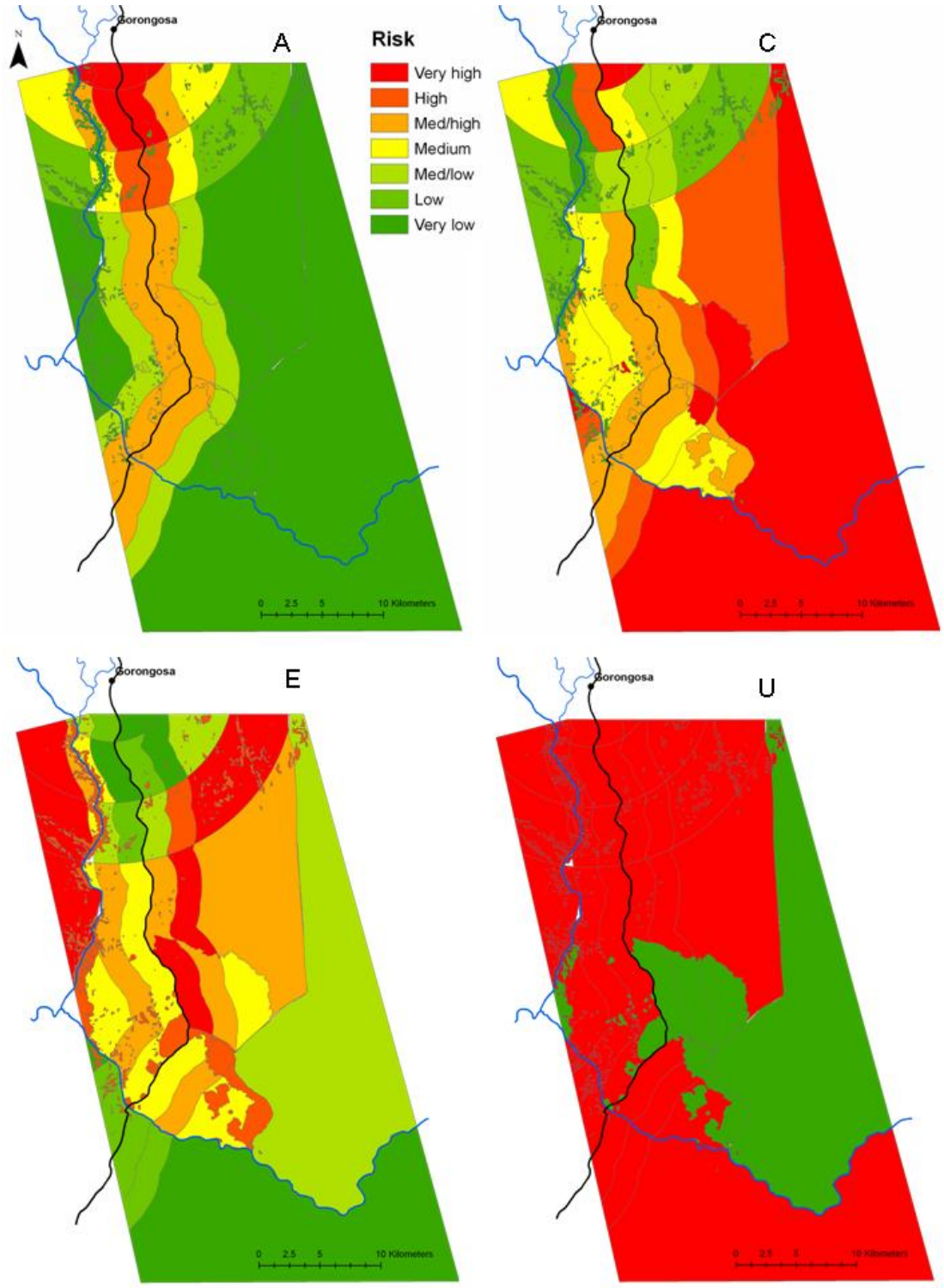

Fig. 8: Estimated risk level associated with each of the four model parameters; A) accessibility risk, C) cultivation risk, E) extractable value and U) protection status. Each zone shows an estimated risk level from very high risk (red) to very low risk (dark green).

Combined ACEU model risk assessment

When each of the ACEU risks are combined (Eq. 1) the resultant estimated risk map (Fig. 9), using qualitative risks, identifies areas that are expected to be at higher risk of deforestation and degradation in our study site. The areas with the highest biomass losses (Fig. 7) were correctly identified as high risk zones in all cases (Fig. 9), although the pattern of risk was not always matching the pattern of AGB changes. For example, a very high risk was assigned to both zones 22 and 23, but lower AGB losses occurred in zone 23 as compared to zone 22.

Several zones were, however, incorrectly assigned a high risk when AGB density change showed medium to low biomass losses. Within the 15 km buffer of Gorongosa town (zones 1-18), the patterns of estimated risks matched well with measured AGB density changes in the outer 10-15 km buffer strip, but the relationship breaks down when within 10 km of Gorongosa. The very high risk zones within 10 km of Gorongosa were estimated to be zones 1 and 5-6. However, measured AGB losses were only moderate in these zones. Zones 2-4 were estimated to have medium/high to high risk, but AGB density showed virtually no changes in biomass in these zones. Zones 23-24 east of the main road were also assigned a high to very high risk level, but AGB density changes were lower than the equivalent high risk zones to the west of the main road, in zones 21-22.

South of the Pungue river risks are generally lower than their counterparts immediately north of the river, but the pattern of observed AGB losses (Fig. 7) were not in agreement with the estimated risk map. A high risk was predicted within 2 km of the road in zone 35, decreasing to low risk with increased distance from the road in zone 33. Zone 35, however, had the lowest AGB losses south of the river, and the

highest losses occurred in zone 34. The protected areas (zones 26-32) and the areas with steep slopes (zone 36) showed very low losses of AGB density and even some growth (Fig.7). This result is in agreement with the estimated risks for these areas, where the protected areas were estimated to have very low risk of biomass loss, and steep sloped areas had a low estimated risk (Fig. 9).

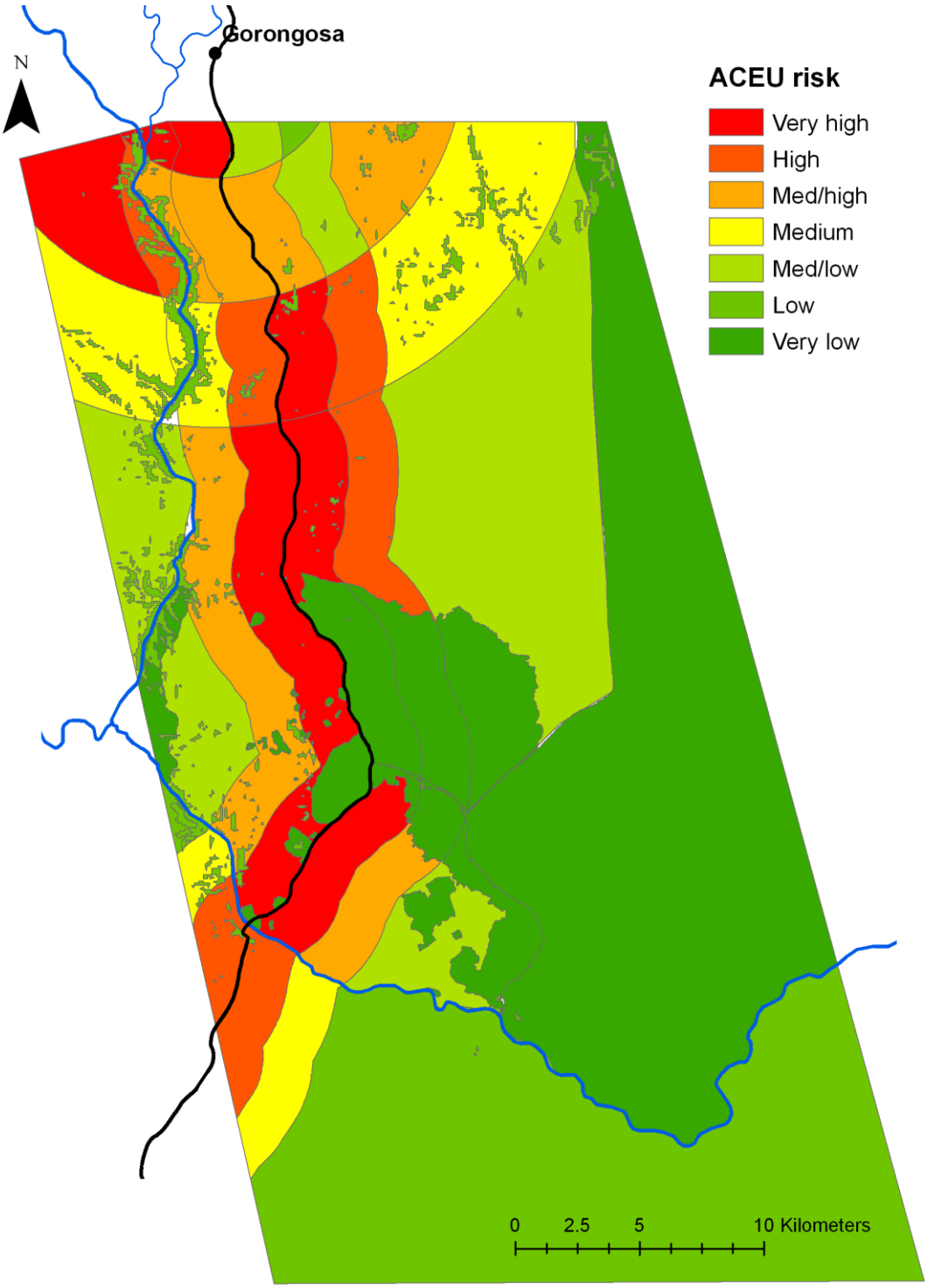

Fig. 9: Map for Gorongosa and Sofala provinces, central Mozambique, of estimated risk of deforestation and degradation under the assumptions of the ACEU model.

Model ability to estimate AGB density change

A linear relationship between estimated ranked risk and mean AGB density change showed that the ACEU model was able to explain 35 % ($r^2 = 0.35$, $P < 0.01$) of variability in mean AGB density change within every zone for our study site (Fig. 10). However, some scatter clearly occurs around the least-squares linear regression, with a RMSE of 1.47 Mg C ha^{-1}. Some of the clear outliers are zones 2 – 4, where a gain in biomass (i.e. negative density change) or very low losses occurred rather than a higher predicted biomass loss. At the higher end of the ranked risk scale, zones 6, 17, 22, and 23 show some scatter, where the zone with the highest biomass density changes were under-estimated by the model, but the highest ranked risk in zone 6 was over-estimated. At the lowest risk, rank 1 (i.e. all the protected areas), there is large scatter of AGB density change ranging from growth in zone 32 to small losses in others. Some of the scatter is most likely associated with radar biomass measurement errors, and the uncertainty in measuring a change in AGB density between years, particularly at lower AGB density changes.

We recognise that errors exist on both axes, which complicates the use of a simple linear regression to characterise the relationship between estimated risks and measured AGB density change. However, the errors which arise from uncertainty in radar estimated mean AGB density change, and the assessment of ranked risk from the model, are difficult to translate to real error estimates. Therefore, although we recognise these errors exist, we chose to use a simple linear regression in order to facilitate a simple comparison between estimated risks and biomass losses, and recognise that some variability and/or error in the fitted relationship is likely.

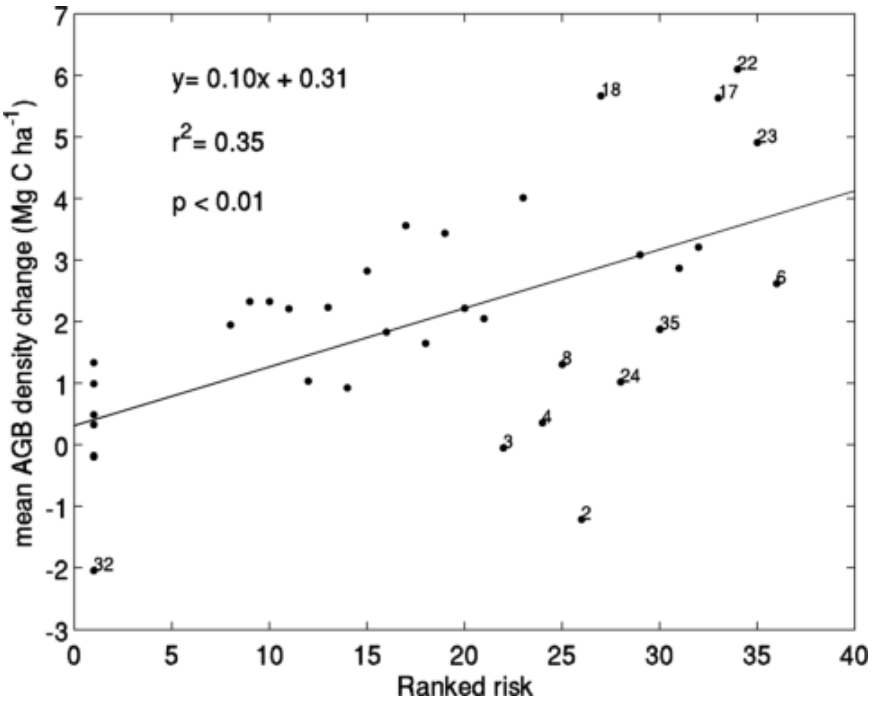

Fig. 10: Linear correlation of mean above-ground biomass (AGB) density change (2007 – 2010) and the ranked risk (1-36) of each zone estimated with the ACEU model. Negative density change values are gains in AGB and positive values are losses of AGB. Numbers on the graph correspond to zone labels. The linear equation, goodness-of-fit (r^2) and the significance (*P*) level is shown.

Discussion

Model performance

In accordance with the ACEU hypothesis, individual parameters showed no correlation to AGB density change, and only in combination did the estimated risk have any relationship with biomass change in each zone. The ACEU model proved to be able to spatially locate the high risk land areas, which experienced greater biomass losses over a short 3 year time period for our study site in central Mozambique, but the model was only moderately good (explained 35 % of AGB density change variability) at accurately predicting the intensity of biomass loss. Where the model failed to correctly identify areas at risk can give us valuable

insights into where our model assumptions and our understanding of deforestation and degradation drivers were flawed.

The risks associated with several zones were not well predicted by the ACEU model. Zones 2 and 3 had relatively high mean slopes (5.6-5.8^{o}), and therefore low cultivation risk, but high risks associated with accessibility and extractable value (Fig. 8), increasing the overall risk estimate (Fig. 9). In zone 4, 6, 8 and 35 the extractable value based on biomass density was very low (10-20 % woody land cover), but the estimated risk was much higher due to high *A* and *C* risks. Therefore, our assumptions of risk associated with *C* and *E* were not well represented at high values of slope or at low values of biomass density, and could be improved by lowering the risk at greater mean slope angles and at low biomass densities in order to lower the overall risk estimated by the ACEU model.

Risks in zone 1, 23 and 24 were estimated as high to very high risk from the ACEU model (Fig. 9), due to a combination of high *A* and *E* in these zones (Fig. 8), but AGB density change was only moderate (Fig. 7). For these cases there is no obvious impact from slope (*C*) to explain the discrepancy. However, these zones were both in areas which could have been influenced by decreased accessibility due to natural barriers (zone 1), or under some form of management (zones 23-24). This discrepancy indicates that the protection status of land was not well defined by a binary rule, and areas that are under some form of managed status, but not fully protected, should be better represented in the risk assessment of protection status (*U*). Also, decreased access due to natural barriers such as rivers should be better represented in model assumptions by lowering accessibility risk (*A*).

Model limitations

Drivers of deforestation and degradation are many and varied (Geist and Lambin 2002), and the ACEU model is limited in that it inherently assumes that deforestation and degradation processes can be adequately explained by only four parameters. Deciding which drivers fit into what categories is subject to large user bias. For example, we assume proximity to larger towns increases access to land areas, when in fact proximity to towns is more likely a measure of population density and increased pressure on resources rather than accessibility. However, the flexibility of defining ACEU parameters and deciding which drivers are important based on what spatial data are available allows the user to define and modify the ACEU method for particular locations and situations, broadening its usability, but limiting its generality: a model calibrated for one particular site or region may not be applicable to all other sites and regions.

The ACEU model, like many other spatial models, is largely limited to and dependent on what spatial data are available, and several assumptions are made. As such, we attempt to represent ACEU processes by using proxy data, such as assuming biomass volume is associated with extractable value or slope is a measure of suitability of land for cultivation. Ideally ACEU parameters would be based on spatial variables directly related to each, informed by extensive ground data. However, this approach is not always practical if the study area is large or if capabilities are limited.

From the ACEU model we cannot ascertain any causal relationships between increased risk and biomass loss. From the risk map we can only infer possible drivers of biomass change related to ACEU and use the spatial information to target further

monitoring for determination of specific factors causing deforestation and degradation. Furthermore, the ACEU model cannot accurately forecast the amount of biomass which might be lost based on the estimated risks, only to identify areas likely to be at most risk of degradation and deforestation.

Lastly, the use of radar-derived biomass maps to validate the risk map and to estimate extractable value limits the use of the method outlined here to locations where high resolution biomass maps are available. However, the capacity to create biomass maps from satellite products is growing (Le Toan et al. 2011), and several pan-tropical biomass maps are already available (Baccini et al. 2012; Saatchi et al. 2011). Alternatively, extensive ground data or other satellite products such as land cover classification could be used to characterise extractable value and validate risk maps, though this might limit the model to assessing risk of deforestation only, excluding degradation processes.

Informing policy and management

From our risk assessment the land areas at greatest risk of deforestation and degradation in our study site primarily occurred along the main road. Between 2007 and 2010 the land areas which experienced high intensity biomass loss (> 4 Mg C ha^{-1}) occurred within 4 km of the main road, suggesting that roads are a major vector for increased deforestation and degradation activities in the study site. Several other studies similarly find that roads act as a major axis for increased forest loss (Chomitz and Gray 1996; Jansen et al. 2008; Nagendra et al. 2003), and in Africa this has been associated with increased access for cultivation and charcoal production purposes (Luoga et al. 2002; Malimbwi et al. 2005; Sprague and Oyama 1999). It is not clear what the causes of biomass loss are in our study, but charcoal production is known to

occur within 2km of the main road where charcoal is sold (Herd 2007). The current rates of net biomass loss surrounding the main road are unsustainable, and if rates continued very little biomass would be left within 2 km of the road by the year 2025. However, it is difficult to project biomass losses into future beyond a few years, as variables and drivers will be changing constantly.

Protected areas in our study site showed very little change in AGB density, even when in close proximity to the main road. However, it is unclear whether these areas experience little change in AGB biomass due to their protected status, or whether other factors such as remoteness or perceptions of land ownership cause the low biomass losses (Nagendra 2008). Several of the avoided deforestation sites were established within the 2007-2010 timeframe (Grace et al. 2010), making it difficult to assess the impact of the newly founded protection status, or whether pre-existing factors influenced the low biomass losses in these locations. Encroachment into protected areas occurs when increased incentives for resource extraction and alternative land use within the reserve boundary override the protection status (Ahrends et al. 2010; Luoga et al. 2002). The continued maintenance of biomass within protected areas may start to be threatened when and if resources in other accessible areas start to decrease, increasing the incentives for biomass extraction and alternative land use within protected areas.

Several land areas outside of the protected areas were at high risk of deforestation and degradation (i.e. within the National Bark buffer zone and in areas west of the Vunduzi river), but between 2007-2010 only experienced moderate to low biomass loses. It is possible that these high risk areas may be at greater risk beyond the 2007-2010 study period, if all other high risk site resources have been exhausted,

increasing the incentives for expansion into new land areas. Some encroachment on woodland areas west of the Vunduzi is already apparent (Ryan et al. 2012), and it is even visible on recent Google Earth imagery (Google 2009).

Despite the ACEU model limitations, the risk map created acts as a useful resource for informing policy and management of land areas likely to be at greater risk of deforestation and degradation in the near future, and can suggest possible causes of biomass loss. Furthermore, the ACEU risk map allows us to postulate which areas may be at higher risk beyond the 3 year observation period in this study, and could inform management of sites in need of further monitoring and/or protection in future for effective sustainable resource management.

Conclusions

With limited spatial data and using a simple rule-based approach we were able to map and identify areas which were at high risk of deforestation and degradation in the near future for our study site in central Mozambique. We tested our model assumptions using a 3 year period of biomass change assessments, and found that the ACEU model was adept at spatially locating high risk sites, though with limited accuracy in some cases, but was not able to accurately predict the quantity of biomass change. Further limitations include an inability to assess causation of deforestation and degradation, the potential for large user bias, and a dependence on radar derived biomass maps or other high resolution biomass maps for the risk assessment. However, the relative simplicity, flexibility, and transparency of the ACEU model makes it accessible to users with limited data and expertise that wish to create risk maps to inform and target management efforts, and biomass maps are likely to become more common in the future as new satellites are launched (Le

Toan et al. 2011). Further application of the ACEU model in different locations and regions would be needed to validate the model under different conditions and with different drivers of deforestation and degradation.

Acknowledgements

Envirotrade Ltd. and Lucy Goodman provided geospatial information on avoided deforestation areas. ARA CENTRO provided geospatial information on land features. The GeoEye Foundation provided the IKONOS imagery. This work was funded by a CASE studentship from the Natural Environment Research Council and Ecometrica. We thank staff of Ecometrica for their helpful comments, and Edward Mitchard and Anthony Bloom at the University of Edinburgh for their helpful discussions.

References

Abbot JIO, Homewood K (1999) A history of change: causes of miombo woodland decline in a protected area in Malawi. Journal of Applied Ecology 36:422-433

Agarwal DK, Silander JA, Gelfand AE, Dewar RE, Mickelson JG (2005) Tropical deforestation in Madagascar: analysis using hierarchical spatially explicit, Bayesian regression models. Ecological Modelling 185:105-131

Ahrends A et al. (2010) Predictable waves of sequential forest degradation and biodiversity loss spreading from an African city. Proceedings of the National Academy of Sciences of the United States of America 107:14556-14561

Angelsen A, Kaimowitz D (1999) Rethinking the causes of deforestation: Lessons from economic models. World Bank Research Observer 14:73-98

ArcGIS (2009) ArcMap (9.3.1). ESRI Inc.

Baccini A et al. (2012) Estimated carbon dioxide emissions from tropical deforestation improved by carbon-density maps. Nature Advance online publication

Chidumayo EN (1991) Woody biomass structure and utilization for charcoal production in a Zambian miombo woodland Bioresource Technology 37:43-52

Chomitz KM, Gray DA (1996) Roads, land use, and deforestation: A spatial model applied to belize. World Bank Economic Review 10:487-512

DeFries RS, Houghton RA, Hansen MC, Field CB, Skole D, Townshend J (2002) Carbon emissions from tropical deforestation and regrowth based on satellite observations for the 1980s and 1990s. Proceedings of the National Academy of Sciences of the United States of America 99:14256-14261

DeFries RS, Rudel T, Uriarte M, Hansen M (2010) Deforestation driven by urban population growth and agricultural trade in the twenty-first century. Nature Geoscience 3:178-181

Farr TG et al. (2007) The shuttle radar topography mission. Reviews of Geophysics 45

Fisher B (2010) African exception to drivers of deforestation. Nature Geoscience 3:375-376

Geist HJ, Lambin EF (2002) Proximate causes and underlying driving forces of tropical deforestation. Bioscience 52:143-150

Google (2009) Google Earth (Version 5.0.11733.9347).

Grace J, Ryan CM, Williams M, Powell P, Goodman L, Tipper R (2010) A pilot project to store carbon as biomass in African woodlands. Carbon Management 1:227-235

Herd ARC (2007) Exploring the socio-economic role of charcoal and the potential for sustainable production in the chicale regulado, Mozambique. MSc thesis, School of GeoSciences, University of Edinburgh, Edinburgh

Houghton RA (2010) How well do we know the flux of CO(2) from land-use change? Tellus Series B-Chemical and Physical Meteorology 62:337-351

Houghton RA, Hackler JL (2006) Emissions of carbon from land use change in sub-Saharan Africa. Journal of Geophysical Research-Biogeosciences 111

Houghton RA, Hall F, Goetz SJ (2009) Importance of biomass in the global carbon cycle. Journal of Geophysical Research-Biogeosciences 114:13

Imhoff ML, Bounoua L, Ricketts T, Loucks C, Harriss R, Lawrence WT (2004) Global patterns in human consumption of net primary production. Nature 429:870-873

INE (2008) Estatisticas do Distrito de Gorongosa. Estatistica Ind.

Jansen LJM, Bagnoli M, Focacci M (2008) Analysis of land-cover/use change dynamics in Manica Province in Mozambique in a period of transition (1990-2004). Forest Ecology and Management 254:308-326

Lambin EF (1997) Modelling and monitoring land-cover change processes in tropical regions. Progress in Physical Geography 21:375-393

Le Quere C et al. (2009) Trends in the sources and sinks of carbon dioxide. Nature Geoscience 2:831-836

Le Toan T et al. (2011) The BIOMASS mission: Mapping global forest biomass to better understand the terrestrial carbon cycle. Remote Sensing of Environment 115:2850-2860

Liu DS, Iverson LR, Brown S (1993) Rates and patterns of deforestation in the Philippines: application of geogrpahic information system analysis. Forest Ecology and Management 57:1-16

Luoga EJ, Witkowski ETF, Balkwill K (2002) Harvested and standing wood stocks in protected and communal miombo woodlands of eastern Tanzania. Forest Ecology and Management 164:15-30

Luoga EJ, Witkowski ETF, Balkwill K (2005) Land cover and use changes in relation to the institutional framework and tenure of land and resources in eastern Tanzania miombo woodlands. Environment Development and Sustainability 7:71-93

Malimbwi RE, Zahabu E, Monela GC (2005) Charcoal potential of miombo woodlands at Kitulangalo, Tanzania. Journal of Tropical Forest Science 17:197-210

Manly BFJ (2007) Randomization, Bootstrap and Monte Carlo Methods in Biology, Third edn. Chapman & Hall/CRC

Mas JF, Puig H, Palacio JL, Sosa-Lopez A (2004) Modelling deforestation using GIS and artificial neural networks. Environmental Modelling & Software 19:461-471

Mertens B, Lambin EF (1997) Spatial modelling of deforestation in southern Cameroon - Spatial disaggregation of diverse deforestation processes. Applied Geography 17:143-162

Nagendra H (2008) Do parks work? Impact of protected areas on land cover clearing. Ambio 37:330-337

Nagendra H, Southworth J, Tucker C (2003) Accessibility as a determinant of landscape transformation in western Honduras: linking pattern and process. Landscape Ecology 18:141-158

Ryan CM (2009) Carbon Cycling, Fire and Phenology in a Tropical Savanna Woodland in Nhambita, Mozambique. PhD thesis, School of GeoSciences, The University of Edinburgh, Edinburgh

Ryan CM et al. (2012) Quantifying small-scale deforestation and forest degradation in African woodlands using radar imagery. Global Change Biology 18:243-257

Ryan CM, Williams M (2011) How does fire intensity and frequency affect miombo woodland tree populations and biomass? Ecological Applications 21:48-60

Saatchi SS et al. (2011) Benchmark map of forest carbon stocks in tropical regions across three continents. Proceedings of the National Academy of Sciences of the United States of America 108:9899-9904

Sloan S, Pelletier J (2012) How accurately may we project tropical forest-cover change? A validation of a forward-looking baseline for REDD. Global Environmental Change-Human and Policy Dimensions 22:440-453

Soares BS et al. (2006) Modelling conservation in the Amazon basin. Nature 440:520-523

Sprague DS, Oyama S (1999) Density and distribution of citemene fields in a miombo woodland environment in Zambia. Environmental Management 24:273-280

Tabuti JRS, Dhillion SS, Luye KA (2003) Firewood use in Bulamogi County, Uganda: species selection, harvesting and consumption patterns. Biomass & Bioenergy 25:581-596

Tinley KL (1977) Framework of the Gorongosa Ecosystem. PhD thesis, Faculty of Science, University of Pretoria, Pretoria

Tinley KL (1982) The Influence of Soil Moisture Balance on Ecosystem Patterns in Southern Africa. In: Huntley BJ, Walker BH (eds) Ecology of Tropical Savannas. Springer-Verlag, Berlin, pp 175-192

Tipper R (2008) A Simple Rule-Based Approach for Setting REDD Project Baselines. Conference on Carbon and Communities in Tropical Woodlands, 16 -18th June, Edinburgh

Wassenaar T, Gerber P, Verburg PH, Rosales M, Ibrahim M, Steinfeld H (2007) Projecting land use changes in the Neotropics: The geography of pasture expansion into forest. Global Environmental Change-Human and Policy Dimensions 17:86-104

Woollen E, Ryan CM, Williams M (2012) Carbon Stocks in an African Woodland Landscape: Spatial Distributions and Scales of Variation. Ecosystems 15:804-818

5. Discussion and key conclusions

The aim of this thesis was to improve our understanding of miombo woodland carbon dynamics. I did this by addressing key unknown aspects of the C cycle at a range of scales, including 1) seasonal controls on C uptake at the leaf level, 2) spatial distributions and scales of variation of C stocks in the landscape, and 3) drivers and spatial patterns of deforestation and degradation at the regional scale. My thesis asked the following questions:

4) What are the controls on photosynthetic productivity of miombo woodland tree species on a diurnal to seasonal time scale?
5) How do C stocks in soil and vegetation vary across a miombo woodland landscape, and to what degree and at what scales are these stocks linked?
6) Based on our understanding of drivers of deforestation and degradation, can a simple spatial model usefully predict risk of forest biomass loss in a region of central Mozambique?

To which the answers were:

a) Primary productivity of miombo woodland tree species showed inter-specific controls on photosynthesis, where *B. spiciformis* had lower assimilation rates in the dry season and *J. globiflora* and *D. condylocarpon* maintained assimilation rates across seasons. Inter-specific differences were related to differing access to soil water, hydraulic conductivity and stomatal regulation on leaf gas exchange, as well as varied photosynthetic capacities related to leaf developmental stage at the time of measurement in the dry season.

b) Spatial distributions of miombo woodland C stocks in soils and vegetation were related to soil textural distributions and topography at scales of a few meters to kilometres. Greater woody C stocks were found on coarse textured soils on elevated ground, and were coupled to top-soil C stocks. Deeper soil C stocks were de-coupled from woody C and top soil C stocks, and were more closely related to soil clay content, with greater soil C stocks found in low lying fine textured soils.

c) A simple rule-based spatial model, based on our understanding of drivers of forest loss, was able to accurately predict areas which were at higher risk of deforestation and forest degradation in the near future for a study site in central Mozambique.

I now review the key conclusions of the thesis relating to the three questions outlined above, in context of the scales of measurement to which they relate: leaf scale, landscape scale, and regional scale. I highlight further research questions arising from each chapter at each scale, and go beyond the scales of this thesis to discuss further research needed in order to understand miombo woodlands role in Africa's carbon cycle.

Leaf scales

Chapter 2 aimed to determine the seasonal limitations to leaf level productivity of miombo woodland tree species, by collecting data on leaf gas exchange and leaf traits in the dry and wet seasons. The key conclusions from chapter 2 were:

1) Responses of leaf level productivity to seasonal drought differed amongst tree species of miombo woodland. *Julbernardia globiflora* and *Diplorhynchus condylocarpon* maintained similar maximum assimilation rates and stomatal

conductance in dry and wet seasons, whereas *Brachystegia spiciformis* maximum assimilation rates and stomatal conductance were lower during the dry season.

2) The inter-specific differences were a result of differing stomatal regulation on leaf gas exchange, varied access to soil water, and variation in leaf traits and photosynthetic capacity for *B. spiciformis* during the dry season.
3) The inter-specific differences in leaf traits and photosynthetic capacities were attributed to differing stages of leaf development during the time of measurement in the dry season, where *B. spiciformis* had less developed leaves.
4) It was unclear what caused differing leaf development between species, but varied timing of leaf flush can create niche separation with regards to resource competition during the early growing season, facilitating the co-existence of tree species in miombo woodlands.

Previous work on leaf level processes of miombo tree species (Choinski and Johnson 1993; Tuohy and Choinski 1990; Tuohy et al. 1991) has focused on understanding how photosynthesis changes with leaf nutrient content and leaf development during the late dry season, and only one of those studies (Choinski and Johnson 1993) made a comparison between dry and wet seasons in *B. spiciformis*. The conclusions from this work have contributed towards a better understanding of the seasonal changes in leaf level productivity of several miombo tree species, and show differences in inter-specific responses, which were previously unknown. Furthermore, the high rates of transpiration measured during the dry season supports the hypothesis that miombo trees have access to deep soil water during the dry

season (Frost 1996), which has previously never been shown. Further questions emerge from this work, including:

Is the timing of leaf flushing coordinated within and between species? The differing stages of leaf development, as evidenced by the leaf trait measurements, were attributed to different timing of leaf flush between the three tree species. Other studies on the phenology of miombo woodland (Chidumayo 1994; Fuller 1999; Ryan 2009) have noted the phenology of the canopy as a whole is largely coordinated in time, and that timing can vary depending on location, but have not distinguished between the phenology of individual tree species. Further work should assess whether phenological timing differs between species, or between individual trees. This could be done by analysing hemispherical photos of the canopy taken during the course of the dry season, when new leaves emerge (Fig. 1). By singling out individual species and trees from the rest of the canopy it would be possible to assess if new leaf emergence is coordinated across the same species, or whether it differs between individual trees. Linking such results with an analysis of resource availability for individual trees would allow further assessment on the mechanisms determining differing phenological timing.

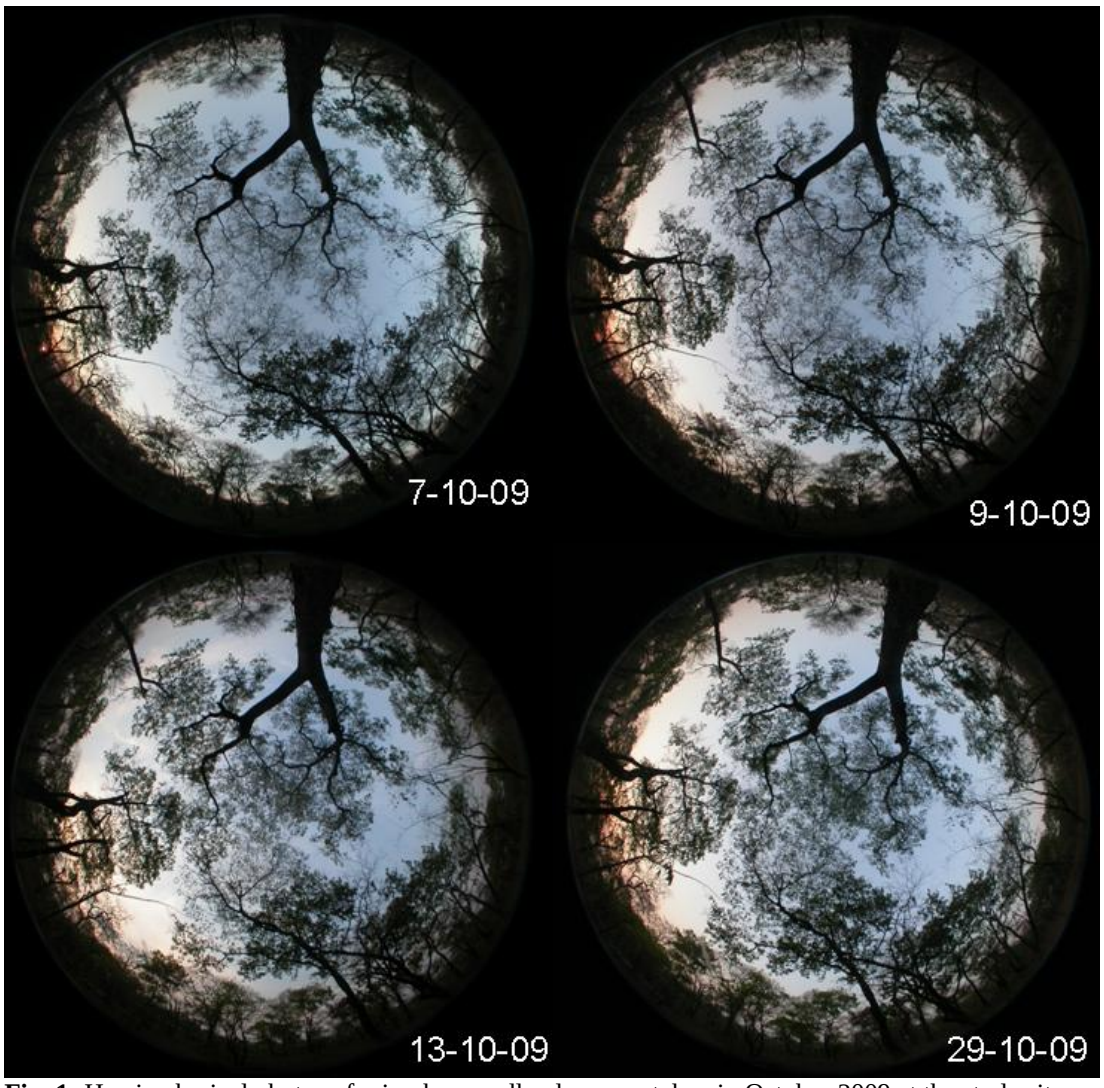

Fig. 1: Hemi-spherical photos of miombo woodland canopy taken in October 2009 at the study site, showing differing timing of leaf emergence between trees. The dominant canopy tree in this photo is *Brachystegia spiciformis*. The photos were taken by Emily Woollen.

Does rooting depth and access to soil water differ between species and tree size classes? If so, does root niche separation determine the timing of leaf flush and the inter-specific responses of leaf level processes to seasonal drought?

There is some evidence in Timberlake and Calvert (1993) to suggest that rooting depths and structures vary widely within and between miombo woodland tree species, depending to some extent on height of trees and soil characteristics. However, it is not known whether roots of co-occurring trees compete for the same soil water and nutrient resources, or whether root niche separation occurs. Further

studies on rooting profiles of trees and pre-dawn leaf water potentials of different species and sizes in conjunction with an assessment of depth of woody plant water uptake, using for example hydrogen and oxygen isotope ratio signals (Rossatto et al. 2012), and nutrient uptake would be needed in order to ascertain whether miombo trees are accessing different soil water and nutrient resources, and assess whether root niche separation occurs.

Do the hydraulic architectures and plant water relations differ between tree species, tree size classes, and seasons? Differing leaf specific conductivity between species and seasons found in this thesis work suggests hydraulic conductivity could be an important mechanism determining the inter-specific responses of leaf level processes to seasonal drought. However, there have been no complete studies of miombo woodland plant water relations and hydraulic architecture, and only few studies in addition to this thesis have measured changes in leaf moisture content and osmotic potentials (Choinski and Johnson 1993; Ernst and Walker 1973). Further data on plant water relations, including hydraulic conductivity, sap flow, sap wood area, and stem water storage capacity of miombo tree species would be needed in order to fully understand plant water relations of miombo trees and their ability to cope with seasonal drought. This information could further be used to parameterise process-based models (e.g. Soil-Plant-Atmosphere model (Williams et al. 1996)) to further determine hydraulic limitations to productivity.

How do other co-occurring miombo tree species respond to seasonal drought, and do the observations of this study apply to other locations with miombo woodland? The results of this thesis study were limited to comparisons

between three co-occurring miombo tree species, in one location and between a few individual trees. Miombo woodlands have many co-occurring tree species and it is unknown how these species respond to seasonal drought, and whether any further inter-specific differences exist. The vast extent of miombo woodland also gives rise to variations in amount of rainfall, lengths of dry season, and soil characteristics (Frost 1996), which could alter how miombo trees in different locations respond to seasonal drought. Further studies on seasonality of productivity, plant water relations, leaf gas exchange and leaf trait measurements need to be conducted across several miombo tree species and locations in order to fully understand seasonality of miombo woodland productivity as a whole.

Landscape scales

Chapter 3 aimed to determine how C stocks in soils and vegetation varied across a miombo woodland landscape, and to assess at what degree and at what scales C stocks were linked. Soil and vegetation C stocks, as well as other variables, were sampled along a 5 km transect through miombo woodland using a cyclic sampling scheme to determine the spatial structure of C stores. Correlation analyses were used to assess if any links between sampled variables occurred. The key conclusions from chapter 3 were:

1) Spatial distributions of vegetation and soil C stocks in a miombo woodland landscape are linked to topography and soil textural distributions.
2) Above-ground woody C stocks were closely linked to topography, as were soil textural distributions, where greater woody C stocks and coarse textured soils were found on higher elevated ground.

3) Soil textural properties restricted woody C stocks to an upper limit so that coarser soils were able to support greater woody C stocks.
4) Top-soil C stocks were coupled to vegetation, with greater amounts found in coarse textured soils on elevated ground. Deeper soil C stocks were de-coupled from top-soil C and vegetation, and were more closely related to soil clay content, with greater C stocks found in fine textured soils at lower elevation sites.
5) Soil C stocks varied significantly at metre scales, whereas vegetation C stocks varied significantly at kilometre scales, reflecting the patchy heterogeneity of miombo woodland vegetation.
6) For optimal sampling and assessment of landscape C stocks in miombo woodland, woody biomass should be sampled in plots that are > 0.5 ha in size separated by distances > 1426 m. Soil C stocks sampled in the top 30 cm of soil should be separated by distances > 26 m, unless the aim is to compare the effect of a treatment, in which case the samples should be < 26 m apart.

Previous work on miombo woodland spatial patterning and vegetation distributions (Campbell et al. 1995; Tinley 1977; Tinley 1982) were largely based on observations and very little quantitative assessments were performed. This study was one of the most complete transect studies ever conducted in a natural miombo woodland, and provides some of the first quantitative insights into the relationships between C stocks, soil properties, vegetation and topography in miombo woodlands over multiple scales. Furthermore, the study was able to inform future studies on optimal sampling for C stock assessments of miombo woodlands. Some interesting questions arise from this study. In particular:

Why do miombo woodland trees prefer well drained soils on elevated ground? A large proportion of the distribution and variability of large miombo woodland trees was linked to topography and soil texture. It is still unclear why miombo trees prefer well drained coarse soils but several mechanisms were suggested, including inundated soils inhibiting tree growth during the wet season (Tinley 1982), root niche separation and competition between trees and grasses (Walker 1987), and fire feedbacks (Ryan and Williams 2011). Of these mechanisms, further work is particularly needed on below-ground processes and rooting structures to assess their impacts on vegetation structure. A very good example of such a study, conducted in Brazilian *cerrado* savanna (Rossatto et al. 2012), assessed the depth of plant water uptake along a topographic gradient, confirming that vegetation at higher elevations extracted water from deeper unsaturated soils and had greater variability in water uptake strategies, allowing a denser more complex woody vegetation layer. Further to this, more work is required on mycorrhizal root associations, as past work (Hogberg 1986a; Hogberg 1986b; Hogberg and Alexander 1995) suggests that they are important determinants of vegetation distributions and structure. Further studies on plant water uptake strategies and mycorrhizal root associations of both trees and grasses would provide further evidence towards the root niche hypothesis and increase our understanding of tree-grass interactions and determinants of vegetation structure in a miombo woodland landscape.

Does the relationship between topography and woody C stocks hold at larger scales? From satellite images of the study site (chapter 3), we see a clear patterning of vegetation, occurring as small islands surrounded by networks of dambos. When we look at larger regional scales of the study site (chapter 4), there is

a general trend of higher biomass to the north west, in areas with higher elevation (~ 400 m), decreasing to lower biomass in the south east in the Gorongosa national park, where the ground is largely flat and at much lower elevations (~ 30 m) (Ryan et al. 2012). There are of course several disturbance factors, such as human impacts and fire, which can supersede the natural spatial pattern of biomass at the regional scale. However, in another study by Mayaux et al. (2004), satellite images over Angolan miombo woodlands (Fig. 2) show clear striation patterns of vegetation, possibly related to the underlying topography and/or hydrology.

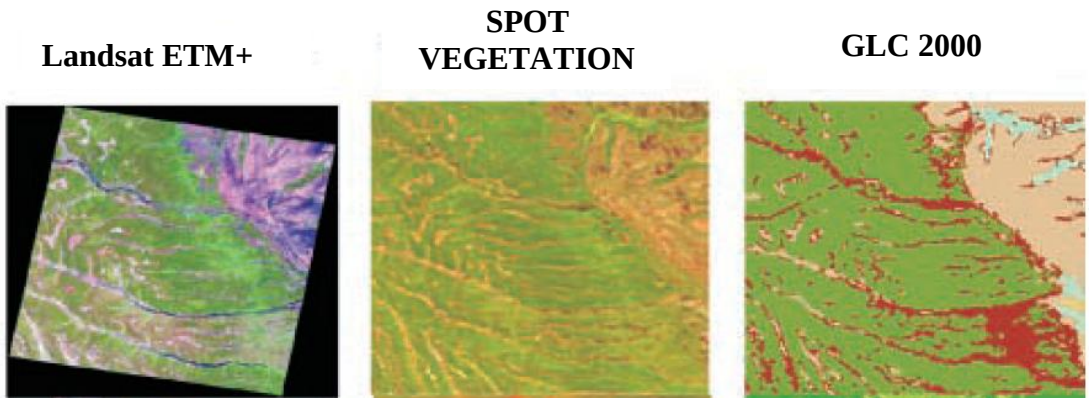

Fig. 2: Optical satellite images of miombo woodlands in Angola, showing the Landsat ETM+ (30 m resolution) and SPOT VEGETATION (1 km resolution) data, and the Global Land Cover 2000 map of the same area. Subset image from Mayaux et al. (2004), p. 875.

Further studies on large scale links between woody biomass, or vegetation cover, and topography might reveal that topography is a consistent predictor of miombo biomass and vegetation distributions at continental scales. This could be tested using recently produced above-ground C stock maps of Africa (Baccini et al. 2012; Saatchi et al. 2011), or the Global Land Cover map (2000), linked to topographic data provided by the Shuttle Radar Topography Mission (Farr et al. 2007) and newer, higher precision missions such as TanDEM-X. If a clear relationship were found, which might be dependent on measurement noise, we could conclude that the

relationship found between woody biomass C stocks and topography in this thesis is a consistent predictor of vegetation cover in miombo woodlands on continental scales. However, other influencing factors such as rainfall gradients (Sankaran et al. 2005) and land use/cover change (Ryan et al. 2012) might de-couple woody biomass and topography at larger scales.

Regional scales

Chapter 4 aimed to develop and test a simple rule-based model of deforestation and degradation, based on our understanding of the main drivers of biomass loss, for a study site in central Mozambique. The model was based on the hypothesis that if land is accessible, cultivable, has extractable value and is unprotected (the ACEU hypothesis) it will be at high risk of deforestation and degradation. The model was applied in a spatial context using geographic information system techniques to produce a risk map of areas more likely to be affected by deforestation and degradation processes in the near future, and was validated against a time series of remotely sensed biomass changes. The main conclusions from this study were:

1) The ACEU model was able to spatially locate and accurately assign a high risk to land areas which experienced a high intensity of biomass loss over the three year study period.
2) The model was only moderately good at predicting the quantity of biomass lost based on the risk classification.
3) Some areas were incorrectly assigned a high risk status, due to the overestimation of risk in sites with steeper slopes, low biomass densities, and in sites protected by natural barriers.

4) Where the model had 'falsely' attributed a high risk of biomass loss, the model could be predicting areas that will be at high risk in the future (i.e. beyond the three year study period) if biomass resources in other locations are exhausted.
5) The ACEU model cannot determine the causes of deforestation and degradation, but can provide spatial information of risks to target further monitoring, and better inform policy and management efforts.
6) The sites of highest risk and greatest biomass losses occurred along the main road, suggesting roads are the major vector for deforestation and degradation in the study site.

The relatively simple approach used in this study to model complex deforestation and degradation processes provides a valuable tool for forest conservation and management groups that wish to assess risk of forest loss in specific locations, in a comprehensive and transparent fashion, without the need for large spatial data sets or particular expertise. Furthermore, the ACEU framework allows flexibility in the model so that it can be adapted to specific locations, and has potential for wider applications. As a case study, the model added to our understanding of the drivers of deforestation and degradation at the study site, and provided valuable insights to managing forest biomass resources. Further questions arising from this study include:

What are the main causes of biomass loss in the study site? From the spatial model and assessment of risk of deforestation and degradation it was possible to predict the likely locations of biomass loss, but it was not possible to determine the cause of biomass change. From previous studies, it is known that charcoal production is a major economic activity occurring within a few kilometres of the

main road (Herd 2007), and from personal observations and other studies (Jansen et al. 2008; Ryan et al. 2012) it is clear that shifting agriculture is a key driver of forest cover and biomass loss in the study area. These are the most likely proximate causes of biomass loss, but the underlying driving forces and extent of these are largely unknown. For example, other studies in Tanzania have found that markets for forest products and economic driving forces largely determined degradation patterns around Dar es Salaam (Ahrends et al. 2010; Hofstad 1997). In order to fully understand what causes biomass loss in the study site, it is necessary to understand the underlying driving forces of deforestation and degradation (Geist and Lambin 2002), and in particular what the market forces and demand for biomass products are. More data collection on market forces for forest biomass resource from centres of demand, and the extent of these forces, is needed. Following a similar method to Ahrends et al. (2010) to ascertain the spatial influence of market forces for forest products around the city of Beira, the largest city in proximity to the study site, would improve our understanding of the underlying driving forces.

How well does the model work when applied to other regions and at bigger scales? In this study the ACEU model was developed and calibrated to the case study site. The use of case studies are important for validating the model, but it is still unclear whether the calibrated model would apply equally well in other areas with similar drivers of deforestation and degradation, or at larger scales where drivers may change. The relative simplicity of the ACEU model allows flexibility in model parameterisation. However, further application of the ACEU model in different locations, regions and scales would be needed to validate the model under

different conditions and with different drivers of deforestation and degradation in order to thoroughly test the model accuracy and usability.

Continental scales

Upscaling of the results from this thesis to larger continental scales would improve our understanding of miombo woodlands role in Africa's C cycle. In order to scale to the continent, however, there is a need for a wider network of C cycle measurements across miombo woodlands of southern Africa, and a further need for model-data integration of miombo woodland C dynamics. Williams et al. (2007) highlighted the need for continent-wide observations that support both bottom-up and top-down methods of estimating carbon sources and sinks for Africa. Despite advancements on integrated C observation networks (e.g. CarboAfrica), there is still a need for enhanced continent wide carbon cycle observations (Ciais et al. 2011), in order to enable a more precise assessment of Africa's C cycle and its sensitivity to natural and anthropogenic pressures and future climate change.

To this end, improving the terrestrial modelling capacity is of key importance. Bombelli et al. (2009) points out the large discrepancy between the modelled and measured estimates of the biogenic C balance of Africa, confirming their current inadequacy when applied to Africa, as these models are usually developed and validated for different latitudes (Ciais et al. 2009; Weber et al. 2009). Increasing eddy covariance measurements across Africa (Merbold et al. 2009), the development and maintenance of a network of permanent samples plots, and combining flux and biometric data with models (Williams et al. 2009) using data assimilation techniques (Williams et al. 2005) would improve analyses of carbon cycle processes. Models can be linked with remote sensing data to allow us to upscale measurements to

continental scales to provide a better understanding of Africa's C cycle and dynamics, now and in the future. Pivotal in any future work on Africa's C cycle is the continued and increased involvement of local scientists. Further capacity building and empowerment of the local research community is needed in order to improve and maintain future research on Africa's C cycle.

Concluding remarks

This thesis has improved our knowledge of seasonality of C uptake, distributions of C stocks, and patterns and drivers of C stock changes of miombo woodlands of southern Africa at several scales. From this work several further research questions were raised, in particular pertaining to below ground processes and their possible impacts on miombo C dynamics. It also highlighted a further need for C cycle observations across the miombo biome, and improved modelling capacity of C cycle dynamics for upscaling to continental scales. Only then can we begin to incorporate miombo woodlands into a broader understanding of Africa's C cycle, and assess the impacts of increasing anthropogenic influences and future climate change on the C cycle of Africa.

References

Ahrends A et al. (2010) Predictable waves of sequential forest degradation and biodiversity loss spreading from an African city. Proceedings of the National Academy of Sciences of the United States of America 107:14556-14561

Baccini A et al. (2012) Estimated carbon dioxide emissions from tropical deforestation improved by carbon-density maps. Nature Advance online publication

Bombelli A et al. (2009) The sub-saharan Africa carbon balance, an overview. Biogeosciences Discuss. 6:2085-2123

Campbell BM, Cunliffe RN, Gambizia J (1995) Vegetation structure and small-scale pattern in Miombo woodland, Marondera, Zimbabwe. Bothalia 25:121-126

Chidumayo EN (1994) Phenology and Nutrition of Miombo Woodland Trees in Zambia. Trees-Structure and Function 9:67-72

Choinski JS, Johnson JM (1993) Changes in Photosynthesis and Water Status of Developing Leaves of Brachystegia-Spiciformis Benth. Tree Physiology 13:17-27

Ciais P et al. (2011) The carbon balance of Africa: synthesis of recent research studies. Philosophical Transactions of the Royal Society a-Mathematical Physical and Engineering Sciences 369:2038-2057

Ciais P, Piao SL, Cadule P, Friedlingstein P, Chedin A (2009) Variability and recent trends in the African terrestrial carbon balance. Biogeosciences 6:1935-1948

Ernst W, Walker BH (1973) Studies on Hydrature of Trees in Miombo Woodland in South Central-Africa. Journal of Ecology 61:667-673

Farr TG et al. (2007) The shuttle radar topography mission. Reviews of Geophysics 45

Frost P (1996) The ecology of miombo woodlands. In: Campbell B (ed) The Miombo in Transition: Woodlands and Welfare in Africa. Center for International Forestry Research, Bogor, Indonesia, pp 11-57

Fuller DO (1999) Canopy phenology of some mopane and miombo woodlands in eastern Zambia. Global Ecology and Biogeography 8:199-209

Geist HJ, Lambin EF (2002) Proximate causes and underlying driving forces of tropical deforestation. Bioscience 52:143-150

GLC (2000) Global Land Cover Map. Institute for the Environment and Sustainability, Global Vegetation Monitoring Unit, Joint Research Centre, European Commission

Herd ARC (2007) Exploring the socio-economic role of charcoal and the potential for sustainable production in the chicale regulado, Mozambique. MSc thesis, School of GeoSciences, University of Edinburgh, Edinburgh

Hofstad O (1997) Woodland Deforestation by Charcoal Supply to Dar es Salaam. Journal of Environmental Economics and Management 33:17-32

Hogberg P (1986a) Nitrogen fixation and nutrient relations in savanna woodland trees (Tanzania). Journal of Applied Ecology 23:675-688

Hogberg P (1986b) Soil nutrient availability, root symbioses and tree species composition in tropical Africa: a review. Journal of Tropical Ecology 2:359-372

Hogberg P, Alexander IJ (1995) Roles of root symbioses in African woodland and forest: Evidence from N15 abundance and foliar analysis. Journal of Ecology 83:217-224

Jansen LJM, Bagnoli M, Focacci M (2008) Analysis of land-cover/use change dynamics in Manica Province in Mozambique in a period of transition (1990-2004). Forest Ecology and Management 254:308-326

Mayaux P, Bartholome E, Fritz S, Belward A (2004) A new land-cover map of Africa for the year 2000. Journal of Biogeography 31:861-877

Merbold L et al. (2009) Precipitation as driver of carbon fluxes in 11 African ecosystems. Biogeosciences 6:1027-1041

Rossatto DR, Silva LDR, Villalobos-Vega R, Sternberg LDL, Franco AC (2012) Depth of water uptake in woody plants relates to groundwater level and vegetation structure along a topographic gradient in a neotropical savanna. Environmental and Experimental Botany 77:259-266

Ryan CM (2009) Carbon Cycling, Fire and Phenology in a Tropical Savanna Woodland in Nhambita, Mozambique. PhD thesis, School of GeoSciences, The University of Edinburgh, Edinburgh

Ryan CM et al. (2012) Quantifying small-scale deforestation and forest degradation in African woodlands using radar imagery. Global Change Biology 18:243-257

Ryan CM, Williams M (2011) How does fire intensity and frequency affect miombo woodland tree populations and biomass? Ecological Applications 21:48-60

Saatchi SS et al. (2011) Benchmark map of forest carbon stocks in tropical regions across three continents. Proceedings of the National Academy of Sciences of the United States of America 108:9899-9904

Sankaran M et al. (2005) Determinants of woody cover in African savannas. Nature 438:846-849

Timberlake JR, Calvert GM (1993) Preliminary Root Atlast for Zimbabwe and Zambia. Zimbabwe Bulletin of Forestry Research

Tinley KL (1977) Framework of the Gorongosa Ecosystem. PhD thesis, Faculty of Science, University of Pretoria, Pretoria

Tinley KL (1982) The Influence of Soil Moisture Balance on Ecosystem Patterns in Southern Africa. In: Huntley BJ, Walker BH (eds) Ecology of Tropical Savannas. Springer-Verlag, Berlin, pp 175-192

Tuohy JM, Choinski JS (1990) Comparative Photosynthesis in Developing Leaves of Brachystegia-Spiciformis Benth. Journal of Experimental Botany 41:919-923

Tuohy JM, Prior JAB, Stewart GR (1991) Photosynthesis in Relation to Leaf Nitrogen and Phosphorus-Content in Zimbabwean Trees. Oecologia 88:378-382

Walker BH (ed) (1987) Determinants of Tropical Savannas. The International Union of Biological Sciences, Oxford

Weber U et al. (2009) The interannual variability of Africa's ecosystem productivity: a multi-model analysis. Biogeosciences 6:285-295

Williams CA et al. (2007) Africa and the global carbon cycle. Carbon Balance Manag 2:3

Williams M et al. (1996) Modelling the soil-plant-atmosphere continuum in a Quercus-Acer stand at Harvard forest: The regulation of stomatal conductance by light, nitrogen and soil/plant hydraulic properties. Plant Cell and Environment 19:911-927

Williams M et al. (2009) Improving land surface models with FLUXNET data. Biogeosciences 6:1341-1359

Williams M, Schwarz PA, Law BE, Irvine J, Kurpius MR (2005) An improved analysis of forest carbon dynamics using data assimilation. Global Change Biology 11:89-105

Appendix 1

From the two field campaigns to measure ecophysiological parameters of miombo woodland trees over two seasons (as described in detail in chapter 2), several further analyses were conducted on the data, which were not presented as part of the main thesis. During the wet season several other measurements were also conducted, as plants were less stressed and therefore more amicable during measurements, and there were less logistical constraints allowing more time for measurements. I present some of the additional analyses and data here.

Additional analyses of data

Ambient light curves

From the diurnal ambient measurements of leaf gas exchange, measured in the dry and wet seasons, I created light response curves to characterise the relationship between assimilation rates and incident photosynthetic active radiation (Fig. 1). A non-rectangular hyperbola was fitted to the data (Ögren and Evans 1993) using a least-squares optimisation method in Matlab, where the curvature term was set to 0.7 (Evans 1987). The fitted hyperbola was not used to give estimates of light saturated assimilation rate (A_{sat}), photosynthetic efficiency (quantum yield, Φ), or light compensation point (I_c), as the large amount of scatter in the data made these estimate unreliable, and were therefore not included in the main thesis chapter. The scatter was caused by variability in other influencing factors, such as stomatal conductance, during the course of the day.

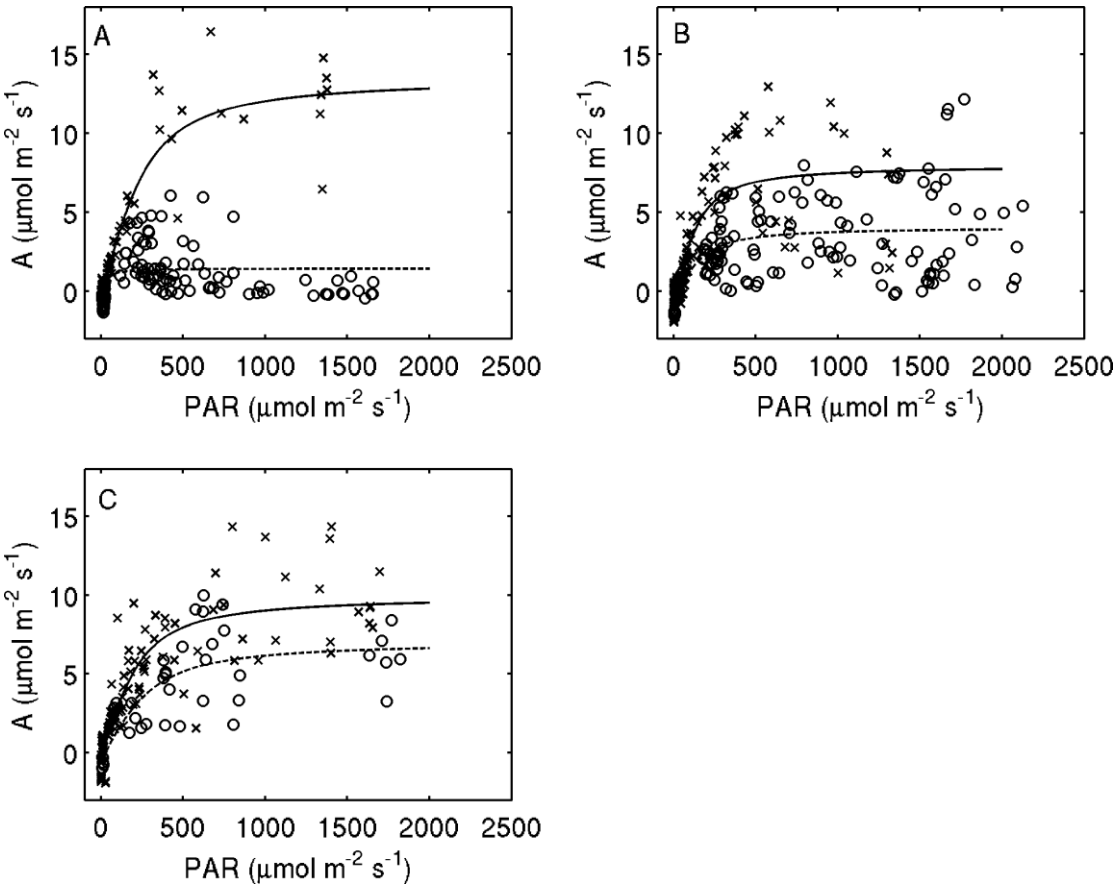

Fig. 1: Light response curves from diurnal ambient measurements of A) *Brachystegia spiciformis*, B) *Julbernardia globiflora*, and C) *Diplorhynchus condylocarpon* during the dry (o) and the wet (x) seasons. Each point is one leaf measurement, taken over the course of several days on several individual trees.

Despite the large variability in the data, and therefore a difficulty in determining significant differences in relationships between seasons, these plots show that *B. spiciformis* did not reach as high saturated assimilation rates over a similar range of *PAR* during the dry season as in the wet (Fig. 1 A). The other two species do not show quite as large a contrast in saturated assimilation rates between seasons (Fig. 1 B-C). This is in agreement with the results discussed in chapter 2, where *B. spiciformis* had lower assimilation rates and lower rates of carboxylation during the dry season. These plots add the additional knowledge that differences

between species responses to seasonal drought were not due to differences in light availability.

Total daily C uptake, water loss, and yearly C uptake estimates

Total assimilated C (A_t, g C m^{-2} leaf area) and total transpired water (E_t, kg H_2O m^{-2} leaf area) were calculated for each diurnal curve (i.e. each tree) in each season (Table 1). To calculate A_t and E_t , I calculated the area under the diurnal curves using a trapezoidal integration function, using Matlab routines (MathWorks 2012). The area under the curve was equal to the total number of mols of each gas being taken up or released per m^2 leaf area over the course of the day. I then multiply total mols of each gas by the respective molecular weights (C = 12 g mol^{-1}, and H_2O = 18 g mol^{-1}) to get the total weight of each gas per m^2 leaf area per day. As A_t and E_t were based on diurnal measurements for each tree, it was not possible to test for significant differences in the means between seasons, as sample size was small (n = 1 – 3 trees in each season), and these measurements were therefore excluded from the main thesis chapter. However, the values shown here are interesting in that they provide a measure of daily net primary productivity and total water loss per unit leaf area.

Tree ID	A_t (g C m^{-2})		E_t (kg H_2O m^{-2})	
	Dry	*Wet*	*Dry*	*Wet*
BS1	0.96	1.63	0.366	0.450
BS2	0.19	1.90	0.307	0.879
BS mean	***0.58***	***1.77***	***0.336***	***0.665***
JG1	1.55	2.35	0.644	0.375
JG2	1.89	1.68	1.021	0.467
JG3	1.02		0.879	
JG4		1.08		0.622
JG mean	***1.49***	***1.70***	***0.848***	***0.488***
DC1	2.31	2.20	1.799	0.597
DC2		1.92		0.772
DC3		2.50		0.986
DC mean	***2.31***	***2.21***	***1.799***	***0.785***

Table 1: Total daily assimilated C (A_t) and transpired H_2O (E_t) measured over a 12 hour period in individual trees of three miombo tree species (*B. spiciformis*, *J. globiflora*, and *D. condylocarpon*) over two seasons (see Ch. 2, Table 1 for further details).

The results are in agreement with the seasonal patterns of maximum assimilation and transpiration rates shown in chapter 2, where *B. spiciformis* has lower total assimilated C and total transpired water in the dry season as compared to the wet, and the other two other species show similar total C uptake values in both seasons and higher transpired water losses in the dry (Fig. 2).

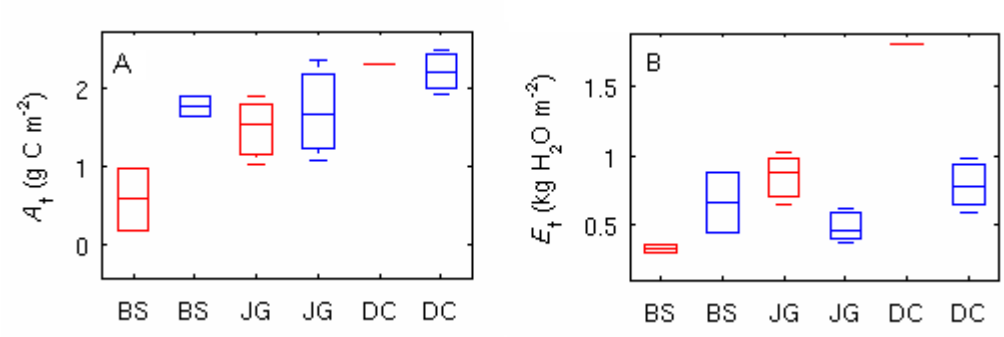

Fig. 2: Boxplots of A) total assimilated carbon and B) total transpired water for trees of species *Brachystegia spiciformis* (BS), *Julbernardia globiflora* (JG) and *Diplorhynchus condylocarpon* (DC) in the dry (red) and the wet (blue) seasons. Each boxplot is based on mean leaf measurements from individual trees (Table 1), where several leaves were sample on each tree (see Ch. 2 for full details). For each box, the central mark is the median, and the edges of the box are the 25th and 75th percentiles. Where $n > 2$, the whiskers indicate the range of mean values.

Across all three species, miombo woodlands have a mean daily C uptake of 1.9 g C m^{-2} leaf area day^{-1} during the wet season. If the leaf area index of miombo woodlands is between 1 - 2 m^2 m^{-2} (as determined from hemispherical photographs) during the wet season, then we can estimate that the total daily C uptake of miombo woodlands would be between 1.9 – 3.8 g C m^{-2} ground area day^{-1}. If we scale this up to the total area of miombo woodlands (2.7 milliom km^2) we can roughly estimate a total C uptake capacity of 0.005 – 0.01 Pg C day^{-1}. If we then assume that these values apply throughout the wet season from November to March (inclusive) (Ryan 2009), or 153 days of the year, total C uptake through net primary productivity of miombo woodland trees would be between 0.76 – 1.53 Pg C $year^{-1}$. However, total daily C uptake is likely to fluctuate across the miombo biome and leaf area index changes both seasonally and spatially. Therefore, this is only a rough estimate of total net primary productivity for all miombo woodlands, assuming our study site is representative of the whole.

Additional measurements in the wet season

Several other leaf trait measurements were taken during the wet season, as stomatal conductance was not limiting gas exchange measurements. Here I present the estimates of dark respiration (Rn), CO_2 compensation point without dark respiration (Γ*), light saturated assimilation rate (A_{sat}), quantum yield (Φ) and light compensation point (I_c). The methods used are briefly outlined followed by the results in Table 2.

Dark respiration in the dark (R_n)

Dark respiration (R_n) was measured on the same attached leaves as were used in the A/C_i measurements during the wet season only (see Ch.2 for details), due to stomatal limitation in the dry season preventing measurements. Leaves were wrapped in aluminium foil following A/C_i measurements to simulate dark conditions for 30 minutes. The leaf was unwrapped and placed quickly into a dark leaf chamber (LI-6400) with ambient humidity and ambient [CO_2], keeping external leaf parts covered in foil, where the leaf was allowed to stabilise for a few minutes. Five point measurements were taken on each leaf to get an average respiration rate. Measurements were not corrected for CO_2 diffusion leaks as we used ambient [CO_2] within the chamber, negating diffusion due to no concentration differences in and out of the chamber. Measured respiration rates were temperature corrected for 25 ^oC following the formula outlined in Tjoelker et al. (2001):

$$R_{25} = R_{Tleaf} Q_{10}^{(25-T_{leaf})/10}$$

where dark respiration at 25 ^oC (R_{25}) is a function of measured dark respiration at the leaf temperature (R_{Tleaf}), the Q_{10} of temperature response (assumed as equal to 2), and the measured temperature of the leaf (T_{leaf}) in ^oC.

CO_2 compensation point without dark respiration (Γ^*)

To determine the CO_2 compensation point without dark respiration (Γ^*) (i.e. the internal [CO_2] at which the rate of photosynthesis equals that of respiration), the method of Laisk (1977) was used [as described in Brooks and Farquhar (1985)]. Assimilation rate of intact leaves during the wet season were measured at three different irradiance levels (50, 100 and 500 μmol m^{-2} s^{-1}) and at each irradiance level

the chamber [CO_2] was decreased gradually from 150 down to 30 ppm for each measurement (Fig. 3). For each irradiance level a least-squares linear regression equation was calculated, and the point where they intersect represents the estimated Γ^* (x-axis C_i concentration) of the leaf. All data was corrected for CO_2 diffusion leaks (as described in Ch. 2), and Γ^* temperature corrected for 25 ^oC using an equation from Brooks and Farquhar (1985):

$$\Gamma^*_{25} = \Gamma^* - 1.88(T - 25) - 0.036(T - 25)^2$$

where CO_2 compensation point at 25 ^oC (Γ^*_{25}) is a function of the measured CO_2 compensation point (Γ^*) at a given leaf temperature (T) in degrees celsius.

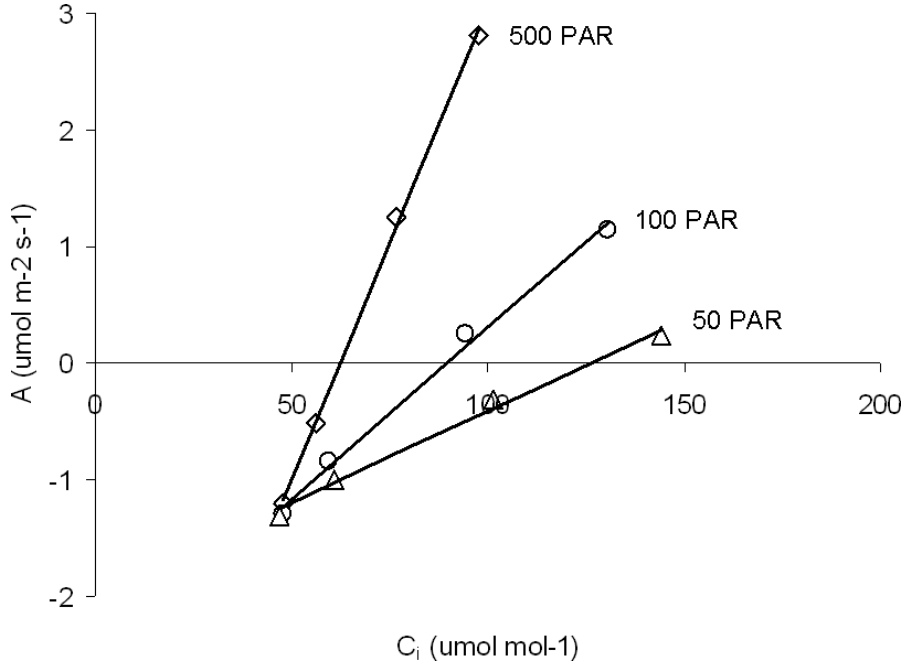

Fig. 3: Example of Laisk method for estimation of CO_2 compensation point (Γ^*)

Light response curves

Light response curves were conducted on intact leaves during the wet season using the LI-6400 fitted with an artificial light source. Temperature, humidity and [CO_2] were kept at ambient conditions throughout the measurement period (approx.

30 min), and irradiance levels were gradually decreased from high levels (2000 µmol m^{-2} s^{-1}) to zero using an automatic programme, and assimilation rates were recorded at each interval. A non-rectangular hyperbola was fitted to the diffusion corrected data (Ögren and Evans 1993) using a non-linear optimisation algorithm (Nelder-Mead method) to obtain a least-squares fit, where the curvature term was set to 0.7 (Evans 1987). The fitted hyperbola gave estimates of light saturated assimilation rate (A_{sat}) and photosynthetic efficiency (quantum yield, Φ). The code for fitting the hyperbola and estimating parameters was written by Joanna Zaragoza-Castells using R software. The light compensation point (I_c), when photosynthetic CO_2 uptake and respiratory CO_2 release are in equilibrium was estimated as the value at which the fitted non-rectangular hyperbola crossed the *x*-axis. All measurements were corrected for diffusion leaks, and parameters temperature corrected for 25^{o}C.

Table 2: Estimates of mean leaf traits per species at 25 ^{o}C (± S.E) in the wet season, based on light response curves, dark respiration measurements, and the Laisk method. Number of replicates (*italicised*) is the number of leaves or replicates used for each mean. None of the mean values were significantly different across species (ANOVA, $P > 0.05$)

Leaf trait	***B. spiciformis***		***J. globiflora***		***D. condylocarpon***	
A_{sat} (µmol CO_2 m^{-2} s^{-1})	*4*	16.16 ± 2.03	*5*	15.35 ± 1.28	*5*	13.21 ± 1.99
Quantum yield Φ	*4*	0.055 ± 0.004	*5*	0.053 ± 0.002	*5*	0.050 ± 0.005
I_c (µmol PAR m^{-2} s^{-1})	*4*	17.52 ± 1.91	*5*	19.32 ± 4.59	*5*	16.20 ± 2.98
R_n (µmol CO_2 m^{-2} s^{-1})	*30*	1.14 ± 0.01	*18*	0.96 ± 0.08	*17*	0.88 ± 0.06
Γ^* (µmol CO_2 mol^{-1})	*4*	39.80 ± 1.69	*4*	41.67 ± 1.76	*4*	37.56 ± 1.94

References

Brooks A, Farquhar GD (1985) Effect of temperature on the CO2/O2 specificity of ribulose-1,5-bisphosphate carboxylase oxygenase and the rate of respiration in the light - estimates from gas-exchange measurements on spinach. Planta 165:397-406

Evans JR (1987) The relationship between electron-transport components and photosynthetic capacity in pea leaves grown at different irradiances. Australian Journal of Plant Physiology 14:157-170

Ögren E, Evans JR (1993) Photosynthetic light-resonse curves- 1. The influence of CO2 partial pressure and leaf inversion. Planta 189:182-190

Ryan CM (2009) Carbon Cycling, Fire and Phenology in a Tropical Savanna Woodland in Nhambita, Mozambique. In: School of GeoSciences, vol. Doctor of Philosophy. The University of Edinburgh, Edinburgh

Tjoelker MG, Oleksyn J, Reich PB (2001) Modelling respiration of vegetation: evidence for a general temperature-dependent Q(10). Global Change Biology 7:223-230

Appendix 2

Leaf trait relations of miombo woodlands

E. Woollen [1]

[1] School of GeoSciences, The University of Edinburgh, Edinburgh, EH9 3JN, UK

Introduction

As a biochemical process, photosynthesis exhibits simple scaling relationships, and one of the most common scaling relationships found is a strong positive correlation between photosynthetic capacity and leaf nitrogen (N) content (Field & Mooney 1986, Evans 1989). Models have used these scaling relationships to predict photosynthetic capacity on a global scale (Kattge et al. 2009; Reich et al. 2007). Universal leaf trait relationships have been shown to exist across several species and biomes (Reich et al. 1997; Wright et al. 2004), which can be used in models to predict photosynthetic activity on a global scale. However, universal leaf trait relationships suffer from a lack of plant physiological measurements from the tropics, biasing global scale leaf trait relations towards species in temperate regions (Reich et al. 2007). Furthermore, large trait variability has been found in different sites and between species (Domingues et al. 2010; Reich et al. 1999; Wright et al. 2005; Wullschleger 1993), making site specific measurements important for accurate local scale modelling. In the tropical biome, Africa as a whole has been vastly underrepresented in global gas exchange datasets, owing to a paucity of leaf gas exchange measurements (Domingues et al. 2010; Meir et al. 2007; Midgley et al. 2004; Mooney et al. 1983; Tuohy et al. 1991). To the knowledge of the author,

miombo woodland photosynthetic carboxylation rates and related leaf traits have never been measured. In this study I asked, what are the leaf trait relationships of miombo tree species, and do leaf trait relations vary seasonally? How do they compare with global leaf trait relations?

Leaf trait measurements were taken on two key miombo canopy species, *Brachystegia spiciformis* and *Julbernardia globiflora*, and one commonly co-occurring understory tree *Diplorhynchus condylocarpon*. Measurements were taken in the dry season during new leaf development (October-November 2009) before the start of the rains, and at the end of the following wet season (April-May 2010) in miombo woodlands of central Mozambique. We compare light saturated assimilation rates (A_{sat}), maximum carboxylation rates (V_{cmax}) and maximum electron transport rates (J_{max}) to leaf nutrient content and physical structure of miombo trees across seasons. We compare our findings to global leaf trait relationships, and to other African ecosystems, and suggest optimal scaling relationships for use in miombo woodlands.

Methods

For a full description of the study site, CO_2 response curve measurements, and other leaf trait measurements, see methods section in chapter 2 of this thesis.

Statistical analyses

Least-squares linear regression analyses were used to test for bivariate relationships between leaf traits on a leaf area basis on all data (all species and seasons combined), and by season (all species combined within each season). No transformations on data were needed, as regression error residuals were all normally

distributed and showed similar variances. To test for significant differences between the slopes and intercepts of bivariate relationships grouped by season we used an analysis of covariance (ANCOVA), where a P value < 0.05 for the interaction term indicated a significant difference in the slopes, and a P value < 0.05 for the differences in group means indicated a significant difference in the intercepts at the 95% confidence interval. All analyses were conducted using Matlab routines (MathWorks 2007). All bivariate relationships were done on a leaf area basis rather than a leaf mass basis, as our leaf-mass-to-area (*LMA*) ratio measurements were not conducted on a leaf level but on a tree level, reducing accuracy on conversion to leaf mass basis using a mean *LMA* rather than a leaf specific *LMA*. Using leaf area basis rather than mass basis relationships has been shown to give weaker relationships between leaf traits (Wright et al., 2004), but using leaf area basis relationships meant that the only variable which needed conversion from mass basis to area basis was leaf nitrogen content, reducing errors due to non-leaf specific *LMA* measurements.

To be able to compare leaf trait relationships to other studies we used the same methodology as employed in Wright et al. (2004) and Domingues et al. (2010), where bivariate relationships between leaf traits on an individual leaf basis were done using standardised major axis (*SMA*) regression fits (Warton et al. 2006) on $\log_{10}$ transformed data. To test for significant differences between slopes and intercepts the routines used in the SMATR software (Falster et al. 2006), which was used to calculate SMA fits, and as outlined in Warton et al. (2006) were used.

Results

Leaf trait relationships

Linear regressions found several significant relationships between leaf traits in both seasons (Table 1). Light saturated assimilation rates (A_{sat}), maximum electron transport (J_{max}) and carboxylation rates (V_{cmax}) showed positive linear relationships with leaf N content in both seasons (Fig. 1). A_{sat} rates were significantly (ANCOVA, $P < 0.05$) lower during the dry season at any given leaf N content (Table 1, Fig. 1 A). J_{max} rates were lower in the dry season at high leaf N content as compared to the wet season (Fig. 1 B), and the slopes of the relationships were significantly (ANCOVA, $P < 0.05$) different between seasons (Table 1). V_{cmax} and leaf N content were linearly correlated in both seasons (Fig. 1 C), and were not significantly different between seasons (Table 1). J_{max} and V_{cmax} show strong linear relationships in both seasons (Fig. 1 D), but the slope of the relationship was significantly lower (ANCOVA, $P < 0.01$) in the dry season than in the wet season (Table 1), as J_{max} rates were lower in the dry season.

Table 1: Linear regression coefficients of relationships between leaf traits (V_{cmax}, J_{max}, A_{sat}) and leaf chemical and physical structure (N, LMA) on a leaf area basis. Coefficients are not shown when regressions were not significant (*ns*, $P > 0.05$).

Model	All data	Dry season	Wet season
$A_{sat} = a + b\ N_a$	$a = 5.78$ $b = 5.04$	$a = 5.34$* $b = 3.09$	$a = 6.90$* $b = 5.33$
	$r^2 = 0.31$	$r^2 = 0.41$	$r^2 = 0.37$
$A_{sat} = a + b\ LMA$	$a = 3.60$ $b = 0.14$	$a = -4.78$* $b = 0.19$	$a = 8.99$* $b = 0.09$
	$r^2 = 0.13$	$r^2 = 0.64$	$r^2 = 0.08$
$J_{max} = a + b\ N_a$	$a = 48.61$ $b = 47.28$	$a = 68.68$* $b = 20.77$*	$a = 38.27$* $b = 59.05$*
	$r^2 = 0.35$	$r^2 = 0.19$	$r^2 = 0.48$
$J_{max} = a + b\ LMA$	$a = 30.43$ $b = 1.24$	$a = 17.39$* $b = 1.09$	$a = 49.48$* $b = 1.15$
	$r^2 = 0.14$	$r^2 = 0.21$	$r^2 = 0.13$
$V_{cmax} = a + b\ N_a$	$a = 32.99$ $b = 32.80$	$a = 38.60$ $b = 26.10$	$a = 29.85$ $b = 35.94$
	$r^2 = 0.40$	$r^2 = 0.30$	$r^2 = 0.46$
$V_{cmax} = a + b\ LMA$	$a = 10.11$ $b = 0.99$	$a = -27.48$ $b = 1.39$	$a = 28.36$ $b = 0.80$
	$r^2 = 0.21$	$r^2 = 0.33$	$r^2 = 0.16$
$J_{max} = a + b\ V_{cmax}$	$a = 6.42$ $b = 1.38$	$a = 28.45$* $b = 0.91$*	$a = 1.70$* $b = 1.51$*
	$r^2 = 0.81$	$r^2 = 0.85$	$r^2 = 0.89$
$LMA = a + b\ N_m$	$a = 60.54$ $b = 8.49$	$a = 45.76$ $b = 15.61$	*ns*
	$r^2 = 0.10$	$r^2 = 0.47$	

* indicates slopes and/or intercepts are significantly different (ANCOVA, $P < 0.05$) between the wet and the dry seasons

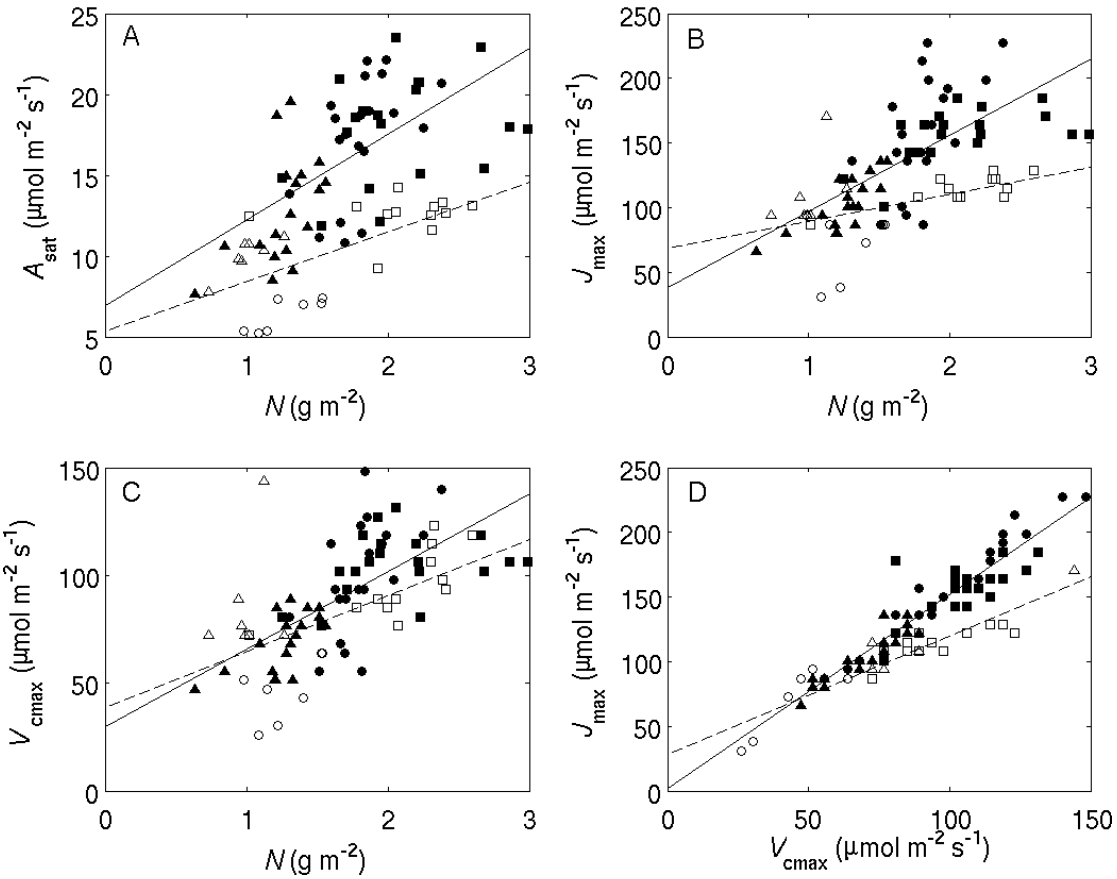

Fig. 1: Relationships between A) light saturated assimilation rate (A_{sat}), B) maximum electron transport rate (J_{max}), C) maximum carboxylation rate (V_{cmax}) and leaf nitrogen (N) content on an area bases, and D) maximum electron transport rate and maximum carboxylation rate in the dry season (open symbols and dashed lines) and the wet season (filled symbols and solid lines) for tree species of *Brachystegia spiciformis* (circles), *Julbernardia globiflora* (squares) and *Diplorhynchus condylocarpon* (triangles). For regression coefficients see Table 1.

Positive linear relationships between *LMA* and A_{sat} rate were strong during the dry season ($r^2 = 0.64$) (Fig. 2 A), when leaves were still developing, but only very weak ($r^2 = 0.08$) during the wet season (Table 1). J_{max} and V_{cmax} relationships with *LMA* were also positively linear in both seasons (Fig. 2 B & C), with stronger relationships in the dry season than in the wet season (Table 1). *LMA* was significantly ($P < 0.05$) positively linearly correlated ($r^2 = 0.47$) to leaf N_m content (on a mass basis) during the dry season, where leaf N_m content increased with leaf physical development (Table 1).

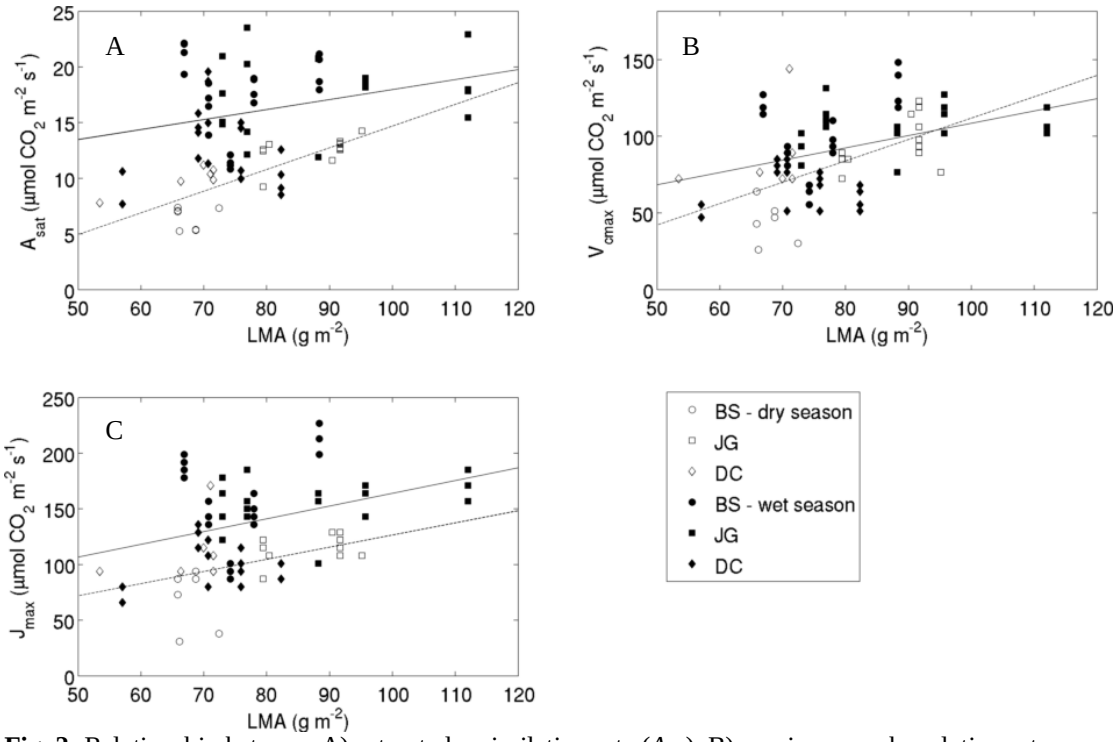

Fig. 2: Relationship between A) saturated assimilation rate (A_{sat}), B) maximum carboxylation rate (V_{cmax}), C) maximum electron transport rate (J_{max}) on an area basis and leaf mass per area in the wet season (filled symbols and solid lines) and the dry season (open symbols and dashed lines) for all three species: *B. spiciformis* (BS), *J. globiflora* (JG) and *D. condylocarpon* (DC). For regression coefficients see Table 1.

Comparing to global leaf trait datasets

The standard major axis fits between pooled A_{sat} rates and leaf N_a content (y = 1.1x + 0.91, $r^2 = 0.38$) and *LMA* (y = 2.41x - 15.58, $r^2 = 0.14$) were significantly ($P < 0.05$) different to the fits found by Wright et al. (2004) using a global dataset, and to Domingues et al. (2010) on a West African woodland dataset (Fig. 3). One exception was that there was no significant difference ($P > 0.05$) between the slope of A_{sat} relationships to leaf N_a content in this study and that of Wright et al. (2004) using a global dataset (Fig. 3 A). A_{sat} values in this study were generally higher than the global dataset average and higher than the west African woodland average at the range of leaf N content and *LMA* measured in this study (Fig. 3).

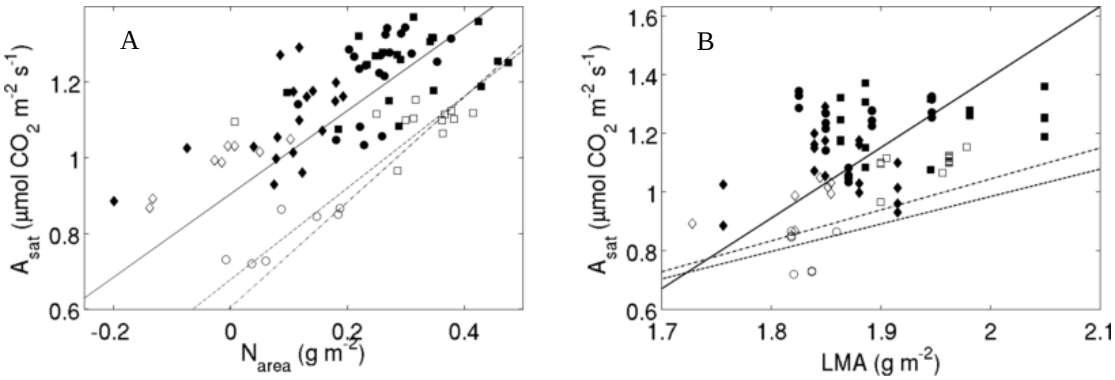

Fig. 3: The relationship between A) leaf level light saturated assimilation rates (A_{sat}) and leaf nitrogen content on an area basis (N_{area}), and B) leaf mass to area ratios (*LMA*). Axes are on log10 scales. Measurements from this study were taken on three species, *Brachystegia spiciformis* (circles), *Julbernardia globiflora* (squares) and *Diplorhynchus condylocarpon* (diamonds), during the dry season (open symbols) and the wet season (filled symbols). Standardised major axis (SMA) line fitting (solid lines) was applied to the whole data set. The dashed line is an SMA fit to a global data set from Wright et al. (2004); the dash-dot line is an SMA fit to a western African woodland data set from Domingues et al. (2010). All slopes and elevations are significantly different between this study and the two other studies ($P < 0.05$), except for (A) the slope between this study and Wright et al.

Discussion

Assimilation and leaf nutrient relations

In all species, A_{sat} rates increased linearly with increasing leaf N content in both seasons. Other studies done in African savanna find only weak relationship between A_{sat} and leaf N content (Midgley et al. 2004). Domingues et al. (2010) demonstrates that both leaf N and Phosphorus (P) content co-limit photosynthetic rates in west African woodlands, and closer relationships between assimilation rates and leaf P content (Meir et al. 2007) suggests that P is more limiting than N in these regions. The majority of trees in miombo woodlands belong to the sub-family Caesalpiniodeae, which are typically non-nodulating (i.e. non-nitrogen fixing) leguminous trees, but have mycorrhizal root associations increasing their ability for P uptake (Hogberg 1986a; Hogberg 1986b). Tuohy et al. (1991) failed to find any correlation between leaf P content and CO_2 assimilation rates in miombo woodlands,

but a strong relationship with leaf N content and assimilation rates exists, suggesting that leaf P content was not limiting to photosynthetic rates but leaf N content was.

Drought stress and photoinhibition

Metabolic impairments to the photosynthetic apparatus during periods of low water availability have been found to occur in plant species of other seasonally dry environments (Nogues and Baker 2000; Tezara et al. 2005), decreasing photosynthetic reaction rates and capacity for C uptake significantly. During drought stress, some plants are susceptible to damage from high irradiance, causing photoinhibition, impairing light-dependent photosynthetic reactions (PSII) and decreasing photosynthetic capacity (Long et al. 1994). Photoinhibition can be exacerbated when multiple stress factors such as water stress and high temperatures co-occur with high light environments (Flexas et al. 1999; Powles 1984). Reduced assimilation rates (A_{sat}) found in this study during the dry season were related to reduced electron transport rates (J_{max}), indicating impairments to PSII. Impaired PSII reaction rates tend to occur early in drought development, at relatively high stomatal conductance (g_s > 150 mmol m^{-2} s^{-1}), whereas Rubisco activity (i.e. Vcmax rates), a part of the dark reaction (PSI) of photosynthesis, does not generally decrease until severe drought stress (g_s < 100 mmol m^{-2} s^{-1}) (Flexas and Medrano 2002). This could explain why the carboxylation rates (V_{cmax}) did not change between seasons in this study, as measurements at low stomatal conductance were excluded. However, we cannot assess whether photoinhibition or other factors caused the lower electron transport rates and reduced photosynthetic capacity in the dry season, and further studies using chlorophyll fluorescence measurements would be needed to ascertain

which mechanisms were reducing or impairing metabolic processes (Tezara et al. 2005).

Mean J_{max}:V_{cmax} ratios ranged from 1.3 in the dry season to 1.5 in the wet season in this study, lower than the average ratio reported for a global datasets of 1.6 (Wullschleger 1993). Other studies conducted in tropical environments report a range of ratios. For example, west African woodlands show a mean ratio of 1.2 (Domingues et al. 2010), along the Kalahari transect it was 1.3 (Midgley et al. 2004), 1.4 in the Sahel, 1.7 in the Cameroonian rain forest (Meir et al. 2007), and 2.1 in tropical rain forest of French Guiana (Coste et al. 2005). It is interesting that in the drier locations, J_{max}:V_{cmax} ratios tend to be lower than the global average, but in wetter locations it is higher. Perhaps this difference is caused by reduced J_{max} rates in areas that are prone to drought stress and high temperatures and irradiance levels. There are no studies to confirm this hypothesis, and further investigation into global variations in J_{max}:V_{cmax} ratios in relation to environmental conditions might shed more light on this theory.

Despite the depressed rates of J_{max} in the dry season, J_{max} rates seem to recover in the wet season, indicating reversible metabolic impairments and no long term damage occurred. It is unclear what impacts a changing climate might have on miombo woodland productivity, but with increased drought stress and temperatures, permanent impairments to metabolic processes is more likely to occur (Flexas and Medrano 2002). Decreased photosynthetic potential can perhaps decrease miombo tree species competitiveness over other co-occurring species, eventually limiting or changing their geographical distributions.

Global context

In west African woodlands, Domingues et al. (2010) report A_{sat} ranges (5-28 μmol CO_2 m^{-2} s^{-1}), J_{max} (30-140 μmol m^{-2} s^{-1}) and V_{cmax} ranges (20-90 μmol m^{-2} s^{-1}) similar to other values reported for the tropics (Coste et al. 2005; Eamus et al. 1999; Meir et al. 2007; Midgley et al. 2004; Tuohy et al. 1991). In this study, A_{sat} values for three miombo tree species in two seasons (6 -18 μmol m^{-2} s^{-1}) fall within the range reported in other tropical studies, but our J_{max} (71-157 μmol m^{-2} s^{-1}) and V_{cmax} (46-105 μmol m^{-2} s^{-1}) values were slightly higher than other tropical values, particularly in the wet season. The high A_{sat}, J_{max} and V_{cmax} rates found in this study were comparable to rates found in several tree species on the arid to semi-arid Kalahari transect in Botswana (Midgley et al. 2004), and rates found in the Sahel (Meir et al. 2007). When comparing to Beerling and Quick (1995) modelled parameter estimates, our mean wet season V_{cmax} and J_{max} values compare well with the tropical seasonal forest vegetation type.

The differences found in photosynthetic parameters between this study and several other studies emphasises the differences which exist between species and sites (Domingues et al. 2010; Wright et al. 2005; Wullschleger 1993). Differing measurement techniques and instrumentation can also create differences (Long and Bernacchi 2003; Rodeghiero et al. 2007; Santiago and Mulkey 2003), even when seemingly similar applications of the Farquhar et al. (1980) model are used for parameter estimation. However, despite variations in leaf trait parameter estimates, leaf trait relationships have been found to be robust across several biomes and species (Reich et al. 1999; Reich et al. 1997; Wright et al. 2005) and miombo woodland is no exception. A_{sat} rates and leaf N content relations on an area basis

followed the same relationship as global leaf trait relations (Wright et al. 2004), although with higher rates. The same could not be said, however, for A_{sat} relations to *LMA*, where a significant deviation from the global dataset relationship was observed, possibly caused by the low accuracy of leaf specific *LMA* and a small range, creating large scatter in the relationship ($r^2 = 0.13$).

References

Beerling DJ, Quick WP (1995) A new technique for estimating rates of carboxylation and electron transport in leaves of C3 plants for use in dynamic global vegetation models. Global Change Biology 1:289-294

Choinski JS, Johnson JM (1993) Changes in Photosynthesis and Water Status of Developing Leaves of Brachystegia-Spiciformis Benth. Tree Physiology 13:17-27

Coste S, Roggy JC, Imbert P, Born C, Bonal D, Dreyer E (2005) Leaf photosynthetic traits of 14 tropical rain forest species in relation to leaf nitrogen concentration and shade tolerance. Tree Physiology 25:1127-1137

Domingues TF et al. (2010) Co-limitation of photosynthetic capacity by nitrogen and phosphorus in West Africa woodlands. Plant Cell and Environment 33:959-980

Eamus D, Myers B, Duff G, Williams D (1999) Seasonal changes in photosynthesis of eight savanna tree species. Tree Physiology 19:665-671

Falster DS, Warton DI, Wright IJ (2006) SMATR: Standardised major axis tests and routines, ver 2.0. http://www.bio.mq.edu.au/ecology/SMATR/.

Farquhar GD, Caemmerer SV, Berry JA (1980) A Biochemical Model of Photosynthetic CO2 Assimilation in Leaves of C3 Species. Planta 149:78-90

Flexas J, Medrano H (2002) Drought-inhibition of photosynthesis in C-3 plants: Stomatal and non-stomatal limitations revisited. Annals of Botany 89:183-189

Hogberg P (1986a) Nitrogen fixation and nutrient relations in savanna woodland trees (Tanzania). Journal of Applied Ecology 23:675-688

Hogberg P (1986b) Soil nutrient availability, root symbioses and tree species composition in tropical Africa: a review. Journal of Tropical Ecology 2:359-372

IPCC (2007) Fourth Assessment Report: Climate Change 2007 (AR4). Geneva, Switzerland

Kattge J, Knorr W, Raddatz T, Wirth C (2009) Quantifying photosynthetic capacity and its relationship to leaf nitrogen content for global-scale terrestrial biosphere models. Global Change Biology 15:976-991

Lawlor DW, Cornic G (2002) Photosynthetic carbon assimilation and associated metabolism in relation to water deficits in higher plants. Plant Cell and Environment 25:275-294

Long SP, Bernacchi CJ (2003) Gas exchange measurements, what can they tell us about the underlying limitations to photosynthesis? Procedures and sources of error. Journal of Experimental Botany 54:2393-2401

Long SP, Humphries S, Falkowski PG (1994) Photoinhibition of photosynthesis in nature. Annual Review of Plant Physiology and Plant Molecular Biology 45:633-662

MathWorks (2007) Matlab (Version 7.4). The MathWorks Inc., Natick, MA.

Meir P, Levy PE, Grace J, Jarvis PG (2007) Photosynthetic parameters from two contrasting woody vegetation types in West Africa. Plant Ecology 192:277-287

Midgley GF, Aranibar JN, Mantlana KB, Macko S (2004) Photosynthetic and gas exchange characteristics of dominant woody plants on a moisture gradient in an African savanna. Global Change Biology 10:309-317

Mooney HA, Field C, Gulmon SL, Rundel P, Kruger FJ (1983) Photosynthetic characteristics of south-African sclerophylls. Oecologia 58:398-401

Reich PB et al. (1999) Generality of leaf trait relationships: A test across six biomes. Ecology 80:1955-1969

Reich PB, Walters MB, Ellsworth DS (1997) From tropics to tundra: Global convergence in plant functioning. Proceedings of the National Academy of Sciences of the United States of America 94:13730-13734

Reich PB, Wright IJ, Lusk CH (2007) Predicting leaf physiology from simple plant and climate attributes: A global GLOPNET analysis. Ecological Applications 17:1982-1988

Rodeghiero M, Niinemets U, Cescatti A (2007) Major diffusion leaks of clamp-on leaf cuvettes still unaccounted: how erroneous are the estimates of Farquhar et al. model parameters? Plant Cell and Environment 30:1006-1022

Santiago LS, Mulkey SS (2003) A test of gas exchange measurements on excised canopy branches of ten tropical tree species. Photosynthetica 41:343-347

Tuohy JM, Prior JAB, Stewart GR (1991) Photosynthesis in Relation to Leaf Nitrogen and Phosphorus-Content in Zimbabwean Trees. Oecologia 88:378-382

Warton DI, Wright IJ, Falster DS, Westoby M (2006) Bivariate line-fitting methods for allometry. Biological Reviews of the Cambridge Philosophical Society 81:259-291

Wright IJ et al. (2005) Assessing the generality of global leaf trait relationships. New Phytologist 166:485-496

Wright IJ et al. (2004) The worldwide leaf economics spectrum. Nature 428:821-827

Wullschleger SD (1993) Biochemical Limitations to Carbon Assimilation in C3 Plants - A Retrospective Analysis of the A/Ci Curves from 109 Species. Journal of Experimental Botany 44:907-920

Appendix 3

Published paper by Ryan et al. (2012) detailing the radar derived biomass maps used in chapter 4 of this thesis:

C.M. Ryan, T. Hill, E. Woollen, C. Ghee, E. Mitchard, G. Cassells, J. Grace, I.H. Woodhouse, and M. Williams (2012) Quantifying small-scale deforestation and forest degradation in African woodlands using radar imagery. Global Change Biology 18: 243-257

Permission to include this paper in this thesis has been obtained from co-authors

Quantifying small-scale deforestation and forest degradation in African woodlands using radar imagery

Casey M Ryan[1], Timothy Hill[1,2], Emily Woollen[1], Claire Ghee[1,3], Edward Mitchard[1], Gemma Cassells[1], John Grace[1,2], Iain H Woodhouse[1] and Mathew Williams[1,2]

1. School of Geosciences, University of Edinburgh, EH9 3JN.

2. The National Centre for Earth Observation, Natural Environment Research Council, UK.

3. Now at: The James Hutton Institute, Invergowrie, Dundee DD2 5DA.

Corresponding Author:

Casey Ryan, tel: +44 131 650 7722 casey.ryan@ed.ac.uk

Abstract

Carbon emissions from tropical land use change are a major uncertainty in the global carbon cycle. In African woodlands, small-scale farming and the need for fuel are thought to be reducing vegetation carbon stocks, but quantification of these processes is hindered by the limitations of optical remote sensing and a lack of ground data. Here we present a method for mapping vegetation carbon stocks and their changes over a three year period in a >1000 km^2 region in central Mozambique at 0.06 ha resolution. L-band synthetic aperture radar imagery and an inventory of 96 plots are combined using regression and bootstrapping to generate biomass maps with known uncertainties. The resultant maps have sufficient accuracy to be capable of detecting changes in forest carbon stocks of as little as 12 MgC ha^{-1} over 3 years with 95% confidence. This allows characterisation of biomass loss from deforestation and forest degradation at a new level of detail. Total aboveground biomass in the study area was reduced by 6.9±4.6% over three years: from 2.13±0.12 TgC in 2007 to 1.98±0.11 TgC in 2010, a loss of 0.15±0.10 TgC. Degradation probably contributed 67% (96.9±91.0 GgC) of the net loss of biomass, but is associated with high uncertainty. The detailed mapping of carbon stock changes quantifies the nature of small-scale farming. New clearances were on average small (median 0.2 ha) and were often additions to already cleared land. Deforestation events reduced biomass from 33.5 to 11.9 MgC ha^{-1} on average. Contrary to expectations, we did not find evidence that clearances were targeted towards areas of high biomass. Our method is scalable and suitable for monitoring land cover change and vegetation carbon stocks in woodland ecosystems, and can support policy approaches towards reducing emissions from deforestation and degradation (REDD).

Key words: carbon mapping, emissions, land use change, agriculture, machamba, carbon stocks, ALOS PALSAR, radar, backscatter

Introduction

Deforestation and other land use change is a major component of the anthropogenic carbon (C) cycle, transferring 0.9-2.2 PgC $year^{-1}$ from the biota to the atmosphere (Houghton, 2010). This number is highly uncertain (Denman *et al.*, 2007, Ramankutty *et al.*, 2007, van der Werf *et al.*, 2009, Houghton, 2010) and estimates often exclude many of the processes leading to degradation of forest land (Houghton, 2010). Deforestation is primarily the result of the clearing of land for agriculture (Geist & Lambin, 2002), both for the large-scale production of global commodities (DeFries *et al.*, 2010), and, particularly in Africa, for small-scale production of food and cash crops (Burgess *et al.*, 2002, Fisher, 2010). In Africa, land use change emissions are thought to be in region of 0.3 ± 0.2 PgC $year^{-1}$ (Houghton & Hackler, 2006, Williams *et al.*, 2007, Ciais *et al.*, in press), but the data underlying these estimates come from extrapolation of outdated, unreliable and inconsistent national estimates (Grainger, 2008, Kindermann *et al.*, 2008, FAO, 2010).

Woodlands, characterised by an open tree canopy and a continuous grass layer, cover 36% of vegetated Africa (Mayaux *et al.*, 2004), and as such represent a low density, but large, stock of vegetation C (Dewees *et al.*, 2010). African countries dominated by woodlands have high population densities, high population growth rates and high, but uncertain, deforestation rates (FAO, 2010). As a result, nations

dominated by woodlands contribute around half of Africa's deforestation emissions (based on data from Mayaux et al. (2004) and FAO (2010)). Woodlands are particularly difficult to monitor with optical/infrared remote sensing due to inter- and intra- annual changes in tree leaf display (Grainger, 1999) and the transient presence of a substantial grass layer which complicates the interpretation of such satellite imagery (Archibald & Scholes, 2007). Consequently, degradation emissions from woodlands are highly uncertain, but are thought to be substantial (Ahrends *et al.*, 2010).

The standard approach to estimating C emissions from deforestation is based on estimates of changes in forest area, aided by increasingly robust estimates of forest area change (Etter *et al.*, 2006, Achard *et al.*, 2007, Hansen *et al.*, 2008, Miettinen *et al.*, 2011). Degradation emission estimates however, require repeat *in situ* measurements of carbon density (GOFC-GOLD, 2010) which are scarce (Ahrends *et al.*, 2010), because they require a large number of plots and strata to estimate accurately any changes in mean C density. Recent airborne approaches (Asner *et al.*, 2010) have not been widely deployed to date. As a result, changes in forest C density resulting from fire (Ryan & Williams, 2011) or the selective extraction of biomass for fuel or timber (Nepstad *et al.*, 1999), are rarely assessed and have not been fully included in emissions estimates (Houghton & Hackler, 2006, Denman *et al.*, 2007).

Even when combined, the methods outlined above yield large uncertainties on estimates of changes in vegetation C stock, let alone on emissions (Houghton *et al.*, 2009). Uncertainty stems from three main issues: 1) The use of arbitrary forest/non-forest thresholds whereas C stocks are a continuous variable. Such

thresholds are a particular problem in woodlands where distinct edges are rare; 2) a lack of *in situ* measurements of C density, and the potential artefacts associated with differential land use on research plots; and 3); land that is deforested or degraded may not be representative of the forest type in which it is found (Loarie *et al.*, 2009, Houghton, 2010). That is, farmers are likely to target areas for deforestation based on careful consideration of agricultural potential. Therefore, land with higher than average soil fertility and/or water availability might be expected to have a greater probability of conversion to agriculture. The same areas might also be expected to have higher than average soil and vegetation C stocks due to the increased productivity.

Small scale, often shifting, cultivation exemplifies the problem of estimating changes in C stocks in forests and woodlands, producing a mosaic landscape that is frequently misclassified (Mertz, 2009) and is rarely well-represented by discrete land cover classes. The landscape C dynamics (Williams *et al.*, 2008) cannot be adequately described by changes between categories such as degraded land, forest or agriculture (Schmidt-Vogt *et al.*, 2009). Furthermore, the scale at which small-scale farmers clear forest is constrained by a lack of mechanical power and transport. This physical limit results in small farms (scale ~ha) that may not be recorded on land use maps or detected with accuracy by coarse-scale (~km^2) satellite-based land cover change analyses.

Thus, there is a clear need for direct measurement at sub-hectare resolution of changes in C stocks due to land cover change (Houghton *et al.*, 2009). Our first aim is to demonstrate a method for such measurements in African woodlands at a spatial resolution sufficient to characterise small scale farming and degradation. This is

achieved by the use of 25 m resolution L-band radar imagery to map C stocks and their changes through the years 2007-10 in an area of central Mozambique. Radar imagery has several advantages for this purpose. Firstly, cloud and atmospheric effects are largely irrelevant allowing observations at cloudy sites. Secondly, L-band (23 cm wavelength) normalised radar cross section (hereafter referred to as backscatter) has been shown to have a reasonably direct relationship to woody biomass up to a saturation at around 50 MgC ha^{-1} (Le Toan *et al.*, 1992, Rignot *et al.*, 1994, Magnusson *et al.*, 2007, Karjalainen *et al.*, 2009). These advantages mean that spaceborne radar imagery is increasingly used in support of land use mapping in the tropics (van der Sanden & Hoekman, 1999, Hoekman *et al.*, 2010, Rahman & Sumantyo, 2010). Previous work has shown that L-band radar backscatter is well-correlated to biomass across several African landscapes (Mitchard *et al.*, 2009). The resultant C maps allow us to ask several questions about the nature of the processes of deforestation and degradation:

- How much carbon is lost to deforestation compared to degradation?
- Are areas of high carbon density preferentially targeted for land cover change?
- What is the carbon density of changed areas before and after land cover change?
- What size are land cover change events, and how are they clustered in space?

Methods

Site description and land use history

Our study area covers 1,160 km^2 in the Gorongosa and Nhamatanda districts of Sofala province in central Mozambique. It is primarily dominated by miombo woodland, the most widespread vegetation type in Southern Africa (Frost, 1996). It has a seasonal wet-dry climate with ~900 mm rain per year, with 82% falling in the five months between November and March (Ryan *et al.*, 2011). The vegetation consists of miombo woodland on the well-drained flanks of the Rift valley, grading to more scattered savanna on the poorly drained valley floor (Tinley, 1977, 1982). The terrain is gently undulating in most of the study area, but in the west there are steep slopes associated with the Pungue and Vunduzi rivers (Fig S1). Ninety seven per cent of the study area has a slope of < 10° (based on 90 m resolution elevation data from the Shuttle Radar Topography Mission (SRTM, Farr *et al.*, 2007, http://srtm.usgs.gov).

The area is undergoing rapid land use change: in 1992, with the end of the Mozambican civil war, there were major population movements in the area, including resettlement of semi-abandoned rural areas such as Nhambita (Fig 1). The only surfaced road in the area, the EN1, was rebuilt, along with a bridge over the River Pungue (rehabilitation of both took place from 1999-2002), connecting the study area and Gorongosa town to the Beira corridor, the major area of economic activity in central Mozambique. Gorongosa town has grown rapidly since 1992 (INE, 2010) with the district population increasing by 50% from 1997 to 2007 to 117,129. Currently, 69% of the population is aged below 18 years (INE, 2010). Forest or woodland loss in the area is primarily the result of: 1) clearance for small scale

agriculture, notably for maize production on farms of between ~1-2 ha and 2) charcoal production, involving the selective removal of medium size stems from an area of ~0.2 ha surrounding temporary kilns. Charcoal is sold along the EN1 highway for transport south to Inchope and Beira, but there is also some demand for charcoal and fuel wood in Gorongosa town. In addition, fire is extensively used to manage the landscape and wild fires are common. Frequent and intense fires can reduce biomass in these woodlands (Furley *et al.*, 2008, Ryan & Williams, 2011).

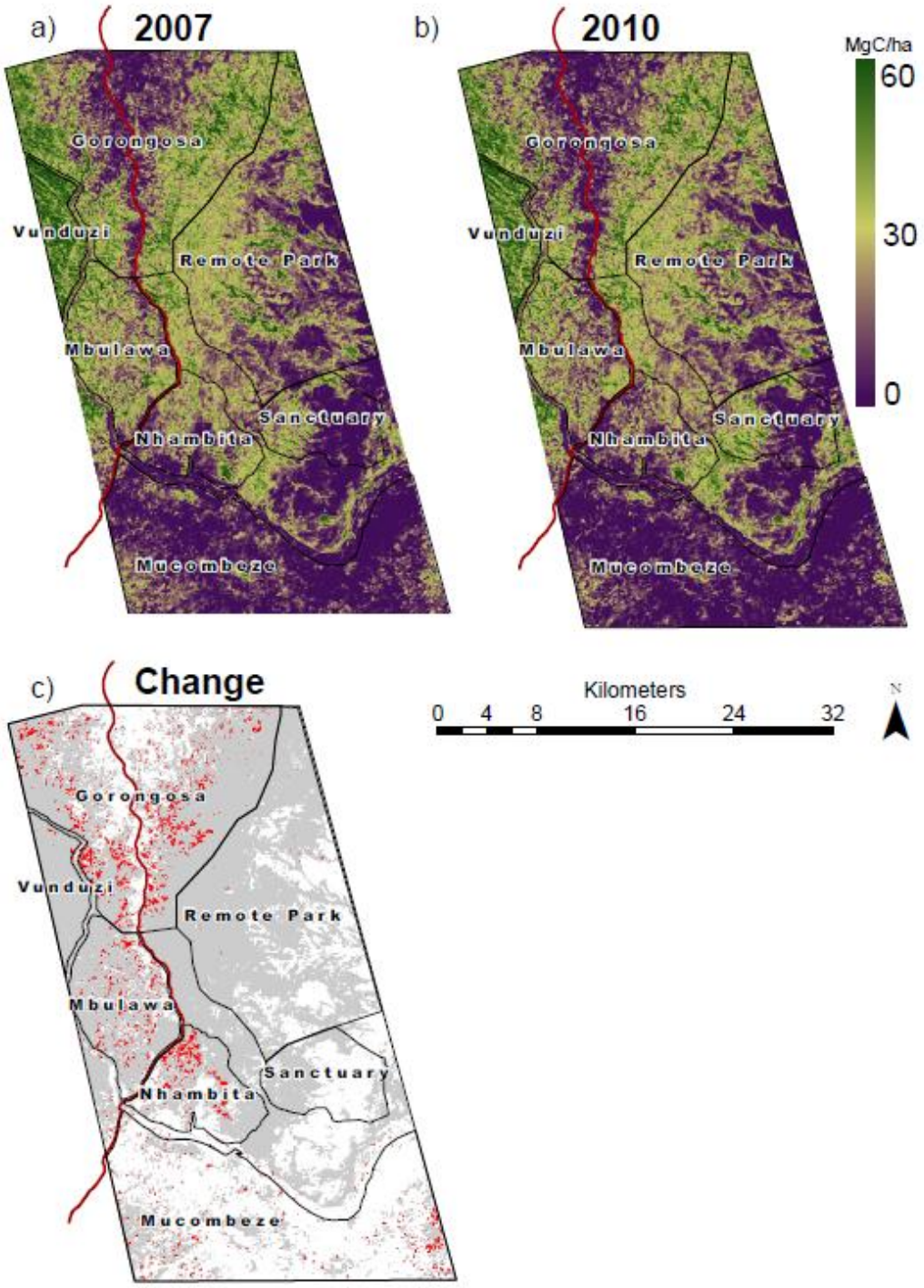

Fig. 1: Estimated carbon stocks in the study area in a) 2007 and b) 2010. Each image is derived from the mean of three ALOS PALSAR scenes from that year's dry season. c) shows the areas detected as undergoing abrupt change (red) with a probability greater than 95% and a reduction in biomass to less than 50% of original biomass. Areas that did not undergo change are indicated in grey, and white indicates areas with < 10tC/ha. The maps are annotated with the local road network and the "sub-areas" used in Fig 7. (GIS data courtesy of ARA-CENTRO).

Carbon stock estimation

The basis of our approach is to produce a three year time series of carbon maps of the area. The maps are produced using a combination of satellite radar images and *in situ* carbon stock inventories. We deal here only with carbon in the aboveground woody vegetation pool (AGB, MgC ha^{-1}), although more information on belowground biomass at this site can be found in Ryan et al (2011).

Radar imagery

Synthetic Aperture Radar (SAR) remote sensing can provide information on vegetation biomass (Le Toan *et al.*, 1992), as well as many other characteristics of the land surface (Woodhouse, 2006a). SAR utilises an active sensor aboard a satellite or plane to send out a beam of energy and measures the intensity of the echoes that return to the sensor. The parameter of interest is the *backscatter* (technically the normalised radar cross-section, a unitless variable (m^2/m^2)). Backscatter can loosely be thought of as the ratio of the power that comes back from a patch of ground to the power sent to that patch of ground (based on the arbitrary assumption that the ground is an isotropic scatterer). The energy that returns to the sensor varies with the proportion of the incident energy that is scattered by the land surface, and the directionality of that scattering. When energy of an appropriate wavelength is used, it interacts with the structural elements of the tree canopy (branches and trunks): typically, more woody biomass results in more diffuse scattering and thus more energy being returned to the sensor and a higher backscatter value is recorded. Backscatter is also affected by soil roughness (as it changes the directionality of the scattering) and moisture (as it changes the total proportion of scattering), as well as other environmental factors. In this study L-band (~23 cm wavelength) SAR imagery

was used, as it is less affected by soil conditions than shorter wavelengths, and is known to be able to detect deforestation and to be sensitive to forest biomass due to its ability to penetrate the forest canopy (Almeida-Filho *et al.*, 2005, Fransson *et al.*, 2007, Karjalainen *et al.*, 2009, Mitchard *et al.*, 2009). Ten images were acquired that covered the study site spanning the dates 23 Jun 2007 to 1 Oct 2010 (Table 1). All images were for the dry season and two or three were available for each year.

Table 1: Regression statistics for the relationship between radar backscatter (unitless) and aboveground woody biomass (MgC ha^{-1}).

Date	RMA Slope (MgC ha^{-1})$^{-1}$		RMA Intercept (MgC ha^{-1})		OLS	Calibration error	Validation error	Validation bias
	Slope	95% confidence interval	Intercept	95% confidence interval	adj R^2	RMSE (MgC ha^{-1})	RMSE (MgC ha^{-1})	Bias (MgC ha^{-1})
23-Jun-07	1562	1315–1810	-20.9	-26.6–-15.1	0.39	10.4	10.9	1.7
08-Aug-07	1268	1082–1453	-13.7	-18.0–-9.5	0.49	9.3	9.9	1.5
23-Sep-07	1329	1153–1505	-11.0	-14.5–-7.5	0.58	8.4	8.7	1.4
10-May-08	1647	1417–1877	-22.6	-27.9–-17.3	0.53	8.9	9.3	1.5
25-Jun-08	1632	1385–1880	-19.9	-25.2–-14.5	0.44	9.8	10.4	1.6
28-Jun-09	1601	1363–1840	-17.5	-22.3–-12.6	0.47	9.6	10.1	1.6
28-Sep-09	1303	1115–1490	-11.2	-15.0–-7.4	0.50	9.2	9.6	1.5
16-May-10	1801	1518–2083	-24.7	-31.0–-18.4	0.41	10.3	10.7	1.7
01-Jul-10	1679	1431–1926	-25.6	-31.6–-19.6	0.48	9.5	9.9	1.6
01-Oct-10	1348	1169–1526	-13.3	-17.0–-9.5	0.58	8.4	8.7	1.4
mean	*1517*	*1295–1739*	*-18.0*	*-22.9–-13.1*	*0.49*	*9.4*	*9.8*	*1.6*

RMA indicates reduced major axis regression. OLS ordinary least squares regression.

The technical details of the imagery and processing now follow. Images were obtained from the Phased Array L-band Synthetic Aperture Radar sensor aboard the Advanced Land Observing Satellite (ALOS PALSAR) in the Fine-Beam Double mode (Shimada *et al.*, 2010). All images were acquired on the ascending pass, have an incidence angle centred on 34.3°, and were provided at a pixel size of 12.5 m with 4 equivalent looks, but then averaged to 25 m for 16 equivalent looks. Only Horizontal-send Vertical-receive data are used here, as previous studies have shown

this polarisation to be more sensitive to biomass than Horizontal-send Horizontal-receive (Le Toan *et al.*, 1992, Mitchard *et al.*, 2009).

The images were processed using the Alaska Satellite Facility's MapReady software v2.3.6 (ASF, 2010), combined with ~90 m elevation data from the SRTM. Each image was converted from digital numbers to backscatter using the calibration coefficients of Shimada *et al.* (2010) and a geometric and radiometric terrain correction was applied. Visual comparison with optical imagery (IKONOS and Landsat) showed that the resulting images were well geolocated (1-2 pixel error, i.e. 25 -50 m) compared to prominent landscape features such as roads, bridges and an airstrip. In particular, the images were very closely geolocated to each other: no geolocation differences were visible between the ten images. Commonly, backscatter values are used on the logarithmic dB scale, but here untransformed values of backscatter are used, as the backscatter-biomass trend is usually linear in untransformed space, but non-linear in dB space.

Ground data

For each radar scene, backscatter values were converted into carbon density using a regression equation based on inventories of 96 plots in the forest, woodland and cropland in the south of the study area. These data come from a range of inventories conducted during 2006-9, and include plots of sizes ranging from 0.1 to 2.2 ha (mean±SD 0.63±0.33 ha, Fig 2). The inventories include standing trees > 5 cm DBH. Many of the woodland inventory data are described in Ryan *et al*. (2011), as is the site-specific allometric equation for converting stem diameter to carbon mass for each stem. Briefly, the data set consist of: fifteen 1 ha square permanent sample plots in the woodland and savanna (Ryan *et al.*, 2011), eight 0.28 ha plots used in the fire

experiments of Ryan and Williams (2011), thirty 0.57 ha plots in a transect from open savanna to woodland (Woollen et al. in prep; these had a nested sampling design, see supplementary information), five 0.5 ha plots in relatively remote woodland, thirty-seven plots of 0.1 to 2.2 ha (mean 0.6 ha) on cropland (Ghee, 2009) and one dense forest plot consisting of three 0.04 ha subplots. Details of the plot data are given in the supplementary information. Every plot is thought to have avoided abrupt land cover change (i.e. deforestation) during the study period, assessed by repeat ground visits or satellite imagery; however we cannot rule out gradual changes due to aggradation or degradation.

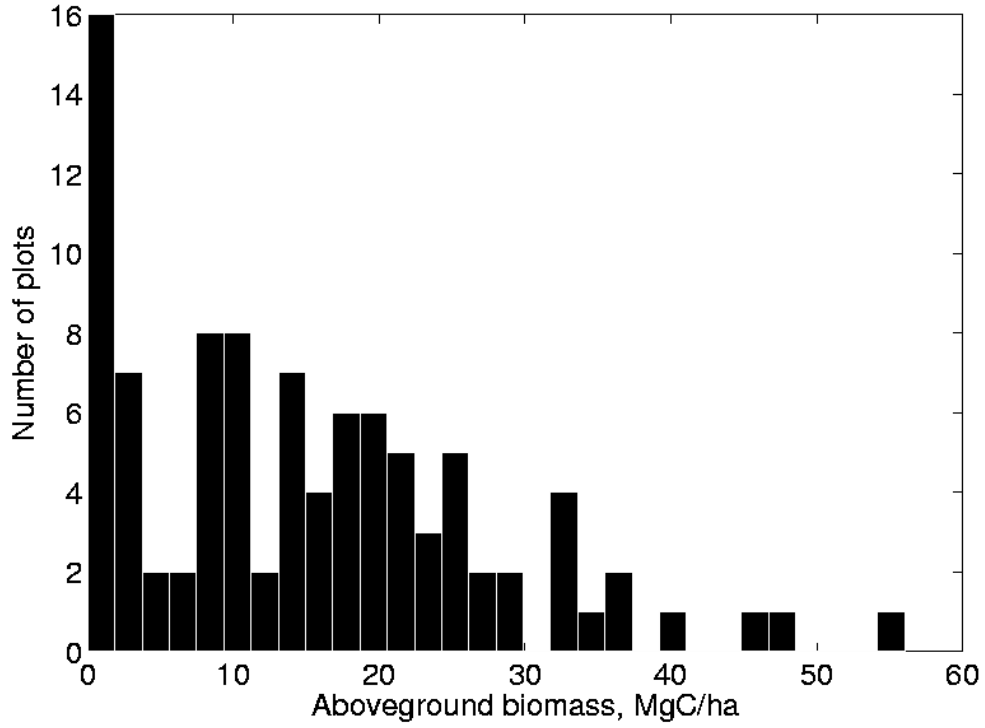

Fig. 2: Histogram of the aboveground biomass (AGB) of the plots used to estimate and validate the AGB-backscatter relationship. Aboveground woody carbon stock is estimated from DBH measurements using a site-specific allometric equation. $n = 96$.

Regression and Error Propagation

To convert backscatter images into aboveground biomass (AGB in units of MgC ha^{-1}), for each timeslice we regress plot mean backscatter against plot AGB, assuming that the plot AGB is consistent over the observational period. We use reduced major axis (RMA) regression (Mitchard 2011, in review) implemented in MATLAB by Trujillo-Ortiz & Hernandez-Walls (2010). RMA regression minimises the errors on both axes (rather than just on the Y-axis as in normal regression), which is appropriate because there are errors in both data sets and the observer controls neither (Sokal & Rohlf, 1995).

To estimate error on the predictions from the regression, a 5,000 x 2-fold cross-validation procedure was employed. Half the dataset was withheld and used to estimate the root mean squared validation error (RMSE), and bias (B) of predictions from each regression. These statistics are defined as (Hui & Jackson, 2007):

$$B = \frac{\sum_i Y_i - \hat{Y}_i}{n}$$

$$RMSE = \sqrt{\frac{\sum_i (Y_i - \hat{Y}_i)^2}{n - 2}}$$

where Y_i is a validation data point (not used in the regression) and $\hat{Y}_i$ is the prediction from the regression. B and RMSE were calculated for all 10 timeslices 5,000 times, each time with a different random split of the data, and the mean values of B and RMSE for the 5,000 validations are reported. For indicative purposes the adjusted R^2 of an ordinary least squares regression is also shown in Table 1.

The temporal covariance of the bias was quantified by looking at the correlation of the bias between time steps for each of the 5,000 validations, i.e. by

asking if the regression is biased high in year *x*, is it likely to be biased high in subsequent years *x*+*n*?

Regression errors were propagated to the carbon maps with a bootstrap procedure. Bootstrapping was used as it implicitly includes any spatial or temporal covariance of the uncertainty resulting from the AGB-backscatter regressions. For each set of 10 carbon maps, 30,000 realisations were created each using a different regression based on randomly selected regression data (resampled with replacement). Derived quantities such as carbon stock change, rates of loss, and the deforestation and degradation totals, were also calculated for each of the 30,000 bootstraps, allowing the uncertainties introduced by the regression to be estimated. All values are reported as the mean ± the standard deviation of the 30,000 bootstraps. The number of bootstraps was chosen after initial analysis showed that repeat calculation with different random number seeds using 10,000 bootstraps yielded identical results to three significant figures.

Change detection algorithm

One of the aims of this paper is to estimate parameters of pixels before and after land cover change. This necessarily involves defining a threshold of change. Here we focus on detecting abrupt losses of AGB and define land cover changes (LCC) of interest as being in pixels where: 1) AGB is >20 MgC ha^{-1} at the start of the study, thus increasing the likelihood that only forested pixels are examined; 2) the AGB of the pixel after the change is reduced to a minimum percentage (φ, default 50%) of its initial AGB, a threshold which should exclude most natural changes in forest structure; and 3) the probability that the change in AGB occurred by chance (given the noise in the data) is $<(1-\alpha)$ (default $\alpha = 0.95$). The use of a ratio to define

change is appropriate with SAR imagery in power space, as ratioing SAR images is generally preferred to differencing because of its noise characteristics (Rignot & van Zyl, 1993, Radke *et al.*, 2005).

The time series $C(t)$, where C is the AGB of a pixel over the t=1,…,10 images, provides a rich data source with which to detect changes, and the 10 time-slices allow more confidence in using noisy data. For change detection, a simple iterative algorithm locates the time-point of change, τ, at which the mean of the preceding values of $C(t)$ is most different to the mean of the remaining part of the time series. The mean AGB before ($C1$) and after ($C2$) τ are then estimated. We use a Monte Carlo procedure to estimate the probability, P, of obtaining the change in AGB ($C1$-$C2$) by chance, based on sampling from the time series and including the RMSE validation errors from the regression (Table 1). A mathematical description is given in the supplementary information.

Once changed pixels have been identified, each LCC event (defined as adjacent changed pixels that have identical τ) was automatically converted to a polygon in ARCGIS (ESRI, CA, USA) and the area of each polygon calculated.

Change detection validation

Two tests were used to produce accuracy statistics for the change detection. To assess successful LCC detection we delineated 92 agricultural fields formed by clearing woodland between March 2007 and June 2009. These conversions were assessed by visual interpretation of multispectral SPOT 4 (20 m resolution) imagery from 7 March 2007 and IKONOS (1 m) imagery from 24 June 2009 (an example is shown in Fig 6). The edges of the new farms were converted by hand to polygons using ARCGIS. These areas of known LCC had a mean area of 1.7±1.5 ha and were

well distributed across the study area. Although the AGB of these new farms is unknown, visual inspection suggests that very few trees remain and that they have crossed the change threshold outlined above. The miss rate is defined as the number of pixels on these farms that are not detected as changed.

To assess false positives, an area of the Gorongosa National Park, termed 'The Sanctuary' (Fig 1) that is extremely unlikely to have undergone human-induced LCC was analysed. The Sanctuary is an electric-fenced area of 5,761 ha designed to retain animals imported to the Park (not including elephants). Note that this definition of false positive is very broad and includes both natural changes to the woodland as well as random errors in detection as 'false positives'.

The sensitivity of the hit rate and false positive rate to the parameters used in the change detection algorithm was assessed: φ, the fraction of AGB remaining on a changed pixel was varied from 80% to 20%, and α, the threshold *P*-value above which a LCC event is considered significant, from 0.8 to 1.

Assessing preferential selection of high biomass areas

To test whether land with high AGB is preferentially selected for LCC, compared with the null hypothesis that LCC is random with respect to AGB, we compare the observed results to a pseudo-data set for which the null hypothesis is true. The pseudo data time series of AGB for each pixel, denoted $C^*(t)$, is constructed as follows: for each pixel, a time series is constructed with a constant mean equal to the observed AGB in 2007. Then a random 4% of pixels are pseudo deforested at a time point randomly selected between t=2 and t=9. At this time point, an abrupt change is imposed and the AGB reduced to a mean of 10 MgC ha^{-1}. Noise was added to the time series by drawing each value from a normal distribution with

means as described above and standard deviations *N(t)*, the RMSE validation errors from the regressions. The change detection algorithm was run as described above to identify pixels that were pseudo-changed, estimating the parameters *C1** and *C2**, the pseudo equivalents of *C1* and *C2*. The resulting distributions of *C1** and *C1* are compared using a two sample Kolmogorov-Smirnov test to test if the distribution of *C1* is larger than *C1**.

Biomass loss due to deforestation and degradation

To compare the contributions of deforestation and degradation to the total carbon loss from the study area, the change (ΔC) between the mean AGB of the three images in 2007 (C_{2007}) and the mean AGB of the three images in 2010 (C_{2010}) was examined. The image is classified into four categories that follow the conventional definition of de/reforestation and de/aggradation based on a binary forest/non-forest pixel classification in 2007 and 2010. The forest/non-forest classification is made using a default AGB threshold of 15 MgC ha^{-1}. However, the effects of varying the threshold from 5 to 20 MgC ha^{-1} were evaluated.

The deforestation AGB loss (Δ_D) is defined as the net sum of ΔC for pixels that shift from the forest to non-forest classes. Reforestation gain (Δ_R) is the net sum of ΔC for pixels moving from non-forest to forest. Forest de/aggradation (Δ_{GF}) is the net sum of ΔC for forest-pixels remaining forest, and non-forest de/aggradation (Δ_{GN}) is the net sum of ΔC for non-forest pixels remaining non-forest. Thus:

$$C_{2007} - C_{2010} = \Delta C = \Delta_D + \Delta_R + \Delta_{GF} + \Delta_{GN}$$

and net deforestation is:

$$\Delta_{D,net} = \Delta_D + \Delta_R$$

Thus for all terms describing a change in biomass stocks, positive numbers indicate loss of biomass and negative values denote gains.

Results

Ground data and regression

The 96 plots ranged in aboveground biomass from 0 to 56 MgC ha^{-1} (mean 15±12 MgC ha^{-1}; Fig 2; ± indicates one standard deviation throughout). The ordinary least squares regression of backscatter against AGB gave values of R^2 from 0.40 to 0.58 (Table 1). For the ten images, regression slopes ranged from 1272 to 1803 (MgC ha^{-1})$^{-1}$ (Table 1; Fig 3) and this translated into moderate variation in estimated carbon stocks through the study period. For instance, backscatter values for a pixel over a pseudo invariant patch of protected forest ranged from 89-107% of the first image, which translated, to a range of 47-61 MgC ha^{-1} (Fig 4).

The validation procedure estimated RMSE validation errors of 8.7 – 10.9 MgC ha^{-1} for the different time slices (mean error 9.8±0.7 MgC ha^{-1}), and mean absolute bias of 1.6±0.1 MgC ha^{-1} (Table 1). The worst-case scenario for change detection is that these biases are random between each scene, but the covariance of these biases through time was high (Table S1), with, for example r>0.86 between the bias in the three scenes from 2007, and r>0.44 for bias between years.

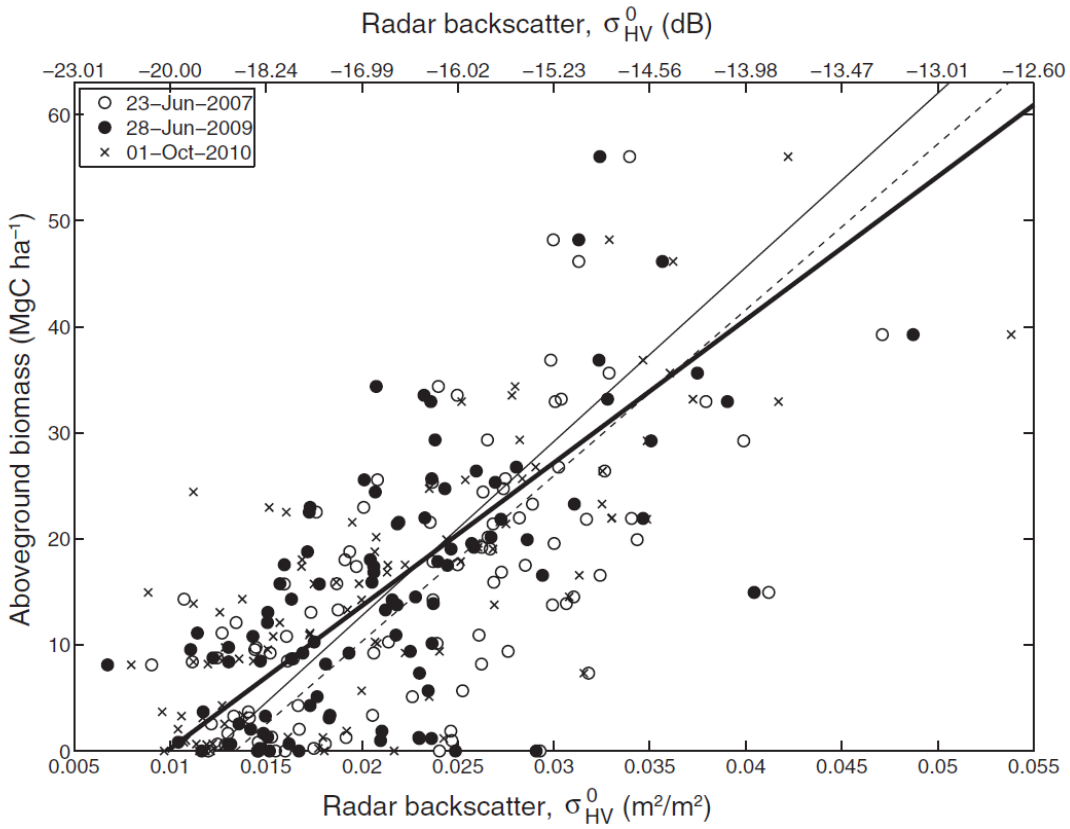

Fig. 3: Regression of radar backscatter from ALOS PALSAR and aboveground biomass. Ten regressions were performed, one for each image in Table 1, but for clarity only the data and regression lines from the first (June-2007, open circle, dashed line), sixth (June-2009, closed circles, light line) and last (Oct-2010, crosses, heavy line) image are shown. Each line is fit to minimise the errors on both axes (RMA regression).

Carbon stocks and changes

The carbon stocks in the study area exhibit an east-west gradient related to the topography, with AGB ~60 MgC ha^{-1} in the undisturbed areas to the west of the Vunduzi river falling to ~30 MgC ha^{-1} in the centre of the study area (Fig 1). East, towards the floor of the Rift valley, substantial biomass is restricted to the river lines and high points. Imposed on this topographic pattern, the effects of human disturbance are obvious, with almost no large blocks of woodland remaining to the south of the River Pungue and along the west side of the highway. However LCC is less apparent to the east of the highway, an area that is part of the buffer zone of the

Gorongosa National Park. The town of Gorongosa marks the epicentre of a zone of reduced biomass.

The study area contained AGB of 2.13±0.12 TgC in 2007 and 1.98±0.11 TgC in 2010, a loss of 0.15±0.10 TgC, or 6.9±4.6% of the 2007 AGB over three years. Pixels that lost > 9 tC/ha contributed half the total loss in AGB, with the remaining loss being in pixels that lost <9 tC.

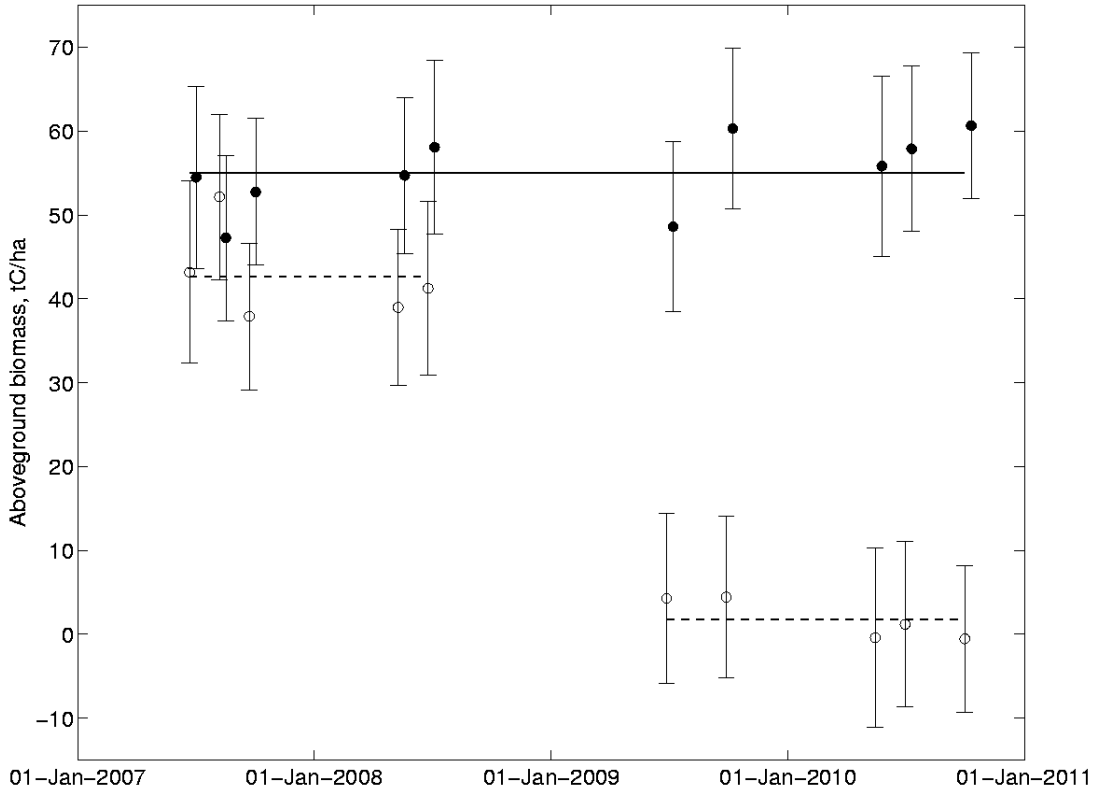

Fig.4: Example time series for a single pixel over a) an undisturbed riverine forest (solid line, filled circles) and b) an area of woodland converted to a farm (dashed line, open circles). The lines indicate the parameters as estimated by the change detection algorithm. Over the protected forest no change was detected (mean AGB of 55.0±4.5 MgC ha^{-1}). The new farm (illustrated in Fig 6) was created between June 2008 and June 2009. AGB before the change point was 42.7±1.8 and 5.3±5.3 MgC ha^{-1} afterwards. The probability of this change being observed by chance is < 0.001. The points representing the forest pixel have been shifted forward by 10 days for clarity.

Spatial patterns of carbon stock change

Looking at the spatial patterns of change in C stocks (Fig 5), there were several areas of increasing AGB mainly in the Park and Sanctuary (A; letters refer to points marked on Fig 5; names to the sub-areas delineated with green lines in Fig 1) as well as decreases (B). Losses were observed all along the highway, but particularly to the west of the road; in comparison, to the east of the road in the buffer zone of the Park there are fewer areas of biomass loss (C). New farms were opened in the area between the Vunduzi river and the road, and a cluster of new farms can be seen in the inaccessible region to the west of the river (D). A new power line built in the Park is visible along the boundary of the Nhambita sub area (E). An area of private land, in which charcoal production and agriculture are not present (Eng. A. Serra, pers comm. 2011) stands out clearly from the surrounding decrease in AGB in Mbulawa (F). In Nhambita a string of new farms along a previously high AGB river line is visible (G).

The probability distribution functions (PDFs) of carbon stocks in the sub areas (Fig 7) provide further insight into the AGB stocks and changes. In the inhabited areas (Gorongosa town, Nhambita, Mucombeze and Mbulawa) the LCC is evident in the difference between the 2007 and 2010 PDFs. In contrast, in the Sanctuary, the 2010 PDF is shifted to higher biomass values compared to 2007, indicating regrowth. The Remote Park shows no change in AGB over the study period. Vunduzi, an almost undisturbed, well wooded area, is the only sub-area with a normal PDF. The bimodal PDF of Gorongosa appears to consist of a deforested PDF similar to Mucombeze combined with a woodland PDF centred on 40 MgC ha^{-1}.

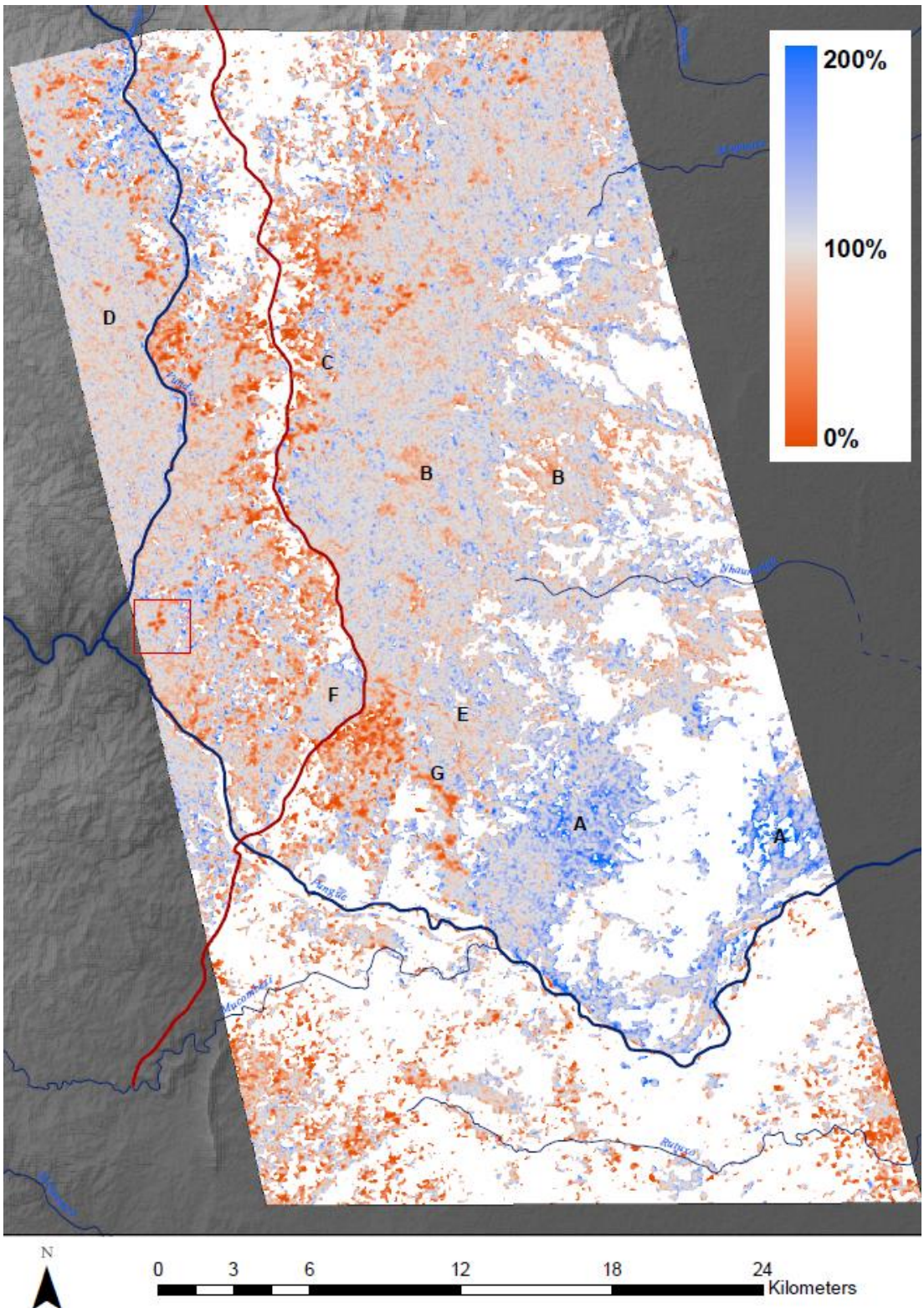

Fig.5: Carbon stock change in the study area. The image shows the aboveground biomass (AGB) in 2010 as a percentage of AGB in 2007. Values greater than 100% indicate areas of biomass gain (blue)and below 100% areas of biomass loss (red). Features lettered A-F are described in the main text. Areas with AGB <10 tC are shown in white. The red box indicates the area shown in Fig 6. The red line shows the EN1 highway. Rivers are marked in blue.

Deforestation and degradation

The loss of AGB across the study area over the three years was 149±101 GgC. Using the default threshold of forest being any pixel with AGB > 15 MgC ha^{-1}, loss of AGB due to deforestation was 92±11 GgC (Table 2). This was offset by a reforestation gain in AGB of -36±4.5 GgC, leading to a net deforestation loss of 55±12 GgC. This can be compared to forest degradation loss of 42±73 GgC and non-forest degradation of 53±43 GgC, so that total degradation is 94±90 GgC. Thus most of the uncertainty in ΔC comes from the degradation term.

Thus, the best guess of the percentage of net biomass loss that can be attributed to degradation is 67% (median of the bootstraps). This result varied only slightly with different thresholds of forest/non-forest: from 69% with 10 MgC ha^{-1} as the threshold to 65% when using 20 MgC ha^{-1} as the threshold. This proportion of biomass loss attributed to degradation is highly uncertain, with an 80% confidence interval of 21 to 80% (Fig S2). There is a 79% chance that degradation was >50% of the net loss of AGB and a 90% chance that it accounted for >21% of the net loss.

Table 2: Change in aboveground biomass (AGB) stocks classified by forest/non-forest transitions over the period 2007-2010.

Transition type	Area (km^2)	AGB loss over three years (GgC)	
Deforestation (forest→ non-forest)	75	92±11	
Aggradation (non-forest→ forest)	48	-36±4.5	55±12 (33%)
Forest degradation (forest→forest)	530	42 ±73	
Non-forest degradation (non-forest→non-forest)	507	53±43	94±90 (67%)
All	1160	149±101	

The threshold for forest is AGB>15MgC ha^{-1}. Negative changes indicate a gain in biomass stocks.

Characteristics of land cover change events

The change detection algorithm was able to detect per-pixel abrupt changes of >12 MgC ha^{-1}, a threshold that is a function of the noise associated with the measurements of AGB, the number of observations and the detection algorithm parameters α and φ. Using the default parameters (α = 0.95 and φ = 50%) abrupt LCC was detected in 2.61 % of the study area.

In total, 3,029 ha were detected as changed in 6,761 events (mean size = 0.45±0.80 ha, median = 0.19 ha). Events larger than the median contributed 88% of the total changed area; events > 0.5 ha, 70%; and events >1 ha contributed 49% of the total changed area. The mean event size (assumed to be false positives) in the Sanctuary (0.14 ha) was smaller than the events in the inhabited sub-areas (means 0.34-0.52 ha). In the inhabited areas, event size was smallest in Mucombeze (mean 0.34 ha), where forested land is very scarce (26% of land was forested in 2007) and largest (mean 0.52 ha) in Vunduzi where all land was forested in 2007. The other inhabited sub-areas have intermediate event sizes and forest cover.

The mean change is AGB when an event occurred was for the area to lose 21.3±5.5 MgC ha^{-1}, being reduced from *C1* = 33.5±9.8 to *C2* = 11.9±18.4 MgC ha^{-1}. The reduction in AGB ranged from 12.2-56.9 MgC ha^{-1}. With the exception of the Vunduzi sub-area, the mean pre-change AGB of changed pixels (*C1*) was never more than 0.7 MgC ha^{-1} higher than if LCC was random with respect to AGB (*C1**), although the differences were significant to P<0.001 (Fig 7). This suggests that the hypothesis that high AGB pixels are preferentially subject to LCC is not true to a substantial extent. However, in the Vunduzi sub-area, *C1* (53.6 MgC ha^{-1}) was 4.7 MgC ha^{-1} higher (P<0.001) than *C1** (48.9 MgC ha^{-1}), suggesting a modest

preference towards high AGB land, but the number of changed pixels is relatively small (n= 345).

Events were significantly clustered (P<0.001) according to the nearest neighbour distance. The observed mean distance from one event to the nearest was 87 m compared to 206 m if the events were evenly spaced. Many cleared areas are the result of small expansions to the frontiers of already cleared land (example in Fig 6).

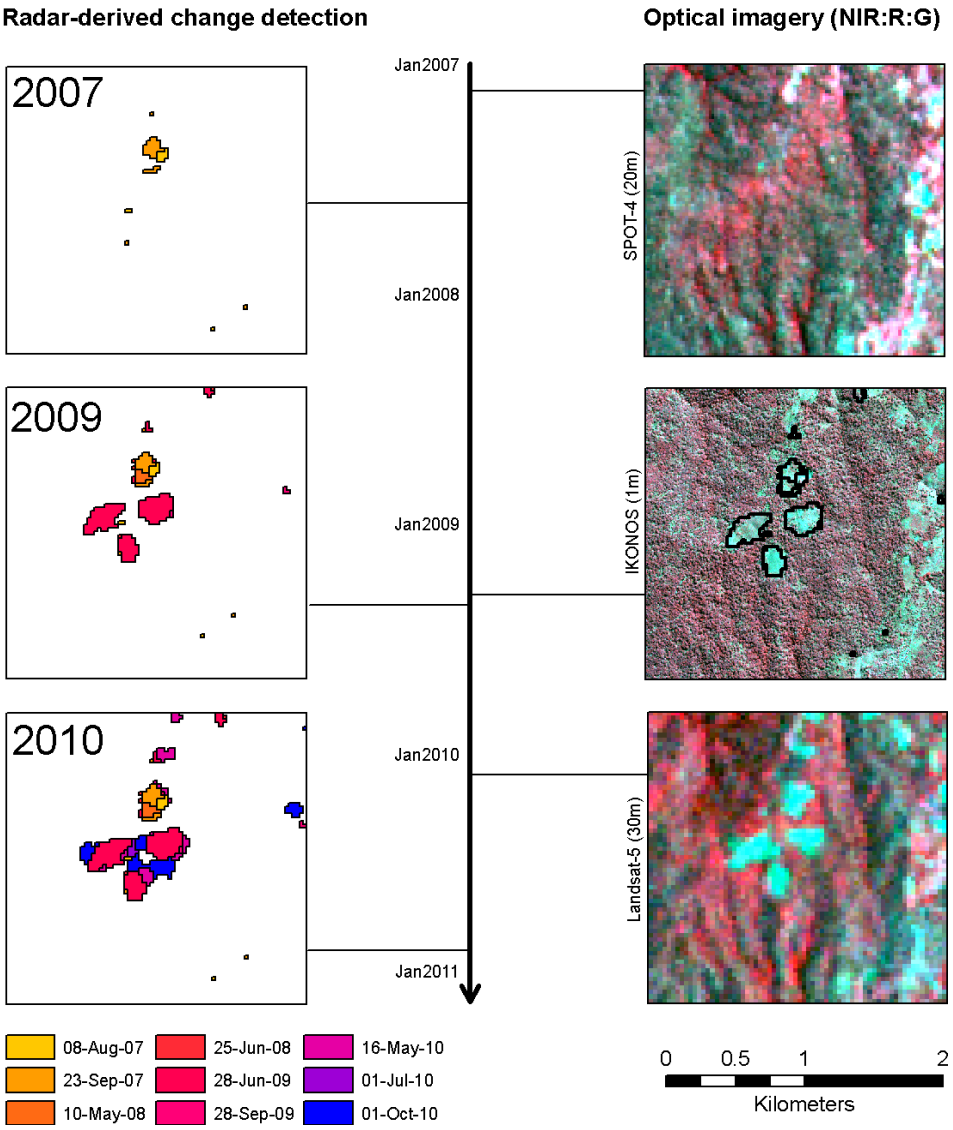

Fig. 6: Detail of Fig 5, showing the detected land cover change events. The temporal evolution of forest clearance as detected by the radar imagery is shown from 2007 to 2010 (left panels). The right hand panels show false-colour optical imagery of the same area for comparison. The outlines of the change events up to July 2009 are overlaid on the middle right image.

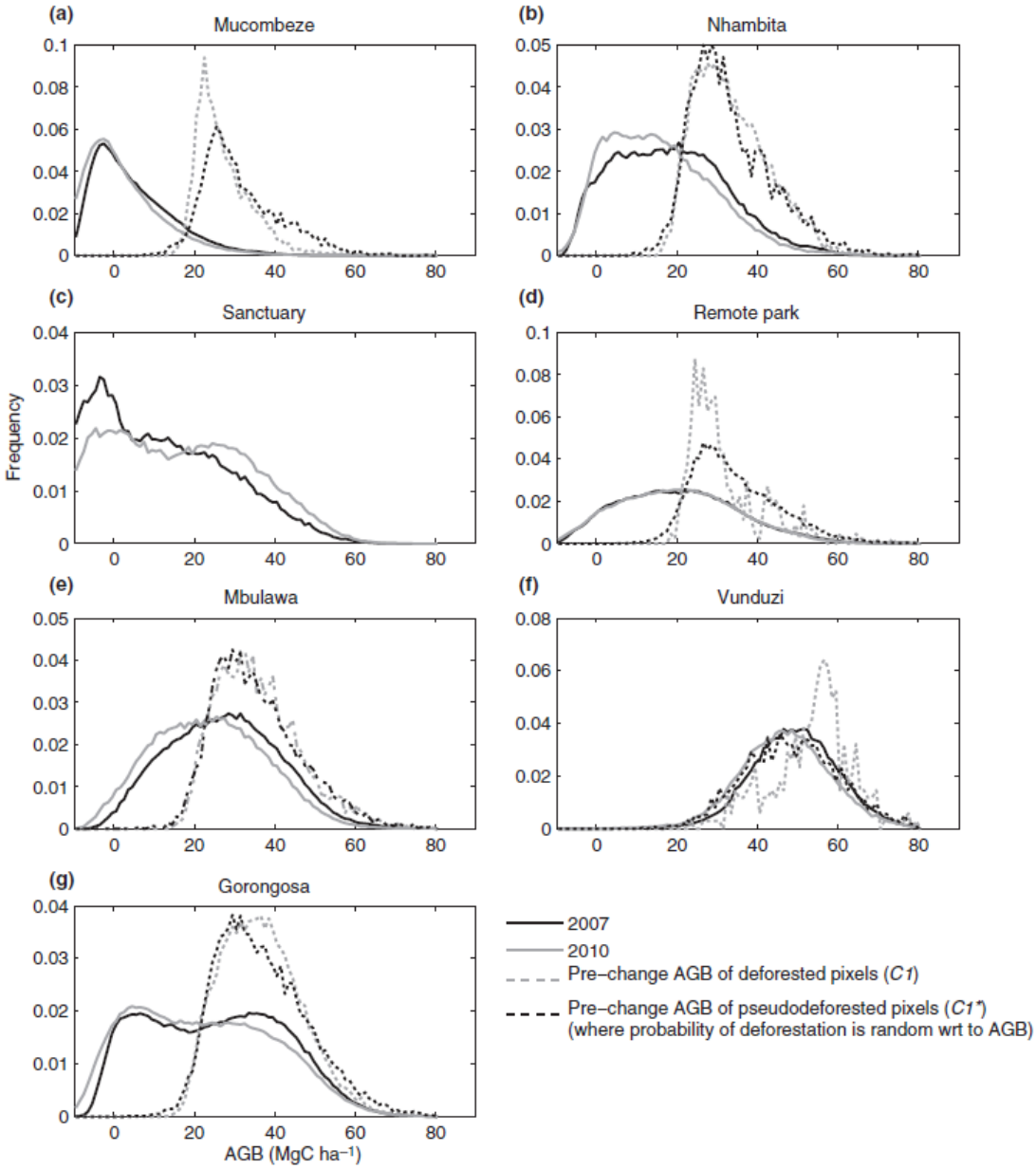

Fig. 7: Probability density functions of aboveground biomass in 2007 (black solid line), 2010 (grey solid line). Also shown is the AGB of changed pixels prior to change (dashed lines). The observed values (grey dashed lines), and the expected value if deforestation was random with respect to biomass (black dashed line) are shown. The 2007 and 2010 data are the mean of three images. The boundaries of each sub-area (a-g) are shown in Fig 1. No data are shown for the changed pixels in the Sanctuary as the number of changed pixels (n=10) was to few to produce a meaningful PDF.

Change detection validation and sensitivity

Using our default parameters, LCC was detected in 1,646 of the 2,611 validation pixels, a miss rate of 35%. Generally, the missed pixels were at the fringes of the events – only in 10 of the 90 validation events was no LCC detected – implying that the misses will affect the size of detected events more than the number. The false positive rate was 0.016% in the Sanctuary, equal to 0.005 % year^{-1}. The sensitivity analysis (Fig 8) showed that it is possible to suppress the false positive rate further, but only at the expense of an increase to the miss rate. A zero false positive rate can be achieved in the Sanctuary by reducing φ to 20% (for $\alpha > 0.95$), but this gives a miss rate of 74%. Conversely, a lower miss rate can be achieved, say 20%, with φ =60% and α=0.9, but this gives a false positive rate of 0.07%.

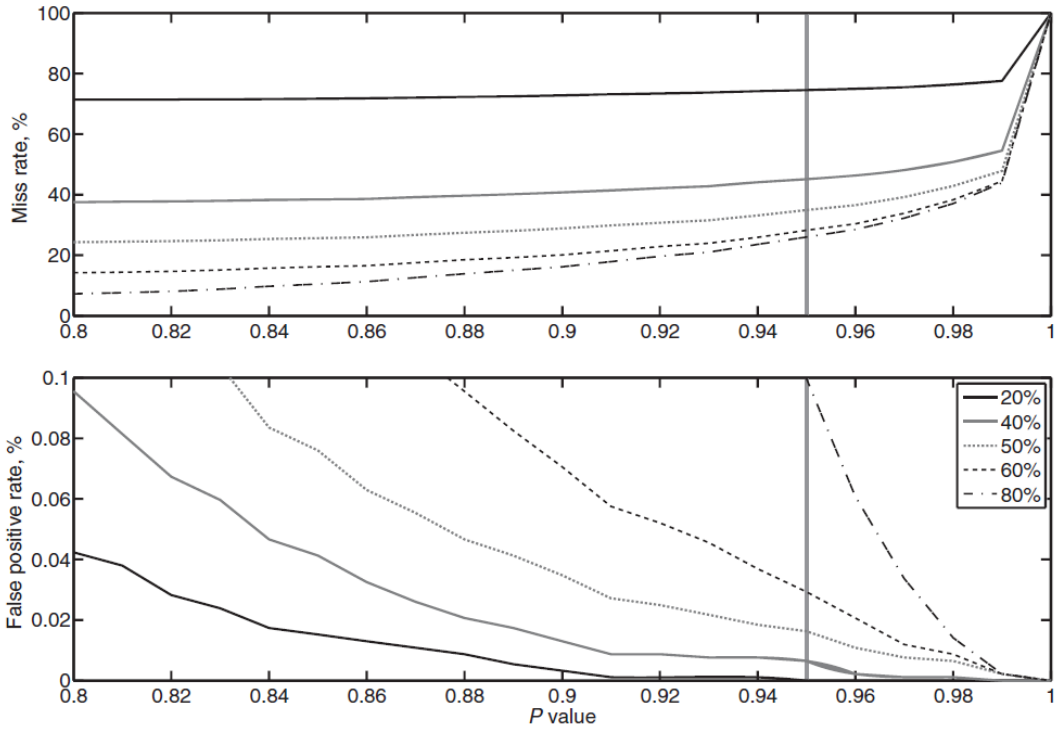

Fig. 8: Miss rates and false positives for the land cover change detection algorithm under a variety of definitions of change. The *P*-value shown on the x axis are the threshold probability above which a change event is considered real. The various lines indicate φ, the fraction of biomass remaining after change, below which the pixel's biomass needs to be reduced for the change to be detected. A *P*-value of 0.95 and φ = 50% were used as default values.

Discussion

Can L-band radar accurately measure changes in biomass?

Our method was able to detect a loss (6.9±4.6%) of biomass from the landscape over a relatively short observation period of three years. This change in biomass (ΔC) is equivalent to a reduction in C density from 18.4 to 17.1 MgC ha^{-1} across the whole study area, a change that would be difficult to detect without very accurate stratification and intensive ground-based sampling. The relative error on the standing stock estimates is 6%, but this increases to 67% for ΔC , the change in stocks (Table 2). Without the high covariance of the regression errors through time (Table S1) the error on the change in stocks would have been higher.

When the net changes in biomass are split between deforestation and degradation, it is clear that most of the uncertainty in ΔC comes from degradation. It is much easier to detect change in the small area (77 km^2) that was deforested and which lost 84.8±9.7 GgC, compared to the very large (643 km^2) forest-remaining-forest area that probably lost a comparable amount of AGB (96.9±91.0 GgC) (Table 2). The nature of the challenge is illustrated by a best guess assessment of the change in C density for the forest-remaining-forest area from 30.3 to 29.4 MgC ha^{-1}.

However, at a pixel scale, abrupt change (including degradation) is detectable at 95% confidence as long as it exceeds 12 MgC ha^{-1}. Per pixel change detection rates were 65%, and in 89% of change events some change was detected. These rates are comparable to another application of L-band SAR to detect >2 ha clear cuts in Sweden (hit rate = 76%, (Pantze *et al.*, 2009)). However it is clear that we are at the limit of the resolution of this technique – the ALOS imagery detects new farms as having a bare centre and then a gradient of biomass into the surrounding woodland,

but on-the-ground observations show that the farm/woodland boundary is normally abrupt. Morphological detection techniques have the potential to improve the very simple per-pixel change detection used here and to reduce false positives. Such techniques may also be more accurate in determining the size of each LCC event.

Backscatter-biomass relationships for space borne L-band backscatter in 'difficult' conditions (i.e. mixed age stands of multiple species) are reported with similar statistics to that found here (e.g. $R^2 = 0.53$ (Karjalainen *et al.*, 2009)) and slightly better results have been found in even-aged stands (RMSE = 30% of biomass (Magnusson *et al.*, 2007)), or when considering a very wide range of biomass (Mitchard *et al.*, 2009). In comparison, airborne LiDAR has regression statistics between the LiDAR metrics and AGB of RMSE of 23.5 MgC ha^{-1}, R^2 = 0.85 in an example from Peru (Asner *et al.*, 2010). In the present study the comparable figures were RMSE = 8.7 tC/h and $R^2 = 0.49$, but the difference in RMSE is probably due to the lower AGB of our study area.

Williams et al (2008) found that regrowing woodland at this site can accumulate between 0.4-0.9 MgC ha^{-1} $year^{-1}$ AGB, and we expect that changes in more mature woodland will be less than this. However, in two parts of the study area (Fig 5, A) rapid increases in AGB beyond this rate are observed. Observations in this area show rapid woody encroachment, probably the result of fire exclusion in the Sanctuary. Stem numbers have approximately doubled in four years (data not shown), but biomass has not increased by that rate because the new stems are small saplings. This unrealistic sensing of biomass accumulation raises the issue of which (combination of) plot characteristics L-band backscatter is most strongly related to – stem number, basal area or biomass (Woodhouse, 2006b)? In mixed age, diverse

sites this question has not yet been resolved (Woodhouse, 2006b). If the biomass-backscatter relationship is not direct, but is mediated by other stand characteristics (Lucas *et al.*, 2010), then the site-specificity of the regression parameters needs to be evaluated (Mitchard *et al.*, 2009).

- How much carbon is lost to deforestation compared to degradation?

The large uncertainty on the degradation loss makes it difficult to estimate the fraction of AGB losses attributable to degradation. However, a best guess is that total degradation was 67% of total net losses of AGB. This analysis thus provides tentative support for the idea of a large and presently un-quantified loss of biomass due to degradation in African woodlands and forests. However, we caution against extrapolating this change in AGB to emissions, because, firstly, it is likely that many of the areas that are degraded are subsequently deforested (Ahrends *et al.*, 2010), and secondly, the time period over which a change in standing stocks translates into a flux to the atmosphere is currently unknown in this ecosystem.

Loss of AGB in our study area (0.43 MgC ha^{-1} yr^{-1}) was lower than has been reported from plot data in the surrounds of Dar es Salaam (0.8 MgC ha^{-1} yr^{-1} (Ahrends *et al.*, 2010)). This is expected given that our study site is ~100 km by road from the nearest city, Chimoio, which has a much smaller population and thus pressure for resource extraction is likely to be lower.

The distinction between deforestation and degradation is logical in the context of the area multiplied by C density approach to C stock estimation. However, the advent of high resolution maps of C stocks and their change, where the resolution is similar to the area of a single tree canopy, means that the distinction becomes ambiguous – in effect degradation is just very small scale deforestation. It may be more useful to

characterise a land cover change regime in terms of the frequency, area (and shape), and intensity of biomass change, as these parameters might be more easily related to the extent of different land uses, which is normally the information policy makers require.

- Are areas of high carbon density preferentially targeted for land cover change?

The difference between the AGB of land that underwent LCC and the mean of comparable surrounding woodland was <1 MgC ha^{-1}, suggesting there is no substantial preference for LCC to be undertaken in high biomass areas (Fig 7). There are some indications that this may not be true in all areas (such as Vunduzi), but for now, the hypothesis that emissions might be substantially higher as a result of preferential deforestation of high AGB areas has not been supported. This suggests that the other criteria for the location of new farms dominate (such as proximity to existing farms, roads or dwellings) or that AGB is not correlated to the agricultural suitability of the land. The latter might be true even if *potential* AGB and soil fertility are correlated because of past land use or other disturbance to AGB.

- What is the carbon density (MgC ha^{-1}) of changed areas before and after land cover change?

After a change event, land was not reduced to zero AGB, but instead averaged 11.9±18.4 MgC ha^{-1}. This result fits with observations on the ground, where large trees are often left in newly cleared areas to provide shade, or because of the disproportionate effort needed to remove them (Ghee, 2009). In addition, trees on deforested land are often ringbarked or otherwise killed, but left standing, and as they dry out will scatter radar waves less as their dielectric properties change. However, there is evidence of non-linearity in the AGB- backscatter regression at low values of

backscatter, so these measurements of very low AGB values may be subject to additional uncertainties. This may be because at very low biomass, backscatter will be strongly influenced by the properties of the ground surface, including surface roughness and soil moisture.

- What size are land cover change events, and how are they clustered in space?

In Central Mozambique, farmers have an arable area of 1.4 ha on average (Simler *et al.*, 2004). However, most LCC events detected in this study were much smaller than this (mean 0.45 ha), indicating that farms are built up in size by repeated small clearances (Fig 6). The significant spatial clustering of LCC events supports this. This 'death by a thousand cuts' type of woodland clearance poses a stiff challenge for rapid monitoring of LCC: A detection system that ignored events < 1 ha would miss the areal majority of LCC in this study area, and so might need to operate over long time scales to be effective.

Limitations

Despite only using dry season imagery, there is considerable variation through time in the backscatter values of the ALOS PALSAR imagery, and the slope of the backscatter-AGB regression. This is presumably due to variations in environmental conditions such as soil moisture, which is well known to influence L-band backscatter (Rignot *et al.*, 1994, Pulliainen *et al.*, 1999, Magnusson *et al.*, 2007, Pantze *et al.*, 2009, Lucas *et al.*, 2010), changes to understory vegetation, or sensor calibration drift. This variation suggests that accurate biomass change detection with this sensor will require either: invariant features to be present in each scene; correction for e.g. the effects of soil moisture with ancillary data sets and models; or recalibration to ground data at each time point. We adopted the latter approach here,

but with an inventory that was not repeated each year, and thus an assumption that plot biomass has not changed during the study period.

Furthermore, there are potentially significant uncertainties associated with the stem diameter-biomass allometry (Chave *et al.*, 2004) even with the use of a site-specific model. This can introduce bias of ~17% (Ryan, 2009). Although the regression procedure used here accounts for the random error, the bias will remain and influence estimates of AGB stocks, but not change.

It should also be noted that the L-band biomass-backscatter response is known to saturate at the level of biomass typically found in closed canopy forests. Studies report saturation at between 30-100 MgC ha^{-1} (Mitchard *et al.*, 2009, Lucas *et al.*, 2010), although this appears to depend on vegetation structure (Lucas *et al.*, 2010). Thus the method presented here which utilises L-band will be most useful in low C density woodlands rather than higher density forests. The proposed BIOMASS mission would employ P-band radar in an effort to overcome this limitation (Le Toan *et al.*).

Conclusions

- Multi-temporal L-band radar imagery can be effective in detecting small-scale deforestation, but may fail to detect small levels of degradation over large areas. Abrupt changes of more than 12 MgC ha^{-1} are detectable at 95% confidence on a 25x25 m pixel scale.
- In this area of Mozambique, land cover change events are mostly small (median = 0.2 ha) but range from 0.06-18 ha and reduce aboveground carbon from 33.5 to

11.9 MgC ha^{-1} on average. They are strongly clustered together, and many events are the expansion of previously cleared land.

- There was no evidence that the areas that were deforested had a higher biomass than the average surrounding woodland.
- Degradation losses are likely to be substantial, with a best guess that they represent 67% of the net biomass loss. This number is extremely uncertain however.

Acknowledgements

The Nhambita community and staff of Envirotrade facilitated fieldwork. Staff of the Gorongosa national park allowed access to plots within the park. The GeoEye Foundation provided the IKONOS image. ESA and JAXA provided the ALOS imagery (C1P.7493). CR was supported by the UK NERC Carbon Fusion project, the Mpingo Conservation & Development Initiative (http://tinyurl.com/mpingo) under their REDD Pilot Project funded by the Royal Norwegian Embassy in Tanzania, and the EU FP7 iREDD+ project. EM is funded by Gatsby Plants. We also thank Iain Cameron for his advice and help. We thank the two anonymous reviewers for their helpful comments.

References

Achard F., Defries R., Eva H. *et al.* (2007) Pan-tropical monitoring of deforestation. *Environmental Research Letters,* **2**.

Ahrends A., Burgess N. D., Milledge S. a. H. *et al.* (2010) Predictable waves of sequential forest degradation and biodiversity loss spreading from an African city. *Proceedings of the National Academy of Sciences,* **107**, 14556-14561.

Almeida-Filho R., Rosenqvist A., Shimabukuro Y. E. *et al.* (2005) Evaluation and perspectives of using multitemporal L-band SAR data to monitor deforestation in the Brazilian Amazoˆnia. *Geoscience and Remote Sensing Letters, IEEE,* **2**, 409-412.

Archibald S., Scholes R. J. (2007) Leaf green-up in a semi-arid African savanna separating tree and grass responses to environmental cues. *Journal of Vegetation Science,* **18**, 583-594.

Asf (2010) *ASF MapReady User Manual*, Alaska Satellite Facility Engineering Group.

Asner G. P., Powell G. V. N., Mascaro J. *et al.* (2010) High-resolution forest carbon stocks and emissions in the Amazon. *Proceedings of the National Academy of Sciences,* **107**, 16738-16742.

Burgess N., Doggart N., Lovett J. C. (2002) The Uluguru Mountains of eastern Tanzania: the effect of forest loss on biodiversity. *Oryx,* **36**, 140-152.

Chave J., Condit R., Aguilar S. *et al.* (2004) Error propagation and scaling for tropical forest biomass estimates. *Philosophical Transactions of the Royal Society of London Series B-Biological Sciences,* **359**, 409-420.

Ciais P., Bombelli A., Williams M. *et al.* (in press) The carbon balance of Africa: synthesis of recent research studies. *Philosophical Transactions of the Royal Society (A),* **369**, 1-20.

Defries R. S., Rudel T., Uriarte M. *et al.* (2010) Deforestation driven by urban population growth and agricultural trade in the twenty-first century. *Nature Geoscience,* **3**, 178-181.

Denman K. L., Brasseur G., Chidthaisong A. *et al.* (2007) Couplings Between Changes in the Climate System and Biogeochemistry. In: *Climate Change 2007: The Physical Science Basis.* (eds Solomon S, Qin D, Manning M, Chen Z, Marquis M, Averyt KB, M.Tignor, Miller HL) pp Page. Cambridge, Cambridge University Press.

Dewees P. A., Campbell B. M., Katerere Y. *et al.* (2010) Managing the Miombo Woodlands of Southern Africa: Policies, Incentives and Options for the Rural Poor. *Journal of Natural Resources Policy Research,* **2**, 57-73.

Etter A., Mcalpine C., Phinn S. *et al.* (2006) Characterizing a tropical deforestation wave: a dynamic spatial analysis of a deforestation hotspot in the Colombian Amazon. *Global Change Biology,* **12**, 1409-1420.

Fao (2010) Global Forest Resources Assessment 2010. In: *FAO Forestry papers.* pp Page.

Farr T. G., Rosen P. A., Caro E. *et al.* (2007) The shuttle radar topography mission. *Reviews of Geophysics,* **45**.

Fisher B. (2010) African exception to drivers of deforestation. *Nature Geosci*, **3**, 375-376.

Fransson J. E. S., Magnusson M., Olsson H. *et al.* (2007) Detection of forest changes using ALOS PALSAR satellite images. In: *Geoscience and Remote Sensing Symposium, 2007. IGARSS 2007. IEEE International.* pp Page.

Frost P. (1996) The ecology of Miombo woodlands. In: *The Miombo in transition : woodlands and welfare in Africa.* (ed Campbell BM) pp Page. Bogor, Indonesia, Center for International Forestry Research.

Furley P. A., Rees R. M., Ryan C. M. *et al.* (2008) Savanna burning and the assessment of long-term fire experiments with particular reference to Zimbabwe. *Progress In Physical Geography*, **32**, 611-634.

Geist H. J., Lambin E. F. (2002) Proximate Causes and Underlying Driving Forces of Tropical Deforestation. *BioScience*, **52**, 143-150.

Ghee C. (2009) Nitrogen and Carbon Dynamics in Mozambican Smallholder Agroforestry Systems. MSc, University of Edinburgh, Edinburgh.

Gofc-Gold (2010) A sourcebook of methods and procedures for monitoring and reporting anthropogenic greenhouse gas emissions and removals caused by deforestation, gains and losses of carbon stocks in forests remaining forests, and forestation. pp Page, Alberta, GOFC-GOLD Project Office.

Grainger A. (1999) Constraints on modelling the deforestation and degradation of tropical open woodlands. *Global Ecology and Biogeography*, **8**, 179-190.

Grainger A. (2008) Difficulties in tracking the long-term global trend in tropical forest area. *Proceedings of the National Academy of Sciences*, **105**, 818-823.

Hansen M. C., Shimabukuro Y. E., Potapov P. *et al.* (2008) Comparing annual MODIS and PRODES forest cover change data for advancing monitoring of Brazilian forest cover. *Remote Sensing of Environment*, **112**, 3784-3793.

Hoekman D. H., Vissers M. a. M., Wielaard N. (2010) PALSAR Wide-Area Mapping of Borneo: Methodology and Map Validation. *Selected Topics in Applied Earth Observations and Remote Sensing, IEEE Journal of*, **3**, 605-617.

Houghton R. A. (2010) How well do we know the flux of CO2 from land-use change? *Tellus B*, **62**, 337-351.

Houghton R. A., Hackler J. L. (2006) Emissions of carbon from land use change in sub-Saharan Africa. *Journal of Geophysical Research - Atmospheres*, **111**.

Houghton R. A., Hall F., Goetz S. J. (2009) Importance of biomass in the global carbon cycle. *Journal of Geophysical Research-Biogeosciences*, **114**.

Hui D., Jackson R. B. (2007) Uncertainty in allometric exponent estimation: A case study in scaling metabolic rate with body mass. *Journal of Theoretical Biology*, **249**, 168-177.

Ine (2010) Estatísticas do Distrito de Gorongosa. pp Page, Instituto Nacional de Estatística.

Karjalainen M., Pyysalo U., Karila K. *et al.* (2009) Forest biomass estimation using ALOS PALSAR images in challenging natural forest area in Finland. In: *ALOS PI 2008 Symposium.* pp Page, Island of Rhodes, Greece, ESA Special Publication SP-664.

Kindermann G. E., Mcallum I., Fritz S. *et al.* (2008) A global forest growing stock, biomass and carbon map based on FAO statistics. *Silva Fennica,* **42**, 387-396.

Le Toan T., Beaudoin A., Riom J. *et al.* (1992) Relating forest biomass to SAR data. *Geoscience and Remote Sensing, IEEE Transactions on,* **30**, 403-411.

Le Toan T., Quegan S., Davidson M. W. J. *et al.* The BIOMASS mission: Mapping global forest biomass to better understand the terrestrial carbon cycle. *Remote Sensing of Environment,* **In Press, Corrected Proof**.

Loarie S. R., Asner G. P., Field C. B. (2009) Boosted carbon emissions from Amazon deforestation. *Geophysical Research Letters,* **36**.

Lucas R., Armston J., Fairfax R. *et al.* (2010) An Evaluation of the ALOS PALSAR L-Band Backscatter–Above Ground Biomass Relationship Queensland, Australia: Impacts of Surface Moisture Condition and Vegetation Structure. *Selected Topics in Applied Earth Observations and Remote Sensing, IEEE Journal of,* **3**, 576-593.

Magnusson M., Fransson J. E. S., Eriksson L. E. B. *et al.* (2007) Estimation of forest stem volume using ALOS PALSAR satellite images. In: *Geoscience and Remote Sensing Symposium, 2007. IGARSS 2007. IEEE International.* pp Page.

Mayaux P., Bartholom, Etienne *et al.* (2004) A new land-cover map of Africa for the year 2000. *Journal Of Biogeography,* **31**, 861-877.

Mertz O. (2009) Trends in shifting cultivation and the REDD mechanism. *Current Opinion in Environmental Sustainability,* **1**, 156-160.

Miettinen J., Shi C., Liew S. C. (2011) Deforestation rates in insular Southeast Asia between 2000 and 2010. *Global Change Biology,* no-no.

Mitchard E. T. A., Saatchi S. S., Woodhouse I. H. *et al.* (2009) Using satellite radar backscatter to predict above-ground woody biomass: A consistent relationship across four different African landscapes. *Geophys. Res. Lett.,* **36**, L23401.

Nepstad D. C., Verssimo A., Alencar A. *et al.* (1999) Large-scale impoverishment of Amazonian forests by logging and fire. *Nature,* **398**, 505-508.

Pantze A., Krantz A. H., Fransson J. E. S. *et al.* (2009) Mapping and monitoring clear-cuts in Swedish forest using ALOS PALSAR satellite images. In: *Geoscience and Remote Sensing Symposium,2009 IEEE International,IGARSS 2009.* pp Page.

Pulliainen J. T., Kurvonen L., Hallikainen M. T. (1999) Multitemporal behavior of L- and C-band SAR observations of boreal forests. *Geoscience and Remote Sensing, IEEE Transactions on,* **37**, 927-937.

Radke R. J., Andra S., Al-Kofahi O. *et al.* (2005) Image change detection algorithms: a systematic survey. *Image Processing, IEEE Transactions on,* **14**, 294-307.

Rahman M., Sumantyo J. (2010) Mapping tropical forest cover and deforestation using synthetic aperture radar (SAR) images. *Applied Geomatics*, **2**, 113-121.

Ramankutty N., Gibbs H. K., Achard F. *et al.* (2007) Challenges to estimating carbon emissions from tropical deforestation. *Global Change Biology*, **13**, 51-66.

Rignot E., Way J., Williams C. *et al.* (1994) Radar estimates of aboveground biomass in boreal forests of interior Alaska. *Geoscience and Remote Sensing, IEEE Transactions on*, **32**, 1117-1124.

Rignot E. J. M., Van Zyl J. J. (1993) Change detection techniques for ERS-1 SAR data. *Geoscience and Remote Sensing, IEEE Transactions on*, **31**, 896-906.

Ryan C. M. (2009) Carbon Cycling, Fire and Phenology in a Tropical Savanna Woodland in Nhambita, Mozambique. PhD, University of Edinburgh, Edinburgh, 257 pp.

Ryan C. M., Williams M. (2011) How does fire intensity and frequency affect miombo woodland tree populations and biomass? *Ecological Applications*, **21**, 48-60.

Ryan C. M., Williams M., Grace J. (2011) Above- and Belowground Carbon Stocks in a Miombo Woodland Landscape of Mozambique. *Biotropica*.

Schmidt-Vogt D., Leisz S., Mertz O. *et al.* (2009) An Assessment of Trends in the Extent of Swidden in Southeast Asia. *Human Ecology*, **37**, 269-280.

Shimada M., Tadono T., Rosenqvist A. (2010) Advanced Land Observing Satellite (ALOS) and Monitoring Global Environmental Change. *Proceedings of the IEEE*, **98**, 780-799.

Simler K. R., Mukherjee S., Dava G. L. *et al.* (2004) Rebuilding after War: Micro-level Determinants of Poverty Reduction in Mozambique. pp Page, Washington DC, International Food Policy Research Institute.

Sokal R. R., Rohlf F. J. (1995) *Biometry : the principles and practice of statistics in biological research*, New York, W.H. Freeman.

Tinley K. L. (1977) Framework of the Gorongosa Ecosystem. D.SC, University of Pretoria, Pretoria, 184 pp.

Tinley K. L. (1982) The influence of soil moisture balance on ecosystem patterns in Southern Africa. In: *Ecology of tropical savannas.* (eds Huntley BJ, Walker BH) pp Page. Berlin, Springer.

Trujillo-Ortiz A., Hernandez-Walls R. (2010) Geometric Mean Regression (Reduced Major Axis Regression). pp Page.

Van Der Sanden J. J., Hoekman D. H. (1999) Potential of Airborne Radar To Support the Assessment of Land Cover in a Tropical Rain Forest Environment. *Remote Sensing of Environment*, **68**, 26-40.

Van Der Werf G. R., Morton D. C., Defries R. S. *et al.* (2009) CO2 emissions from forest loss. *Nature Geosci*, **2**, 737-738.

Williams C., Hanan N., Neff J. *et al.* (2007) Africa and the global carbon cycle. *Carbon Balance and Management*, **2**, 3.

Williams M., Ryan C. M., Rees R. M. *et al.* (2008) Carbon sequestration and biodiversity of re-growing miombo woodlands in Mozambique. *Forest Ecology And Management*, **254**, 145-155.

Woodhouse I. H. (2006a) *Introduction to microwave remote sensing*, New York ; London, Taylor & Francis.

Woodhouse I. H. (2006b) Predicting backscatter-biomass and height-biomass trends using a macroecology model. *Geoscience and Remote Sensing, IEEE Transactions on*, **44**, 871-877.